Sol-Gel-Derived Bioactive Borate Glasses for Mineralized Tissue Repair

William Cole Lepry

Department of Mining and Materials Engineering

McGill University, Montreal, QC, Canada

May 2017

A thesis submitted to McGill University in partial fulfillment of the requirements of the degree of Doctor of Philosophy

For my parents.

Abstract

Factors such as the increasing ageing population, bone degenerative diseases, fractures, and injuries have led to a great demand for synthetic bone replacement materials. Of these, bioactive glasses have risen as a primary choice due to their ability to convert to bone-like hydroxycarbonated apatite (HCA) mineral in biological solutions, which allows them to both chemically and physically bond to bone. In addition, their ability to homogeneously release ions can help stimulate the body's natural repair mechanisms. While the majority of bioactive glasses are melt-quench derived silicates, other glasses such as those based on borates, or ones fabricated through the sol-gel process have the added benefits of lower chemical durability and enhanced textural properties, respectively, which both aid in potentially providing more rapid bone repair. Yet, combining these properties to make a bioactive sol-gel derived borate glass (SGBG) has so far not been investigated, possibly due to the unique chemistry of the boron ion which makes sol-gel processing difficult. In this thesis, a wide range of nine SGBG compositions in the B_2O_3-CaO-Na_2O-P_2O_5 system were created through a novel sol-gel process. These calcined materials maintained their amorphous structure after processing and possessed specific surface areas and porosities at least two orders of magnitude higher than their melt-quench derived equivalents. These properties translated to a 25-fold increase in HCA conversion rates, in simulated body fluid. Beyond composition, SGBG processing parameters were systematically examined to determine their effects on the glass properties and bioactivities. Various precursor materials led to different gelling behaviors yet also demonstrated rapid HCA conversion. Of these parameters, calcination temperature had the greatest influence on the structure, creating a partially crystalline material, which led to reduced textural and bioactive properties. This work also methodically demonstrated the effect of sodium on SGBG composition, where decreased sodium content led to higher surface areas, but did not substantially influence bioactivity. Furthermore, the potential to enhance bioactivity in composite systems was demonstrated by the addition of SGBG particles into an electropsun polycaprolactone scaffold. With as little as 5 w/v% SGBG addition, these scaffolds demonstrated conversion to HCA, *in vitro*. In conclusion, this dissertation has introduced a new class of rapidly HCA converting bioactive glasses, fabricated using a unique sol-gel processing method, resulting in enhanced the textural properties and making SGBGs promising candidates for bone tissue engineering applications.

Résumé

Des facteurs tels que la croissance de la population vieillissante, les maladies dégénératives osseuses, les fractures et les blessures ont entraîné une forte demande pour des matériaux synthétiques en tant que remplacement osseux. Parmi ceux-ci, les verres bioactifs sont devenus un choix premier en raison de leur capacité à se convertir en minéraux d'hydroxyapatite carbonatées (HCA) dans des solutions biologiques, ce qui leur permet de se lier chimiquement et physiquement aux os. En outre, leur capacité à libérer des ions de manière homogène peut aider à stimuler les mécanismes de réparation naturels du corps. Bien que la majorité des verres bioactifs soient des silicates dérivés de fusion à haute température, d'autres verres tels que ceux à base de borates ou ceux fabriqués par le procédé sol-gel ont les avantages d'une plus basse durabilité chimique et de propriétés texturales supérieures, respectivement, qui aident à potentiellement fournir une réparation osseuse plus rapide. La combinaison de ces propriétés pour fabriquer un verre de borate bioactif dérivé par le procédé sol-gel (SGBG) n'a pas encore été étudiée, probablement en raison de la chimie unique des ions de bore qui rend le traitement par sol-gel difficile. Dans cette thèse, une large gamme comportant neuf compositions de SGBG dans le système B_2O_3-CaO-Na_2O-P_2O_5 a été créée grâce à un nouveau procédé de sol-gel. Ces matériaux calcinés ont maintenu leur structure amorphe après traitement et possédaient des surfaces spécifiques et des porosités d'au moins deux ordres de grandeur supérieurs à leurs équivalents dérivés fusion à haute température. Ces propriétés se traduisent par une conversion en HCA 25 fois plus rapide dans le fluide corporel simulé. Au-delà de la composition, les paramètres de traitement SGBG ont été systématiquement examinés pour déterminer leurs effets sur les propriétés du verre et sur les activités biologiques. Divers matériaux précurseurs ont conduit à différents comportements gélifiants, mais ont également démontré une conversion rapide en HCA. Parmi ces paramètres, la température de calcination a eu la plus grande influence sur la structure, créant un matériau partiellement cristallin, ce qui a conduit à des propriétés texturales et d'activités biologiques réduites. Ce travail a également démontré méthodiquement l'effet du sodium sur la composition du SGBG, où la teneur en sodium diminuée a conduit à des zones de surface plus élevées, mais n'a pas influencé de manière significative les activités biologiques. De plus, le potentiel d'améliorer les activités biologiques dans des systèmes composites a été démontré par l'ajout de particules de SGBG dans un échafaudage en polycaprolactone électrofilées. Avec seulement 5 p/v%

d'addition de SGBG, ces échafaudages ont été convertis en HCA in vitro. En conclusion, cette thèse a introduit une nouvelle classe de verres bioactifs qui se convertissent rapidement en HCA. Ces verres bioactifs ont été fabriqués à l'aide d'une méthode unique de traitement sol-gel, ce qui a permis d'améliorer les propriétés texturales et de rendre les SGBG des candidats prometteurs pour des applications en ingénierie des tissus osseux.

Acknowledgements

I would first and foremost thank my supervisor, Prof. Showan Nazhat, for his invaluable guidance and support. His initial trust in my proposed project allowed me to take many risks and truly make my dissertation my own. I'm also especially thankful for the numerous travel opportunities he provided which allowed me to collaborate with international researches across the world – something that I will always be grateful for. Moreover, his support and encouragement to always aim high, apply for grants, and participate in events outside of engineering have been irreplaceable learning experiences.

To all the co-authors, I am appreciative of your hard work that contributed to some manuscripts in this thesis. I'd like to give special thanks the current members of the Nazhat Laboratory: Shiva Naseri, Gabriele Griffanti, and Hyeree Park. You guys made my graduate experience fun and almost more importantly, stress-free (#NSG). I'd also like to thank former lab member Christoph Stähli for his helpful advice and showing me around when I first arrived and also to Sophia Smith who is the most diligent and hardworking undergrad student that I could have ever asked for.

I believe the most important parts of well-run, successful research environments are the secretaries and technicians and I feel lucky to have had the best. I'm extremely grateful for Barbara Hanley who answered approximately one million of my questions and whose immense knowledge of McGill's "inner workings" made my life significantly easier. I'm also thankful for Monique Riendeau for allowing me to make a second home in the common lab and for the insightful conversations ranging from the gym to cookies to travel and even science. I'm also appreciative of Ranjan Roy and Andrew Golsztajn for their ICP expertise and the following professors: Kristian Waters for use of DVS, Nate Quitoriano for use of nitrogen glovebox, and In-ho Jung for the use of the DSC.

I'd like to thank the numerous funding sources over the course of my PhD: The McGill Engineering Doctoral Award (MEDA), Les Vadasz Engineering Fellowship, Fonds de recherche du Québec (FQRNT) – Bourses de doctorat en recherche, Graduate Research Excellence Award (GEF), Graduate Research Mobility Award (GRMA), Graduate Research Enhancement and Travel Award (GREAT), D.F.A.T.D. Canada-Brazil Award- Joint Research Projects, and the German Academic Exchange Service (DAAD) short-term research grant.

Thank you to my gracious hosts during my travels: Prof. Ifty Ahmed at the University of Nottingham, UK, Prof. Eliton Medrios and Prof. Jonny Blaker at the Federal University of Paraíba, BR, and Prof. Aldo Boccaccini at the Friedrich-Alexander-Universität Erlangen-Nürnberg, DE. I'm also grateful for all the people that made each of those places memorable: All seven inhabitants of 282 Papa Zulu, Neymara and Eudes for teaching me all about Brazil, and to the numerous graduate students who helped me navigate Germany, made conferences more than notable, and to the whole ICG São Carlos gang. I'm also deeply grateful for Andre and Roberta in Brazil who are two of the nicest people I've ever known and made my stay significantly better - muito obrigado!

Furthermore, there were many people who influenced me before I went to graduate school. My great TAs at Alfred University (Harlan Brown-Shaklee, Jake Amoroso, Matt Brophy, and Mark Naylor) who I think subconsciously showed me grad school could be fun and worthwhile. At Johns Manville, to Jeff Shock and Elam Leede for igniting my interest in glass science. At PNNL, to all the former interns, technicians, and post-bacs that made for an excellent science-social life. To John McCloy, Joe Ryan, Dong-Sang Kim, and Ashutosh Goel for their one-on-one conversations about grad school and beyond. I'd like to especially thank Brian Riley for his mentorship, teaching me about "due diligence", Photoshop, and the importance of nice figures. If I had his work ethic this would be the acknowledgments section of my 4th PhD dissertation. Every positive laboratory skill or research ability that I have now is directly related to him (#MP4L).

I'd also like to give a special shout-out to all the exchange students I met during my first two years in Montreal. If it wasn't for you guys, I'd probably have finished my thesis a year earlier – thanks for reminding me how to live life. To Hillary, for constantly reminding me of my age and skiing friendship – congrats, you've officially won the graduation race! Thanks to Montreal, for being the best place to be a student, and in particular Vin's Café, Frostbite, Thompson House, Blue's Pub, BDA, Segal's Market, poutine, Blades of Wood, and PGSS for enhancing my graduate school experience.

Most of all, I'd like to thank my family; my brother Miles, sister Anna, and Mom, for their steadfast support and encouragement, especially these last few months. This thesis is dedicated to my parents who have given me every opportunity to succeed in life. To my mother, who early-on installed in me the importance of learning, discipline, and sleep and to my late father who taught me how to be inquisitive, creative, and to always go for the big ideas. During these last few years when we'd talk about my PhD, he would always say, with encouragement, "Short-term pain for long-term gain" to which I would jokingly reply, "Long-term pain for long-term gain" making us both laugh. If there was only one person in the world who got to know that I finished my PhD I would have chosen you.

Contents

Abstract i
Résumé ii
Acknowledgements iv
Contents vi
List of Figures viii
List of Tables xiii
Glossary of Abbreviations and Symbols xiv
Contributions to Original Knowledge xvii
Contribution of Authors xviii

1 General Introduction 1
1.1 Introduction 1
1.2 Aim, Hypothesis and Objectives 2
2 Literature Review 4
2.1 Bone 4
2.1.1 Calcium 5
2.1.2 Phosphorous 6
2.1.3 Silica 6
2.1.4 Boron 6
2.2 Tissue Engineering 7
2.2.1 Scaffolds for tissue engineering 8
2.3 Bioactive Glasses 9
2.3.1 Glass structure and properties 9
2.3.2 Borate glass structure 14
2.3.3 Bioactivity 17
2.3.3.1 Silicate-based bioactive glasses 19
2.3.3.2 Borate-based bioactive glasses 20
2.4 Glass Processing Techniques 24
2.4.1 The melt-quench technique 24
2.4.2 The sol-gel technique 25
2.4.2.1 Sol-gel derived borate glasses 28
2.4.3 Sol-gel silicate-based bioactive glasses 30
3 Statement of the Problem 33

4 Highly Bioactive Sol-Gel-Derived Borate Glasses 35
4.1 Introduction 38
4.2 Experimental 39
4.3 Results and Discussion 42
4.4 Conclusions 54
4.5 Supporting Information 55
5 Effect of Processing Parameters on Sol-Gel-Derived Borate Glasses 63
5.1 Introduction 66
5.2 Experimental 67
5.3 Results and Discussion 69
5.4 Conclusions 78
5.5 Supporting Information 79
6 Effect of Sodium on Sol-Gel Derived Borate Glasses 82
6.1 Introduction 85
6.2 Experimental 86
6.3 Results and Discussion 88
6.4 Conclusions 95
7 Acellular Bioactivity of Sol-Gel Derived Borate Glass-Polycaprolactone Electrospun Scaffolds 96
7.1 Introduction 99
7.2 Methods 100
7.3 Results 102
7.4 Discussion 107
8 General Discussion 112
8.1 SGBG composition and structure 113
8.2 SGBG sol-gel processing parameters 116
8.3 SGBG textural properties 117
8.4 SGBG Reactivity, dissolution, and HCA formation 118
9 Conclusions and Future Perspectives 123
9.1 Conclusions 123
9.2 Future Perspectives 124
10 References 126

List of Figures

Figure 2.1 The hierarchical structural organization of bone including cortical ('compact') and cancellous ('spongy') bone, collagen fibre assemblies of collagen fibrils, and bone mineral crystals (Nalla 2006). 5

Figure 2.2 A glassy ("random") network model from Zachariasen's 1932 paper, The atomic arrangement in glass with the black circles as cations (network former) and white circles as oxygens. To imagine a 3D structure, place an oxygen above the cation. (Note: in his original drawing two oxygen atoms are missing in the top center). 11

Figure 2.3 The effect of temperature on the enthalpy of glass forming melt (Shelby 2005). 12

Figure 2.4 Schematic of glass structure showing the network former (i.e., Si) in blue, network modifier (i.e., Na) in gray as well as the oxygens, both bridging (dark teal) and non-bridging (light green). 13

Figure 2.5 Schematic of vitreous borate glass with high proportion of boroxol rings (B_3O_6, example shown in green) and trigonal borate groups ($B\emptyset_3$, example shown in blue) with filled circles representing boron and hollow circles representing oxygen (adapted from Kroghe-Moe 1969). 14

Figure 2.6 The five major Borate $B^{(n)}$ structural units ($0 \leq n \leq 4$) represented in 2 dimensions adapted from Wright (2015). (Key: Blue, tetrahedral boron; yellow, trigonal boron; dark teal, bO; aqua, nbO) 15

Figure 2.7 Frequently occurring borate superstructures in either the glassy and/or vitreous state adapted from Wright (2015). (Key: Blue, tetrahedral boron; yellow, trigonal boron; dark teal, bO) 15

Figure 2.8 Simplified overview on the variation of borate super-structural units with increasing alkali oxide additions (Shelby 2005). Experimental data represented by solid lines and dashed line indicates theory. 16

Figure 2.9 Borate glass short-range order changes with modifier (M_2O) additions which contribute to the boron anomaly (Brauer and Moncke 2016). 17

Figure 2.10 Schematic showing the dissolution of 45S5 glass and borate substituted 45S5 (Huang 2006). 21

Figure 2.11 An overview of the two main glass processing methods: Sol-gel and melt-quench. Due to the aqueous nature of the sol-gel process, there is greater processing flexibility which can result in a wide variety of final forms. 26

Figure 2.12 A basic overview of the sol-gel process taken from Jones (2013). Variations of this method exists where nanofibers and aerogels, amongst other forms can be produced. 27

Figure 2.13 Hydrolysis and condensation reactions under neutral conditions via the SN mechanism through nucleophilic attack of OH or OR ligands on electrophilic, trigonal boron followed by the elimination of alcohol of water (Brinker and Scherer 1990). 29

Figure 4.1. An overview of the sol-gel process; (i) mixing of precursor materials, (ii) casting and ageing, (iii) gel monoliths at day 10, (iv) drying, and (v) post calcination at 400 °C (scale bars = 1 cm). (iii) Demonstrates the scaling up possibilities. 43

Figure 4.2 Effect of calcination temperature on SGBG structure. XRD diffractograms of calcined glasses indicate the amorphous characteristics by the presence of two broad humps. Crystallization of the glasses was initiated at higher calcination temperatures and was dependent on SGBG composition. All SGBG compositions crystallised at 600 °C.....43

Figure 4.3 Characterisation of calcined SGBGs. (a) ATR-FTIR spectra of the SGBGs calcined at 400 °C and 45B5 indicate typical borate bonding modes. (b) 11B MAS NMR of the SGBGs calcined at 400 °C including 45B5. (c) Glass forming ability as indicated by the trend of the difference between T_c and T_g versus N_C. Compositions with higher borate content were more likely to form a glass, as demonstrated by the increase in the difference between T_c and T_g. 45

Figure 4.4 Reactivity through vapour adsorption. (a) The stepwise increase in % RH, with adsorption (solid line) and desorption (dashed line), indicated that lower borate content glasses experienced higher % mass changes. (b) The direct exposure to 90% RH showed a rapid increase in mass. The rate and extent of mass change were dependent on SGBG composition, and increased with a decrease in glass borate content suggesting greater extents of reactivity. 47

Figure 4.5 SGBG ion release. (a) Boron, (b) Calcium, (c) Sodium, and (d) Phosphorus ion release in DIW as measured through ICP-OES. 48

Figure 4.6 Mineralization in SBF solution. ATR-FTIR spectra before and after immersion in SBF for 6 h, 1 d, 3 d, and 7 d. The bending mode (ν3) of PO_4^{3-} at ~1020 cm^{-1}, which is characteristic of apatite formation, was observed at the 6 h time point and became more defined at longer times in SBF. 49

Figure 4.7 Mineralization in SBF solution. XRD diffractograms before and after immersion in SBF for 6 h, 1 d, 3 d, and 7 d. Characteristic hydroxyapatite ("•" JCPDS 9-0432) peak formation initiated at the 6 h time point and became more defined at longer times in SBF. 50

Figure 4.8 Morphological characterization of B46 and 45B5 as a function of time in SBF. The initial textured surface of the calcined B46 increased in roughness with time in SBF. As-made 45B5 demonstrated a smooth surface that became rougher with time in SBF. EDA EDAX of B46 at 6 h indicated a Ca/P ratio of 1.6, closely resembling that of hydroxyapatite. EDAX of both glasses at day 7 indicated similar Ca/P ratios.....51

Figure 4.9 Mineralization rates of B46 and 45B5 in SBF solution. (a) ATR-FTIR spectra demonstrated that B46 rapidly (in 0.5 h) converted to carbonated-apatite compared to 45B5 (3 d). (b) XRD diffractograms indicated typical hydroxyapatite peak formation ("•" JCPDS 9-0432) after 3 h for B46 compared to 3 d for 45B5. 53

Figure S4.10 Gel network formation. A schematic showing the suggested route to borate glass network formation during the sol-gel process (recreated from Brinker et al. 1990 [187]. 55

Figure S4.11 Sol-gel derived borate-based glasses. (a) Visual representation of the gels cast over the 10-day gelation period. B36 did not form a gel until day 3, where two distinct phases were observed. (b) XRD diffractograms of the as-made glasses displayed two broad humps indicating their amorphous nature. B36, on the other hand displayed a number of minor peaks, which may be due to a precipitated phase. 56

Figure S4.12 ATR-FTIR spectra of the SGBGs, as-made (AM) and calcined at different temperatures. Sharp, doublet peaks indicate increasing crystallization with calcination temperature, corroborating the XRD diffractograms shown in Figure 4.2. 57

Figure S4.13 Properties of calcined SGBGs. (a) Percentage weight loss of SGBGs post calcination at 400 °C. Glasses with lower borate content experienced greatest extent of weight loss upon calcination. (b) Effect of calcination temperature on B46 SSA and pore volume. There was a decrease in these parameters with an increase in calcination temperature. 58

Figure S4.14 Effect of SGBG dissolution on the pH of (a) DIW and (b) SBF. The increase in pH values corresponded with SGBG composition, where glasses with lower borate content (i.e., higher soda content) resulted in greater extents of pH increase. 59

Figure S4.15 Morphology of SGBGs. SEM micrographs of all as-made and 400 °C calcined SGBGs as a function of time in SBF (scale bar = 2 μm, inset = 500 nm). Glass surfaces became more textured with time in SBF; attributable to HCA formation. 60

Figure S4.16 Mineralization rates of B46 and 45B5 in 0.02 M K_2HPO_4 solution. (a) ATR-FTIR spectra and (b) XRD diffractograms indicated that apatite peak formation initiated after 6 h in both glasses demonstrating that the K_2HPO_4 solution is prone to giving favorable in vitro mineralization results. 61

Figure 5.1 Schematic of the sol-gel processing route and adjusted parameters (in bold). For the boric acid precursor route, images referring to BA 400 are shown. For the TMB and TEB precursor routes, images for TEB are shown with TMB giving similar results. 70

Figure 5.2 Structural characteristics of the various glasses using (a) ATR-FTIR and (b) XRD. The spectra and diffraction patterns remain similar for all glasses except for BA 500, which indicated the initiation of crystallization as shown by the sharp doublet peaks in ATR-FTIR and crystallization peaks in XRD. 72

Figure 5.3 ATR-FTIR spectra as a function of immersion time in SBF. Glass conversion to HCA was initiated in as little as 0.5h as indicated by the formation of the large phosphate peak around 1020 $cm^{-1.}$ 73

Figure 5.4 XRD diffractograms as a function of immersion time in SBF. All particles produced through the various sol-gel processing methods converted to HCA ("•", JCPDS 9-0432) at a rapid rate. 74

Figure 5.5 Release of boron, calcium, and phosphorus in SBF as measured through ICP-OES. Rapid ion release was observed with boron. The decreasing release trend of calcium and phosphorous suggested their re-precipitation on the glass surface. 76

Figure 5.6 SEM micrographs of TMB, TEB, BA 300, BA 400, and BA 500 as a function of time in SBF. Typical flower-like crystals, indicative of hydroxyapatite formation was initiated at 2h and became well-defined by 6h. White scale bars = 1 μm and black scale bars = 500 nm. ..77

Figure S5.7 Linear isotherm plots for each glass during surface area measurements through BET..79

Figure S5.8 Effect of calcination temperature on specific surface area for BA 300, BA 400, and BA 500. Weight loss upon calcination is inversely proportional to specific surface area measurements. 80

Figure S5.9 SEM micrographs of the calcined glasses demonstrating the nano-textured surfaces of the SGBGs. Upon higher calcination temperature, the glass surface becomes less porous as verified by textural analysis data. 80

Figure S5.10 SEM micrographs of 0d and 30d aged samples at 7d in SBF. The flower-like crystals suggest hydroxyapatite formation as confirmed by FTIR and XRD analyses. 81

Figure 6.1 An overview of the effect of sodium content on the gelling of SGBGs. (i) casting and ageing, (ii) gel monoliths at day 10, (iii) drying at RT for 1 day, (iv) drying at 120 C for 2 days. Sodium influences the gelation behaviour of the glasses, possibly due to increasing pH. 89

Figure 6.2 Characterisation of the calcined SGBGs (a) ATR-FTIR spectra and (b) XRD diffractograms of the glass particles produced as a function of sodium content. 91

Figure 6.3 Reactivity through vapor adsorption using DVS. The direct exposure to 90% RH showed rapid increase in mass change which increased with sodium content. 92

Figure 6.4 ATR-FTIR spectra as a function of immersion time in SBF. Characteristic apatite-like peaks began to form after 30 min in SBF for higher sodium containing glasses. Peak formation was less defined in lower sodium containing glasses. 93

Figure 6.5 XRD diffractograms as a function of immersion time in SBF. All SGBG compositions rapidly converted to HCA ("•", JCPDS 9-0432). 94

Figure 6.6 Release of boron, calcium, sodium, and phosphorus in SBF as measured through ICP-OES. Rapid ion release was observed with boron depending on composition and the decreasing release trend of calcium and phosphorous suggested their re-precipitation on the glass surface. 95

Figure 7.1 Characterization of BG particles. (a) Particle size distribution of the calcined BG particles. (b) Nanotextured morphology of the glass surface via SEM. (c) ATR-FTIR spectra showing the bonding moments for the BG particles and (d) XRD diffractograms displaying the typical amorphous humps. 103

Figure 7.2 Morphology of as-made PCL and PCL-BG scaffolds. (a) SEM micrographs showing the fibrous morphologies and BG incorporation in composite scaffolds (inset scale bars = 2 μm). (b) Range of fibre diameters for the various scaffolds, indicating wider distribution of diameters with BG incorporation. (c) A macro view of PCL-5BG showing the cotton-wool like nature and (d) ease of handling of the scaffold. 104

Figure 7.3 Structural analyses of as-made PCL and PCL-BG scaffolds. (a) ATR-FTIR spectra showing representative bonding moments of the electrospun PCL and PCL-BG scaffolds. (b) XRD diffractograms showing typical semi-crystalline peaks associated with PCL 105

Figure 7.4 Reactivity of PCL and PCL-BG scaffolds through vapour sorption. The direct exposure to 90% RH, resulted in a rapid increase in mass of BG and BG incorporated PCL scaffolds. At 6 hours, the equilibrium increase in mass increased with BG content in composite scaffolds. The return to near 0% mass change after 12 hours for the PCL samples demonstrated their hydrophobic nature. 106

Figure 7.5 SEM micrographs of PCL and PCL-BG scaffolds as a function of immersion time in SBF. For PCL-5BG composite scaffolds, apatite-like crystals were visible at day 3 and rapidly increased by day 7. Surface changes were visible in the non-doped PCL samples at day 7. 107

Figure 7.6 ATR-FTIR spectra of PCL and PCL-BG scaffolds as a function of immersion time in SBF. The presence of the peak at 1020 cm-1 in BG incorporated PCL scaffolds at day 7 suggested apatite peak formation. 109

Figure 7.7 XRD diffractograms of PCL and PCL-BG scaffolds as a function of immersion time in SBF. Apatite conversion ("•", JCPDS 9-0432), which was initiated at day 3 for the BG incorporated PCL scaffolds were more defined by day 7 in SBF. 110

Figure 8.1 Aqueous interactions of a borate substituted Bioglass in 4 different size fractions. Above 75 μm, there seems to be no effect on the mass change. 120

Figure 8.2 XRD diffractograms of (a) B46 submerged in 4 different types of media after 7d and (b) four different particle size fractions of B46 in SBF for 7d. Calcite formation is observed by the sharp peaks. 121

List of Tables

Table 4.1 Glass compositions 42

Table 4.2 Glass Textural and Thermal Properties: Average Median Diameter (D_{50}), Specific Surface Area (SSA), Average Pore Width and Average Pore Volume as well as Glass Transition Temperature (T_g) and Crystallization Temperature (T_c) 44

Table 5.1 Overview of the Sol–Gel Processing Parameters Investigated in this Study 69

Table 5.2 Glass particle textural properties (n=3): average mean (D_{AVG}) and median (D_{50}) diameter, specific surface area (SSA), average pore width and average pore volume 71

Table 6.1 SGBG Compositions and Codes (mol%) 88

Table 6.2 Glass particle textural properties: Average Median (D_{50}) and Mean (D_{AVG}) Diameter, Specific Surface Area (SSA), Average Pore Width and Average Pore Volume 90

Table 7.1 Scaffold compositions and their average fibre diameters as measured from SEM micrographs (n = 200) 104

Table 8.1 Summary of all glass compositions and selected properties 112

Table 8.2 Ionic Concentrations of Various Dissolution Media 120

Glossary of Abbreviations and Symbols

13-93B3	(53)B_2O_3-(20)CaO-(12)K_2O-(6)Na_2O-(5)MgO-(4)P_2O_5 (in wt. %)
3D	Three dimensional
45B5	(46.1)B_2O_3-(26.9)CaO-(24.4)Na_2O-(2.6)P_2O_5 (mol%)
45S5	(46.1)SiO_2-(26.9)CaO-(24.4)Na_2O-(2.6)P_2O_5 (mol%)
ATR	Attenuated total reflectance
B	Boron (element)
B_2O_3	Borate
B36	(36.2)B_2O_3-(31.9)CaO-(28.9)Na_2O-(3.0)P_2O_5 (mol%)
B41	(41.1)B_2O_3-(29.4)CaO-(26.6)Na_2O-(2.8)P_2O_5 (mol%)
B46	(46.1)B_2O_3-(26.9)CaO-(24.4)Na_2O-(2.6)P_2O_5 (mol%)
B51	(51.1)B_2O_3-(24.4)CaO-(22.1)Na_2O-(2.4)P_2O_5 (mol%)
B56	(56.1)B_2O_3-(21.9)CaO-(19.8)Na_2O-(2.2)P_2O_5 (mol%)
B61	(61.3)B_2O_3-(19.3)CaO-(17.5)Na_2O-(1.9)P_2O_5 (mol%)
BG or SGBG	Sol-gel derived borate glass
bO or "Ø"	Bridging oxygen
°C	Degrees Celsius
Ca	Calcium (element)
CN	Coordination number
CaO	Calcium oxide
CO_2	Carbon dioxide
CaP	Calcium phosphate
CTE	Thermal expansion coefficient
d	Day
DVS	Dynamic vapor sorption
ECM	Extracellular matrix
ES	Electrospinning
EDS	Energy dispersive spectroscopy
FTIR	Fourier transform infrared spectroscopy

h	Hour
HA	Hydroxyapatite
HCA	Hydroxycarbonated apatite
hMSC	Human mesenchymal stem cells
ICP-OES	Inductively coupled plasma optical emission spectroscopy
K_2HPO_4	Potassium phosphate
M	Metal
M_f	Molar fraction
mM	Millimolar
Mol	Molar
Na	Sodium (element)
Na_2O	Sodium oxide
Na24	(46.1)B_2O_3-(26.9)CaO-(2.6)P_2O_5-(24.4)Na_2O (mol%)
Na16	(51.1)B_2O_3-(29.8)CaO-(2.4)P_2O_5-(16.3)Na_2O (mol%)
Na8	(56.0)B_2O_3-(32.7.8)CaO-(3.2)P_2O_5-(8.1)Na_2O (mol%)
Na0	(61.0)B_2O_3-(35.6)CaO-(3.4)P_2O_5 (mol%)
nbO	Non bridging oxygen
N_C	Network connectivity
NMR	Nuclear magnetic resonance
O	Oxygen
Ø or bO	Bridging oxygen
OH	Hydroxide
P	Phosphorous (element)
P_2O_5	Phosphate
PCL	Polycaprolactone
PGA	poly(glycolic acid)
pKa	Acid dissociation constant
R^+	Alkali ion
R^{2+}	Alkaline earth ion
R_2O	Alkali oxide
RO	Alkaline earth oxide
SBF	Simulated body fluid

SEM	Scanning electron microscopy
SGBG or BG	Sol-gel-derived borate glass
Si	Silicon (element)
SiO_2	Silica
SSA	Specific surface area
T_c	Crystallization temperature
T_g	Glass transition temperature
TEB	Triethyl borate
TEOS	Tetraethyl orthosilicate
TMB	Trimethyl borate
TMES	Trimethylethoxysilane
x_M	Network modifier fraction
XRD	X-ray diffraction

Contributions to Original Knowledge

This thesis describes the processing and *in vitro* characterization of four- and three-component sol-gel-derived borate glasses (SGBGs) for bone tissue engineering applications. Chapter 4 describes the first iteration of SGBGs as bioactive glasses. It was shown that a wide range of chemistries could be created using a novel sol-gel processing method. Furthermore, for the first time, a four-component SGBG has been evaluated in terms of its textural, thermal, structural, reactivity, and bioactivity properties. This study serves as a basis for the creation of further SGBG formulations.

Chapter 5 highlights the numerous processing parameters inherent to the sol-gel method that can be altered to affect the final properties of an SGBG composition. These parameters have been extensively examined and reviewed for other glass systems, such as those based on silica. However, since the literature on sol-gel borate glasses is sparse, so far there has been no comprehensive study investigating the processing parameters. It was demonstrated that the calcination temperature was critical in determining the final structural and bioactivity properties. Despite the higher calcination temperatures, which resulted in partially crystallized glasses, the bioactivity was still relatively high and the conversion to bone-like mineral in simulated body fluid was observed within one day. These findings provide significant contributions to the sol-gel borate glass literature for future applications beyond bone tissue engineering.

Although sodium is typically added as a flux to lower the melting temperature in melt-quench derived glasses, its addition to the sol-gel process is unnecessary. Yet, in order to directly compare to previously generated melt-quench derived compositions, sodium was included in the first generation SGBGs. Chapter 6 examines the effect of varying the amount of sodium inclusion on SGBG processing and the final structural, textural, reactivity, and bioactivity properties.

Polycaprolactone (PCL) is a Food and Drug Administration (FDA) approved biodegradable polymer that is biocompatible, but not bioactive. Since SGBGs were demonstrated to be highly bioactive, Chapter 7 investigated their effect on the bioactivity of PCL by their incorporation into electrospun fibers. It was shown that with only 5 wt. % SGBGs addition, a layer of bone-like mineral was formed on the surface of the PCL-matrix composites. This study demonstrated how SGBGs can endow bioactivity of otherwise non-bioactive materials and will serve as the basis for other hybrid and composite systems.

Contribution of Authors

This dissertation contains a collection of published and to-be-submitted manuscripts written by the candidate under the supervision of Prof. Showan N. Nazhat. As the first author of all the manuscripts, I proposed, designed, conducted the majority of the experiments, analyzed all the data, and wrote each manuscript. Critical guidance for all research activities along with a thorough review was provided by Prof. Nazhat. Shiva Naseri assisted with experimental set up and tests examining different bioactive glasses in Chapter 5. Sophia Smith operated essential equipment to provide analysis on composite materials in Chapter 6. Dr. Liliana Liverni assisted with the electrospinning set-up and Prof. Aldo Boccaccini hosted me in his laboratory for the study in Chapter 7. All co-authors reviewed the respective manuscripts and provided significant critical feedback.

1 General Introduction

1.1 Introduction

There is an ever-growing need for bone replacement materials, largely due to the ageing population, bone degeneration, fractures, and osteoporosis; factors that affect millions of people worldwide [1]. Since bone is a living tissue with vasculature, it can often heal itself, but in the case of severe injuries and diseases that lead to large defects, intervention with bone grafts, or "scaffolds", are needed [2]. Indeed, in the USA alone, 500,000 bone graft procedures are performed annually and worldwide, this number is estimated to be more than 2.2 million [3].

After blood, bone is the most widely transplanted tissue in the human body [4]. The clinical 'gold standards' for repairing bone tissue are traditionally donor based, which can be autografts from the same patient, allografts from other human donors, or xenografts from other animal sources [3, 5, 6]. These grafts can be advantageous because the supplied materials match the complex hierarchical tissue structure of native bone. Although rejection is rare with autografts, donor site morbidity and limited supply present some issues of concern. On the other hand, the factors that impact allografts and xenografts, include limited donor supply, particularly in the former, as well as the potential for disease transmission and rejection in both cases, which require these grafts to undergo thorough processing prior to implantation [6-8]. These disadvantages have created a great push to develop synthetically engineered grafts and are some of the main drivers for the recent growth of the bone tissue engineering field.

While all material classifications have been used to replace bone, bioactive glasses have emerged as a leader attributable to their capacity to convert to hydroxycarbonate apatite (HCA), the mineral component of bone, their ability to release ions to help stimulate regeneration and their capability to bond with both hard and soft tissues [9-11]. Dr. Larry Hench invented the first bioactive glass in 1969, Bioglass® 45S5 $(46.1)SiO_2$-$(26.9)CaO$-$(24.4)Na_2O$-$(2.6)P_2O_5$ (mol%), which has gone on to become the most commonly used and researched composition, achieving great commercial success [12]. The success of the this glass lies in its bone bonding mechanism, which is due to a surface HCA formation, after an initial glass dissolution phase [13]. However, Bioglass®, along with the majority of all other bioactive formulations, have generally been based on melt-quench-derived silica (SiO_2) glasses, and while these glasses can stimulate bone formation, their dissolution is often slow and

incomplete [14]. To improve these properties, the sol-gel technique, an aqueous based low temperature processing method, can be implemented to create glasses with higher surface areas and porosities, which can improve dissolution rate and conversion to HCA [15].

Despite improvements to the textural properties, the chemical composition still limits the dissolution and reactivity rates of silicate-based glasses. An alternative route to improve the bioactivity of a glass is through changing the chemistry [14]. Borate-based glasses are less chemically durable compared to silicate glasses due to the three-coordinated preference of the boron ion, which leads to lower network coordination of the glass network and translates into more rapid dissolution and conversion rates [16-18]. Therefore, borate glasses have gained great attention in the past decade for biomedical applications [19] with many based on previously reported bioactive, silicate glasses such as "45B5" (46.1)B_2O_3-(26.9)CaO-(24.4)Na_2O-(2.6)P_2O_5 (mol%) [17] and "13-93B3" (53)B_2O_3-(20)CaO-(12)K_2O-(6)Na_2O-(5)MgO-(4)P_2O_5 (wt.%) [16]. While these glasses have demonstrated greater HCA conversion rates than silicate-based equivalent formulations, opportunities exist in improving the dissolution rates by adjusting the textural properties. Furthermore, although the sol-gel method has been extensively studied in silicate-based systems [20], limited literature exists on sol-gel-derived borate glasses, with most of the research focusing on structural investigations [21]. Therefore, there is a need to explore sol-gel-derived borate glasses (SGBGs) for potential biomedical applications and more specifically in bone repair and tissue engineering.

1.2 Aim, Hypothesis and Objectives

The aim of this doctoral thesis was to create bioactive SGBGs and examine their potential for bone tissue engineering applications, *in vitro*. It was hypothesized that the lower chemical durability and faster conversion to bone-like mineral of borate glasses, compared to silicate-based glasses, could be further enhanced by producing the glasses via the sol-gel method. Moreover, this method would also allow for the creation of a wider range of compositions and specifically, the tailoring of textural properties. To achieve these goals, the following objectives were created:

1) Fabricate a range of SGBGs based on a previously used, melt-quench-derived equivalent glass, and examine the textural properties, reactivity, and *in vitro* bioactivity.
2) Examine the effect of different sol-gel processing parameters on the textural and bioactivity properties of these glasses.
3) Investigate the effect of sodium content on textural, reactivity and bioactivity of SGBGs.

4) Assess the effect of SGBG on the bioactivity of composite scaffolds through incorporation into a degradable electrospun polymer.

To meet the first objective, a borate substituted Bioglass® with composition ("B46" – (46.1)B_2O_3-(26.9)CaO-(24.4)Na_2O-(2.6)P_2O_5 (mol%) was fabricated where the amount of borate was increased or decreased by 5% increments, while maintaining the original ratios of CaO, Na_2O and P_2O_5, thus creating six unique glasses ranging from 36 to 61 mol% borate (B_2O_3). Furthermore, a melt-quench derived borate substituted Bioglass® (45B5) was used as a control. Visual observations of the sol-gel process for each glass were recorded and the resultant glass textural properties were examined. Additionally, the structural characteristics, reactivity, dissolution, and bioactive properties were extensively characterized for all glasses.

To satisfy the second objective, the B46 glass composition was processed using different modifications of the sol-gel method including precursor materials, ageing time and temperature, as well as calcination rate and temperature. These conditions were shown to influence the final textural, structural, and bioactive properties of the calcined glass.

In order to meet the third objective, the sodium content in SGBGs was incrementally decreased from the original B46 composition until no sodium remained, thus creating four unique glass compositions, all processed using similar conditions. Unlike in melt-quench derived glasses, sodium is typically not added during sol-gel processing, and this study investigated the effect of reduced sodium content on the structure, reactivity, dissolution, and bioactivity of the SGBGs.

To meet the fourth objective, the B46 SGBG was incorporated into polycaprolactone (PCL), a common medical polymer that is biodegradable, yet not bioactive. It was anticipated that due to the high bioactivity degree of SGBGs, they might be able to improve the bioactivity of other materials, by their addition in a composite material. PCL-BG composites were electrospun in order to create three-dimensional (3D) cotton wool-like scaffolds. The electrospinning processing conditions were examined as a function of different B46 filler amounts and the resultant fibrous composites were characterized in terms of their structure, reactivity, and bioactivity.

2 Literature Review

2.1 Bone

In an adult human, the skeletal system is composed of 206 bones of various shapes and sizes, which can be generally classified into three main categories: long (*e.g.,* femur or tibia), short (*e.g.,* vertebra) and flat (*e.g.,* skull) [22, 23]. The function, composition, and size of the various types of bones can vary greatly, and working together, they provide structural support, transmit mechanical forces, protect vital organs, and store minerals within the body [23, 24]. An overview of the structure of bone can be seen in Figure 2.1. A single bone is comprised of two main components: cortical and cancellous bone. Cortical bone, also called compact bone, is located on the exterior of all bones and possesses a dense structure with low porosity. Internally, bone is highly porous; called cancellous, spongy, or trabecular bone [22, 25, 26]. Cancellous bone, also called "spongy" bone accounts for the majority of the total bone mass (~80 %) in an adult skeleton whereas trabecular bone has significantly more surface area [26-30]. The trabeculae that make up cancellous bone appears sponge-like, and consists of the basic cellular structures: rod-rod, rod-plate, or plate-plate with a typical trabecular rod being about 50 – 300 μm in diameter [31].

Approximately 65 wt.% of bone is an inorganic, mineral phase called hydroxycarbonated apatite (HCA; $Ca_5(PO_4,CO_3)_3(OH)$) [32, 33]. The high inorganic content makes bone one of the most mineralized tissues in the body along with tooth enamel and dentine [34, 35]. The remaining 35 wt.% of bone is composed of the organic phase, which mainly consists of type I collagen (> 90 wt.%) along with smaller quantities of non-collagenous proteins, proteoglycans, and water [23, 32, 36]. These highly organized phases play critical roles in the properties of bone: the mineral phase provides compressive strength and stiffness while the organic phase provides toughness and ductility [24, 32].

At the cellular level, bone is made up of osteoblasts (bone forming cells) osteocytes (mature bone cells), and osteoclasts (bone resorbing cells). Bone is constantly being remodeled through the functions of osteoblasts and osteoclasts [23, 24, 31], which can be controlled through the action of chemical factors [37-39]. Osteoblasts can be activated by increased secretion of the osteoid, the non-mineralized portion of organic bone extracellular matrix (ECM), which is stimulated by the emission of growth factors by various glands [40]. There are also many bone matrix non-collagenous proteins, such as osteonectin and bone sialoprotein, that play significant roles in bone mineralization and have

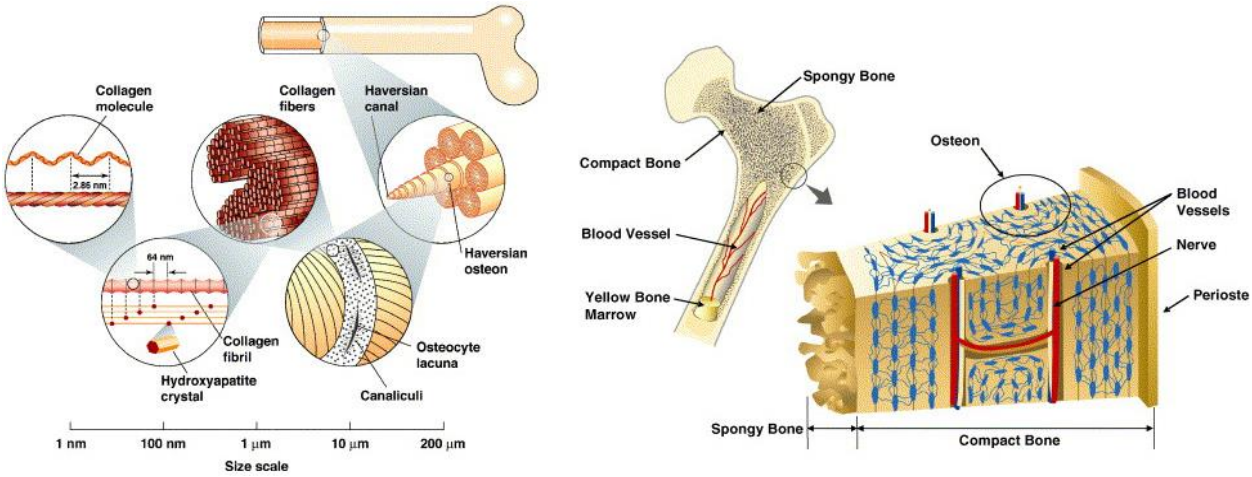

Figure 2.1 The hierarchical structural organization of bone including cortical ('compact') and cancellous ('spongy') bone, collagen fibre assemblies of collagen fibrils, and bone mineral crystals (Nalla 2006).

broad functions that include control of cell proliferation and differentiation, cell-matrix interactions, and mediation of HCA deposition [38, 39]. An imbalance in the dynamics of bone remodeling can lead to osteoporosis, a skeletal disorder characterized by low bone density and deterioration of the microarchitecture of bony tissue. This ultimately leads to an increase in fracture risk, a condition that affects millions of people worldwide [41-43]. Bone health relies on many different factors and since it is a highly-mineralized tissue, inorganic elements from diet or those released from synthetic bone scaffold materials, such as bioactive ceramics or glasses, play a crucial role in its health as discussed below.

2.1.1 Calcium

Calcium (Ca) is synonymous with bone health. Over 99% of all calcium in the body is found in bones in the form of HCA making it a crucial structural component [44]. This element also mediates many effects at cellular and tissue levels, such as acting as a signal transduction molecule for producing cellular responses, which if not maintained, can cause bone disease [45]. Hypercalcemia occurs when osteoclast activity increases causing the release of calcium stored in the extra cellular matrix, which provides structural support for tissues and cells, as well as cell adhesion and in signaling [46], leading to a decrease in bone density [47]. The opposite response can occur when bone production exceeds bone resorption, requiring additional calcium to form new bone mineral, which is supplied by the free calcium, thus decreasing HCA formation [45]. The amount of calcium and its effect on skeletal production is thought to have a threshold zone, that is, if calcium levels are below the threshold zone then increasing its levels will increase bone production, but if calcium levels are already above the threshold zone, then increasing calcium will likely not have an effect on bone production (for adults

the suggested dietary intake is about 1500 mg/day) [44, 45]. For these reasons, calcium is often a major component in bone replacement materials and is one of the most important elements in bone health that has been extensively studied and reviewed [48-52].

2.1.2 Phosphorous

Most of the phosphorous in the body is in the form of phosphates, which are generally classified into two categories: orthophosphates (PO_4^{3-}) and polyphosphates which can take many forms [53]. Inorganic phosphate (P_i), also known as orthophosphate, is the second most abundant mineral element in the human body and plays an essential role in many bodily processes including bone mineralization [45, 53, 54]. In fact, approximately 85% of the phosphates in the body are present in bone and teeth as an orthophosphate [44, 45] and constituting an important regulator of skeletal development, mineral metabolism, and intracellular signaling [54, 55]. During osteoblastic differentiation, phosphates provide cell signaling functions [56, 57] and can also control mineralization processes by moderating gene expression [58]. Orthophosphate couples with calcium ions to form HCA in bone, dentine and enamel, as well as extracellular fluid and soft tissues [53, 54]. In contrast to singular orthophosphates, polyphosphates, and in particular pyrophosphate ($P_2O_7^{4-}$) are well known to inhibit mineralization, and thus bone growth [45].

2.1.3 Silica

Although silicon (Si) is not naturally present within the body, it has been shown to play an important role in bone health [59-61]. Dietary silica can come from many sources including plant based foods, beer, and some mineral water which is broken down by the gastrointestinal tract in the form of orthosilicic acid [61]. Since silica (SiO_2) is the main network former in the majority of bioactive glasses, Si release is very important when understanding mineralization. Si is essential to skeletal development [62-64] by promoting matrix synthesis and the differentiation of osteoblastic cells [65, 66], where its ionic release from glass has been shown to stimulate osteoblast proliferation and differentiation, *in vitro* [67]. Advanced mapping techniques have recently shown that Si is located in only the mineralized tissue areas and thus may play a biological role in bone formation due to its distribution near these mineralized sites [68].

2.1.4 Boron

Although boron (B) is not an essential nutrient where no dietary intakes have been set [69, 70], it is present in several foods, including fruits, eggs, milk, wine, and legumes (fruit or seeds of the third largest land plant family, *e.g.,* peas or beans) [71]. Despite this, boron has been shown to affect

bone health, where in a study by Nielsen et al. it was found that boron supplements given to postmenopausal women, along with a diet high in fruits and vegetables, helped prevent calcium loss and bone demineralization [72]. Similar studies have also shown that low boron supplements given to postmenopausal women decreased urinary calcium loss, which is a marker thought to decrease osteoporosis risk [73-75]. Animal models have also investigated the effects of boron on bone health. In a recent study by Hakki and colleagues, it was found that boron enhances the strength and alters the mineral composition of bones in rabbits [76]. Here, New Zealand rabbits were fed high energy diets supplemented with varying amounts of boron. It was found that all boron treatments significantly increased magnesium and calcium concentrations whereas higher boron supplements also increased the phosphorous concentrations in the tibia and femur [76]. Other studies have shown that a decrease in dietary boron can lead to a reduction in bone strength in pigs [77] and rats [78].

2.2 Tissue Engineering

The human body is a collection of cells that form various tissues, which when damaged due to injury or disease, need to be repaired or replaced. The current "gold standards" for tissue engineering implants are traditionally donor based, *i.e.,* either through autografts (from the patient), allografts (from human donors) or xenografts (from animal sources) [79]. However, the associated disadvantages with some of these grafts have created a push to develop engineered tissue grafts and are some of the main reasons behind the rapid growth of the field of tissue engineering. According to Ratner, tissue engineering is a "broad term describing a set of tools at the interface of the biomedical and engineering sciences that use living cells or attract endogenous cells to aid tissue formation or regeneration, and thereby produce therapeutic or diagnostic developments" [79]. This general definition mimics the broad scope and diversity of the tissue engineering field which encompasses many disciplines from materials science to medicine.

The biomaterials created and used in tissue repair or replacement can be split into three distinct generations. *First generation* biomaterials, used in the mid-twentieth century, were widely available, "off the shelf" materials that, typically were not specifically designed for biomedical use. These were intended to be *bioinert*, meaning that they would not react with, or cause a response from, the host tissue [80]. However, it is now well known that no material is completely inert in the body and some type of biological response will always be triggered. *Second generation* biomaterials realized this short coming and were designed to elicit a controlled reaction when implanted into the body. In other words, they were designed to be bioactive. Bone bonding materials such as bioactive glasses and

ceramics, as well as drug delivery systems such as drug-eluting vascular stents, were included in this era along with new resorbable polymers *e.g.,* poly(glycolic acid) (PGA) [79, 81]. Presently, the current era is considered *third generation* biomaterials [81]. These materials acquire many of the second generation biomaterials properties, but are also distinguished by their advanced modes of drug delivery and ability to stimulate certain growth factors depending on the application [81].

2.2.1 Scaffolds for tissue engineering

Tissue engineering relies on the development of a porous, resorbable, three dimensional scaffold, that can be seeded with cells that eventually degrades after the targeted tissue has been regenerated [82, 83]. For bone tissue engineering, a scaffold should be *osteoconductive* (property of a material to host direct bone formation on or within its structure) or *osteoinductive* (incorporation of a biological, mechanical, or chemical signal that will induce osteogenic differentiation in a cell population to form bone cells) or both [2]. Hutmacher originally listed the five key aspects of an ideal scaffold [83] which were later modified by Jones [82] below:

i. be biocompatible and bioactive, promoting osteogenic cell attachment and osteogenesis;
ii. bond to the host bone without fibrous tissue sealing it off from the body;
iii. have an interconnected porous structure that can allow fluid flow, cell migration, bone ingrowth and vascularization;
iv. be able to shaped in theatre so that it can fit the defect (for some applications, clinicians may prefer porous granules to a single block);
v. degrade at a specified rate and eventually be remodeled by osteoclast action;
vi. share mechanical load with the host bone and maintain an appropriate level of mechanical properties during degradation and remodeling;
vii. be made by a fabrication process that can be up-scalable for mass production;
viii. be sterilizable and meet regulatory requirements for clinical use.

Not all bones and injuries are the same and there is a growing need for a bone substitute with controllable bioactivity [81]. The goal of creating a synthetic bone graft is to make a three-dimensional scaffold to serve as an impermanent guide for bone repair that will also stimulate bone formation [82, 83]. For bone tissue, porosity and pore size on both the macro- to nanoscopic levels are important factors to consider when designing a scaffold for bone regeneration [84, 85]. Since bone shape, size, and morphology can vary, there is no standard or set pore size that should be targeted, but in general,

an interconnected network with large pores (>100 μm) [86] to enable tissue ingrowth and *osseointegration* (ability of scaffold to integrate itself into bone) after implantation is desirable [84]. For example, pore size and 3D printed scaffold strut size, have been shown to be important factors to consider during design since they also influence cell migration and vascularization [87]. Furthermore, micropores (<2 nm) and mesopores (2 nm < 50 nm) can help promote adsorption of biological molecules and cell adhesion [88].

Many types of materials have been studied for bone repair including ceramics [89], polymers [90, 91] and glasses [45, 82, 92]. In addition, combining these materials into multifunctional, hybrid or composite scaffolds, such as collagen with bioactive glass, offers synergistic benefits when targeting a specific area of repair [93]. Another common technique to create ECM mimicking scaffolds is electrospinning, which generates continuous, submicron fibers created on the basis a viscoelastic solutions (typically polymers) that are uniaxially stretched using electrostatic forces [94]. The resultant fibers achieve many of the required scaffold characteristics listed above, and have been used in various mineralized tissue engineering applications [95-97].

Although the combination of different materials is beneficial to scaffold production, often, a singular material, such as bioactive glass, can be used in either particulate or in a porous construct form [82, 98]. For non-load bearing bone sites, the bioactive glass particles can simply be packed into the defect. Other techniques include mixing the particles with the patient's own blood or a polymer to form a paste that can be used to fill a defect [82]. While many of these materials have had success, there are still opportunities to improve the rate of bone healing by altering their chemical or physical properties. To this end, bioactive glasses have emerged as a promising option attributable to their ability to release ions, which allows them to both chemically and physically bond to native bone [12, 13].

2.3 Bioactive Glasses

2.3.1 Glass structure and properties

Glasses are in a sub-family of ceramics that are characterized by their lack of crystallinity and amorphous nature, meaning they lack long-range, periodic arrangement. Hence, glasses are often referred to as or *non-crystalline solids* or *amorphous solids* [99]. Glasses also exhibit a glass transition temperature (T_g), which is the temperature that indicates when the solid (*e.g.,* glass precursor materials, typically oxides), upon heating begins to behave as viscoelastic material or, equally, during cooling when the supercooled liquid (*e.g.*, glass melt) converts to a solid [99]. If any material meets these two

requirements, it can be considered a glass and thus, according to Shelby, a glass can be defined as "an amorphous solid completely lacking long-range, periodic atomic structure, and exhibiting a region of glass transformation behavior" [99]. Although human use of glass can be tracked back to 7000 B.C., it was not until about a century ago did scientists begin to examine and postulate about the structure of glass.

The earliest, and most simple, theory on glass structure was from Goldschmidt, who believed that the ratio of cation to anion radii for simple oxides must be between 0.2 and 0.4 in order to form a glass. This ratio implies tetrahedrally-coordinated cations are favorable for glass formation (although this was not proven with any empirical evidence) [99]. A few years later, in 1932, *The atomic arrangement of glass* was published by Zachariasen in an attempt to describe why glass formation might be favored by certain coordination numbers [100]. He noted that silicate crystals have a tetrahedral network, and instead of a close-packed structure similar to crystals, atomic arrangement in glasses were not periodic or symmetric and that these networks stretch in all three dimensions resulting in isotropic behavior. According to Zachariasen, this "vitreous network" formed the baseline requirement for glass formation who went on to postulate the rules for glass formation as summarized below [100]:

1) Oxygen ions are bonded to no more than two cations.
2) Coordination number (CN) of a glass forming cation tends to be small (CN = 3 or 4).
3) Adjacent polyhedral connected at corners do not share edges or faces.
4) At least 3 corners must be shared to create a 3D network.

These statements make up what was later termed "Random Network Theory" (illustrated in Figure 2.2) which became the basis for modeling glass structure. Despite some of Zachariasen's predictions not holding true (*i.e.,* Sb_2O_5, P_2O_3, As_2O_5, Nb_2O_5, and Ta_2O have not been made into a glass along with the advent of non-oxide glasses - *e.g.,* covalently bonded chalcogenide glasses), much of his theory is still relevant today.

In addition to structural considerations for glass formation theory, there are also kinetic theories which don't question if a material will form a glass, but rather how rapid the material must be cooled in order to prevent crystallization in order to form a glass. As stated above, one of the

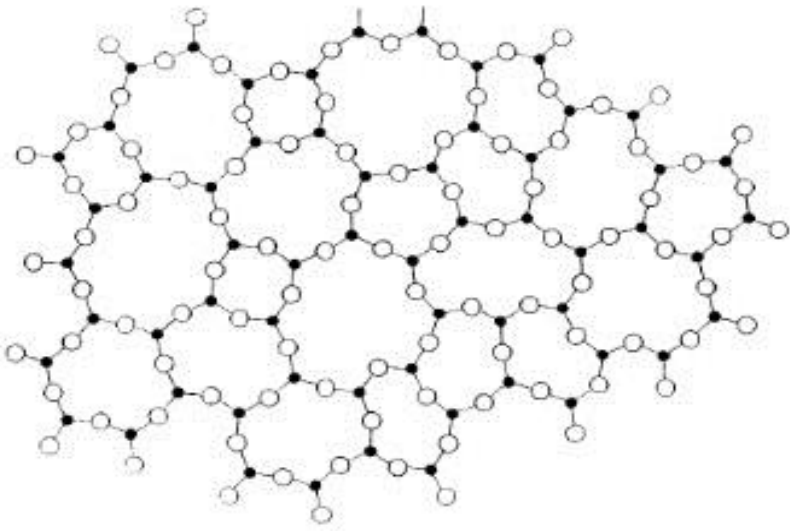

Figure 2.2 A glassy ("random") network model from Zachariasen's 1932 paper, *The atomic arrangement in glass* with the black circles as cations (network former) and white circles as oxygens. To imagine a 3D structure, place an oxygen above the cation. (Note: in his original drawing two oxygen atoms are missing in the top center).

requirements for a materials to be considered a glass is that it must exhibit a T_g, in that, the melt must maintain it's liquid-like structure as it is supercooled below the melting point of the crystal, in order to transform into a solid upon further cooling [101]. This behavior is often represented in the relationship of either enthalpy or volume and temperature (Figure 2.3) [99]. Cooling the liquid (melt) below the melting temperature (T_m) typically results in the material transformation to the crystalline state (*i.e.,* periodic arrangement of atoms, long-range order). However, a supercooled liquid is obtained if taken below T_m without crystallization, allowing the structure to keep re-arranging with no sudden decrease in enthalpy. Further cooling results in increased viscosity, which increases until it becomes high enough that the atoms can no longer rearrange themselves causing a deviation from the equilibrium line, and resulting in a gradually decreasing slope until the structure becomes fixed (*i.e.,* enthalpy becomes dependent on heat capacity of the "frozen liquid") [99]. Thus, the glass transformation region lies between the enthalpy region of the equilibrium liquid and the frozen solid (*i.e.,* glass), and is time-dependent. However, it is typically easier to define T_g as one temperature and typically determined using thermal analysis or expansion curves usually through differential scanning calorimetry (DSC). Since the experimental methods of these techniques (*e.g.,* heating rate) can vary [101], T_g cannot be regarded as a true property of the glass, but rather an indicator of the approximate temperature of when the solid, upon heating behaves as a viscoelastic material or, upon cooling, the

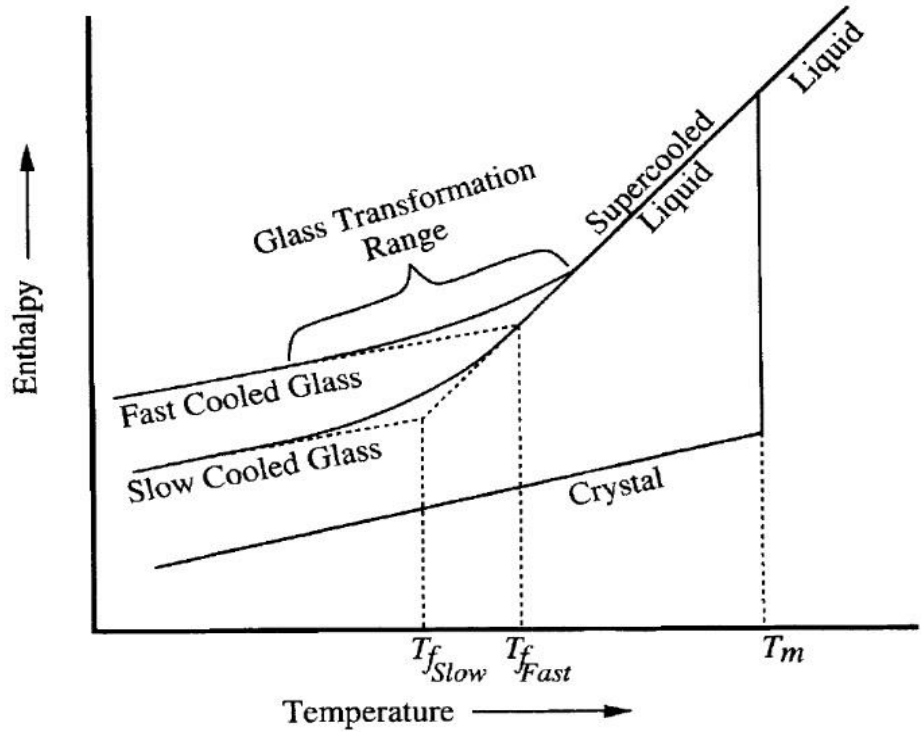

Figure 2.3 The effect of temperature on the enthalpy of glass forming melt (Shelby 2005).

supercooled liquid converts to a solid [99]. While glasses do not have crystals in their structures, it is also important to understand their potential formation and thus crystal nucleation and growth of glasses has been extensively studied and reviewed [99, 102, 103].

The structure of glass is often in reference to the number and arrangement of non-bridging oxygens (nbOs), *i.e.,* the oxygens that do not link to the network polyhedral, and the number of bridging oxygens (bOs or "Ø"), *i.e.,* those oxygens that link the network polyhedral [99]. Quantitatively, the network forming units can be described by Q^i species where the "i" represents the number of bO atoms. For example, pure vitreous silica would be designated Q^4 since all the network tetrahedral are bonded together. As more alkali oxides (R_2O) are added, then the network becomes more disrupted (*i.e.,* less bonded) and the glass forming tetrahedra become Q^3, Q^2, Q^1, and even Q^0 species [99]. For silicate glasses, generally, a decrease in the Q number translates to a decrease in T_g and lower chemical durability, however the amount of modifying alkali (R^+) or divalent alkaline earth ions (R^{2+}) will also influence these properties. However, for invert glasses (e.g. modifier/network former >1) the inverse affect has been observed [104]. This trend does not always hold true for phosphate or borate glasses (discussed later).

The majority of glass formulations today are silica based (SiO_2, commonly called "sand") where silicon (Si) is the glass forming cation, which forms a silicon tetrahedron (SiO_4^{4-}) creating a

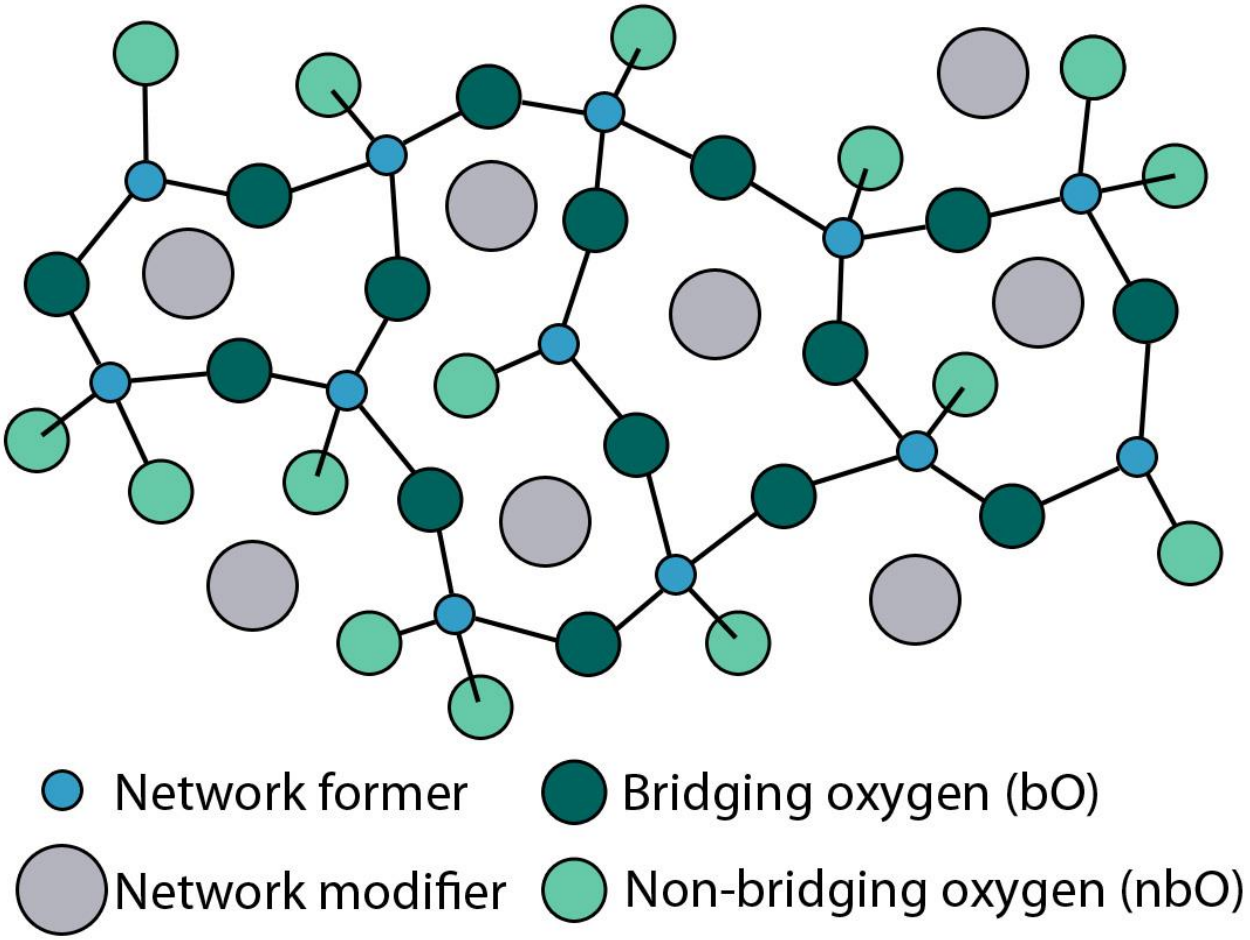

Figure 2.4 Schematic of glass structure showing the network former (i.e., Si) in blue, network modifier (i.e., Na) in gray as well as the oxygens, both bridging (dark teal) and non-bridging (light green).

network of -Si-O-Si- bridging oxygen bonds in three dimensions [82, 92]. Since silica is the main ingredient and most abundant mineral in forming the amorphous network, it is termed the glass network former. However, silica melts at relatively high temperatures (>1700 °C) so it is not practical to make glasses that are only silica-based although it is possible for specialized applications (*e.g.,* fused quartz) [99]. For this reason, additional elements, called *network modifiers*, are often incorporated into the glasses. These network modifiers do not form the main polyhedral network, but rather modify the SiO_4^{4-} network, which in turn lowers T_m and/or affects the final properties, partly due to increased nbO formation. Some of the most common network modifiers are calcium oxide (CaO, also known as "lime") and sodium oxide (Na_2O, also known as "soda") [99] making "soda-lime-silicate" glasses, which have been extensively studied and make up nearly 90% of all the glasses produced today [105].

While silicate based glasses are the most common, glasses can also be based on other network formers such as phosphate or borate. Similar to silicate based glasses, the network former in

phosphate glass is a tetrahedrally coordinated PO_4^{3-} unit. However the main difference is that one of the terminal oxygens in phosphate is double-bonded meaning that, in terms of Q^i notation, the highest a phosphate group can achieve is Q^3 [106]. Due to the ability to share only three oxygens, therefore in the vitreous form it becomes P_2O_5 to charge balance akin to silicate glasses, when network modifiers are added, these convert to Q^2, Q^1, and Q^0 species [107]. However, unlike silicate glasses, P_2O_5 is very hygroscoptic, and the addition of glass modifiers increases the chemical durability by forming P-O-M^+ bonds [108, 109]. Phosphate glasses have a less rigid structure due to this three-coordinated bonding and are able to have a wider glass forming range and thus a wide range of properties [110].

2.3.2 Borate glass structure

In contrast to vitreous silicate glasses, vitreous borate glasses consist of planar, trigonally coordinated $BØ_3$ groups (Figure 2.5) [99]. Since these building blocks are planar, the 3D structure is created by "crumpling" the network, akin to crumping a piece of paper into a ball. This "pseudo" 3D network consists of van der Waals bonds in the third dimension which allow for an easily disrupted glass structure. This is observed by the low T_g (≈ 260 °C) of vitreous borate versus that (≈ 1100 °C)

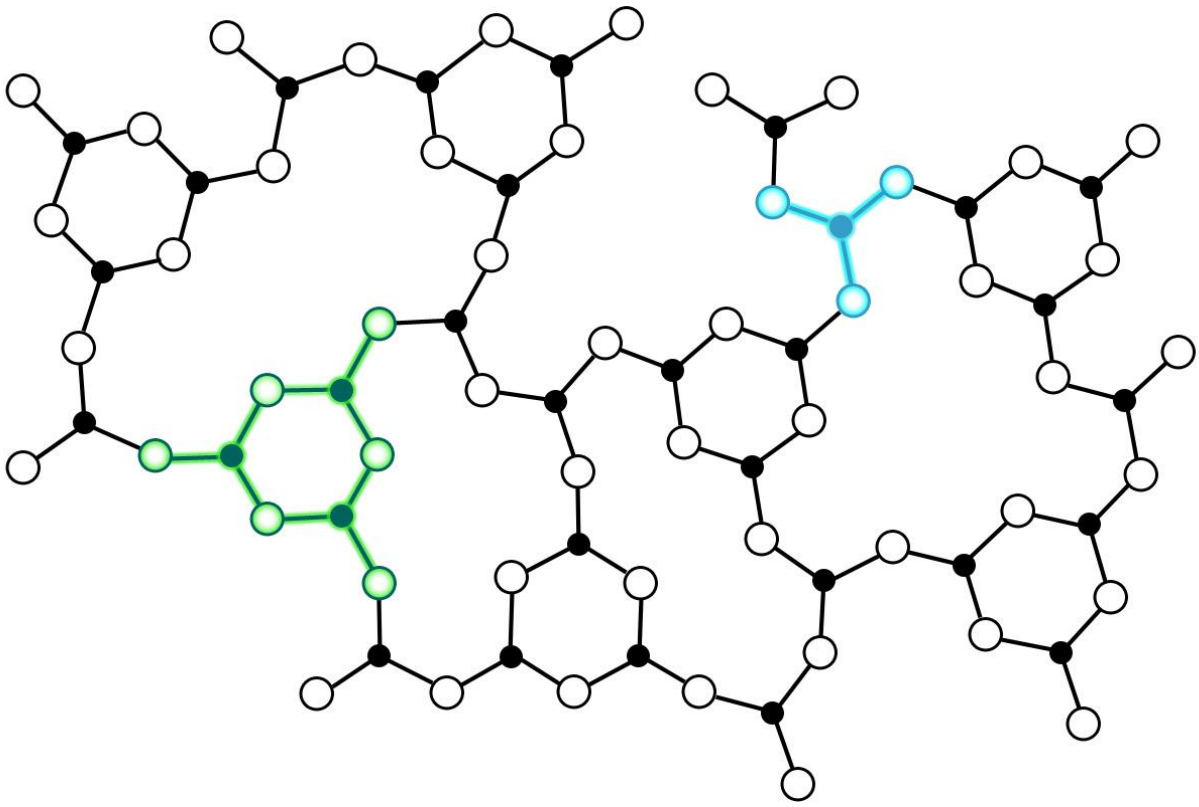

Figure 2.5 Schematic of vitreous borate glass with high proportion of boroxol rings (B_3O_6, example shown in green) and trigonal borate groups ($BØ_3$, example shown in blue) with filled circles representing boron and hollow circles representing oxygen (adapted from Kroghe-Moe 1969).

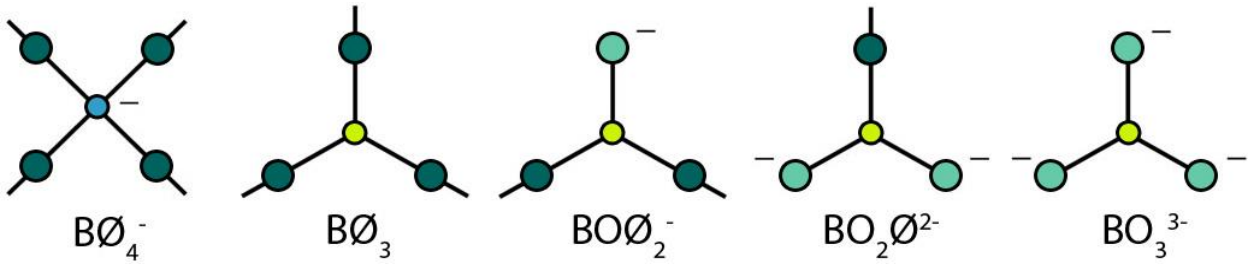

Figure 2.6 The five major Borate $B^{(n)}$ structural units ($0 \leq n \leq 4$) represented in 2 dimensions adapted from Wright (2015). (Key: Blue, tetrahedral boron; yellow, trigonal boron; dark teal, bO; aqua, nbO)

of vitreous silica [99]. Along with the planar $BØ_3$ groups, vitreous borate also contains a number of intermediate units, mainly boroxol rings (B_3O_6) [111]. Although the occurrence of these groups was first proposed by Goubeau & Keller in 1953 [112], it was not accepted for many decades, until neutron diffraction and Nuclear magnetic resonance spectroscopy (NMR) data, confirmed that in vitreous borate, approximately 70-80% of the boron atoms are in boroxol groups [113]. Borate glass is based on five basic structure groups: i) $BØ_4^-$, ii) $BØ_3$, iii) $BOØ_2^-$, iv) $BO_2Ø^{2-}$, and v) BO_3^{3-} as seen in Figure 2.6. Also unlike in silicate glasses, the addition of modifying oxides (M_2O) to B_2O_3 does not increase the formation of nbOs but rather increases the coordination. The neutrally charged, three-fold [$BØ_3$] units convert to negatively charged, four-fold [$BØ_4^-$] tetrahedra which are charge balanced by the

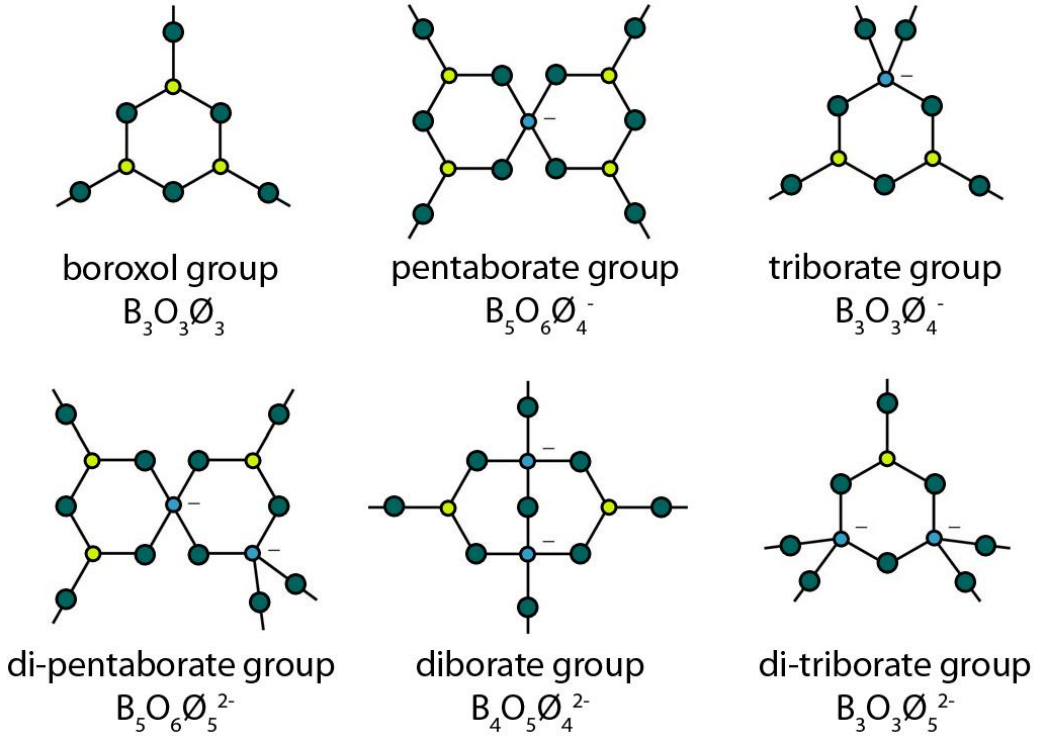

Figure 2.7 Frequently occurring borate superstructures in either the glassy and/or vitreous state adapted from Wright (2015). (Key: Blue, tetrahedral boron; yellow, trigonal boron; dark teal, bO)

network modifying cation [M^+] [99, 104]. One to three of these four coordinated units can be incorporated into borate rings or in superstructures such as di-borates (Figure 2.7). These super structural units are based on three-membered rings of the basic structural units (six-atom rings), and are unique in that they have no internal degrees of freedom in the form of variable bond angles or bond torsion angles except for the diborate group, which is rigidly planar. Numerous structural units exist as reviewed by Wright and Vedishceva, some examples of which are presented in Figure 2.7 [114]. A further increase in modifying oxide addition causes the borate units to convert back to the trigonal coordination, creating more nbOs and increasing the depolymerzation of the network.

In borate glasses, increased alkali results in higher T_g and a decrease in coefficient of thermal expansion (CTE) which is the opposite effect to that observed in silicate glasses [99]. However, what makes borate glasses unique, is that with further increased alkali additions these properties reverse again, thus giving rise to the *borate anomaly* [113] (Figure 2.8). This unique structure-property relationship was first thought to depend on the conversion of three to four-fold coordination occurring up to a critical amount of tetrahedrally-coordinated borate (≈ 13 mol% R_2O) until further addition caused more nbOs to form [115]. This model was widely accepted until the advancement of NMR which could directly measure the amount of three and four-coordinate boron units and then it was found that a maximum number of tetrahedrally coordinated boron units occurs around 35 – 40 mol% alkali oxide

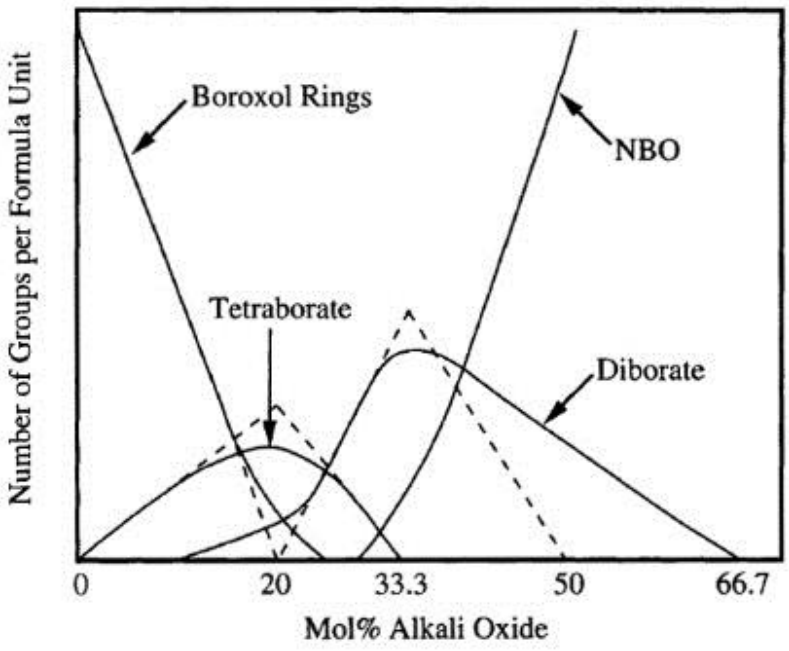

Figure 2.8 Simplified overview on the variation of borate super-structural units with increasing alkali oxide additions (Shelby 2005). Experimental data represented by solid lines and dashed line indicates theory.

[99]. This concentration is beyond the composition where the reversal of properties is observed, so using four-coordinated boron values to explain this anomaly alone is not sufficient [114]. Further measurements show that maximum T_g occurs around 27 mol % R_2O while the lowest CTE occurs near 20 mol % R_2O. This confirms, that while there is a reversal of properties, they occur at different alkali oxide concentrations. An explanation of this anomaly can be through the equilibrium reactions for the two isomers of metaborate or orthoborate units (Figure 2.9) [104]. These metaborate units are either 3 or 4-coordinated and equilibrium occurs between the two which occurs at different modifier concentrations. These glass properties also depend on the cross-linking capability of the modifier cations [116].

2.3.3 Bioactivity

According to Hench et al., a bioactive material is one, "that elicits a specific biological response at the interface of the material which results in the formation of a bond between the tissues and material" [10]. For glasses and ceramics, *bioactivity* is defined by their to undergo surface reactions when implanted into the body which leads to the formation of an HCA-like layer that can form a bond with both hard and soft tissue [117]. It is also generally accepted that a material is bioactive if it forms an HCA-like surface layer *in vitro* usually through immersion in simulated body fluid (SBF) according to Kokubo [118]. However, due to conflicting *in vitro* and *in vivo* results, this assumption has been challenged by Bohner and Lemaitre [119]. Their main criticisms of the original SBF test approach are that the procedure is long and tricky (reduced reproducibility), the solutions are not filtered (may contain insoluble contaminants that affect precipitation), and the carbonate content is not controlled. Additionally, it has been shown that SBF testing can cause both false negative and positive results meaning the *in vitro* and *in vivo* results do not always correspond [119]. While they suggest modified formulas and procedures to test *in vitro* bioactivity, they are not as commonly practiced as Kokubo's original solution. A more recent, alternative approach to overcome some of

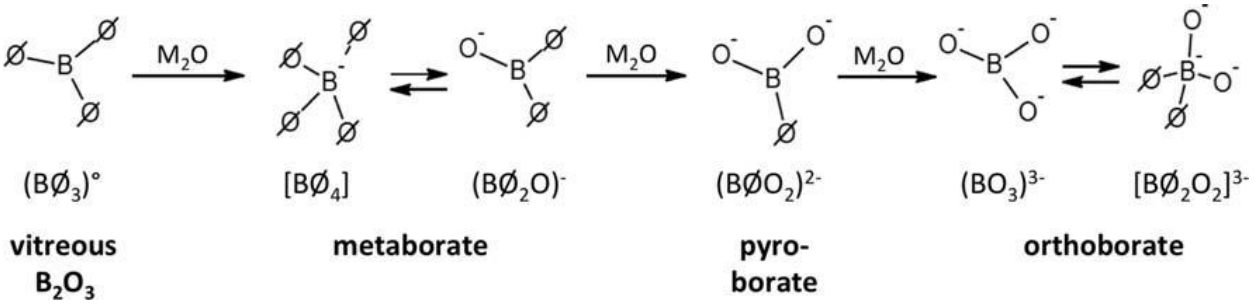

Figure 2.9 Borate glass short-range order changes with modifier (M_2O) additions which contribute to the boron anomaly (Brauer and Moncke 2016).

these drawbacks is to standardize Kokubo's SBF testing procedure and evaluation time points while also taking into account particle size and porosity [120]. In this study, consistent, repeatable results were shown using the same glass compositions at different universities demonstrating that this should be the preferred method of evaluation. Furthermore, the definition of bioactivity is evolving since now bioactive glasses are being targeted specifically for soft tissue engineering applications [121].

Compared to glasses, ceramics have been a popular choice for bone tissue repair since they offer better mechanical properties and their mineral compositions can be tailored to almost identically match the high mineral content of native bone [122]. An example of this is synthetic hydroxyapatite (HA, $Ca_{10}(PO_4)_6OH_2$) which is one of the most prevalent materials used for bone repair since for its osteoconductivity, bioactivity, and similar composition to native bone HCA [123]. However, it has been shown that the high levels of crystallization, such as those associated with ceramics, limits their bioactivity [124] and favored degradation of the amorphous regions also delays the onset of HCA formation compared to fully amorphous glass [125]. This has been previously shown with Ceravital, a 45S5 glass-ceramic with small additions of MgO and K_2O, that could bond to bone [126], but the crystal phase boundary instability of the structure leads to implant failure [12]. Therefore, although bioactive glasses have been demonstrated to typically be more bioactive compared to ceramics due to their amorphous nature, they have yet to achieve similar commercial success [82]. Furthermore, they have the advantage of homogenous degradation and ion release, which can help stimulate the body's natural healing process [81]. However, the majority of glasses have poor mechanical properties compared to bone and other hard tissues and are mostly limited to non-load bearing applications [82].

Structurally, bioactive glasses are in general of lower network connectivity (*i.e.,* lower ratio of network formers to modifiers) which promotes quicker dissolution rates when exposed to body fluid [92]. Similar to the Q^i species quantitative approach in section 2.3.1, Hill proposed an alternative view on the degradation of Bioglass® to supplement the reactive stages of HCA formation (discussed later) [127]. In this study, it was emphasized that the structure (composition) of glass network ("network connectivity") was the most influential property in predicting bioactivity, and tested this theory on data on glass literature and understanding of glass structure at the time (*i.e.,* phosphorous was part of the glass network). In 2011, Eden developed the "split network model" which focused on each network former through assessment of the mean number of bO and nBO as well as the average network polymerization in multi-component glass systems [128]. Both of these models suggest SiO_2–P_2O_5–CaO–Na_2O containing glasses with silicate chains (Q^1 or Q^2 structures) can dissolve without Si-O-Si bond hydrolysis which is in contrast to the original dissolution mechanism proposed by Hench

[13]. Later, also in 2011, Hill and Brauer [129] proposed an updated modified network connectivity (N_C) model to predict the bioactivity of a glass based on its nominal composition in mol %, as given by equation (1):

$$N_C = \frac{4(M_f) - 2[M_2^I O + M^{II} O] + 6[M_{P_2O_5}]}{[M_f]} \quad (1)$$

where M_f is the molar fraction of the network forming oxide (*e.g.,* silica) and $M_2^I O$ and $M^{II} O$ represent the mono and divalent molar fraction of the modifier oxides, while $M_{P_2O_5}$ represents the molar fraction of P_2O_5 in the glass network. Since the structure (*e.g.,* composition) is the prime determinate factor for predicting the bioactivity of a glass [82], through this equation, it has been found that glasses with an N_C between 2 and 2.6 are generally regarded as bioactive according to Eden [128] and near 2.0 < 2.4 for Hill [127]. For example, Bioglass® 45S5, has an N_C value of 2.12 [82, 129]. It is important to note that NMR and modeling studies, have indicated that the phosphorous remains as an orthophosphate [PO_4^{3-}] and does not enter the glass network (*i.e.,* no Si – O – P bonds are formed) [129] yet Si – O – P bonds can form at higher phosphate concentrations (*e.g.,* > 50 mol%) [130]. This has been taken into account in the model proposed by Hill and Brauer. The model also assumes that the phosphates form their own network and are charge balanced by divalent cations and that the network former is always four-coordinated, which is not always the case for all bioactive glass systems such as those based on phosphate and borate.

2.3.3.1 Silicate-based bioactive glasses

The most commonly used glasses today are silicate-based [92]. As mentioned above, silica is termed the glass network former while oxides of calcium (CaO) and sodium (Na_2O) are called network modifiers since they are added for easier processing (*i.e.,* lowering the glass melting temperatures) and tailored properties through the creation of Si-O^- (Ca^{2+}/Na^+) bonds [82, 92]. In the late 1960s, Dr. Larry Hench created the first silicate bioactive glasses, with his most successful formula: (45)SiO_2-(24)Na_2O-(24)CaO-(6)P_2O_5 in wt. % [82, 92, 110], being Bioglass® "45S5" (Note: Only bioactive glass with the 45S5 composition should be called Bioglass® since it is trademarked by the University of Florida where it was invented while all other compositions should be referred to as "bioactive glass" (BG) [82].) *In vivo* studies using rats found that this glass formulation chemically bonded to bone [11]. Since this initial discovery, Bioglass® has been extensively studied for use in bone tissue engineering [12, 82, 92].

Compared to traditional silicate glasses, the high amounts of CaO and Na_2O in 45S5, promotes rapid ion exchange during dissolution, while the P_2O_5 addition creates a less chemically durable glass which helps promote rapid HCA conversion and bone bonding rates [45]. The process of how the surface of Bioglass® dissolves and forms a crystallized apatite layer has been extensively reviewed [45, 81, 82, 92]. In brief, the process can be divided into the following five stages [10, 82]:

1) Rapid cation exchange of the Na^+/Ca^{2+} with H^+ or H_3O^+ from solution (body fluid/SBF). This creates Si-OH bonds on the glass surface, increases the pH of the solution, and forms a Si-rich area at the glass surface. The phosphate component of the glass is lost at this stage.
2) The high pH leads to the break-up of the silica glass network through OH^- which continues to break the Si-O-Si bonds. Soluble $Si(OH)_4$ is lost in solution which generates more Si-OH on the glass surface.
3) Condensation of the Si-OH groups occurs and the silica rich layer is repolymerized
4) Ca^{2+} and PO_4^{3-} groups then migrate to the surface through the silica-rich layer and form a solution rich in amorphous $CaO-P_2O_5$ on the silica-rich layer.
5) The hydroxyls and carbonates from the solution are incorporated and the $CaO-P_2O_5$ film is crystallized to HCA.

In contrast, the mechanism of HCA formation in other glass systems has not been as extensively studied, which may be because those glass systems have not been as well studied for bone tissue regeneration. The main disadvantage of silicate bioactive glasses are their relatively slow degradation rate (depending on the composition) and concerns on the extended effects of concentrated SiO_2 sources in the body [92].

2.3.3.2 Borate-based bioactive glasses

Similar to other non-silicate-based glasses, such as phosphate, borate glasses tend to have lower chemical durability which increases their degradation rate, limiting their commercial potential for many industrial applications [17, 131]. However, in potential bone tissue engineering applications, these glasses have been demonstrated to have good *in vitro* cell compatibly with osteogenic stem cells and exhibit rapid conversion to HCA [132]. Day et al. provided the first major review of how borate glasses can be customized for biomedical applications [133]. Since, these glasses have only recently been investigated for tissue engineering applications, many of the formulations have been based on silicate based glasses (*e.g.,* 45S5 and 13-93) where the borate is either fully or partially substituted for the silica.

One of the first melt-quench derived bioactive borate glass was based on the original "45S5" composition [17], where borate was substituted for the silica either completely or in 1/3 or 2/3 molar ratios to the silica amount. The glasses were ground and separated into three different particle size ranges then subjected to a 0.02 molar K_2HPO_4 solution held at 37 °C (an alternative to using SBF since this solution makes the calcium content in the glass the determining factor for conversion). Higher borate content led to a more rapid HA conversion rate while also lowering the pH of the phosphate solution. Fully substituted borate glass particles in the size range of 150 – 300 μm completely converted to HA after 4 days while the partially substituted borate glasses did not completely convert to HA, even after 70 days in solution [17] (Figure 2.10). The borate substituted 45S5 system was also investigated by Ning and colleagues who produced borate glass microspheres through the flame spraying technique [134]. Again, bioactivity was characterized by submersion in K_2HPO_4 solution and cell viability was tested using goat bone marrow stromal cells (BMSCs) with cell proliferation being measured using an MTT assay. Quick conversion to HA (~ 10 days) along with positive MTT assay results again confirmed the potential of these glasses for bone tissue engineering applications [134]. Fu et al. created another borate substituted 45S5 glass and fabricated scaffolds via the polymer foam replica method [135]. Cellulose-based porous foams were initially covered by a

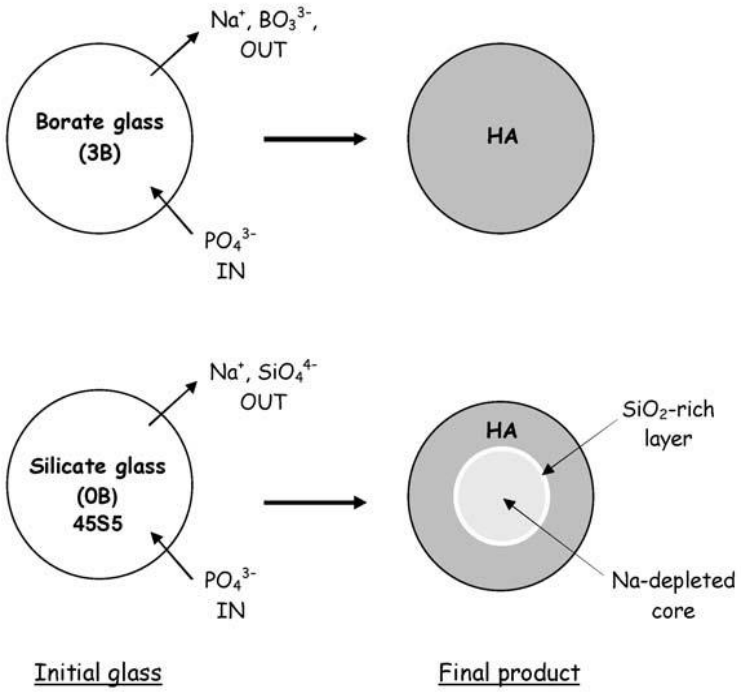

Figure 2.10 Schematic showing the dissolution of 45S5 glass and borate substituted 45S5 (Huang 2006).

slurry of borate glass, which were then heat treated create trabecular bone-like amorphous scaffolds. The scaffolds formed a layer of HA after 7 days in a solution of 0.02M K_2HPO_4. Cell viability using BMSCs was also tested and it was found that boron concentrations under 0.65 mM were conducive to their proliferation [135]. In addition, murine MLO-A5 cells were tested, demonstrating good proliferation and function. These tests suggested that borate substituted 45S5 was a promising composition for bone tissue engineering applications.

More simpler, ternary borate glasses, in the Na_2O-CaO-B_2O_3 system, have also been studied for bone tissue engineering [136]. Particles in the size range of 212 – 355 μm were loosely compacted into disks and soaked in a 0.25 molar K_2HPO_4 solution for 1 or 7 days where partial and nearly full conversion to calcium phosphate (CaP) was observed, respectively. Additionally, bone marrow derived human mesenchymal stem cells (hMSCs) adhered to the pores of the bioactive glass and the levels of alkaline phosphatase, an early osteogenic marker, increased [136]. Furthermore, Liang et al. investigated another ternary borate glass composition (though the formulation was not specified), where particles and microspheres of different sizes were loosely compacted and sintered at different temperatures to form 3D constructs with approximately 25 – 40% porosity [137]. Full conversion of the glass to HA took place in less than 6 days in K_2HPO_4 (0.25M, pH 9). *In vitro* cell culture demonstrated that hMSCs adhered to the scaffolds and produced alkaline phosphatase [137]. This conversion of borate glass to HA has also been investigated by Han and Day [138]. Their randomly shaped glass particles or microspheres based on (1 or 2)CaO-(2)Na_2O-(6)B_2O_3 in molar ratios were reacted with a phosphate solution that was prepared by dissolving K_2HPO_4-3H_2O in distilled water at different temperatures. The amount of HA produced was limited by the calcium content since the amount of phosphate was very high and it was shown that conversion could be achieved by further submersion in a K_2HPO_4 solution at pH 9. Both glass compositions converted to HA and the reaction rate was controlled by a variety of factors including temperature, Ca content in glass, and P content in solution [138].

Borate glasses have also been doped with other ions thought to improve bone healing. Pan et al. investigated a strontium doped borate glass of the composition (36)B_2O_3-(18)SiO_2-(6)Na_2O-(22)CaO-(8)K_2O-(2)P_2O_5-(12-x)MgO-(x)SrO (where x = 0, 6, 12 in mol %) [139]. Bioactivity was tested by immersion in Dulbecco's modified Eagle's medium and cytotoxicity was tested through the MTT assay, where osteoblast-like cells were seeded on the glasses and the increase of strontium was shown to enhance cell adhesion [139]. In addition, strontium in this glass system was shown to control the release of boron. Lithium containing borate glasses have also been investigated by Yao et al. [140],

who created microspheres of (10)LiO_2-(10)CaO-(80)B_2O_3 (wt. %) glass which were then converted to hollow HA spheres through immersion in K_2HPO_4. While no cell compatibility was performed, this novel method of creating hollow HA microspheres might serve as potential drug delivery systems [140].

Borate glasses have also indicated positive results, when tested *in vivo*. Using the 13-93B3 composition, Bi et al. fabricated trabecular, oriented, and fibrous scaffolds [141]. The scaffolds were placed in a rat calvarial defect model and examined after 12 weeks. According to histomorphometric and SEM analyses 33, 23 and 15% new bone was formed by using trabecular, oriented, fibrous scaffolds, respectively. As a comparison, implanted 45S5 formed 19% new bone. It was found that all of the implanted scaffolds fully converted to HCA, and interestingly, doping 13-93B3 with 0.4 wt.% copper increased the amount of new bone formed from 15% to 33% for the fibrous scaffold, but had little effect on the other scaffolds. However, the extent of new blood vessel formation was higher in the trabecular scaffold [141]. In another study, silicate 13-93 and borate 13-93B3 grid-like scaffolds, along with an oriented 13-93B3 glass scaffold, were compared to autografts in critical-size segmental defects in rat femurs [142]. The percentage of new bone formed according to histomorphometric analysis of the scaffolds (25 – 28%) was not significantly different from the autografts (38%). Furthermore, the grid-like 13-93 scaffolds showed significantly higher cartilage formation (18%) compared to 13-93B3 scaffolds (8%) and autografts (8%) [142].

In terms of applications that extend beyond bone tissue engineering a borate glass nanofiber mat termed DermaFuse™ has recently been investigated for wound healing by the MO-SCI Corporation (Rolla, Missouri, USA) [143]. The glass fiber mat has a is borate substituted 13-93 glass with a composition of (53)B_2O_3-(20)CaO-(12)K_2O-(6)Na_2O-(5)MgO-(4)P_2O_5 in wt.% [143]. The researchers were interested in this composition because of the high boron content which allows for rapid dissolution as well as the high calcium content was also desirable since it is suspected to assist in epidermal cell migration, critical in wound healing [143]. With DermaFuse™ treatment, patients with chronic open wounds, experienced an increase in wound closure rates from 0.3 mm/day to 0.8 mm/day and after complete treatment there was minimal to no scaring present [143]. More recently ETS Wound Care, LLC has gained FDA approval for their flagship product MIRRAGEN™ (formally DermaFuse™) for the treatment of acute and chronic wounds [144]. Although only recently studied, the inherent lower chemical durability of borate glasses offers superior flexibility in the tissue engineer realm compared to the silicate based glasses.

2.4 Glass Processing Techniques

Glass is not a solely man-made material. In fact, there are many naturally occurring forms of glass such as Obsidian generated by the quenching of volcano molten rock, Fulgurites, which are formed when lightning strikes the beach or in the desert, and Tektites, which are due to meteorite impacts. Some animals, such as sea sponges, even possess siliceous, glass-like skeletons [167]. While some early ancestors relied on these glasses, such as obsidian for tools or weapons, it wasn't until about 7000 B.C. when the first isolated examples of glass production were discovered [99]. Glass production became more prevalent by 2500 B.C., where there were multiple locations of production which likely started in Mesopotamia and then Egypt [168]. Motivation for the first glass production was decorative, possibly to simulate gems, then transforming into bead production, which was helped with the discovery of colorants such as iron salts, copper, and manganese [168]. This was followed by the glass blowing technique, of which, the first pieces were made about 2000 years ago. This technique became popular and was used extensively by the Roman Empire to create bowls and drinking vessels [168]. From here, glass production grew at a rapid rate and glass use has become an integral part of our society today. A thorough review of this rise is given by Kurkjian and Prindle [168]. Like the approach of the ancient Egyptians, the most common and frequent production method involves using heating raw materials (*e.g.,* oxides) to high temperatures then immediately followed by their rapid cooling (*i.e.,* melt-quench technique) to preserve their amorphous structure as discussed in section 2.3.1. While this basic approach of glass production has its roots in ancient history, the sol-gel process was developed much more recently, in the 1930s [21]. However, both of these production methods offer distinct advantages for many applications as discussed below.

2.4.1 The melt-quench technique

Glasses are traditionally made by mixing precursor materials in powder form such as silica, boron oxide, sodium oxide, and calcium oxide, which are then heated until melting at high temperatures (>~1000 °C depending on the composition) [99]. Since many glass forming materials, like silica, melt at relatively high temperatures (>1700 °C) it is not practical to make glasses that are only based on silica (*e.g.*, fused quartz) although it is possible for specialized, high temperature applications [99]. For this reason, network modifiers are added to lower the melting temperature and/or affect the final properties [99]. Borate based glasses tend to have lower melting temperatures due to their lower network connectivity, as discussed in sections 2.3.2.

Once the melt has reached a low viscosity, it is quickly cooled ("quenched") to maintain its amorphous structure [99]. This can be done by pouring the melt directly on a cool steel plate or in a graphite mold. It is also possible to heat treat the glass, through annealing, at a lower temperature than the glass T_m in order to remove any residual stresses and create a more durable glass, thus one that degrades more slowly [169] and has increased mechanical properties [45]. Once cooled, glasses can be mechanically ground to yield small particles. Additionally, changing the glass composition can significantly alter their intrinsic and thermal properties. On the other hand, some glasses are very difficult to form through melt-quenching, and consequently are made by using the sol-gel method.

2.4.2 The sol-gel technique

The sol-gel processing method is as a robust, low temperature, solution based approach that is the basis for creating many nanostructured forms. The method is advantageous to traditional high temperature glass processing in that it can be carried out at room temperature making it easier to adjust the composition, and since the raw materials are in liquid form, uniform mixing and homogeneity are easier to achieve. Additionally, near end-shape forming is achievable with sol-gel produced materials [82], although cracking upon drying can make monolithic shape formation difficult. Another drawback is that the sol-gel process is expensive due to the raw materials and time consuming when compared to the melt-quench technique. Nevertheless, it is the most suitable technique for producing amorphous, highly porous materials amongst other specialty materials [145].

Early investigations of the sol-gel process occurred in the mid-1800s by Ebelman who noticed that silica alkoxides (*e.g.,* tetraethylorthosilicate ($Si(OC_2H_5)_4$ or TEOS) in the presence of moisture, hydrolyze slowly forming hydrated silica, "a glass-like material" [146]. However, it was not until the 1910s that a solid structure was produced by this technique [147]. In the 1930s, Geffcken made oxide films from alkoxides [148], a process that was further developed by the Schott glass company [149]. Yet, there was sparse interest in the sol-gel route until the 1970s when Yoldas [150] and Yamane [151] made bulk glass from alkoxide gels. This revitalized this technique, which has since greatly expanded in terms of the types of materials that are made today. A schematic overview of both the sol-gel and melt-quench methods can be seen in Figure 2.11.

To understand the sol-gel process, some key concepts must first be defined. A suspension in which the dispersed phase is so small (< 1 μm) that short range forces, such as van der Waals attraction and surface charges dominate is termed as a *colloid* [21]. Due to the relative size of the dispersed phase, it exhibits random motion, created from collisions with molecules of the suspending medium, known as *Brownian motion*. A colloidal suspension of solid particles in a liquid is called a *sol* [21], and an

interconnected, ridged network with polymeric chains or coalesced particles, with average length greater than a micrometer and contains sub-micrometer pores, that forms a solid network, is called a *gel* which forms [152]. Thus, the final goal of the sol-gel process is to obtain a gel from the initial sol, an overview of which can be found in Figure 2.12.

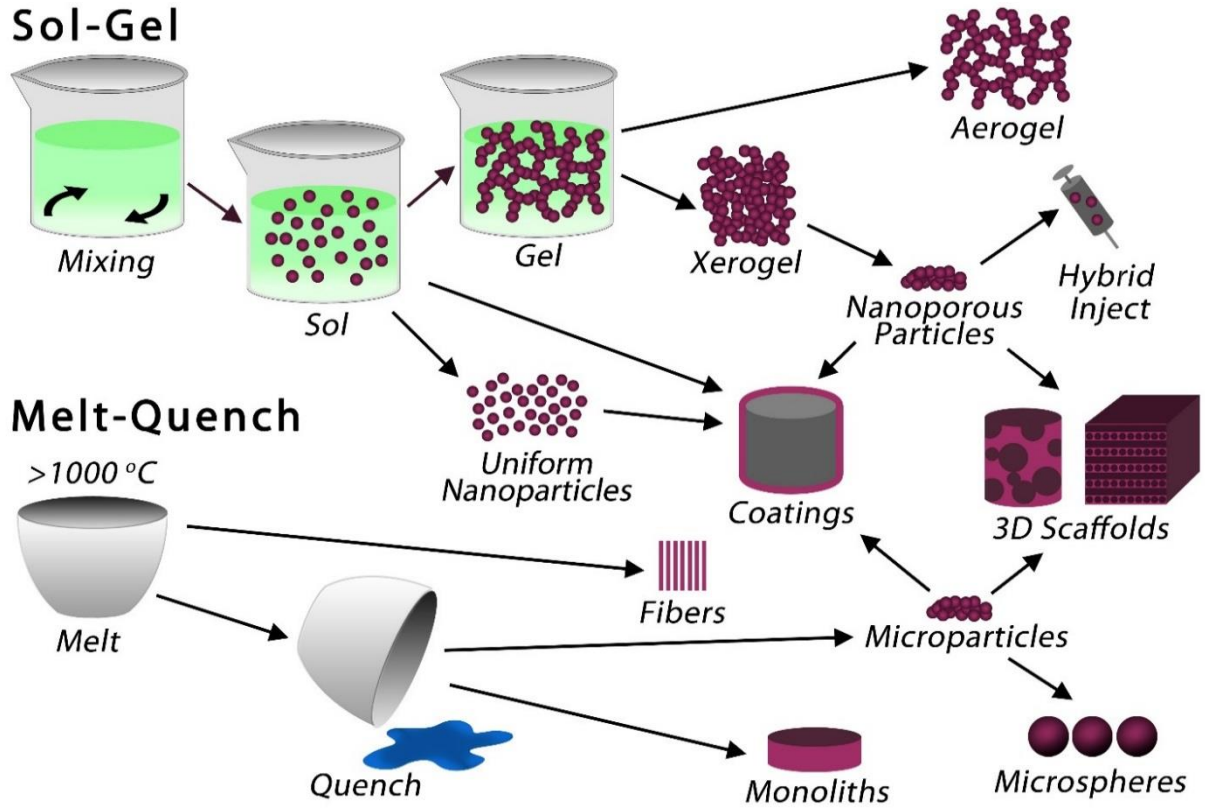

Figure 2.11 An overview of the two main glass processing methods: Sol-gel and melt-quench. Due to the aqueous nature of the sol-gel process, there is greater processing flexibility which can result in a wide variety of final forms.

There are a couple basic approaches for making sol-gel monoliths as described by Hench et al. [152]: 1) gelation of a solution of colloid powders, and 2) hydrolysis and polycondensation of alkoxide precursors. Both approaches are followed by ageing, drying, and calcination stages. The most common method for biomaterials based applications involves using metal-organic precursors (*e.g.,* metal alkoxides) which are converted to inorganic materials in an organic solvent or water [153]. The majority of sol-gel processing uses TEOS as the silica source, and thus network former. When mixed with water, TEOS undergoes hydrolysis that creates a sol (Eqn. 2). This solution of particles then undergoes polycondensation (Eqn. 3) to form nanoparticles which then coalesce during gelation to form a fine, interconnected gel [34]:

$$Si(OCH_2CH_3)_4 + H_2O \rightarrow Si(OCH_2CH_3)_3OH + CH_3CH_2OH \quad (2)$$

$$Si(OCH_2CH_3)_3OH + Si(OCH_2CH_3)_3OH \rightarrow (CH_3CH_2O)_3Si–O–Si(OCH_2CH_3)_3 + H_2O \quad (3)$$

Silicon alkoxides are typically not sensitive to water and can take days to hydrolyze. To improve this process, either acidic or basic catalysts are added. Acid catalysts work by protonating the negatively-charged alkoxide ligands making it become a better leaving group. Basic catalysts provide better nucleophilic OH^- groups for hydrolysis and deprotonated silanol groups $Si\text{-}O^-$ for condensation. Acid catalysts mostly increase the hydrolysis rates as opposed to basic catalysts, which enhance condensation, though they both increase the rate of both events [154].

After the gel has formed, it must be further processed to generate a useable material since excess organic materials from the process are typically not desired in the final product, especially for biomedical applications. Before drying, gels undergo an ageing step, where the gel network is strengthened by forming more interconnected bonds, usually resulting in the slight shrinkage of the gel [21, 152]. To eliminate the organic materials (generally an alcohol, *e.g.,* ethanol, or water or both), the gel must be dried which, depending on the method, can produce drastically different final products

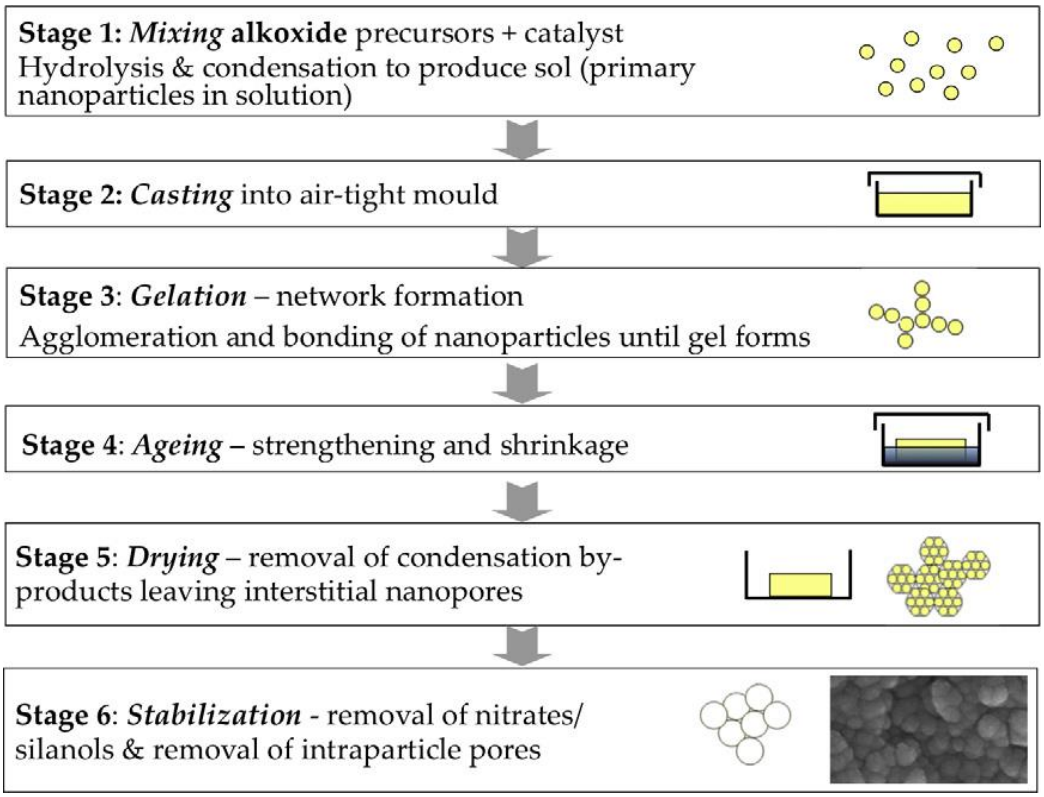

Figure 2.12 A basic overview of the sol-gel process taken from Jones (2013). Variations of this method exists where nanofibers and aerogels, amongst other forms can be produced.

in terms of porosity and microstructure. The two most common final forms are xerogels or aerogels. Xerogels are produced when the gel is allowed to dry in atmospheric conditions. During this drying process, the nanostructured porous layers are under large surface tension and exposed to capillary forces causing the fine microstructure to collapse and the gel to shrink [152]. The resulting monolith structure has significantly reduced porosity compared to the original gel network. Creating a xerogel as a final product is often desirable if it is going to be in particle form since it can be easily ground.

To make aerogels, a more controlled method of drying called *critical point drying* or *supercritical drying* is required. The principle of this technique relies on the critical point of the solvent liquid. The physical characteristics of a liquid and gas are not distinguishable at the critical point, thus a gel soaked in a fluid raised to its critical point can be converted to a gaseous phase without damaging the nanostructure of gel. Often, the as prepared gel is soaked in ethanol or acetone to remove all the water and then supercritically dried using liquid carbon dioxide which is miscible with alcohol. The near zero surface tension of the CO_2 *liq* and solvent prevents the structure from collapsing upon drying, thus preserving the nanopores. As a result, aerogels are highly porous, low-density materials consisting of nano-sized pores, which can be used in a number of applications such as catalysis, drug delivery, thermal insulation, and more recently in tissue engineering [155, 156].

2.4.2.1 Sol-gel derived borate glasses

While the sol-gel process has been extensively studied for silicate systems, there is a distinct lack of literature of sol-gel derived borate glasses. This may be due to the more complicated bonding nature of borate glass systems (section 2.3.2), which tends to form three- and four-coordination compared to the typically four-coordinated silicate glasses [21, 157]. Lower coordination leads to greater difficulty in forming a gel due to reduced bonds in the z-direction, thus reducing the 3D character. Alkyl borates rapidly hydrolyze to form boric acid (Eqn. 4) and, in an aqueous solution, it can further hydrolyze to form borate ions (Eqn. 5):

$$B(OR)_3 + 3H_2O \rightarrow B(OH)_3 + 3ROH \quad (4)$$

$$B(OH)_3 + H_2O \rightarrow B(OH)_4^- + H^+ \quad (5)$$

It is thought that the coordination of boron depends on the concentration of water and pH [157] leading to polyborate formation which are thought to be the backbone of the gel. In alcoholic solutions of alkali borates, it is speculated that a critical concentration of a tetrahedrally coordinated boron is needed. This may require a minimum level of alkali addition or perhaps sufficiently high pH

where tetrahedrally coordinated borate is dominant [21]. Brinker described a mechanism of polyborate formation (Figure 2.13). In this proposed mechanism, it is thought that both the hydrolysis and condensation reactions occur via the SN mechanism, which involves nucleophilic attack of either the OR or OH ligands of the electrophilic, trigonal boron with the elimination of water or alcohol [21].

Despite this lack of literature, the fabrication of sol-gel borate glasses was first reported by Tohge and colleagues, which was based on a simple binary system (80)B_2O_3-(20)Na_2O (mol%) [158]. Other borate-based systems have been reported only for binary sodium [159], lithium [160], and barium [161] compositions with little detail of chemistries, except that large additions of water result in precipitation [157]. Other elements such as Si [162] and Ti [163] have also been examined yet, studies regarding applications of any of these glasses are scarce. Brinker and colleagues studied a borate-lithium aerogel and noted that B-O-B linkages between primary units required at least one four-coordinated boron unit [157]. More recently, Bengisu created a series of high borate containing (> 87% B_2O_3) di and tri-borate glasses doped with lithium or phosphate or both [164]. However, only compositions with lithium formed bulk gels while the other compositions resulted in direct precipitation.

Borate has also been added as a structural element in other sol-gel systems. For example, Carta el al. examined gel formation in the $40(P_2O_5)–x(B_2O_3)–(60−x)(Na_2O)$ ($10 \leq x \leq 30$ mol%) system [165]. It was reported that replacing sodium oxide with borate led to improved glass thermal stability, decreased its hygroscopic nature, and increased its bond strength by forming new P-O-B bonds, where

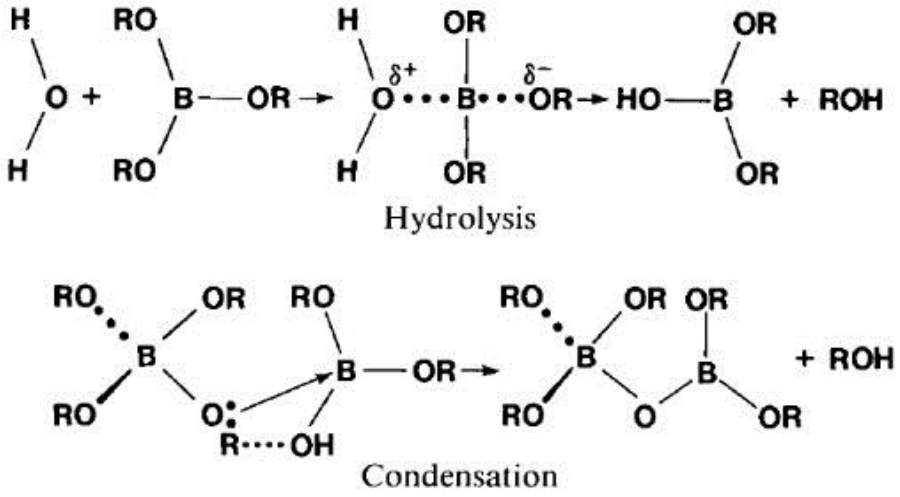

Figure 2.13 Hydrolysis and condensation reactions under neutral conditions via the SN mechanism through nucleophilic attack of OH or OR ligands on electrophilic, trigonal boron followed by the elimination of alcohol of water (Brinker and Scherer 1990).

the boron was almost entirely in four-fold coordination. In a follow-up study, Carta et al. explored the effect of borate addition in $40(P_2O_5)–x(B_2O_3)–(60−x)(Na_2O)$ ($10 \leq x \leq 25$ mol%) glasses [166] and confirmed that increasing the amount of borate led to a greater amorphous character and an increase in B-O-P bonds.

2.4.3 Sol-gel silicate-based bioactive glasses

As discussed in section 2.4.2, the sol-gel method is a flexible, solution based approach to making glass. Post hydrolysis, the precursors undergo condensation reactions to form the initial sol, which is then followed by additional polycondensation reactions to generate a gel (*i.e.,* the glass network). While melt-quench derived glasses require a SiO_2 content of $\leq$ 60 mol% in order to be bioactive, HCA formation is possible up to 90 mol% SiO_2 content when produced via sol-gel processing [15]. This is due to the excess –OH groups that are incorporated into the glass network during processing, which lowers N_C to a greater extent [170]. Furthermore, inherently, sol-gel processed glasses have nanoscale porosity, which are generated by the elimination of the organic precursor species during the drying step. This greatly increases their specific surface area and allows for their rapid degradation and HCA conversion when placed in physiological environments [170].

The first sol-gel derived bioactive glasses were created in the early 1990s, which were based on the ternary system $[(100\text{-}x)SiO_2–(x\text{-}4)CaO–(4)P_2O_5$, x = 40, 30, 20 (mol%)] [15, 171]. Fourier Transform Infrared (FTIR) Spectroscopy of these glasses post immersion in tris-buffer solution and SBF, identified HCA associated phosphate peak formation. Attributable to the enhanced textural properties of this sol-gel derived composition, these glasses converted more rapidly to bone-like mineral when compared to melt-quench derived glasses [172]. One of the compositions from Li et al. [15] became a 'standard' sol-gel composition "58S" $[(60)SiO_2\text{-}(36)CaO\text{-}(4)P_2O_5$ (mol%)] and has since been well studied [172, 173].

Christoduoulou et al. showed that the ionic release products from a sol-gel derived 58S glass exposed to primary human osteoblasts promoted the upregulation and gene expression of common osteogenic markers such as alkaline phosphatase, osteocalcin, and osteopontin. However, the results were not statistically significant when compared to non 58S treated well plates [174]. This study also identified that a narrow range of 58S glass dissolution products (Si > 50 ppm) enhanced the occurrence of mature, terminally differentiated osteoblast with prolonged periods in culture.

Another commonly studied silicate-based composition is "70S30C" $[(70)SiO_2\text{-}(30)CaO$ (mol %)]. Although this glass is phosphorous free, it has been shown to be bioactive [175], for example, Radev and coworkers used FTIR to demonstrate phosphate peak formation after soaking in 1.5X SBF

[176]. Lin and coworkers were able to tailor the nanoporosity of this composition by adding specific amounts of trimethylethoxysilane (TMES) during the sol–gel process [177]. Further work studied the effect of protein interactions with these glasses and found that modal pore diameters > 6 nm were accessible to fibrinogen while < 2 nm diameters inhibited their penetration [178]. Along with the addition of TMES, the glass surface could also be controlled by its composition, gelling pH, and final calcination temperature, all of which can affect its bioactivity. Zhang et al. found that sol-gel derived 70S glass particles could be encapsulated with alginate to help with murine embryonic stem cell expansion and differentiation using a bioreactor system [175]. This therapy showed promising results for bone transplantation where the glass particles could improve the bone bonding rate by rapidly forming HCA within the implanted matrix.

Since melt-derived glasses often require a flux in order to lower the melting temperature of the glass as discussed in section 2.4.1, one of the main advantages of the sol-gel process is that it negates the use of sodium, thus allowing for simplified compositions. Since the glass network is essentially formed at room temperature no fluxes are needed and thus are not often included in sol-gel compositions [82]. Notwithstanding this, Na containing sol-gel-derived glasses have been made which are thought to help increase the dissolution rates of glasses. To improve the textural properties of Bioglass®, the sol-gel process has been implemented. For example, Pirayesh et al. created 45S5 glass-ceramic particles through this process [179] where a calcination temperature of 700 °C resulted in 80% crystallinity. However, upon immersion in SBF, an HCA layer was detected after 21 days similar to that of the melt-quench derived glass. However, the HCA layer for the sol-gel glass appeared to be finer [179]. Cacciotti et al. also created a gel-derived 45S5 glass and demonstrated that the calcination temperature and dwell time influenced crystalline phase evolution and microstructure thus impacting the dissolution rate which is important for bone repair [180].

Faurea and researchers recently developed a new method to create a sol-gel derived 45S5 glass by replacing the commonly used nitric acid catalyst with citric acid [181]. These glasses showed increased Ca and P amounts using energy dispersive spectroscopy (EDAX) and SEM within 4 hours, thus demonstrating a significantly more rapid HCA formation compared with the melt-quench derived equivalent. It was also reported that the more mild processing conditions of the citric acid route can be more attractive as it allows for the addition and encapsulation of biomolecules (*e.g.,* drugs, growth factors, etc.) that can help accelerate bone growth [181]. Similarly, by using a multi-step, nitrate-free method, Rezabeigi et al. created a 45S5 sol-gel derived glass with 10 times greater surface areas than that of melt-quench derived glasses [182].

While sol-gel derived glasses show more rapid conversion rates to HCA, they often have low strength (2–3 MPa) [183], and thus are mainly used in low-load sites only. Furthermore, they are often limited to particulate form after calcination since it is difficult to maintain a crack free monolith during drying. To overcome these limitations, the conversion of these glasses to 3D scaffolds may tailor the mechanical and dissolution properties, and potentially widening their potential range of applications. While most bioactive glasses suffer from poor mechanical properties, 3D printing aligned bioactive silicate glass scaffolds has proven successful in large segmental bone defects in a rabbit femur segmental defect model [184].

As discussed in section 2.4.2.1, borate-based sol-gel glasses are uncommon and their applications have so far not been intended for biomedical applications. However, there has also been recent work of incorporating borate in silicate-based sol-gel systems to help improve bioactivity. Cicero et al. doped a silicate based sol-gel glass $(x)B_2O_3[100-x](61)SiO_2$-$(9)P_2O_5$-$(30)CaO$ (x = 0 – 30, mol%) and found that the amount of borate effected the structure and type of HCA formation in SBF [185]. Partially crystalline glasses were obtained with samples up to 10 mol% B_2O_3 while higher borate content produced more vitreous forms. Furthermore, less than 10 mol% B_2O_3 lead to both A-type HCA and HA formation while increasing the amount of borate resulted in amorphous B-type HCA formation. Seyedmomeni et al. found that in a $(64)SiO_2$–$(26-x)CaO$–$(5)P_2O_5$–$(5)ZnO$–$(x)B_2O_3$ (x = 5, 10, 15 in mol%) composition, increasing the borate amount to ≥10 mol% led to both increased crystallinity of the as-made glass but also increased its bioactivity in SBF [186].

3 Statement of the Problem

Bone repair is a major health concern due to an ever-increasing ageing population. While traditional methods such as autografts, allografts, and xenografts have demonstrated success, their drawbacks have led to a great push for novel synthetic bone graft materials. Bioactive glasses offer distinct advantages as their chemistry can be tailored to convert to bone-like mineral while homogeneously releasing ions which help trigger the body's natural healing mechanisms.

Today, the most common and successful bioactive glass, is the Bioglass® 45S5 formulation [82]. While hundreds of studies have been performed on this glass composition along with achieving great commercial success [12], problems still remain with its slow and incomplete dissolution [92], along with its limited processing flexibility and the tendency to crystalize [82]. Although the advent of sol-gel processing has improved the textural properties of these glasses and greatly expanded the compositional range that are considered to be bioactive [15], the dissolution rate is still slow and incomplete due the inherent silicate chemistry.

This has led to investigating alternate bioactive glass systems such as those based on phosphates [110] or borates [19]. While phosphate glasses can fully and linearly dissolve, their dissolution products typically do not increase the pH locally [187], which may reduce the ability for HCA deposition thus impacting their potential in bone repair applications. Due to the unique chemistry of borate glasses, their lower chemical durability allows for rapid and complete conversion to bone-like mineral [17]. Therefore, there has been an increase in interest in using borate glasses for a wide variety of tissue engineering applications from bone repair to wound healing [92]. However, there is potential to improve the reaction rates and widen the compositional range of these glasses to potentially provide rapid, tailored healing.

While sol-gel derived silicate [152] and phosphate glasses [166, 188-191] have been well studied, literature on sol-gel borate glasses is sparse and to the best of our knowledge there are no studies on bioactive sol-gel-derived borate glasses. Thus, this dissertation focuses on the fabrication and characterization of novel, sol-gel derived borate glasses for bone tissue engineering applications. It also expands the processing knowledge of sol-gel borate glasses that can possibly be used in other tissue engineering applications. Despite the great potential of borate-based glasses to be used in bone tissue engineering applications, the use of borate in sol-gel processing is relatively not well documented

and the few existing examples mainly examine the overall glass structure [146, 157, 158, 160, 162, 164]. Thus, there is an opportunity to combine the inherently lower chemical durability of borate glasses with increased textural properties through the sol-gel process to create highly bioactive sol-gel-derived borate glasses for bone tissue engineering applications.

4 Highly Bioactive Sol-Gel-Derived Borate Glasses

Borate glasses have recently gained much interest in bone tissue engineering applications since they are less chemically durable than silicate-based glasses, thus allowing for the rapid conversion to bone-like mineral. It is also well known that the sol-gel process can increase the rate of bone bonding due to its ability to enhance the glass textural properties. While sol-gel borate glasses have been previously fabricated, there are no studies on assessing bioactive compositions. Thus, the objective of Chapter 4 is to describe the processing of six SGBG compositions based on a borate-substituted "45S5" glass and their resultant structural, textural, reactive, and bioactive properties. This work was reported in a manuscript published in the peer-reviewed journal *Chemistry of Materials* and is reproduced below.

Highly Bioactive Sol-Gel Derived Borate Glasses

William C Lepry and Showan N Nazhat*

Department of Mining and Materials Engineering, McGill University, Montreal, QC, Canada
*corresponding author showan.nazhat@mcgill.ca

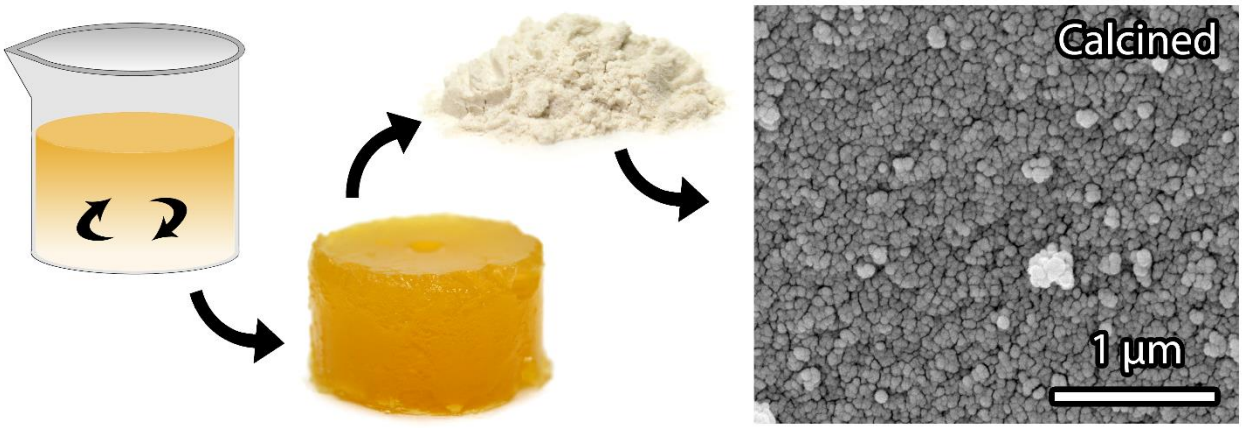

Abstract

Attributable to their low chemical durability, borate-based glasses have been demonstrated to convert rapidly to hydroxy-carbonated apatite (HCA), the inorganic component of bone. However, the effect of sol-gel processing on the bioactivity of borate-based glasses has not been investigated. In this study, the gel and glass forming abilities of six different borate-based glass formulations with borate content ranging from 36 to 61 mol% and based on a previously studied four component melt-derived glass system [$(46.1)B_2O_3$-$(26.9)CaO$-$(24.4)Na_2O$-$(2.6)P_2O_5$; mol%], were investigated. Compared to melt-quench, sol-gel processing fabricated nanoporous glass particles with at least two orders of magnitude greater values for specific surface areas and total pore volumes, which translated to dramatically higher aqueous interaction and ion release rates. Surprisingly, when immersed in simulated body fluid, HCA conversion was achieved in as little as 3 hours for sol-gel derived borate based glasses, demonstrating a 25-fold increase in mineralization rate when compared to melt derived equivalents. The ability of the sol-gel derived borate-based glasses to rapidly convert to bone-like HCA holds promise in numerous potential tissue engineering applications, including the repair and augmentation of mineralized tissues.

4.1 Introduction

Since their initial conception more than 45 years ago, bioactive silicate-based glasses have been widely studied, of which Bioglass® ("45S5"; (46.1)SiO_2-(26.9)CaO-(24.4)Na_2O-(2.6)P_2O_5, by mol%), has been in clinical use for more than two decades [10, 35, 92, 192]. Owing to their ability to release ions in physiological environments, a layer of hydroxy-carbonated apatite (HCA) is formed on the surface of bioactive glasses, which has been shown to promote bonding to bone tissue. However, as a consequence of the slow and incomplete dissolution of silicate-based glasses, there has been a recent growth in interest in bioactive glasses based on other network forming oxides (*e.g.* phosphates, borates) [193, 194]. In particular, and attributable to their lower chemical durability, borate-based glasses have been shown to undergo more rapid degradation and conversion to HCA when compared to silicate-based glasses [16, 17, 19, 131, 138, 195]. Furthermore, while the excess release of boron can be toxic [196], borate-based glasses have been demonstrated to support the proliferation and differentiation of stem cells, *in vitro* [135, 136, 197]. Numerous studies have also shown that these glasses are able to regrow bone with no toxicity, *in vivo* [141, 198, 199]. More widely, borate-based glasses are being used as substrates to treat bone infection [200-202], in wound healing applications [143, 203-205], as well as neural substrates for axon growth [206].

While the majority of bioactive glasses are melt-quench derived, the sol-gel process has demonstrated distinct advantages, including increased surface area, nanoporosity, purity, and homogeneity, coupled with reduced processing temperatures [82, 152, 173, 207]. In contrast to silicate-based sol-gels where the main network former is tetrahedrally coordinated [SiO_4] resulting in a strongly interconnected network [20], in borate-based glasses, the boron ion is typically trigonally coordinated giving it a pseudo three-dimensional character since the BO_3 network is more planar. However, it is also known that in many borate-based glass systems a fraction of the boron can be four-coordinated [BO_4], which depends on the amount of alkali metal present [208, 209]. Nevertheless, this combination of three- or four-fold coordination lowers the network connectivity (N_C), which in turn reduces the chemical durability and increases the dissolution rate of the glasses [17]. More importantly, this makes gel formation difficult, which may have resulted in the sol-gel processing of borate-based glasses being relatively poorly studied. Notwithstanding this, the first sol-gel borate-based glasses, fabricated by Tohge and colleagues [158], were typically either two- or three-component systems often modified with alkali metals such as Na, K, and Li [160, 210] along with other elements such as Si [162] and Ti.[163] Yet, studies regarding their applications are scarce.

Today, borates are commonly added to increase the thermal shock resistance of silicate-based glasses and used to produce non-linear optical materials (*e.g.,* beta-barium borate thin films) through the sol-gel method [161, 211]. For more biomedical focused compositions, boron has been used as a modifier in the sol-gel process [166, 212, 213] and as the main component in a sol-gel precipitation method [214]. Recently, the addition of up to 20 mol% borate was shown to improve the apatite forming ability of silicate-based glasses produced through a sol-gel process [185]. However, to date, a multi-component glass with borate as the network forming oxide has not been made using sol gel processing, and the effect of sol-gel processing on the bioactivity of such borate based glasses has not yet been investigated.

Herein, the creation of bioactive sol-gel derived borate-based glasses (SGBGs) has been attempted for the first time. The gel and glass forming abilities of six different SGBG formulations with borate content ranging from 36 to 61 mol%, based on a previously studied four component melt-derived boron substituted 45S5 glass ("45B5") [17, 134], were investigated. The effect of sol-gel processing and composition on the glass nanoporous properties were analysed. Furthermore, in order to investigate the reactivity and bioactivity of SGBGs, their aqueous interactions, ion release and mineralization in simulated body fluid (SBF) were characterized.

4.2 Experimental

Materials

Boric acid (≥99.5%), monosodium phosphate (>99%), sodium carbonate (≥99.5%), calcium carbonate (≥99%), and anhydrous ethanol were all purchased from Sigma Aldrich (Canada). Triethyl phosphate (>99.8%) and sodium methoxide (25 wt.% in methanol) were obtained from Fisher Scientific (Canada). Calcium methoxyethoxide (20% in methoxyethanol) was purchased from Gelest (USA).

Sol-gel processing

All materials were used as received and all sol-gel processing took place within a nitrogen gas purged glove box. Boric acid was first added to anhydrous ethanol in a watch glass-covered Teflon beaker, and magnetically stirred at 40±3 °C to aid dissolution. Once the solution was clear, triethyl phosphate, calcium methoxyethoxide, and sodium methoxide were added in a drop wise manner at 30 min intervals. After the final addition, the solution was mixed for a further 30 min or until the viscosity was too high for any further stirring. The sol was then cast into polypropylene vials, sealed, and stored at 37 °C for further gelation and ageing. After 10 days, the gels were removed and placed

in crystallization dishes and dried in air at room temperature for 1 day, followed by oven drying at 120 °C for a further 2 days. Table 4.1 gives the investigated SGBG compositions.

To investigate the effect of calcination temperature on the properties of the SGBGs, calcination of the as-made particles were carried out in air at 400, 450, 500, 550 and 600 °C. All temperatures were reached at a heating rate of 3 °C/min, followed by a 2 h dwell time, and then furnace cooled. Following calcination, the particles were ground and sieved to isolate a particle size fraction of 25 – 75 μm and stored in a desiccator until analysis. A melt-derived borate glass ("45B5"), equivalent to B46, was generated through melt-quenching, as previously described.[17]. Here, boric acid, monosodium phosphate, sodium carbonate, and calcium carbonate were thoroughly dry mixed and placed in a Pt crucible then heated at 1100 °C for 2 h with intermediate stirring to insure homogeneity. The melt was then rapidly quenched between two steel plates and the resultant glass was ground to 25 – 75 μm particles.

Particle characterization

The particle size (D_{50}) of the sieved glass powders was determined using a Horiba LA-920 (ATS Scientific Ink., Canada). The specific surface area of the calcined powders (400 °C, n=3) sieved to 25 – 75 μm were measured with nitrogen gas adsorption and desorption isotherms collected with a Micromeritics TriStar 3000 (Micromeritics Instrument Corporation, USA) gas sorption system. Specific surface area (SSA) values were determined from the isotherm with the Brunauer–Emmett–Teller (BET) method.[215] The Barrett–Joyner–Halenda (BJH) method,[216] using the adsorption isotherms, provided the average pore width and pore volume values.

Thermal analysis

Differential scanning calorimetry was performed with a Jupiter STA 449 (Netzsch, Germany) using 30 mg of calcined glass powder in a Pt crucible under flowing argon purge. Analysis was carried out between 50 and 1000 °C at a heating rate of 10 °C/min and the output was used to calculate glass transition and crystallization temperatures (T_g and T_c, respectively).

X-ray diffraction

X-ray diffraction (XRD) diffractograms of the glasses were analyzed with a Bruker D8 Discover X-ray diffractometer (Bruker AXSS Inc., USA) equipped with a CuKα (λ = 0.15406 nm) target set to a power level of 40 mV and 40 mA. Using an area detector, three frames of 25° were collected from 15 – 75 2 theta (°) and merged in post processing. Phase identification was carried out using X'Pert Highscore Plus (PANalytical, Netherlands).

Attenuated total reflectance-Fourier transform infrared spectroscopy

Attenuated total reflectance-Fourier transform infrared (ATR-FTIR) spectroscopy was carried out using a Spectrum 400 (Perkin-Elmer, USA) between 4000 and 650 cm^{-1} with a resolution of 4 cm^{-1} using 64 scans per sample. All spectra were baseline corrected and normalized to the total area surface area under absorption bands using Spectrum software (Perkin-Elmer, USA).

Nuclear magnetic resonance

Solid state ^{11}B nuclear magnetic resonance (NMR) was used to examine the structure of the glasses. ^{11}B NMR spectra were recorded on an Agilent/Varian VNMRS300 spectrometer with a ^{11}B frequency of 96.2 MHz. Approximately 2000 accumulations for each spectra were obtained by applying a 90 degree pulse of microseconds every 8 seconds with proton decoupling.

Dynamic vapour sorption

In order to investigate the aqueous interactions of SGBGs, their vapour sorption was examined using a DVS Intrinsic (Surface Measurement Systems Ltd., UK), which measures mass changes (± 0.1 μg) under controlled humidity and temperature. Approximately 5 mg of SGBG particles was placed in an aluminum pan and inserted into a chamber at 37±0.05 °C. Two methods of analysis were carried out: 1) the relative humidity (RH) was increased stepwise at 5% RH up to 90% RH then back down to 0% RH while the relative mass change was measured when equilibrium was reached or after maximum of 4 h; 2) the glass particles were directly exposed to 90% RH for 6 h, and then to 0% RH for a further 6 h.

Inductively coupled plasma optical emission spectrometry

Release of boron, calcium, sodium and phosphorus ions from glass powders in deionized water (DIW) at a 1.5 mg/mL ratio, were quantified using an inductively coupled plasma– optical emission spectrophotometer (ICP-OES, Thermo Scientific iCAP 6500, USA). Aliquots of 10 mL were filtered through a 0.2 μm nylon filter and stored in a 15 mL falcon tube to which 4% (w/v) nitric acid (Fisher Scientific, Canada) was added. NIST standards were used as calibration values. The pH of the DIW solution was measured at each time point using an Accumet XL20 pH meter (Fisher Scientific).

Scanning electron microscopy

Scanning electron microscopy (SEM) was used to investigate the morphological properties of the glass powders. Samples were sputter coated with Au/Pd and analysis was performed with an Inspect F50 Field Emission Scanning Electron Microscope (FEI Corporation, USA) at 10kV. To determine HCA conversion, Energy Dispersive Spectroscopy (EDS) using an attached EDAX and a

TEAM EDS Analysis System was performed at 20kV on 8 unique glass surface areas to determine the Ca/P ratio at the 6 h and 7 d time points.

Bioactivity

The *in vitro* mineralization of the glasses was examined using Kokubo's SBF (pH 7.4) [117]. Glass powder was added to sterile 50 mL falcon tubes containing SBF at a 1.5 mg/mL ratio and stored at 37±1 °C. Twice per day, the vials were gently agitated in order to prevent agglomeration. Mineralization of the glasses was examined at 6 h, 1 d, 3 d, and 7 d time points when the powders were gently rinsed twice with DIW then twice with ethanol, dried overnight at room temperature, and then dried in an oven at 60 °C for 1 d. The pH of the SBF solution was measured at each time point using an Accumet XL20 pH meter (Fisher Scientific).

4.3 Results and Discussion

Sol-gel processing

Figure 4.1 provides an overview (using B46) of the sol-gel process. During this process, boric acid was dissolved in ethanol, which created excess water, thus allowing for hydrolysis and polycondensation reactions, and eventually leading to the gelling of the precursor materials. A schematic of this proposed network formation is presented in Figure S4.10. All compositions formed a gel, as qualitatively confirmed by placing the storage vials upside down and noting no flow. The viscosity of all compositions increased post mixing and sol formation was initiated almost immediately, except for B36, which exhibited two distinct phases; a bottom precipitate layer, and a clear gel layer similar to the other compositions (Figure S2). Monolithic gels also formed in larger containers (Figure 4.1) demonstrating the scalability of this process. Upon monolith drying, as-made particles were generated, as often observed with non-silicate-based sol-gel systems [158, 166]. XRD

Table 4.1 Glass compositions

Glass	Composition (mol %)				Composition (wt %)			
ID	B_2O_3	CaO	Na_2O	P_2O_5	B_2O_3	CaO	Na_2O	P_2O_5
B36	36.2	31.9	28.9	3	38.6	27.4	27.4	6.6
B41	41.1	29.4	26.6	2.8	43.6	25.2	25.2	6.1
B46	46.1	26.9	24.4	2.6	48.6	22.9	22.9	5.6
B51	51.1	24.4	22.1	2.4	53.6	20.7	20.7	5.1
B56	56.1	21.9	19.8	2.2	58.6	18.4	18.4	4.6
B61	61.3	19.3	17.5	1.9	63.6	16.2	16.2	4.1
45B5	46.1	26.9	24.4	2.6	48.6	22.9	22.9	5.6

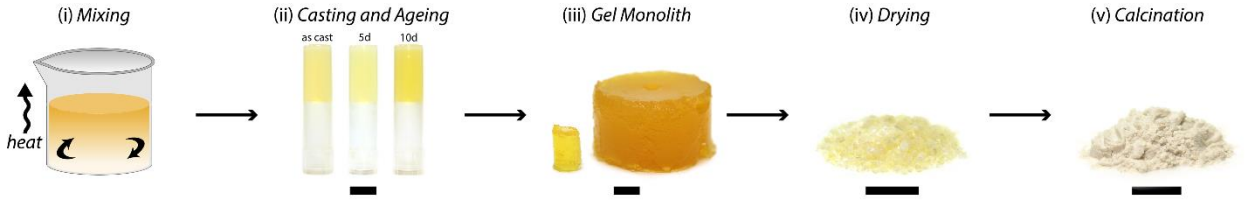

Figure 4.1. An overview of the sol-gel process; (i) mixing of precursor materials, (ii) casting and ageing, (iii) gel monoliths at day 10, (iv) drying, and (v) post calcination at 400 °C (scale bars = 1 cm). (iii) Demonstrates the scaling up possibilities.

diffractograms of the as-made glass particles displayed two broad humps indicating their amorphous and homogenous nature, except for B36, which displayed a number of minor peaks, attributable to a precipitate phase (Figure S4.11).

XRD diffractograms of SGBGs calcined at different temperatures indicated their progressive crystallization with temperature, with low borate content glasses crystallizing at lower temperatures (Figure 4.2). All SGBGs underwent crystallisation when calcined at 600 °C, with the majority resulting in a form of Na-Ca-B phase, indicating the successful incorporation of the precursors into the glass network during processing. It was also found that glasses with higher sodium content tended to crystallise at lower temperatures; an effect previously observed in sol-gel derived silicate-based glasses [163]. This was corroborated by ATR-FTIR spectroscopy which showed sharp, doublet peaks at increased calcination temperatures, indicating crystallization (Figure S4.12).

Properties of calcined SGBGs

Since all SGBGs remained amorphous post calcination at 400 °C, this temperature was chosen in this study to investigate the properties of the various glasses. Calcination at this temperature yielded glass particles of high SSA and large pore volume values (Table 4.2). There was an increase in these parameters with an increase in glass borate content, indicating that the low borate content glasses

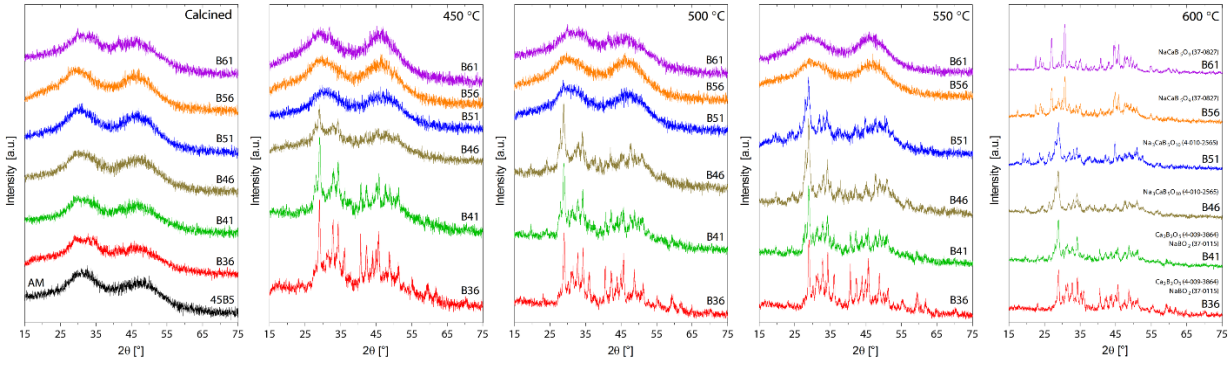

Figure 4.2 Effect of calcination temperature on SGBG structure. XRD diffractograms of calcined glasses indicate the amorphous characteristics by the presence of two broad humps. Crystallization of the glasses was initiated at higher calcination temperatures and was dependent on SGBG composition. All SGBG compositions crystallised at 600 °C.

Table 4.2 Glass Textural and Thermal Properties: Average Median Diameter (D_{50}), Specific Surface Area (SSA), Average Pore Width and Average Pore Volume as well as Glass Transition Temperature (T_g) and Crystallization Temperature (T_c)

ID	D50 (μm)	SSA (m^2/g)	Pore Width (nm)	Pore Volume (cm^3/g)	T_g (°C)	T_c (°C)
B36	34.7	54.9 ± 7.7	32.8 ± 2.0	0.42 ± 0.06	431	474
B41	34.6	71.8 ± 8.3	33.2 ± 1.9	0.65 ± 0.11	441	510
B46	43.8	93.8 ± 8.2	28.9 ± 0.7	0.74 ± 0.05	453	525
B51	33.7	114.2 ± 14.9	32.9 ± 1.0	0.94 ± 0.18	474	579
B56	38.8	121.0 ± 12.9	29.6 ± 0.4	0.98 ± 0.11	485	632
B61	47.1	138.4 ± 11.8	29.0 ± 0.7	1.18 ± 0.12	484	639
45B5	44.1	0.238 ± 0.017	34.0 ± 8.6	0.00089 ± 0.00006	473	531

underwent greater extents of densification at lower temperatures, likely leading to their earlier crystallization (Figure S4.13) [217]. In contrast, the average pore width remained consistent, which can be attributed to the uniform processing conditions. Compared to the melt-derived 45B5, the SSA and total pore volume of B46 were ~400 and ~800 times greater, respectively. On the other hand, an increase in the calcination temperature of B46 led to a decrease in these parameters (Figure S4.13). Thermal analysis of the calcined SGBGs indicated that there was an increase in both T_g and T_c with an increase in glass borate content and corroborated their crystallization trends observed through XRD. Previously, it has been shown that the addition of B_2O_3 increased the T_g of phosphate-based glasses [165].

ATR-FTIR spectroscopy was used to analyse the bonding regions of the calcined SGBGs (Figure 4.3). The three main regions associated with borate-based glasses were present at 850 – 1200 cm^{-1} (B–O stretching of BO_4 units), 1200 – 1500 cm^{-1} (B–O stretching of BO_3 units), and a band at ~720 cm^{-1} attributable to the B–O–B bending of BO_3 units, which was more defined in lower borate content glasses [218-220]. With a decrease in glass borate content, the broad band between ~942 and ~1000 cm^{-1}, attributable to the B–O linkages of BO_4 [165, 221-223], formed a defined shoulder peak at ~870 cm^{-1}, which is characteristic of the B–O stretching of boroxol rings as observed in the B36 to B51 range of the SGBGs. A comparison of the spectra of 45B5 and B46 indicated that both glasses were of analogous structures as they displayed similar peaks.

^{11}B MAS NMR spectroscopy provided geometrical information on the borate unit (Figure 4.3). All calcined SGBGs exhibited a large, sharp peak near 0 ppm, which can be attributed to ^{11}B nuclei occupying a relatively symmetric site in the chemical structure. The small broadening to the right of this peak, as seen in B46 – B61, may be due to ^{11}B in less symmetric sites. B36, B41, and B61 showed

greater broadening on the left side, which may indicate ^{11}B in asymmetric sites (*i.e.,* BO_3) or the same amount but in sites of less symmetry. The resonance associated with BO_4 was quite narrow located in a chemical shift range of 0 and -11 ppm due to its small quadrupole coupling constant. Conversely, BO_3 has a stronger quadrupole interaction and produces a more broad resonance between 14 and 18 ppm. Furthermore, when ^{11}B occupies a state of low symmetry, the relaxation times are relatively short (100 ms) due to its quadrupole nucleus. The glasses analyzed in this study required an 8-second delay between pulses, which suggested that the ^{11}B were in a state of high symmetry and likely to be tetrahedrally coordinated, supporting the ATR-FTIR spectra.

A plot of the relationship between N_C (Supporting Information) and the difference between T_c and T_g of each glass composition, demonstrated a linear correlation (R^2 = 0.9384; Figure 4.3). An increase in the difference between T_c and T_g provides a good estimate of the tendency of the glass to remain amorphous [224, 225], which was used to predict the glass forming ability of the SGBGs. As verified by XRD and ATR-FTIR (Figure 4.2 and Figure S4.12, respectively), glasses with higher borate content remained amorphous at higher calcination temperatures and suggested that these compositions favored glass formation.

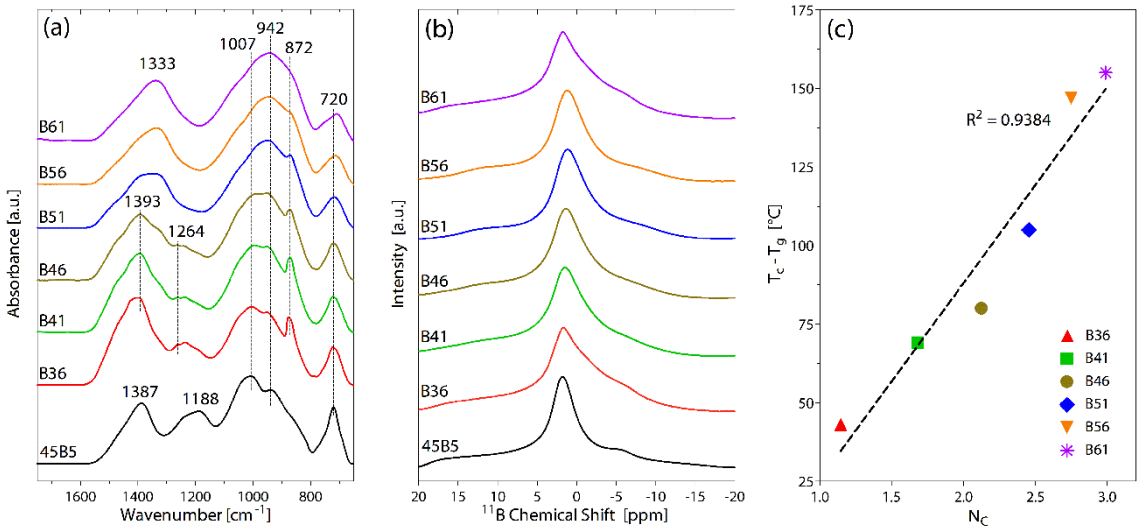

Figure 4.3 Characterisation of calcined SGBGs. (a) ATR-FTIR spectra of the SGBGs calcined at 400 °C and 45B5 indicate typical borate bonding modes. (b) 11B MAS NMR of the SGBGs calcined at 400 °C including 45B5. (c) Glass forming ability as indicated by the trend of the difference between T_c and T_g versus N_C. Compositions with higher borate content were more likely to form a glass, as demonstrated by the increase in the difference between T_c and T_g.

SGBG aqueous interactions and ion release

Attributable to their relatively lower chemical durability, borate-based glasses have been shown to undergo more rapid dissolution when compared to silicate-based glasses [17, 226]. In this study,

DVS was used to investigate the immediate aqueous interactions of SGBGs as an indicator of their reactivity and potential solubility, by gravimetrically measuring their sorption and desorption of water vapour at different RH values [227]. Under a stepwise increase in RH, the % mass change for all SGBGs was similar up to 60% RH, above which there was a significant increase in mass (Figure 4.4). The mass change at 90% RH correlated with glass composition with the lower borate content glass, B36, resulting in ~74% increase, compared to ~36% for B61. Upon decreasing RH, desorption mainly occurred between 90 and 55% RH, and the final mass change at 0% RH ranged between 19.5 and 23.7%, which correlated with SGBG composition. With regard to the melt-derived 45B5, there was no mass change up to 65% RH, above which there was a gradual increase up to ~11% at 90% RH. Desorption in 45B5 mainly occurred between 90 and 65% RH reaching a final mass change of ~3%.

Under the direct exposure of SGBGs to 90% RH, there was an immediate rapid increase in mass within the first 2 h that was followed by a slower rate of increase up to 6 h (Figure 4.4). The rate and extent of mass change (~58 to ~41%) were dependent on SGBG composition, and increased with a decrease in glass borate content suggesting greater extents of reactivity. Upon immediately lowering the RH to 0%, there was a rapid decrease in mass with lower borate content glasses indicating greater extents of final % mass change. In contrast to SGBGs, the direct exposure of 45B5 to 90% RH resulted in ~11% mass increase at 6 h, and was less than that of B46 (~48%). In addition, beyond the first 2 h, 45B5 experienced a relatively linear rate of % mass increase, similar to that experienced by melt-derived silicate [228] and phosphate-based glasses [227].

Therefore, reactivity, as indicated by vapour sorption, was found to be highly dependent on SGBG composition, where atomic and molecular structures play prominent roles in the chemical durability of multi-component glasses [82, 229] and can be related to N_C [127, 129]. It is likely that in the case of lower borate content glasses, the fewer boron units resulted in more terminal groups, specifically OH^-, which were more prone to aqueous interaction and resulted in higher extents of mass change. This is particularly relevant to sol-gel derived glasses as these terminal groups are not fully removed during drying and calcination [82]. On the other hand, the role of SGBG textural properties (SSA and pore volume) were prominent as B46 and 45B5 experienced drastically different % mass changes.

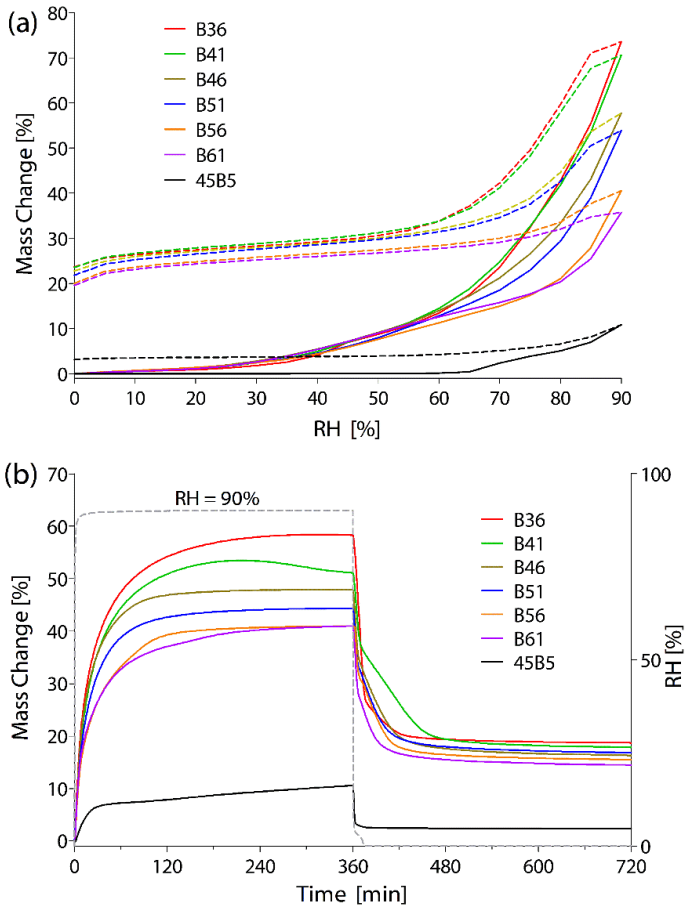

Figure 4.4 Reactivity through vapour adsorption. (a) The stepwise increase in % RH, with adsorption (solid line) and desorption (dashed line), indicated that lower borate content glasses experienced higher % mass changes. (b) The direct exposure to 90% RH showed a rapid increase in mass. The rate and extent of mass change were dependent on SGBG composition, and increased with a decrease in glass borate content suggesting greater extents of reactivity.

ICP-OES measurements up to day 7 in DIW revealed the release of all four SGBG components (Figure 4.5). There were rapid rates of release of boron and sodium ions, which were dependent on borate and soda contents in the SGBGs, respectively. Beyond the 6 h time point, boron and sodium ion concentrations remained constant, indicating their full release. Interestingly, while the release rates of calcium and phosphorus ions were also rapid within the first 6 h, the extents of the release of these ions was inversely related to glass composition. Furthermore, beyond the 6 h time point, there was a concomitant decrease in the concentrations of these ions in solution that was presumably due to their complexing. The rates of ion release from the SGBGs were supported by changes in DIW pH, rapidly increasing within the first 6 h, then stabilising at a constant value, which suggested full ion release (Figure S4.14).

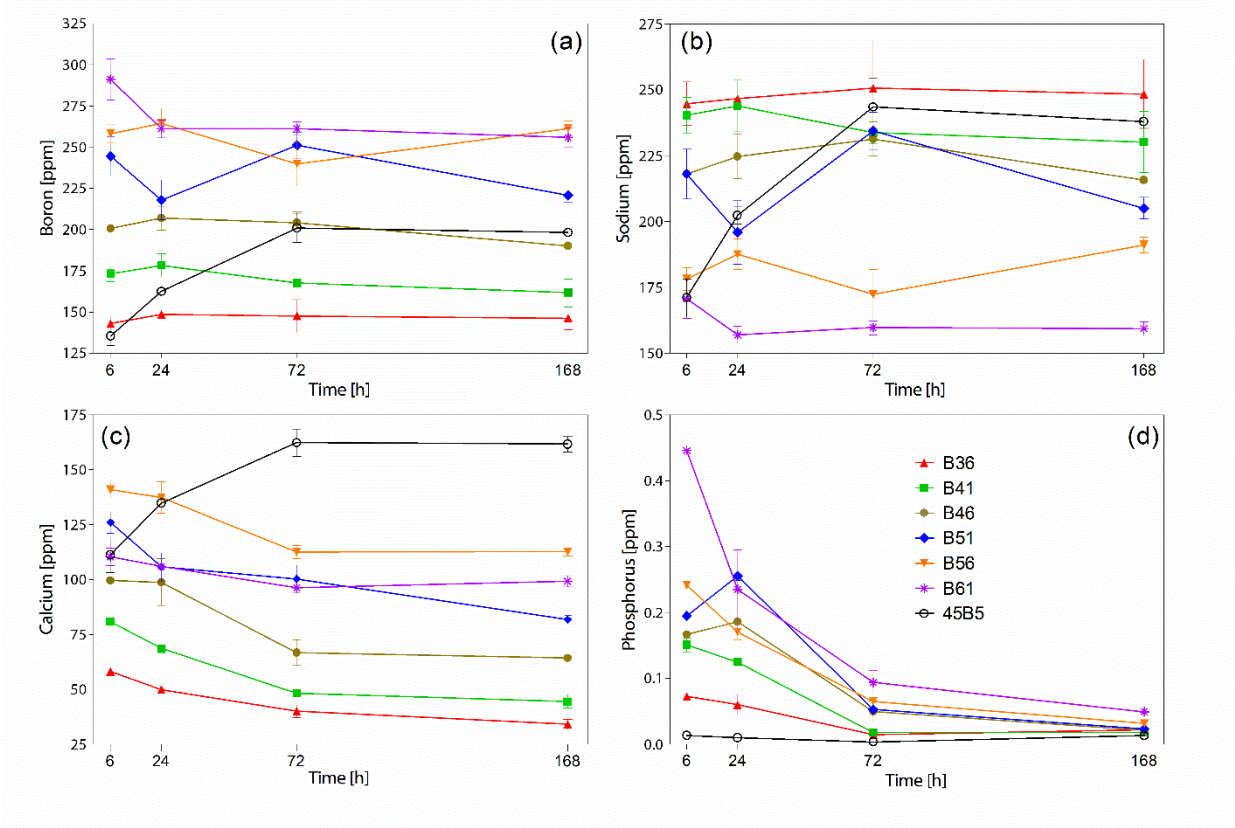

Figure 4.5 SGBG ion release. (a) Boron, (b) Calcium, (c) Sodium, and (d) Phosphorus ion release in DIW as measured through ICP-OES.

The ion release profiles from SGBGs were distinct from those of the melt derived 45B5, which demonstrated a slower, more gradual release rate, where by day 3, the concentration of boron ions in solution reached a similar level to that of B46 achieved after 6 h. Sodium ion release was also higher in 45B5, which may be due to the lower release of boron ions, leading to a more basic solution, as previously reported [17]. The higher extent of sodium ion release resulted in higher pH values, even with the significantly lower textural properties of the melt-derived 45B5. Furthermore, the release of calcium ions from 45B5 displayed a contrasting trend to that of B46, where after the 6 h time point, it steadily increased in concentration and eventually stabilized at day 3. The extent of phosphorus ion release from 45B5 was found to be at least 10-fold lower when compared to B46.

Bioactivity in SBF

The bioactivity of the various SGBGs was investigated up to day 7 in SBF. ATR-FTIR spectroscopy indicated that carbonated-apatite was initiated in as little as 6 h for all SGBGs, through the formation of a strong band at ~1020 cm^{-1} along with shoulders at ~961 and 1062 cm^{-1}, which are characteristic of the bending modes ν1 and ν3 of PO_4,$^{3-}$ [230] respectively (Figure 4.6). In addition,

the broad bands at ~1470 and ~1421 cm^{-1} can be attributed to the stretching mode (ν1) and (ν3) of CO_3^{2-}, respectively, [231, 232] while the weak band at ~1640 cm^{-1} is due to the bending mode (ν2) of water [233, 234]. The sharp peak at 870 cm^{-1} also indicates the bending mode (ν2) of CO_3^{2-} as is commonly associated with carbonated-apatite [231, 232]. However, this peak was also observed in the as-made SGBGs (Figure 4.3), particularly in lower borate content glasses as the B-O stretching of boroxol rings, suggesting a combination of both structural forms. An increase in exposure time to SBF corresponded with these peaks becoming sharper and more defined, indicating the progressive

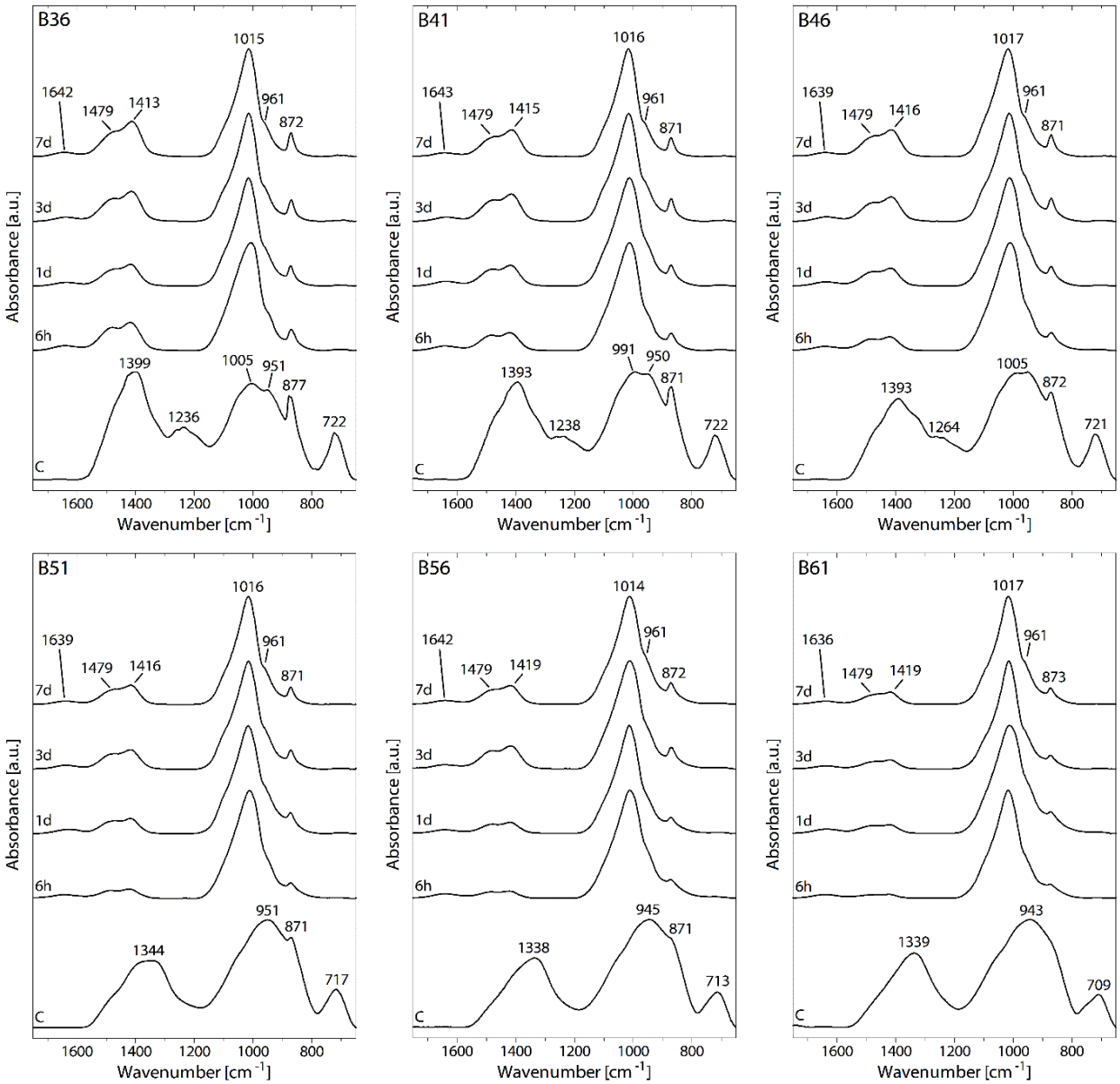

Figure 4.6 Mineralization in SBF solution. ATR-FTIR spectra before and after immersion in SBF for 6 h, 1 d, 3 d, and 7 d. The bending mode (v3) of PO_4^{3-} at ~1020 cm^{-1}, which is characteristic of apatite formation, was observed at the 6 h time point and became more defined at longer times in SBF.

crystallization of HCA. While higher borate containing SGBGs presented more defined phosphate peaks at earlier time points, the spectra at day 7 indicated smaller carbonate peaks.

XRD analysis confirmed apatite formation in 6 h as indicated by the appearance of peaks at ~25 and ~32° 2θ; characteristic of hydroxyapatite ("•", JCPDS 9-0432) where higher borate content glasses indicated more defined peaks (Figure 4.7). At day 1, all SGBGs displayed more prominent broad apatite peaks, which may indicate the formation of nanometer-sized or partially crystalized HCA [17]. On the other hand, B36 showed the formation of a calcite phase ("□", JCPDS 5-0586),

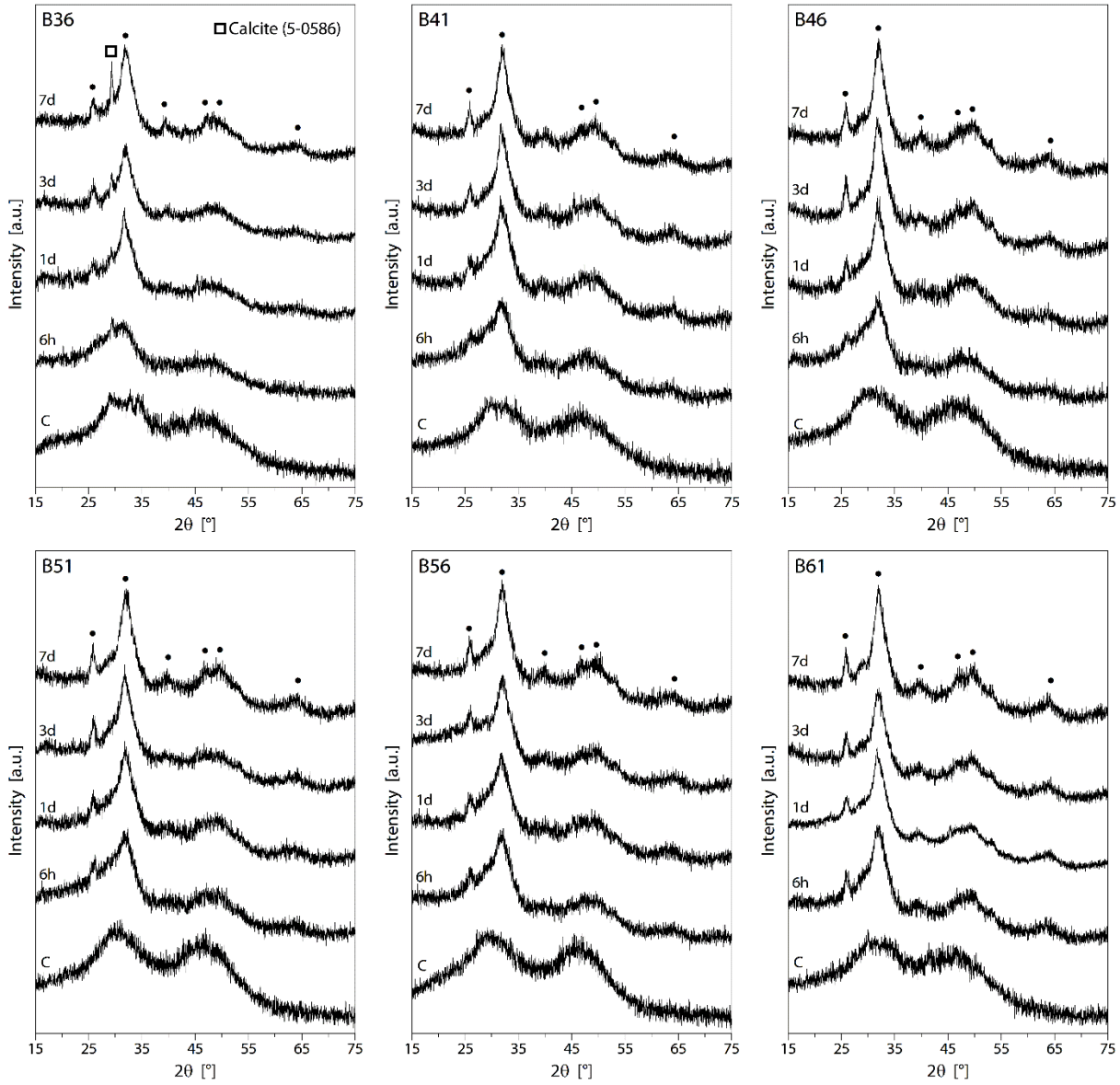

Figure 4.7 Mineralization in SBF solution. XRD diffractograms before and after immersion in SBF for 6 h, 1 d, 3 d, and 7 d. Characteristic hydroxyapatite ("•" JCPDS 9-0432) peak formation initiated at the 6 h time point and became more defined at longer times in SBF.

attributable to its higher lime content, along with the lower N_C likely resulting in calcite forming terminal groups. Furthermore, and in line with that observed in DIW, the increase in the pH of SBF solution corresponded with glass borate content, thus favoring HCA formation (Figure S4.14). Indeed, the conversion mechanism of borate-based glasses to hydroxyapatite is thought to be similar to that of Bioglass® 45S5, but without the formation of an SiO_2 rich layer [17, 219]. It has been described that in the case of borate-based glasses, an HCA is initially formed on the outer glass surface which then continually reacts towards its center, causing a reduction in volume, until full conversion has taken place [219]. This has been attributed to the relatively rapid release of BO_3^{3-} and Na^+ ions, while the remaining Ca^{2+} and PO_4^{3-} ions from the glass migrate to the surface and react with similar ions in the SBF solution leading to formation of an amorphous calcium-phosphate layer that eventually crystalizes into HCA. With the SGBG formulations investigated in this study, it is proposed that a similar mechanism of conversion occurs, yet at a significantly more rapid rate compared to melt-derived glasses, attributable to their significantly higher textural properties and rapid ion release rates. Therefore, in order to further examine the effect of sol-gel processing on the bioactivity of borate-based glasses, the rates of mineralization of B46 and 45B5 were directly compared. Figure 4.8 shows

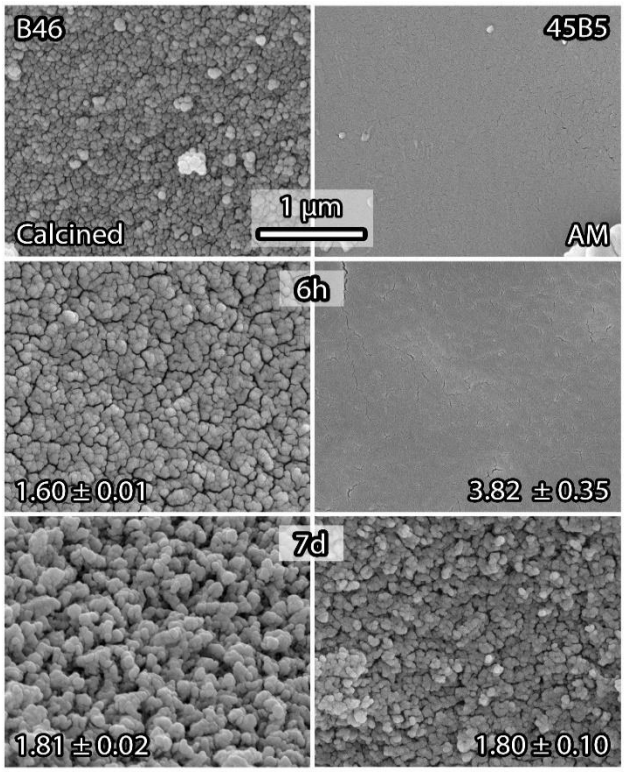

Figure 4.8 Morphological characterization of B46 and 45B5 as a function of time in SBF. The initial textured surface of the calcined B46 increased in roughness with time in SBF. As-made 45B5 demonstrated a smooth surface that became rougher with time in SBF. EDA EDAX of B46 at 6 h indicated a Ca/P ratio of 1.6, closely resembling that of hydroxyapatite. EDAX of both glasses at day 7 indicated similar Ca/P ratios.

the SEM micrographs of these glasses as a function of time in SBF (Figure S4.15 shows the SEM micrographs of all glasses at more extensive time points in SBF). Attributable to sol-gel processing, the surface of calcined B46 exhibited a rough, nanoporous texture [82]; corroborating the textural properties in Table 4.2. In contrast, 45B5 displayed a relatively smooth surface appearance, typical of melt-derived glasses. However, surface roughness in both glasses became more apparent with time in SBF, as has been previously observed in borate-based glasses [219, 235]. EDAX analysis of B46 after 6 h in SBF indicated the rapid formation of an apatite-like calcium-phosphate layer, with a Ca/P ratio approaching that of HCA (1.60 ± 0.01). This was in contrast to 45B5, where the Ca/P ratio at the 6 h time point was more reflective of the glass composition. However, by day 7 in SBF, a comparable Ca/P ratio was observed in both glasses. ATR-FTIR spectroscopy of the glasses at earlier time points in SBF indicated that HCA-like formation was achieved in as little as 0.5 h in B46, compared to 3 d in the case of 45B5 (Figure 4.9). Furthermore, XRD diffractograms showed that HCA formation was initiated after 3 h for B46, compared to 3 d for 45B5. This demonstration of the highly bioactive nature of SGBGs, is unprecedented, and can be attributed to their ability to release greater extents of phosphate ions, thus favoring rapid HCA formation in SBF. Indeed, in assessing the bioactivity of melt-derived borate-based glasses, numerous studies have utilized either 0.02 M or 0.2 M K_2HPO_4 solution [226, 235-238], which provide supraphysiological concentrations of phosphate ions (20 and 200 fold higher compared to that in SBF, respectively) to enable calcium-phosphate formation and the eventual conversion to hydroxyapatite [17]. As a comparison to SBF, this study also investigated the mineralization of B46 and 45B5 in 0.02 M K_2HPO_4. It was found that apatite formation initiated within 6 h in both glasses, indicating that K_2HPO_4 artificially promoted rates of mineralization in melt

derived borate-based glasses (Figure S4.16). Therefore, while the use of SBF in assessing *in vitro* bioactivity has been questioned [119], it can be regarded as more representative than K_2HPO_4 solution.

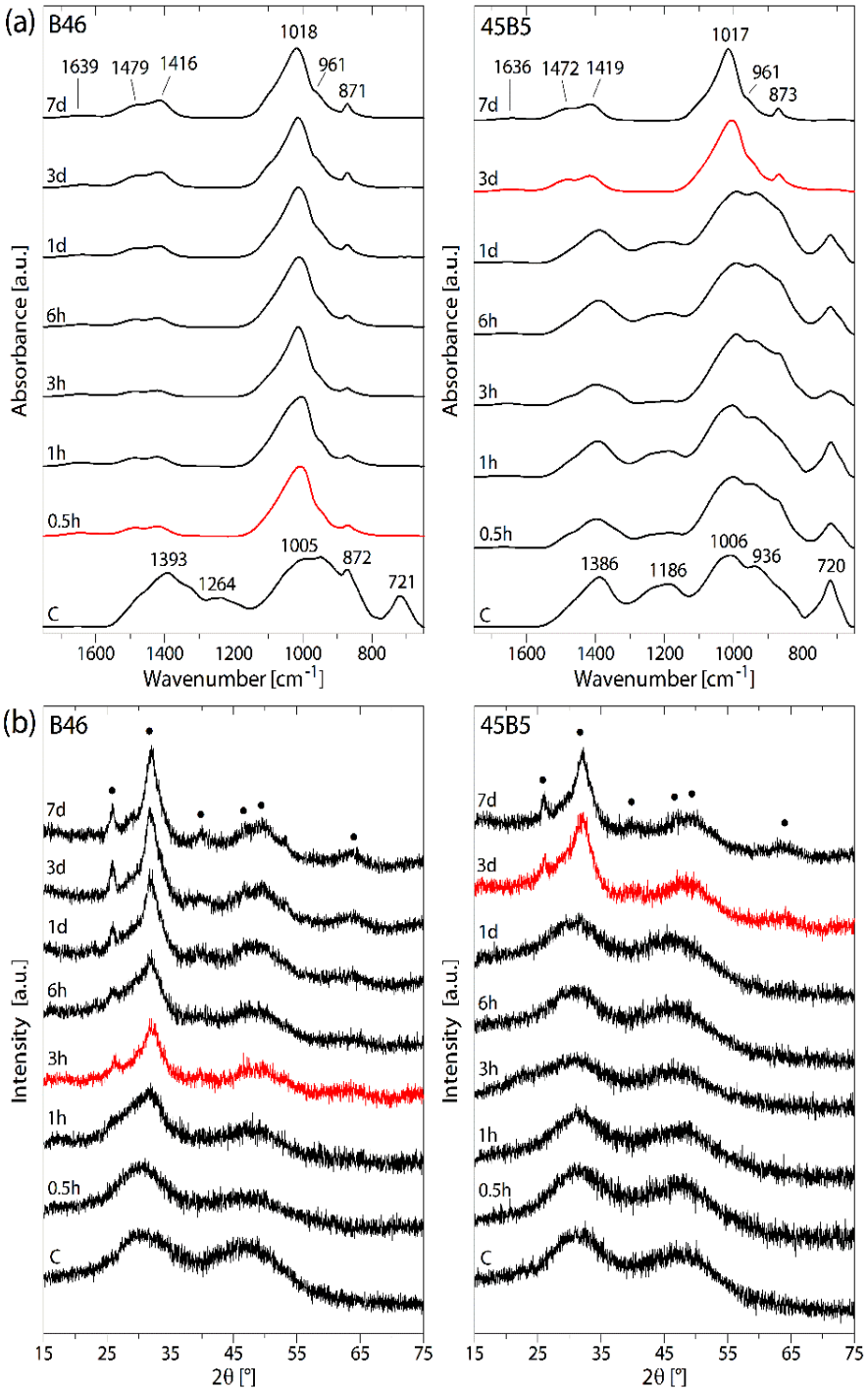

Figure 4.9 Mineralization rates of B46 and 45B5 in SBF solution. (a) ATR-FTIR spectra demonstrated that B46 rapidly (in 0.5 h) converted to carbonated-apatite compared to 45B5 (3 d). (b) XRD diffractograms indicated typical hydroxyapatite peak formation ("•" JCPDS 9-0432) after 3 h for B46 compared to 3 d for 45B5.

In terms of potential uses for the repair and augmentation of mineralized tissues (bones and teeth), a rapid mineralization rate may be desirable as it can potentially lead to faster tissue repair. However, a compromise may be necessary between rapid rates of ion release and biological responses. To this end, and as has been demonstrated with silica-based glasses combined with the sol-gel processing, numerous parameters can be easily adjusted to alter the properties and chemical durability of the glasses, ultimately leading to the control release of therapeutically relevant ions for targeted healing and repair [82]. This will be the subject of further research including the role of higher borate containing glasses in regulating mineralization as well as cellular and tissue responses *in vitro* and *in vivo*.

4.4 Conclusions

Highly bioactive borate-based glasses have been created using a novel sol-gel processing route. All glasses remained amorphous after calcination at 400 °C and demonstrated nanoporosity through high specific surface areas and large pore volumes. Reactivity and ion release from the sol-gel derived glasses were found to be composition dependent. Furthermore, the onset mineralization of all SGBG compositions occurred within 3 hours in SBF, demonstrating at least a ~25 fold increase in bioactivity rate relative to melt-derived borate-based glasses. The ability of the SGBGs to rapidly convert to bone-like HCA holds promise for the repair and augmentation of mineralized tissues. Future work will investigate the effect of these glasses on cellular functions as well as the role of other ionic doping for a broader potential range of tissue engineering, antibacterial, and would healing applications.

Supporting Information

Details on gel network formation, a visual overview of gelation, XRD of the as-made glasses, ATR-FTIR at higher calcination temperatures, pH, SEM, bioactivity using a K_2HPO_4 solution as well as the effect of calcination temperature on weight loss, specific surface area, and pore volume can be found in XXX.

Acknowledgements

This study was supported by Canada NSERC, Québec MEIE, CFI and McGill University Faculty of Engineering Hatch Faculty Fellowship for S.N.N. W.C.L. is also supported by the McGill Engineering Doctoral Award. Drs. Kristian Waters and Fred Morin are gratefully thanked for use of the DVS and NMR, respectively.

4.5 Supporting Information

Sol-gel processing

A proposed process of gel formation is presented in Figure S4.10. It is thought that the hydrolysis and condensation reactions can both occur using the S_N mechanisms involving the nucleophilic attack of either the OR or OH ligands of the electrophilic, trigonal boron with the elimination of water or alcohol [239].

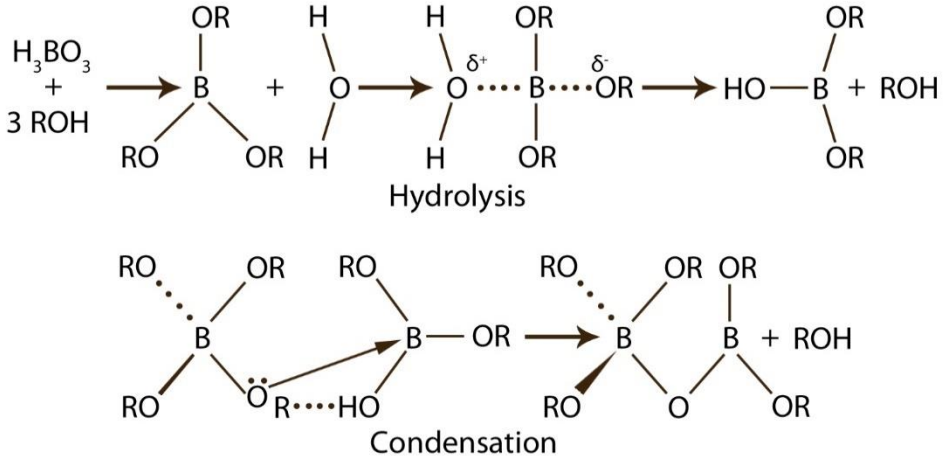

Figure S4.10 Gel network formation. A schematic showing the suggested route to borate glass network formation during the sol-gel process (recreated from Brinker et al. 1990 [187].

The ability of B36 in forming a gel monolith may have been impacted by its low borate (network forming oxide) content. Nevertheless, both of the formed phases were dried together and used for comparison purposes. Lower borate content gels appeared darker orange in colour (Figure S4.11), and upon calcination, all glass particles appeared off-white (Figure 4.1). XRD diffractograms of as-made glass particles displayed two broad humps indicating their amorphous and homogenous nature, except for B36, which displayed a number of minor peaks attributable to a precipitate phase (Figure S4.11).

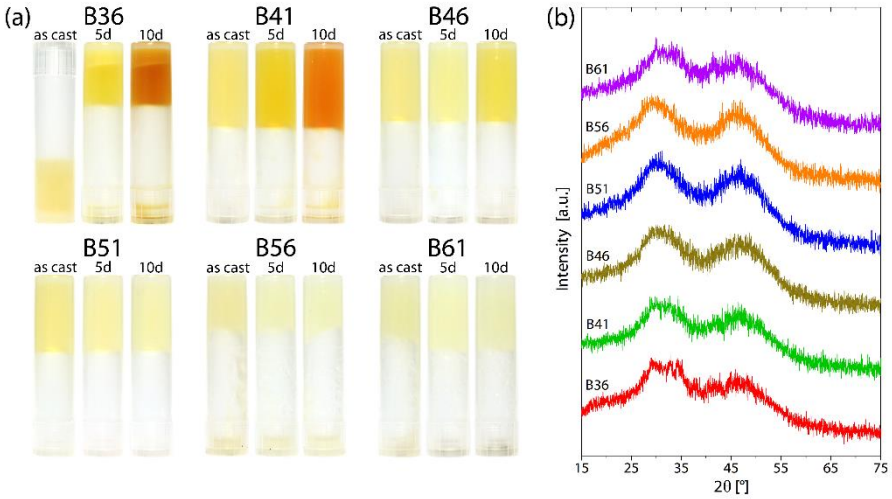

Figure S4.11 Sol-gel derived borate-based glasses. (a) Visual representation of the gels cast over the 10-day gelation period. B36 did not form a gel until day 3, where two distinct phases were observed. (b) XRD diffractograms of the as-made glasses displayed two broad humps indicating their amorphous nature. B36, on the other hand displayed a number of minor peaks, which may be due to a precipitated phase.

ATR-FTIR spectra of the as-made (AM) glasses displayed the peaks associated with borate-based glasses [218-220], which were similar to and more defined than those of the calcined glasses (Figure S4.12). An increase in calcination temperature led to greater extents of crystallization as confirmed by the conversion of rounded peaks to more defined, sharp, doublet peaks. A calcination temperature of 400 °C ("Calcined") was chosen for the remainder of the study since all glasses remained amorphous at this temperature (Figure 4.2), which are likely to be more bioactive compared to partially crystallised glasses [82].

Properties of calcined SGBGs

Reduction in glass surface area is the driving force in densification [217] and the SGBGs with lower borate content indicated the greatest extent of weight loss through calcination (Figure S4.13). On the other hand, an increase in the calcination temperature of B46 led to a decrease in glass particle SSA and pore volume (Figure S4.13).

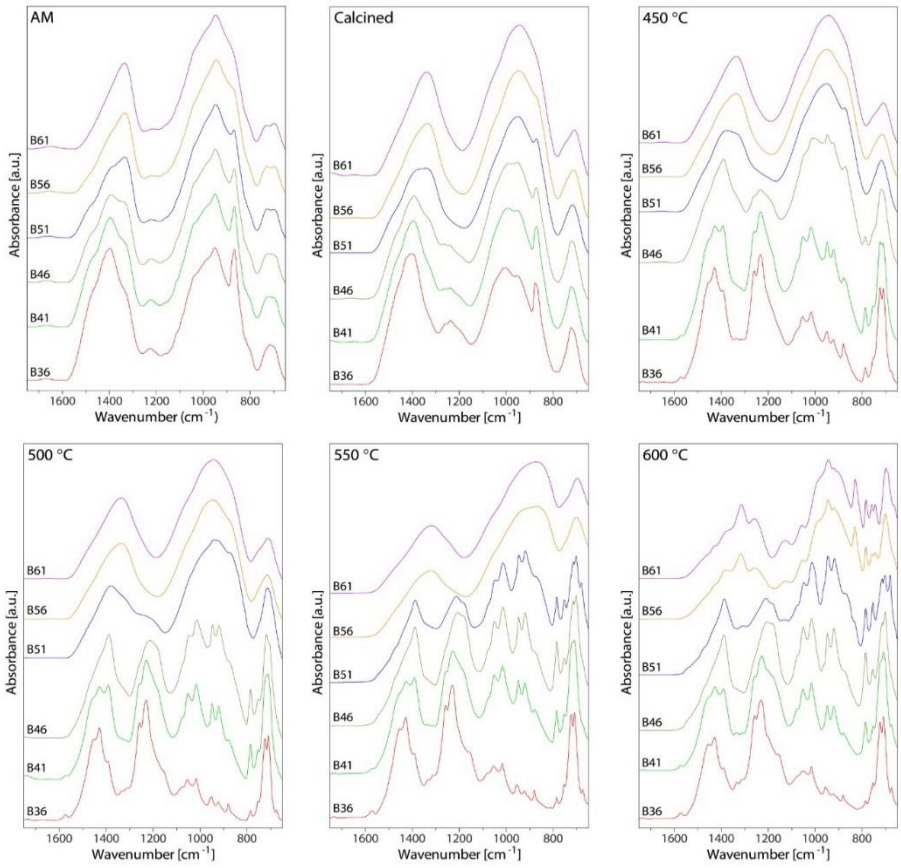

Figure S4.12 ATR-FTIR spectra of the SGBGs, as-made (AM) and calcined at different temperatures. Sharp, doublet peaks indicate increasing crystallization with calcination temperature, corroborating the XRD diffractograms shown in Figure 4.2.

Calculation of SGBG network connectivity

Network connectivity (N_C), which has been used to predict the bioactivity of glasses [127, 129], is a measure of the bridging oxygen bonds per network former (usually calculated for an Si atom in silicate-based glasses). N_C is measured on a scale of 0 to 4, with 4 indicating a fully connected, chemically most stable network (e.g., quartz). On the other hand, glasses with an N_C between 2 and 2.6 have generally been regarded as bioactive [128], *e.g.,* Bioglass® (45S5), which has an N_C of 2.12 [129] as calculated using equation (6):

$$Nc = \frac{4(SiO_2) - 2[M_2^I O + M^{II} O] + 6[P_2O_5]}{[SiO_2]} \quad (6)$$

where M^I and M^{II} represent glass network modifiers sodium and calcium, respectively. Modeling and NMR studies, have indicated that the phosphorous does not enter the glass network (*i.e.,* no Si – O – P bonds are formed) and remains as an orthophosphate [PO_4^{3-}], which is accounted for in the above

calculation [129]. However, Si – O – P bonds can occur at higher P concentrations (> 50 mol%) [130].

In the case of borate-based glasses, while it is also possible to form B – O – P bonds [240], as in the case of silicate-based glasses, it is assumed that the phosphorous does not enter the glass network and is present in an orthophosphate. In addition, if it is assumed that boron is 4-coordinted, as supported by the ATR-FTIR and NMR data (Figure 4.3), then a similar N_C value can be calculated as that for Bioglass®. However, it should be noted that there are three main limitations to using this

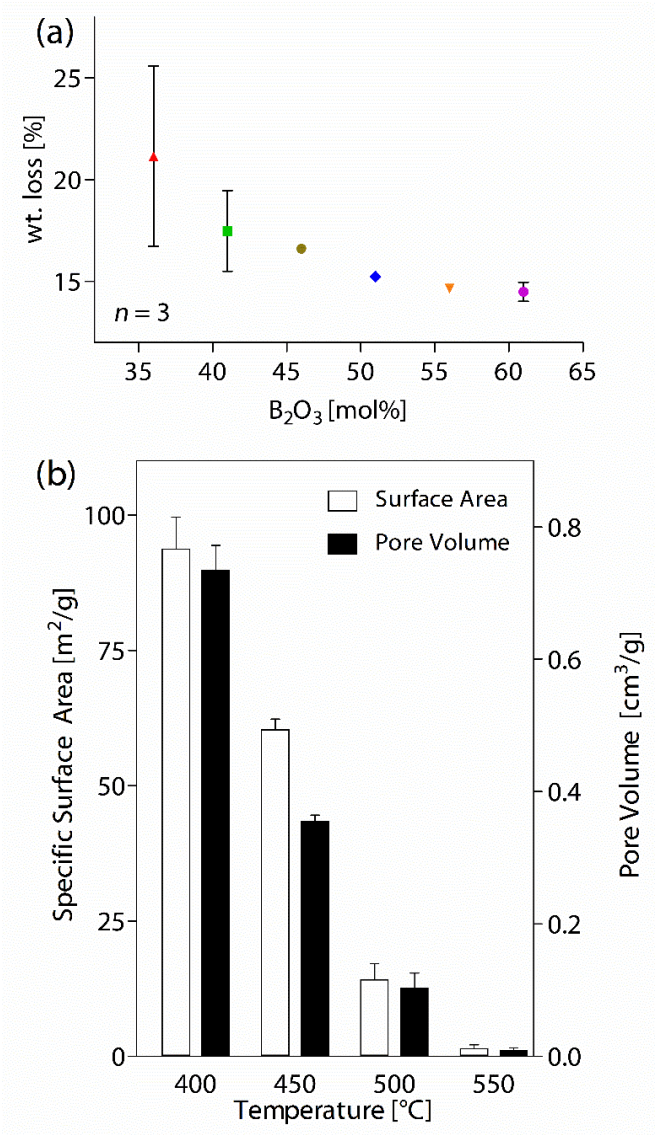

Figure S4.13 Properties of calcined SGBGs. (a) Percentage weight loss of SGBGs post calcination at 400 °C. Glasses with lower borate content experienced greatest extent of weight loss upon calcination. (b) Effect of calcination temperature on B46 SSA and pore volume. There was a decrease in these parameters with an increase in calcination temperature.

approach with sol-gel derived glasses, where: 1) the above calculation does not take into account the increased surface area and porosity; 2) not all boron is 4-coordinated; and 3) the sol-gel process results in residual OH^- groups on the surface, which may contribute to the bioactivity rates of the SGBGs in this study, even in N_C ranges where bioactivity is thought to be inhibited [128]. The latter, has been previously demonstrated for sol-gel derived silicate-based glasses [15].

Measurement of DIW and SBF pH values in the presence of SGBGs

The extent of change in pH of the DIW and SBF solutions was dependent on SGBG composition (Figure S4.14), where lower borate content SGBGs resulted in higher pH values in both solutions, and can be attributed to higher extent of Na^+ ion release [17].

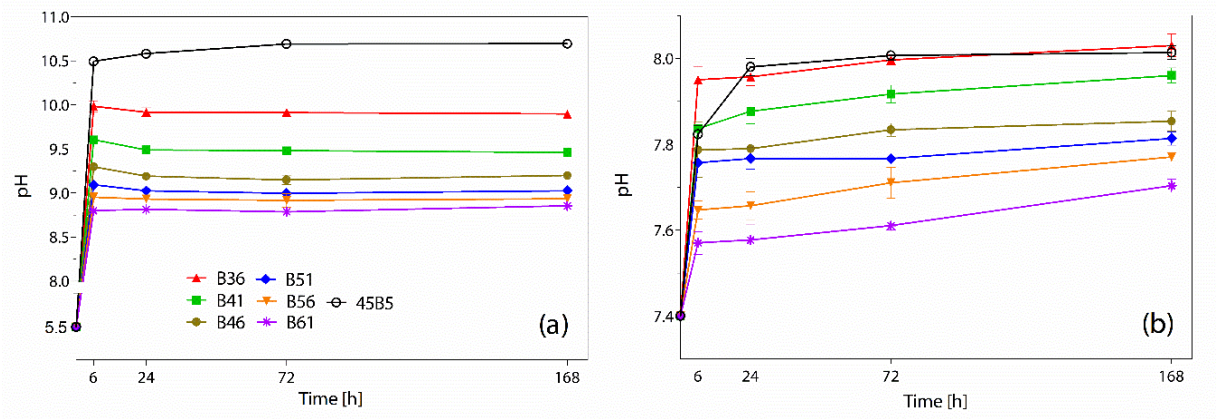

Figure S4.14 Effect of SGBG dissolution on the pH of (a) DIW and (b) SBF. The increase in pH values corresponded with SGBG composition, where glasses with lower borate content (i.e., higher soda content) resulted in greater extents of pH increase.

SGBG mineralization in SBF

Figure S4.15 shows the SEM micrographs of all as-made and calcined (at 400 °C) SGBGs as a function of time in SBF. As-made and calcined SGBGs were comprised of textured porous surfaces, which became smoother after 6 h in SBF, attributable to the washing of loose nanoparticles. However, the surfaces regained their textured appearance with time in SBF, and by day 7, the typically observed HCA morphology was apparent, which correlated with ATR-FTIR and XRD (Figure 4.6 and Figure 4.7, respectively).

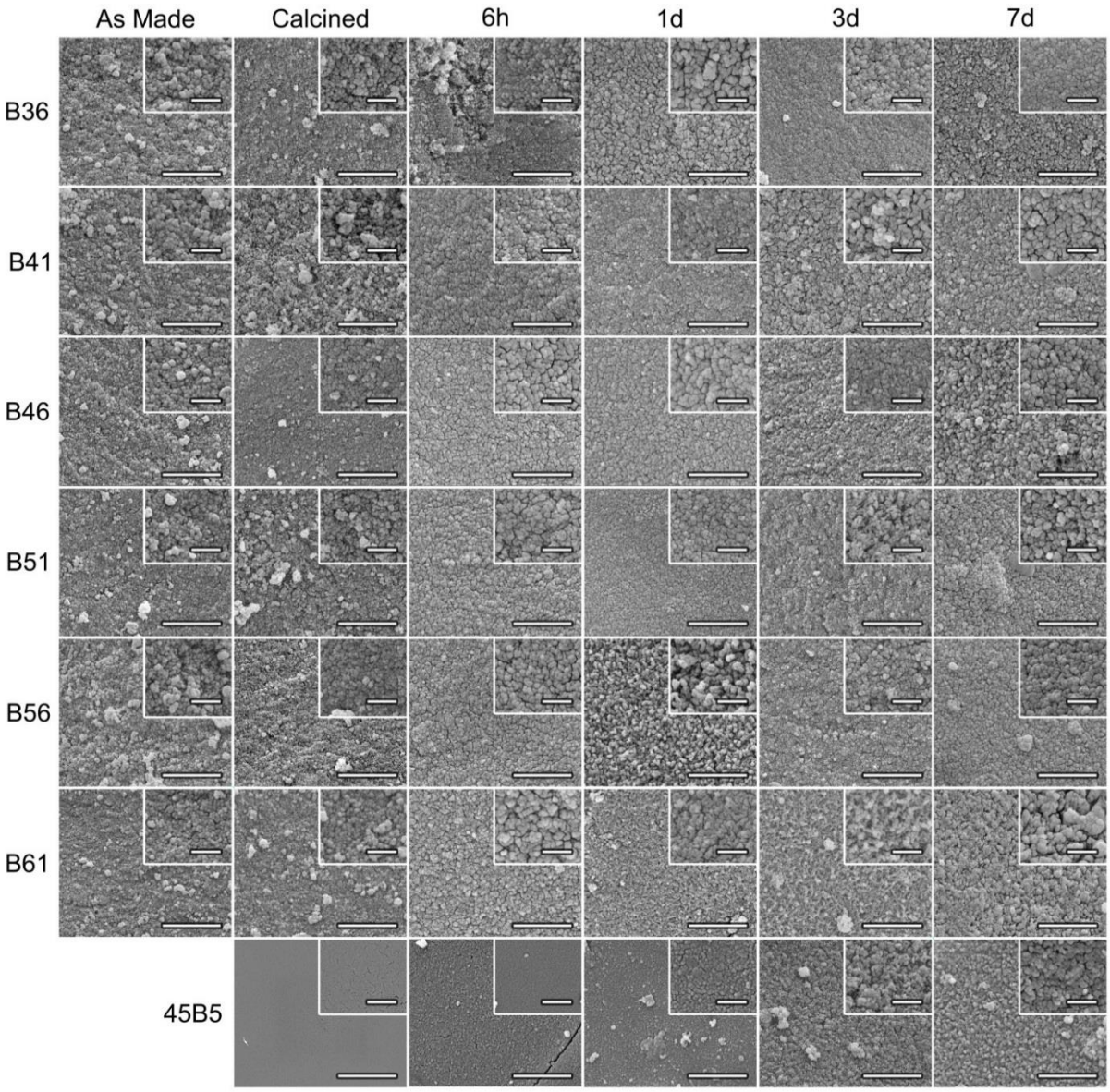

Figure S4.15 Morphology of SGBGs. SEM micrographs of all as-made and 400 °C calcined SGBGs as a function of time in SBF (scale bar = 2 μm, inset = 500 nm). Glass surfaces became more textured with time in SBF; attributable to HCA formation.

Comparing the mineralization of B46 and 45B5 in 0.02 M K_2HPO_4 solution

As a comparison to SBF, this study also investigated the mineralization of B46 and 45B5 in 0.02 M K_2HPO_4, which provided a 20 fold increase in phosphate content compared to SBF. It was found that apatite formation initiated within 6 h in both glasses, indicating that K_2HPO_4 artificially promotes rates of *in vitro* mineralization through the provision of excess, non- physiological concentrations of phosphate ions (Figure S4.16). Furthermore, the appearance of a sharper PO_4^{3-} peak and more pronounced shoulder regions in the ATR-FTIR spectra, indicated that the exposure to

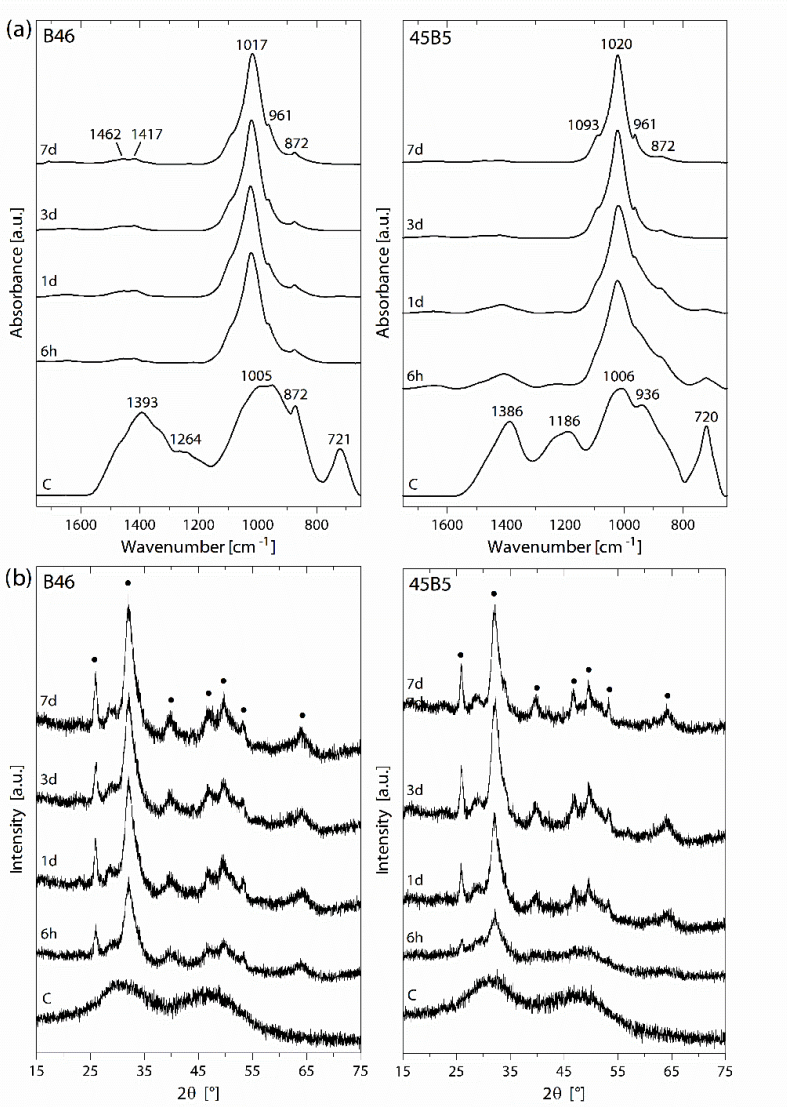

Figure S4.16 Mineralization rates of B46 and 45B5 in 0.02 M K_2HPO_4 solution. (a) ATR-FTIR spectra and (b) XRD diffractograms indicated that apatite peak formation initiated after 6 h in both glasses demonstrating that the K_2HPO_4 solution is prone to giving favorable *in vitro* mineralization results.

K_2HPO_4 did not favor the production of CO_3^{2-} and OH^- peaks, indicators of carbonated-apatite formation.

5 Effect of Processing Parameters on Sol-Gel-Derived Borate Glasses

The sol-gel method has many different processing parameters that can be adjusted to tailor the final glass properties. These parameters have been extensively studied and reviewed for silicate glasses but little literature exists for borate-based glass systems. In the previous chapter, the ability of the sol-gel process in fabricating a range of SGBG compositions was examined. Chapter 5 investigates the effect of various sol-gel processing parameters, on the resultant structural, textural, and bioactive properties of a single SGBG composition. While it was found that, these properties remained relatively similar through each processing variable, calcination at higher temperature, created a glass-ceramic, yet maintained a rapid rate of HCA conversion. This work was published in the Special Larry Hench memorial issue of the peer-reviewed journal, *Journal of Materials Science*, and is reproduced below.

Effect of Processing Parameters on Textural and Bioactive Properties of Sol-Gel Derived Borate Glasses

William C. Lepry, Shiva Naseri, and Showan N. Nazhat*

Department of Mining and Materials Engineering, McGill University, Montreal, QC, Canada
*corresponding author showan.nazhat@mcgill.ca

Abstract

A compositional range of recently developed bioactive sol-gel derived borate glasses (SGBGs) have demonstrated remarkably rapid rates of conversion to hydroxy-carbonated apatite (HCA) in simulated body fluid (SBF). Although the composition of SGBGs did not greatly impact HCA conversion rates, it is still unknown how the sol-gel processing parameters affect the textural properties and thus bioactivity of the glass. In this study, a borate substituted Bioglass® "45S5" formulation [(46.1)B_2O_3-(26.9)CaO-(24.4)Na_2O-(2.6)P_2O_5; mol%], was fabricated using different sol-gel processing parameters including; precursor materials, ageing time and temperature, along with calcination rate and temperature. It was found that a higher calcination temperature led to a partially crystallized glass with almost a magnitude decrease in specific surface area relative to the other glasses. All processing routes resulted in highly bioactive glasses according to Fourier-transform infrared spectroscopy, x-ray diffraction, and scanning electron microscopy, which confirmed HCA formation in SBF in as little as 2 hours. The majority of ion-exchange occurred within 30 minutes, facilitating this rapid conversion to bone-like HCA. Interestingly, the partially crystallized glasses (i.e., glass-ceramics) also underwent full conversion to HCA in SBF. Furthermore, ageing time and temperature did not affect the bioactive properties of these glasses, which allow for significantly reduced processing times. In summary, this study demonstrates that SGBGs can be tailored for targeted tissue engineering applications by varying the sol-gel processing parameters.

5.1 Introduction

Silicate-based bioactive glasses have been extensively investigated for bone tissue engineering applications due to their ability to form a hydroxy-carbonated apatite (HCA) bone-like mineral layer on their surfaces when exposed to physiological fluid, both *in vitro* and *in vivo* [12, 241]. Recently, borate-based glasses have been shown to undergo more rapid conversion to HCA when compared to silicate-based glasses attributable to their lower chemical durability [16, 17, 19, 131, 138, 195]. The combined enhanced and full dissolution rates of borate-based glasses have contributed to an increase in interest in their potential application in bone tissue engineering. Indeed, accelerated HCA conversion rates may be advantageous for mineralized tissue repair, since shorter conversion times could translate to more rapid healing, as has been demonstrated in various bone defect models *in vivo* [141, 198, 199]. Borate-based glasses have also been successfully used as substrates to treat bone infection since they can be loaded with antibacterial drugs such as teicoplanin [200, 242], gentamicin [201] and vancomycin [202]. Furthermore, more recent interest in the potential application of borate-based glasses has expanded into soft tissue such as wound healing [204, 205, 243, 244] and nerve repair [245, 246].

Bioactive glasses have traditionally been made using the melt-quench technique which involves the melting of precursor oxide powders at high temperatures to generate a melt and followed by its rapid cooling (quenching) to maintain the amorphous network. Alternatively, the sol-gel process typically uses liquid based precursors, such as metal alkoxides to allow for the gelling of the glass network through hydrolysis and condensation reactions at ambient conditions. The gelling process is then typically followed by drying and calcination steps to remove any remaining organic products, which also lead to the densification of the resultant amorphous glass [20, 152]. Compared to melt–quench, sol-gel derived glasses offer a number of advantages for biomedical applications such as increased surface area and porosity attributable to lower processing temperatures. These enhanced textural properties translate to quicker ion release and degradation rates and increase the HCA conversion rate [15, 82, 173]. Furthermore, the reduced processing temperatures allow for the incorporation of metallic elements that are typically difficult to include through the melt-quench method, which have been implicated in creating positive biological responses [247].

While sol-gel derived borate-based glasses have been previously fabricated [158, 160, 162, 163, 210, 248], their intended applications have not been biomedically focused. However, in an attempt to increase the bioactivity of sol-gel derived glasses, borate has been added as a modifier to either silicate-

or phosphate-network forming glasses [166, 185, 212]. Furthermore, we have previously demonstrated that sol-gel derived borate glasses (SGBGs) based on B_2O_3;CaO;Na_2O;P_2O_5 with a wide compositional range (36 – 61 mol% B_2O_3) rapidly converted to bone-like mineral in SBF [249]. In particular, and compared to a melt-quench derived equivalent [17, 134], the sol-gel processing of a borate substituted Bioglass® 45S5 formulation [(46.1)B_2O_3-(26.9)CaO-(24.4)Na_2O-(2.6)P_2O_5; mol%] demonstrated at least a 25 fold increase in HCA conversion rates. In order to investigate the impact of processing parameters on the properties of these highly promising SGBGs, in this study, the effects of varying precursor materials, ageing time and temperature, as well as calcination rate and temperature, on their morphological, textural and bioactivity properties were investigated. By adjusting these properties, we aim to tailor these glasses for targeted tissue engineering applications.

5.2 Experimental

Materials and methods

Boric acid (BA; ≥99.5%), trimethyl borate (TMB; ≥ 99%), triethyl borate (TEB; ≥ 99%), and anhydrous ethanol were all purchased from Sigma Aldrich (Canada). Triethyl phosphate (>99.8%) and sodium methoxide (25 wt.% in methanol) were purchased from Fisher Scientific (Canada) and calcium methoxyethoxide (20% in methoxyethanol) was purchased from Gelest (USA). All materials were used as received and all sol-gel processing was carried out in a nitrogen gas purged glove box.

A borate substituted Bioglass® 45S5 formulation (BA 400) [(46.1)B_2O_3-(26.9)CaO-(24.4)Na_2O-(2.6)P_2O_5; mol%], was fabricated as previously described [249]. Briefly, boric acid was added to anhydrous ethanol in a watch glass-covered Teflon beaker, and magnetically stirred at 40±3 °C to aid dissolution in nitrogen atmosphere. After the solution became clear, triethyl phosphate, calcium methoxyethoxide, and sodium methoxide were added in a drop wise manner at 30 minute intervals. After the final addition, the solution was mixed until gelation (< 30 minutes). The sol was then cast in polypropylene vials, sealed, and stored at 37 °C for further gelation and ageing. After 10 days, the gels were removed and placed in crystallization dishes, then dried in air at room temperature for 1 day, and followed by oven drying at 120 °C for a further 2 days. The as-made glasses (oven dried; AM) were calcined to 400 °C at a rate of 3 °C/min, with a 2 hour dwell time, and then furnace cooled.

Table 5.1 and Figure 5.1 provide a summary of the different processing parameters investigated in this study. Both TMB and TEB were used as a substitute for the boric acid precursor, which were added without the addition of ethanol. For the boric acid precursor materials, the following processing parameters were investigated: ageing temperatures of 25 °C (RT) and 65 °C

(65C), ageing times of 0 day (0d) and 30 days (30d), calcination rates of 1°C/min (1C/min) and 10 °C/min (10C/min), and calcination temperatures of 300 °C (BA300), 400 °C (BA400), or 500 °C (BA500). 0d ageing was initiated after the final precursor material was added, which was stirred until gelation, then immediately placed in a crystallization dish to start the drying step, as described above. All glasses followed similar drying and calcination schedules to that used for BA 400, unless otherwise stated. Post processing, all particles were ground and sieved to 25 – 75 μm particle size fraction and stored in a desiccator until further analysis.

Particle characterization

The average particle size (D_{avg}) and median diameter (D_{50}) of the sieved glass powders were determined using a Horiba LA-920 (ATS Scientific Inc., Canada). The specific surface area of the powders (n=3) sieved to 25 – 75 μm was measured with nitrogen gas adsorption and desorption isotherms collected with a Micromeritics TriStar 3000 (Micromeritics Instrument Corporation, USA) gas sorption system. Specific surface area (SSA) values were determined using the Brunauer–Emmett–Teller (BET) method [215] while the Barrett–Joyner–Halenda (BJH) method [216], using the desorption isotherms, provided the average pore width and pore volume.

Bioactivity

The *in vitro* mineralization of the glasses was examined using Kokubo's SBF (pH 7.4) [117]. Glass powder was added to sterile 50 mL falcon tubes containing SBF at a 1.5 mg/mL ratio and stored at 37±1 °C. Twice daily, the vials were gently agitated in order to prevent agglomeration. Mineralization of the glasses was examined at 0.5h, 2h, 6h, 1d, 3d, and 7d time points where the powders were gently rinsed with deionized water then twice with anhydrous ethanol, dried overnight at RT, and then dried in an oven at 60 °C for 1 day.

Attenuated total reflectance-Fourier transform infrared spectroscopy

Attenuated total reflectance-Fourier transform infrared (ATR-FTIR) spectroscopy was carried out using a Spectrum 400 (Perkin-Elmer, USA) between 4000 and 650 cm^{-1} with a resolution of 4 cm^{-1} using 64 scans per sample. All spectra were baseline corrected and normalized to the total area surface area under absorption bands using Spectrum software (Perkin-Elmer, USA).

X-ray diffraction

X-ray diffraction (XRD) diffractograms of the glasses were analyzed with a Bruker D8 Discover X-ray diffractometer (Bruker AXSS Inc., USA) equipped with a CuKα (λ = 0.15406 nm) target set to a power level of 40 mV and 40 mA. Using an area detector, three frames were collected

from 15 – 75 2 theta (°) and merged in post processing. Phase identification was carried out using X'Pert Highscore Plus (PANalytical, Netherlands).

Inductively coupled plasma optical emission spectrometry

Release of boron, calcium, and phosphorus from glass powders in SBF at a 1.5 mg/mL ratio, were quantified using an inductively coupled plasma–optical emission spectrophotometer (ICP-OES, Thermo Scientific iCAP 6500, USA). Aliquots of were filtered through a 0.2 μm nylon filter and stored in a 15 mL falcon tube to which 4% (w/v) nitric acid (Fisher Scientific, Canada) was added followed by dilution. Serial diluted standards of boron (1, 10, 100 ppm), calcium (1, 10, 100 ppm), and phosphorous (0.1, 1, 10 ppm) were used.

Scanning electron microscopy

Scanning electron microscopy (SEM) was used to investigate the morphology of the glasses. Samples were sputter coated with Au/Pd and analysis was performed with an Inspect F50 Field Emission Scanning Electron Microscope (FEI Corporation, USA) at 5kV.

5.3 Results and Discussion

Effect of precursor material on gel formation

In addition to boric acid, glasses were also fabricated using two other borate sources; TMB and TEB. Both of these precursors have been previously used in borate sol-gel synthesis [162, 164, 250] that can potentially provide a processing advantage since they do not require the addition of a solvent (*i.e.,* boric acid with ethanol) and can be added directly to the process. Despite not forming a free standing gel, upon evaporation, an almost translucent gel-like layer was found on the bottom of the crystallization dish when using these precursors and processing methods (Figure 5.1). This layer

Table 5.1 Overview of the Sol–Gel Processing Parameters Investigated in this Study

ID	Boron Precursor	Ageing time (d)	Ageing Temperature (°C)	Firing rate (°C/min)	Calcination Temperature (°C)
AM	Boric Acid	10	40 ± 3	—	—
TMB	Trimethyl Borate	10	40 ± 3	3	400
TEB	Triethyl Borate	10	40 ± 3	3	400
0d	Boric Acid	0	40 ± 3	3	400
30d	Boric Acid	30	40 ± 3	3	400
RT	Boric Acid	10	25 ± 3	3	400
65C	Boric Acid	10	65 ± 1	3	400
1C/min	Boric Acid	10	40 ± 3	1	400
10C/min	Boric Acid	10	40 ± 3	10	400
BA 300	Boric Acid	10	40 ± 3	3	300
BA 400	Boric Acid	10	40 ± 3	3	400
BA 500	Boric Acid	10	40 ± 3	3	500

was then dried for 2 days at 120 °C and calcined at 400 °C, resulting in glass powder similar to that produced using boric acid as the precursor material. Change in ageing time and temperature appeared not to impact gel formation. However, gels aged for 30d in storage vials appeared to have more pore liquid on the surface, which was attributed to greater network formation and gel shrinkage with increased ageing time.

Typically, in sol-gel processing, water is added to hydrolyze the precursors and form OH groups, which allow for the condensation reactions to form the gel and essentially glass network [152]. In this study, while no water was explicitly added, it was created through the mixing of boric acid and ethanol, which is thought to hydrolyze the remaining species [249]. When TMB and TEB were used during processing, neither water nor ethanol were added, and as a consequence prevented hydrolysis to occur, which may explain the lack of gel formation. Often, boric acid is precipitated when water is added to either of these precursors [160, 164] which is why it was avoided. However, it is recognized that further work is required to optimize the processing of SGBGs through these precursors. It is hypothesized that by changing the glass composition or processing parameters, TMB or TEB based sol-gels can result in free standing gel monoliths similar to those seen in Figure 5.1. Nevertheless,

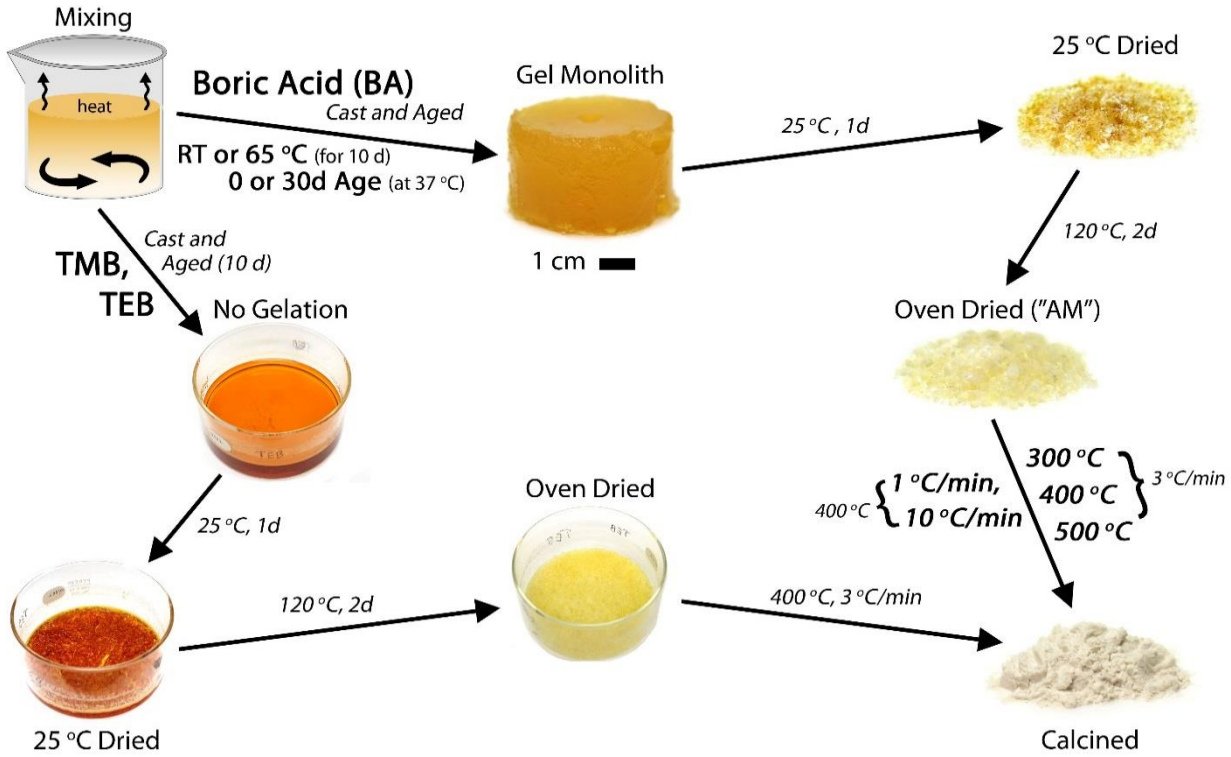

Figure 5.1 Schematic of the sol-gel processing route and adjusted parameters (in bold). For the boric acid precursor route, images referring to BA 400 are shown. For the TMB and TEB precursor routes, images for TEB are shown with TMB giving similar results.

despite the lack of gel formation, both precursors resulted in glass compositions with high surface areas and porosities.

Textural properties

The average particle diameter (42.8±5.5 μm) and median particle size (34.6±7.3 μm) values were consistent across all glasses (Table 5.2). All glasses resulted in high SSA values, which were at least two orders of magnitude higher than that of a similar glass composition made through melt-quenching [249]. AM (91±6 m^2/g) , BA 300 (106±1 m^2/g), and BA 400 (95±3 m^2/g) resulted in similar ranges of SSA values, as previously reported [249]. However, calcination at 500 °C (BA 500) led to an almost magnitude of order decrease in SSA (15±1 m^2/g). The linear isotherm plots for each of these glasses are shown in Figure S5.7. This was due to increased densification at higher temperatures, thus reducing porosity and SSA (Figure S5.8).

Despite the lack of gelation, both TMB and TEB generated particles of high SSA values (75±4 and 81±2 m^2/g, respectively), which were in a similar range to that of BA 400 (95±3 m^2/g). Ageing time, also appeared to influence SSA, where 0d (131±7 m^2/g) indicated higher values than those of either 30d or BA 400 (aged for 10 days), which in turn were similar. While RT and BA 400 were of similar SSA values, ageing at 65 °C resulted in a slight increase (119±6 m^2/g). Calcination rate played a minor role as the slower (1 °C/min) and faster (10 °C/min) calcination rates resulted in similar SSAs (89±3 and 104±20 m^2/g), respectively. Figure S5.9 shows typical SEM micrographs of the investigated glass surfaces which all appear very similar (except for BA 500) and are in contrast to gel-

Table 5.2 Glass particle textural properties (n=3): average mean (D_{AVG}) and median (D_{50}) diameter, specific surface area (SSA), average pore width and average pore volume

ID	Particle Size (μm)		SSA (m^2/g)	Pore Width (nm)	Pore Volume (cm^3/g)
	D_{AVG}	D_{50}			
AM	50.7	45.4	91± 6	20 ± 3	0.6 ± 0.2
TMB	53.9	49.1	75 ± 4	12 ± 0.1	0.3 ± 0.02
TEB	47.9	40.7	81 ± 2	13 ± 0.1	0.4 ± 0.03
0d	44.1	36.8	131 ± 7	16 ± 0.4	0.8 ± 0.1
30d	44.8	35.1	97 ± 1	22 ± 2	0.7 ± 0.1
RT	40.2	30.5	103 ± 2	18 ± 0.2	0.7 ± 0.03
65C	39.2	30.3	119 ± 6	19 ± 1	0.8 ± 0.1
1C/min	37.1	28.5	89 ± 3	25 ± 1	0.8 ± 0.1
10C/min	36	26.7	104 ± 20	24 ± 5	0.8 ± 0.1
BA 300	39.2	28.5	106 ± 1	22 ± 1	0.8 ± 0.1
BA 400	36.9	25.1	95 ± 3	23 ± 2	0.7 ± 0.1
BA 500	43.6	38.5	15 ± 1	38 ± 3	0.2 ± 0.04

derived 45S5 glass-ceramics in which the ageing conditions were found to affect the surface morphology [251].

Pore volume and pore width values generally followed a similar trend to the SSAs. Average pore volumes of TMB (0.3±0.02 cm^3/g) and TEB (0.4±0.03 cm^3/g), were lower than that of BA 400 (0.7±0.1 cm^3/g) which may be due to their lack of gel formation. Furthermore, average pore widths for TMB (12±0.1 nm) and TEB (13±0.7 nm) were also noticeably smaller than that of BA 400 (23±2 nm). The lower pore volume (0.2±0.04 cm^3/g) and increased pore width (38±3 nm) of BA 500, relative to BA 400, further shows the effect of increasing calcination temperature on glass textural properties. Based on the wider textural property ranges observed for TMB, TEB, 0d, 30d, BA300, BA400, and BA500, these glasses were chosen for further analyses and assessment of bioactivity.

Structural analysis

The bonding regions of the SGBGs were examined using ATR-FTIR spectroscopy (Figure 5.2). Three main regions are associated with borate-based glasses: 850 – 1200 cm^{-1} (B–O stretching of BO_4 units), 1200 – 1500 cm^{-1} (B–O stretching of BO_3 units), and a band at ~720 cm^{-1} attributable to the B–O–B bending of BO_3 units [218-220]. The broad band between ~942 and ~1000 cm^{-1} can

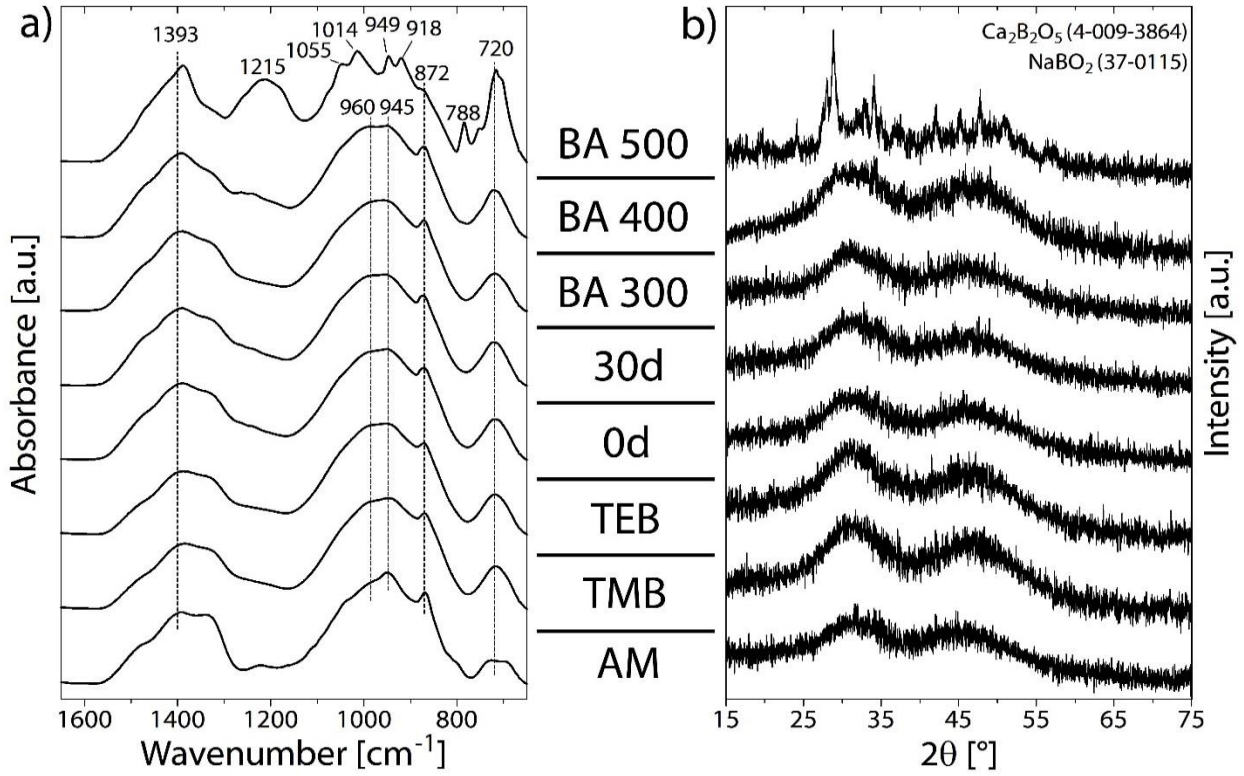

Figure 5.2 Structural characteristics of the various glasses using (a) ATR-FTIR and (b) XRD. The spectra and diffraction patterns remain similar for all glasses except for BA 500, which indicated the initiation of crystallization as shown by the sharp doublet peaks in ATR-FTIR and crystallization peaks in XRD.

be attributable to the B–O linkages of BO_4 [165, 221-223], while the defined shoulder peak at ~870 cm^{-1} is characteristic of the B–O stretching of boroxol rings. The spectrum of AM was not as smooth as those of the calcined glasses, which may be due the presence of residual precursor organics. Furthermore, the spectrum of the BA 500 indicated sharp, doublet peaks at ~1000 cm^{-1}, indicating greater extent of crystallization.

XRD diffractograms (Figure 5.2) showed that all glasses remained amorphous, as indicated by the two broad humps after calcination, except for the glass calcined at 500 °C, which was partially crystallized into $Ca_2B_2O_5$ (JSPDS 4-009-3864) and $NaBO_2$ (JSPDS 37-0115) as previously reported [249], corroborating the ATR-FTIR spectra.

HCA conversion in SBF

The *in vitro* bioactivity of the SGBGs was examined up to day 7 in SBF. ATR-FTIR spectroscopy showed a phosphate peak was formed in as little as 0.5h, as indicated by the strong band at ~1020 cm^{-1} along with shoulders at ~961 and 1062 cm^{-1}, which are characteristic of the bending modes ν1 and ν3 of PO_4^{3-} [252], respectively (Figure 5.3). Furthermore, carbonate peaks were formed

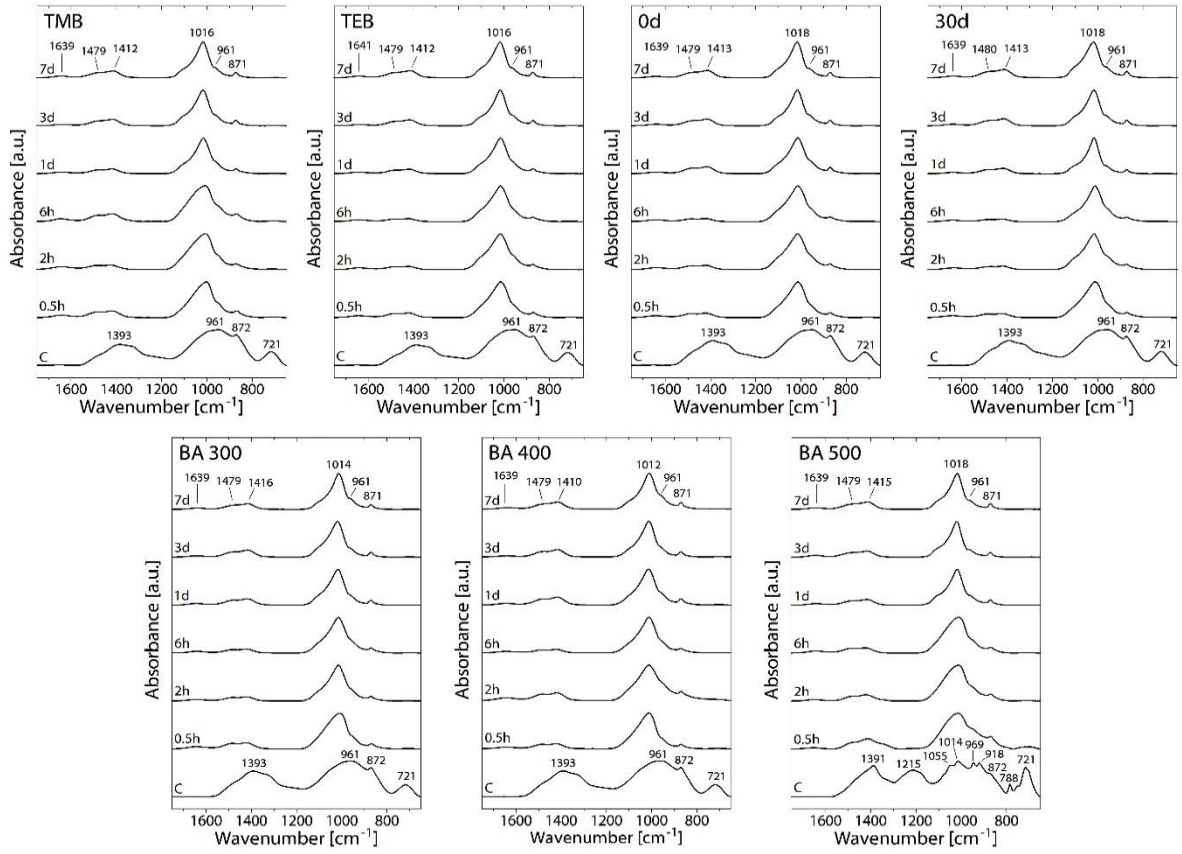

Figure 5.3 ATR-FTIR spectra as a function of immersion time in SBF. Glass conversion to HCA was initiated in as little as 0.5h as indicated by the formation of the large phosphate peak around 1020 cm^{-1}.

as indicated by the broad bands at ~1470 and ~1421 cm^{-1} represent the stretching modes ν1 and ν3 of CO_3^{2-} while the sharp peak at 870 cm^{-1} indicating the bending mode ν2 of CO_3^{2-} [231, 232]. This band was also observed in the calcined glasses (Figure 5.2), which represents the B-O stretching of boroxol rings, suggesting a combination of both structural forms. The broad band at ~1640 cm^{-1} was due to the bending mode (ν2) of water [233, 234]. Increasing time in SBF led to sharper and more defined peaks, suggesting formation of carbonated apatite.

XRD patterns confirmed the formation of HCA through the development of hydroxyapatite characteristic peaks at ~25 and ~32° 2θ ("•", JCPDS 9-0432), that were observed at the 2h time point in SBF in all glasses except for BA 500, which did not indicate peak formation until day 1 (Figure 5.4). The more prominent, broad apatite peaks maybe in nanometer-sized or partially crystallized HCA [17]. At longer immersion times, the apatite indicating peaks become more defined suggesting a greater extent of crystallization. On the other hand, BA 500 indicated an interesting mineralization trend. Once immersed in SBF, the partially crystallized glass initially (at 0.5h) became more amorphous, as indicated by the loss of the shaper more defined peaks in ATR-FTIR and XRD (Figure

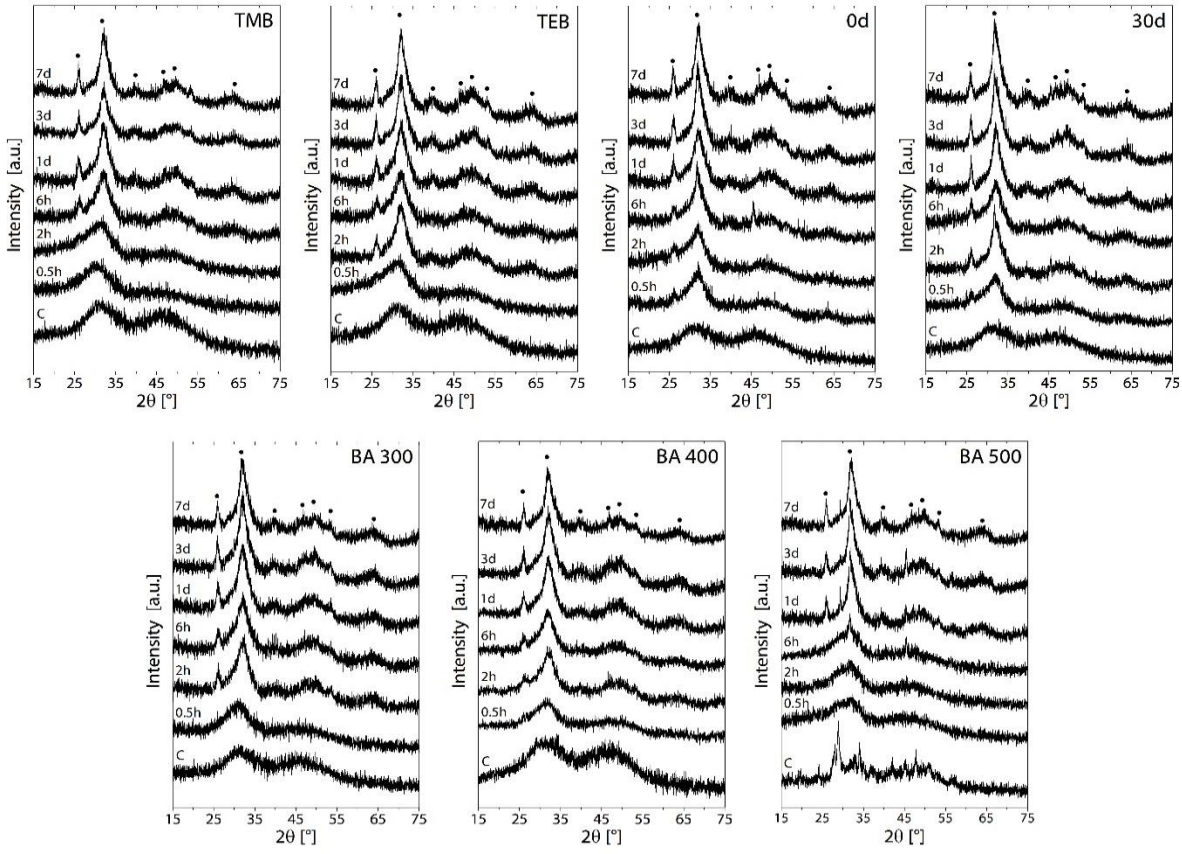

Figure 5.4 XRD diffractograms as a function of immersion time in SBF. All particles produced through the various sol-gel processing methods converted to HCA ("•", JCPDS 9-0432) at a rapid rate.

5.3 and Figure 5.4, respectively). At longer times in SBF, characteristic HCA peaks became more prominent and by day 1, there was little evidence of the initial partially crystallized glass structure (Figure 5.4). This was surprising since glass-ceramics typically maintain some of their crystal structure after exposure to SBF according to XRD [253, 254]. However, it has also been shown that hydroxyapatite can be the sole-remaining crystal structure after immersion in SBF, although it can take up to a week [179] or even longer [255] to form and is dependent upon the glass composition and calcination temperature. Despite their reduced SSA values, rapid HCA rates were still maintained in BA 500. Since glass-ceramics typically are of higher toughness and flexural strength compared to glasses [256], this finding indicates that it may be possible to create mechanically strong, partially-crystallized SGBGs without compromising bioactivity as was previously shown with sol-gel derived compositions based on Bioglass® 45S5 [251]. This also confirms the dominant effect of atomic and molecular composition on the chemical durability and bioactivity of multicomponent glass systems [82, 229].

SGBG ion release and bioactivity

In addition to ATR-FTIR and XRD analyses it is also important to examine the ion release of these glasses to better understand their bioactivity [120]. The release of boron, calcium, and phosphorous from the SGBGs in SBF were measured up to day 7 through ICP-OES (Figure 5.5) with the neat SBF concentrations of Ca and P included as dashed lines (B levels < 0.01ppm). Except for BA 500, which showed a relatively more gradual release rate, all other glasses indicated that the majority of the boron was released within 0.5h, beyond which, its concentration remained relatively constant, as previously observed [249]. Similar release rates were observed for calcium and phosphorous in the glasses. However, beyond the 6h time point, there was a concomitant decrease in their concentration in solution, suggesting their re-precipitation, and corroborated the surface HCA formation results observed through ATR-FTIR and XRD for between 0.5 and 2h [120, 249]. Since the decrease was particularly prominent in the case of phosphorous, it can be proposed that this decline in concentration maybe be used as an indicator for HCA formation in bioactive glasses. This also confirms that the increased surface area and composition of the SGBGs allows for rapid ion release and thus conversion to HCA. Further studies are needed to accurately pinpoint the rapid rates of HCA conversion in these glasses by measuring phosphorous and calcium release at time points earlier than 0.5h.

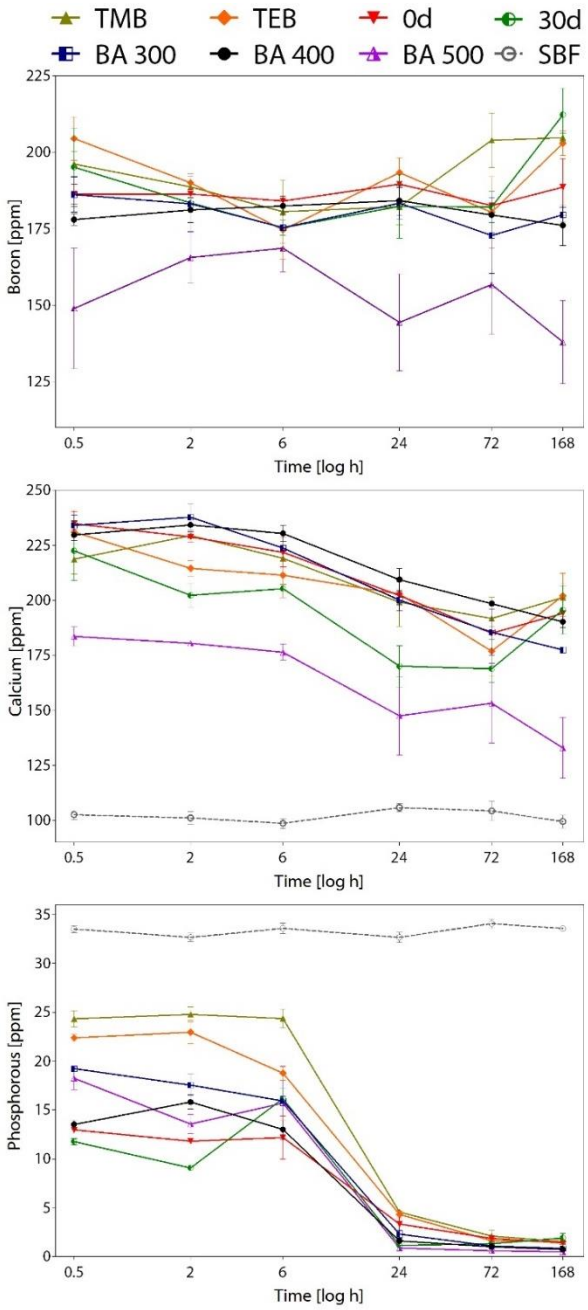

Figure 5.5 Release of boron, calcium, and phosphorus in SBF as measured through ICP-OES. Rapid ion release was observed with boron. The decreasing release trend of calcium and phosphorous suggested their re-precipitation on the glass surface.

The ion release data also supported the theory that HCA formation in borate glasses follow a "volume reduction" model, driven by dissolution-precipitation reactions, in which HCA is initially formed on the glass surface then continually reacts towards its center until full conversion has taken place [17, 219]. This was indicated by rapid release of boron while the remaining calcium and

phosphorous from the glass migrate to the surface, as observed by the decreasing trend, and react with similar ions in the SBF solution leading to the formation of an apatite layer that ultimately crystallizes to form HCA. However, further studies are needed to explore the HCA conversion mechanisms of the SGBGs.

Due to discrepancies in mineralization findings when carried out using *in vitro* and *in vivo* studies [119], there has been a recent drive to create a unified method to examine the *in vitro* mineralization behavior of bioactive glasses when using SBF [120]. One approach to do this would be by correcting for the surface area of the glasses. However, it was found that the amount of particles required for sol-gel derived glasses, compared to melt-quench derived glasses, becomes impractical for SBF studies [120]. Therefore, in order to investigate the effect of glass surface area on bioactivity, in this study, a commonly used glass/SBF ratio (1.5 mg/mL), was applied [120].

SEM micrographs confirmed surface HCA formation (Figure 5.6). After 2h in SBF, the glass surfaces became coarser and by 6h, flower-like crystals were observed, which become more defined and pronounced with immersion time. In the case of BA 500, the conversion appeared to be slower, with HCA crystals observed only after day 1, as also indicated by XRD. However, by day 7 in SBF,

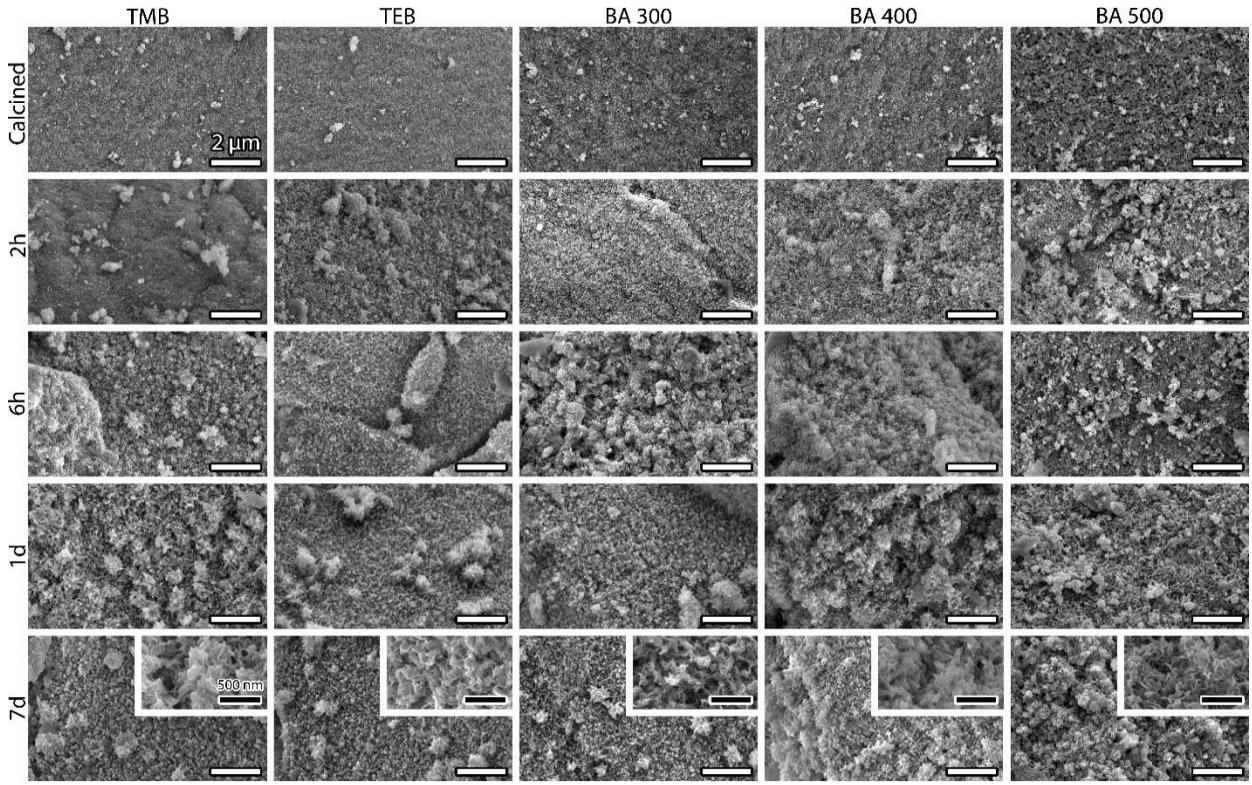

Figure 5.6 SEM micrographs of TMB, TEB, BA 300, BA 400, and BA 500 as a function of time in SBF. Typical flower-like crystals, indicative of hydroxyapatite formation was initiated at 2h and became well-defined by 6h. White scale bars = 1 µm and black scale bars = 500 nm.

the surface of BA 500 was completely covered by HCA crystals. 0d and 30d samples also showed HCA formation at day 7 (Figure S5.10).

5.4 Conclusions

The effects of processing parameters on the structural, textural and bioactivity of a sol-gel derived borate substituted Bioglass® 45S5 formulation were investigated. While the different precursor materials affected the gelation properties, all of the resulting glasses were of high specific surface areas and porosities. Calcination temperature had the greatest effect on these properties as calcination at 500 °C formed glass-ceramics that resulted in a magnitude reduction in specific surface area. The majority of the glasses converted to HCA within 2 hours of SBF immersion according to XRD. This corroborated with ion release measurements, which showed rapid release of boron within 30 minutes and a decreasing release profile of both calcium and phosphorus, which was attributed to their re-precipitation. Future work will investigate the effect of these glasses on cellular functions as well as the role of other ionic doping for a broader potential range of tissue engineering, antibacterial and wound healing applications.

Supporting Information

The surface area linear isotherm plots, a graphical representation of percent weight loss and SSA upon calcination at different temperatures, morphology of the all glasses investigated and hydroxyapatite formation of 0d and 30d samples are shown.

Acknowledgements

This study was supported by Canada NSERC, CFI and McGill University Faculty of Engineering Hatch Faculty Fellowship for S.N.N. W.C.L. and S.N. are supported by the McGill Engineering Doctoral Award and W.C.L. is also supported by the Fonds de recherche du Québec (FQRNT) – Bourses de doctorat en recherché.

5.5 Supporting Information

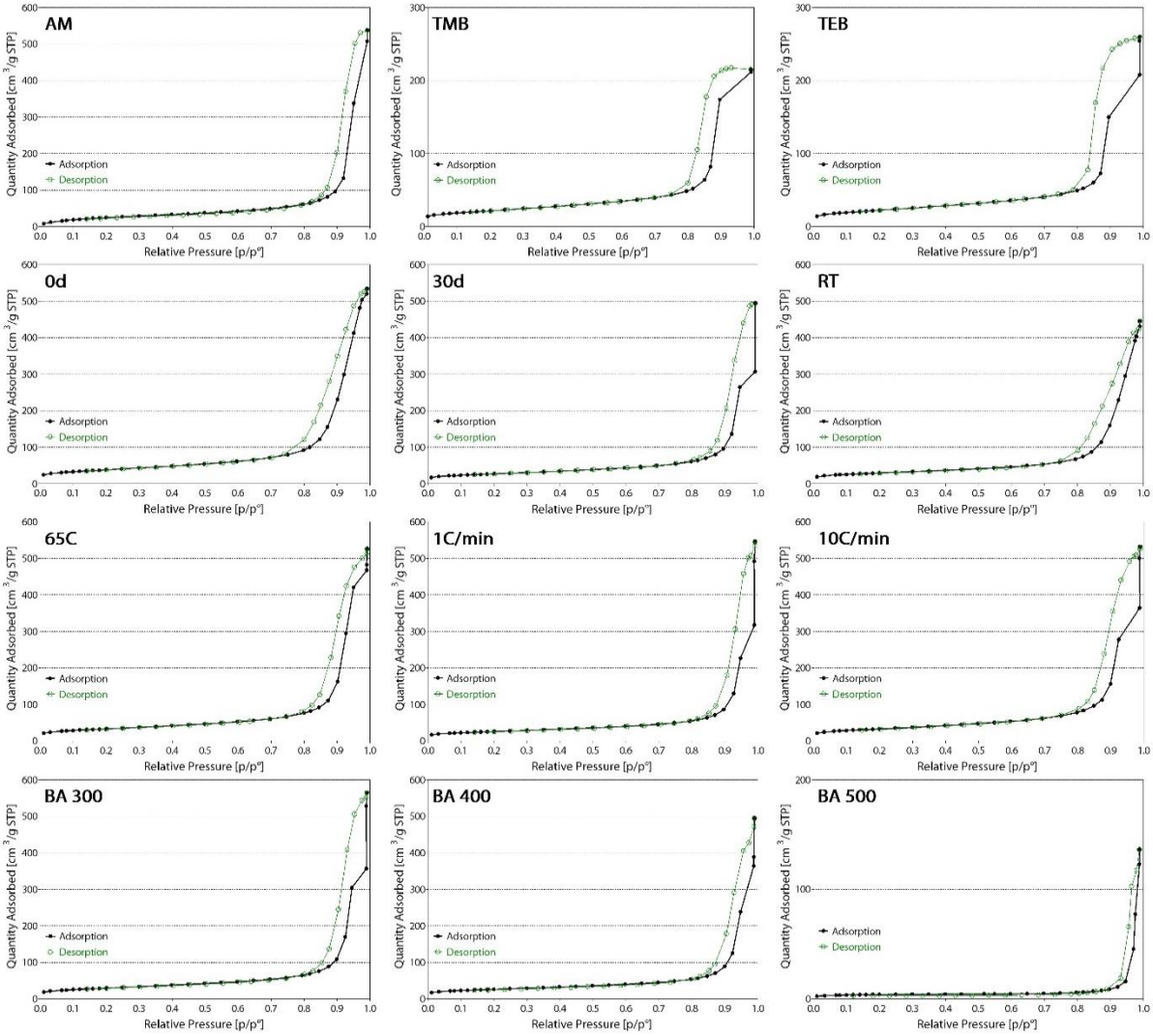

Figure S5.7 Linear isotherm plots for each glass during surface area measurements through BET.

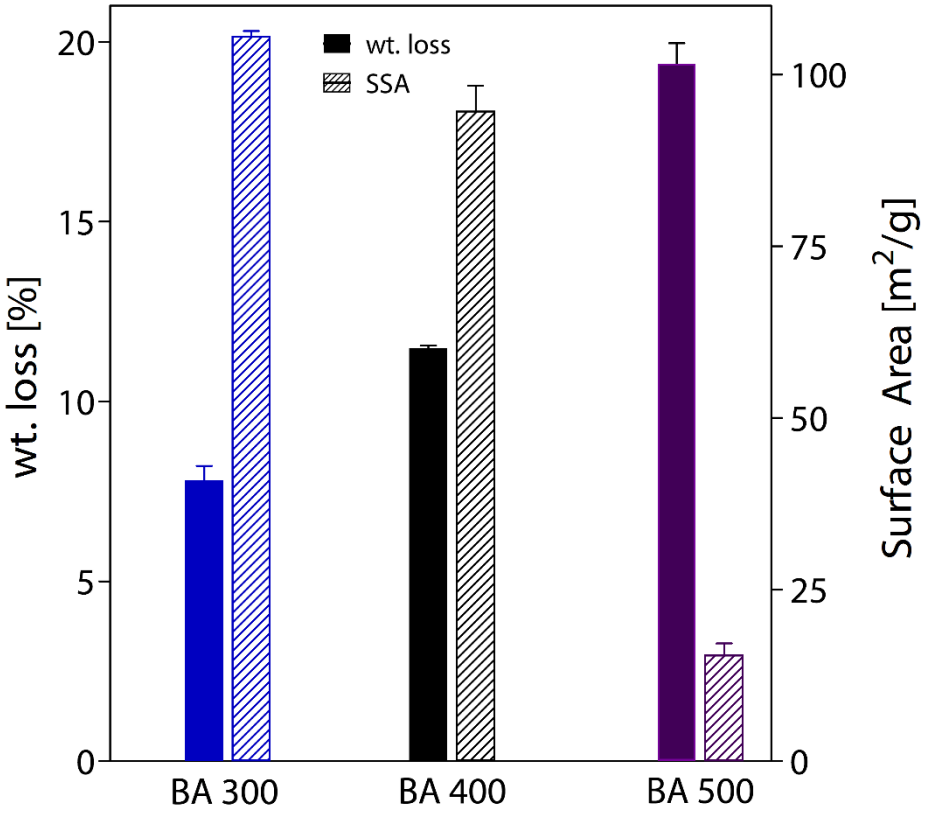

Figure S5.8 Effect of calcination temperature on specific surface area for BA 300, BA 400, and BA 500. Weight loss upon calcination is inversely proportional to specific surface area measurements.

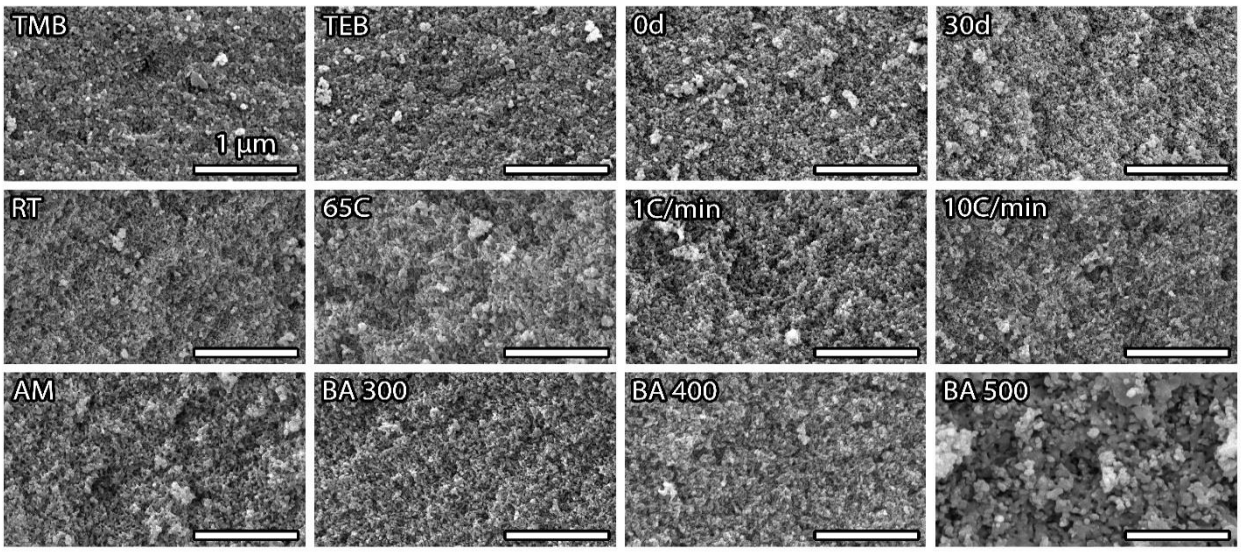

Figure S5.9 SEM micrographs of the calcined glasses demonstrating the nano-textured surfaces of the SGBGs. Upon higher calcination temperature, the glass surface becomes less porous as verified by textural analysis data.

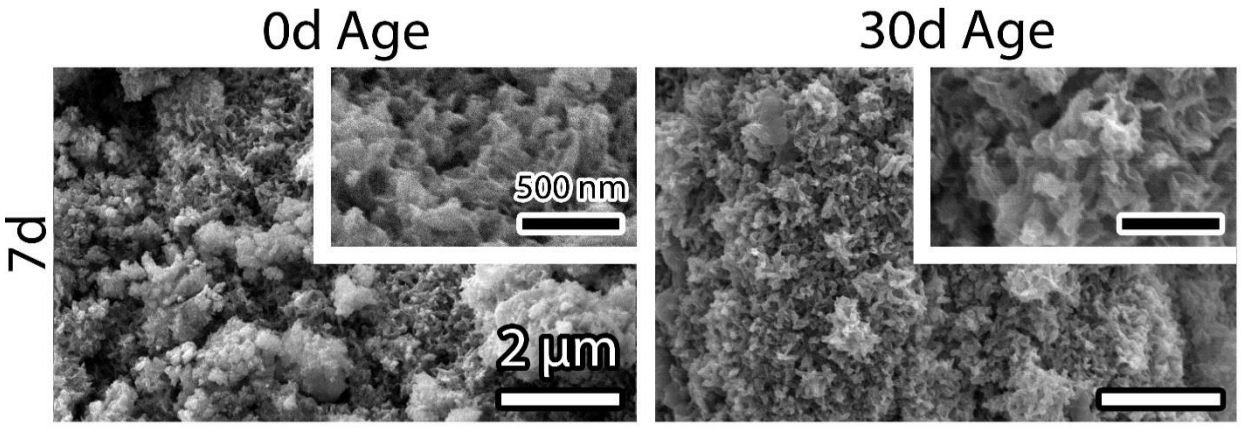

Figure S5.10 SEM micrographs of 0d and 30d aged samples at 7d in SBF. The flower-like crystals suggest hydroxyapatite formation as confirmed by FTIR and XRD analyses.

6 Effect of Sodium on Sol-Gel Derived Borate Glasses

The previous two chapters have demonstrated that highly bioactive SGBGs can be achieved over a large compositional range and after many different processing techniques. Yet, there has been no study that examines the effect of adjusting a single compositional component on the properties of these glasses. One of the benefits of the sol-gel process is that sodium is not required due to the aqueous nature of the sol-gel processing. However, sodium was included in the original SGBG composition to directly compare to a previously made melt-quench derived equivalent. Therefore, Chapter 6 examines the effect of systematically decreasing the sodium content in a four-component system until a three-component system was generated. It was found that although sodium content greatly influenced the processing and textural properties of the SGBGs, surprisingly, it did not greatly affect their bioactivity. This chapter contains a manuscript that is to be submitted to a peer-reviewed journal and is presented below.

Effect of Sodium on Bioactive Sol-Gel-Derived Borate Glasses

William C. Lepry, Sophia Smith, and Showan N. Nazhat*

Department of Mining and Materials Engineering, McGill University, Montreal, QC, Canada
*corresponding author showan.nazhat@mcgill.ca

Abstract

Bioactive, sol-gel derived borate glasses (SGBGs) can rapidly convert to hydroxy-carbonated apatite (HCA) in simulated body fluid (SBF). The processing conditions and compositional changes in four-component glasses have previously been investigated, yet the effect of certain elements, such as sodium, on the processing and bioactivity has not been investigated. Therefore, in this study, a borate substituted Bioglass® 45S5 of the formulation $(46.1)B_2O_3$-$(26.9)CaO$-$(24.4)Na_2O$-$(2.6)P_2O_5$; mol%, was created as the baseline glass and the amount of sodium was incrementally decreased three times by approximately 8% until a sodium-free, three-component composition was generated. It was found that the decreasing sodium content altered the gelation behaviour and resultant glass textural properties. It also greatly affected the glass reactivity, as measured through gravimetric changes when exposed to water vapour. Interestingly, there was very little effect on the bioactivity rate in SBF according to x-ray diffraction and Fourier-transform infrared spectroscopy. Furthermore, ion release profiles were not greatly affected by the sodium content either. This study serves as the basis to develop more simplified SGBG systems for tissue engineering applications.

6.1 Introduction

Silicate-based bioactive glasses have demonstrated great clinical success in mineralized tissue repair due to their ability to convert to bone-like, hydroxycarbonated apatite (HCA) [10, 12, 257]. Attributable to their ability to homogenously release ions to help stimulate healing, recently they are also being targeted for soft tissue applications [121]. Compared to silicate-based glasses, borate glasses are of lower chemical durability which can allow for quicker conversion rates to HCA [16, 17, 19, 131, 138, 195] and ion release for soft tissue engineering applications such as wound healing [203-205, 244].

Regardless of composition, the majority of bioactive glasses are traditionally generated through the melt-quench process, which involves the high temperature melting of oxides followed by their rapid cooling ("quenching") to preserve the amorphous structure. With the advent of the sol-gel process - a robust, low temperature, aqueous based processing approach - it was possible to create bioactive glasses with orders of magnitude higher specific surface area values [15]. This process typically uses a mixture metal alkoxide precursors (the "sol"), which undergo hydrolysis and condensation reactions to form a "gel", essentially the glass network. This gel then undergoes heat treatment (calcination) to eliminate excess precursor organic materials and to densify the glass. However, given that the calcination temperatures are relatively low, sol-gel derived glasses maintain their high specific surface area and porosity characteristics.

From a biomedical materials prospective, sol-gel derived glasses offer distinct advantages when compared to their melt-quench derived equivalents. For example, the increased surface area and porosity values allow for more rapid ion release rates and thus increased conversion rates to HCA [15, 82, 173]. In fact, these improved textural properties have enabled the expansion of the bioactive silicate-glass compositional range; up to 90 mol% SiO_2 compared to the melt-quench derived limit of 60 mol% SiO_2 [15]. Furthermore, based on the precursors, which are typically metal alkoxides, a wide variety of metal ions can be more easily incorporated into the glass structure attributable to lower processing temperatures. Thus, fluxes such as sodium, used to improve the processability of traditional melt-quenching methods through decrease of melting temperature and to also increase the solubility of bioactive glasses, are not necessary in the sol-gel process [82].

Nonetheless, Chen et al. created the first sol-gel derived Bioglass® "45S5" [$(46.1)SiO_2$-$(26.9)CaO$-$(24.4)Na_2O$-$(2.6)P_2O_5$ (mol%)] with the intention of increasing the mechanical properties while creating a more biodegradable crystalline phase [255]. After calcination, the resultant glasses were semi-crystalline, which has been commonly been found in other sol-gel derived "45S5" glasses

[179, 181, 251, 258, 259]. This is mainly due to the requirement of reaching high enough calcination temperatures to eliminate the precursor nitrates. A similar 45S5-like composition [(49.2)SiO_2-(25.8)CaO-(23.3)Na_2O-(1.7)P_2O_5 (mol%)] has also been reported to partially crystallize after calcination [260]. However, amorphous versions of this glass are possible by adjusting the precursors, processing routes, and most importantly, the calcination temperatures [180, 261].

While sol-gel derived borate glasses have been far less investigated [160, 162, 163, 210], the first reported compositions incorporated sodium [158]. Borate has also been added as a modifier in sol-gel derived silicate- and phosphate-systems to help improve glass bioactivity [166, 185, 212]. Furthermore, we have previously reported on a wide compositional range of highly bioactive sol-gel derived borate glasses (SGBGs, with 36 – 61 mol% B_2O_3) based on variations of the Bioglass® "45S5" composition, *i.e.,* [(46.1)B_2O_3-(26.9)CaO-(24.4)Na_2O-(2.6)P_2O_5; mol%] whose melt-quench derived composition has been previously studied [17, 134]. Recently, we have shown that similar sodium containing SGBG compositions, can be produced through various sol-gel processing methods and are highly bioactive converting to HCA in less than 3 h according to X-ray diffraction (XRD) [262]. However, while it is known that sodium is not needed for the sol-gel process, there has yet to be a systematic study reporting on the effect of sodium content on the properties of SGBGs. Therefore, this study examined the effect of systematically decreasing sodium content on the processing, structural, reactivity and bioactivity properties of these glasses.

6.2 Experimental

Materials and methods

Table 6.1 gives an overview of the SGBG compositions investigated. The original composition was based on a borate substituted Bioglass® (24Na) [(46.1)B_2O_3-(26.9)CaO-(24.4)Na_2O-(2.6)P_2O_5; mol%], and the amount of sodium was incrementally decreased by ≈ 8 mol% until a three component, sodium free SGBG composition (0Na) [(61.0)B_2O_3-(35.6)CaO-(3.4)P_2O_5; mol%] was generated, while the ratios of the other components were maintained. The glasses were fabricated following a previously described [249]. Briefly, boric acid (≥99.5%) and anhydrous ethanol (both from Sigma Aldrich, Canada) were mixed and magnetically stirred in a watch glass-covered Teflon beaker at 40 ± 3 °C to aid dissolution. Once the solution became clear, triethyl phosphate (>99.8%; Fisher Scientific, Canada), calcium methoxyethoxide (20% in methoxyethanol; Gelest, USA), and sodium methoxide (25 wt.% in methanol; Fisher Scientific, Canada) were added in a drop wise manner at 30 min intervals. Once the final addition was complete, the sol was mixed for an additional 30 min

or until gelation occurred, followed by transferring into sealed polypropylene vials, and aged at 37 °C for 10 days. The gels were then transferred to crystallization dishes and dried in air at room temperature (RT) for 1 day, followed by oven drying at 120 °C for 2 days. Finally a calcination step was undertaken at 400 °C at a rate of 3 °C/min, with a 2 h dwell period, followed by furnace cooling. The calcined glasses were then ground to a particle size fraction of 25 – 75 μm and stored in a desiccator until analysis.

Glass particle characterization

The average particle size (D_{avg}) and median diameter (D_{50}) of the glass powders was determined using a Horiba LA-920 (ATS Scientific Inc., Canada). The specific surface area (SSA) of each powder was measured with nitrogen gas adsorption and desorption isotherms collected with a Micromeritics TriStar 3000 (Micromeritics Instrument Corporation, USA) gas sorption system. SSA values were determined using the Brunauer–Emmett–Teller (BET) method [215] while the average pore width and pore volume were calculated using the Barrett–Joyner–Halenda (BJH) method [216].

X-ray diffraction (XRD)

XRD diffractograms of the glasses were analyzed with using a Bruker D8 Discover X-ray diffractometer (Bruker AXSS Inc., USA) equipped with a CuKα (λ = 0.15406 nm) target set to a power level of 40 mV and 40 mA. Three frames were collected from 15 – 75 2 theta (°), using an area detector, and merged in post processing while phase identification was carried out using X'Pert Highscore Plus (PANalytical, Netherlands).

Attenuated total reflectance-Fourier transform infrared spectroscopy (ATR-FTIR)

ATR-FTIR spectroscopy was carried out between 4000 and 650 cm^{-1} with a resolution of 4 cm^{-1} using 64 scans per sample using a Spectrum 400 (Perkin-Elmer, USA). The collected spectra were baseline corrected then normalized to the total area surface area under absorption bands using Spectrum software (Perkin-Elmer, USA).

Reactivity and bioactivity

The aqueous interactions of SGBG particles were investigated through dynamic vapour sorption (DVS) using a DVS Intrinsic (Surface Measurement Systems Ltd., U.K.), which measures mass changes (±0.1 μg) under controlled relative humidity (RH) and temperature. Approximately 5 mg of glass powder were placed in an aluminium pan and inserted into a chamber at 37 ± 0.05 °C which were then directly exposed to 90% relative humidity for 6 h and then to 0% RH for a further 6 h. Kokubo's SBF (pH 7.4) was used to examine the *in vitro* mineralization of the glasses [117]. Glass powder was added to sterile 50 mL falcon tubes containing SBF at a 1.5 mg/mL ratio and stored at

37±1 °C. The vials were gently agitated twice per day to prevent agglomeration. The ability of the glasses to form HCA were examined at 30 min, 2h, 6h, 1d, 3d, and 7d time points where the powders were gently rinsed with deionized water then twice with anhydrous ethanol, dried overnight at room temperature, and then dried in an oven at 60 °C for 1d.

Inductively coupled plasma optical emission spectrometry

The release of boron, calcium, sodium and phosphorus ions from glass powders at a 1.5 mg/mL ratio in SBF, were quantified using an inductively coupled plasma–optical emission spectrophotometer (ICP-OES, Thermo Scientific iCAP 6500, USA). Collected aliquots of were filtered through a 0.2 μm nylon filter then stored in a 15 mL falcon tube which contained 4% (w/v) nitric acid (Fisher Scientific, Canada) followed by dilution with DIW. Serially diluted solutions of Boron (1, 10, 100 ppm), Calcium (1, 10, 100 ppm), and Phosphorous (0.1, 1, 10 ppm) were used as standards.

6.3 Results and Discussion

Effect of sodium content on gelling

Figure 6.1 provides an overview of the SGBG sol-gel process as a function of sodium content. While the compositions with less sodium did not form gels during the ageing process, Na8 and Na0 formed a gel-like layer after drying at RT for 1d. Furthermore, it took approximately 1d for Na16 to form a gel after casting. Together this suggests that sodium may be a key component in the gelation process and that higher pH is needed for gel formation (pH of Na precursor ~12). It has also been previously shown that at higher pH, BOH_4^- species dominate [21] thus allowing for easier gel formation since the network former exists as a four-coordinated structure, allowing for more

Table 6.1 SGBG Compositions and Codes (mol%)

Glass ID	B_2O_3	CaO	P_2O_5	Na_2O
Na24	46.1	26.9	2.6	24.4
Na16	51.1	29.8	2.9	16.3
Na8	56	32.7	3.2	8.1
Na0	61	35.6	3.4	0

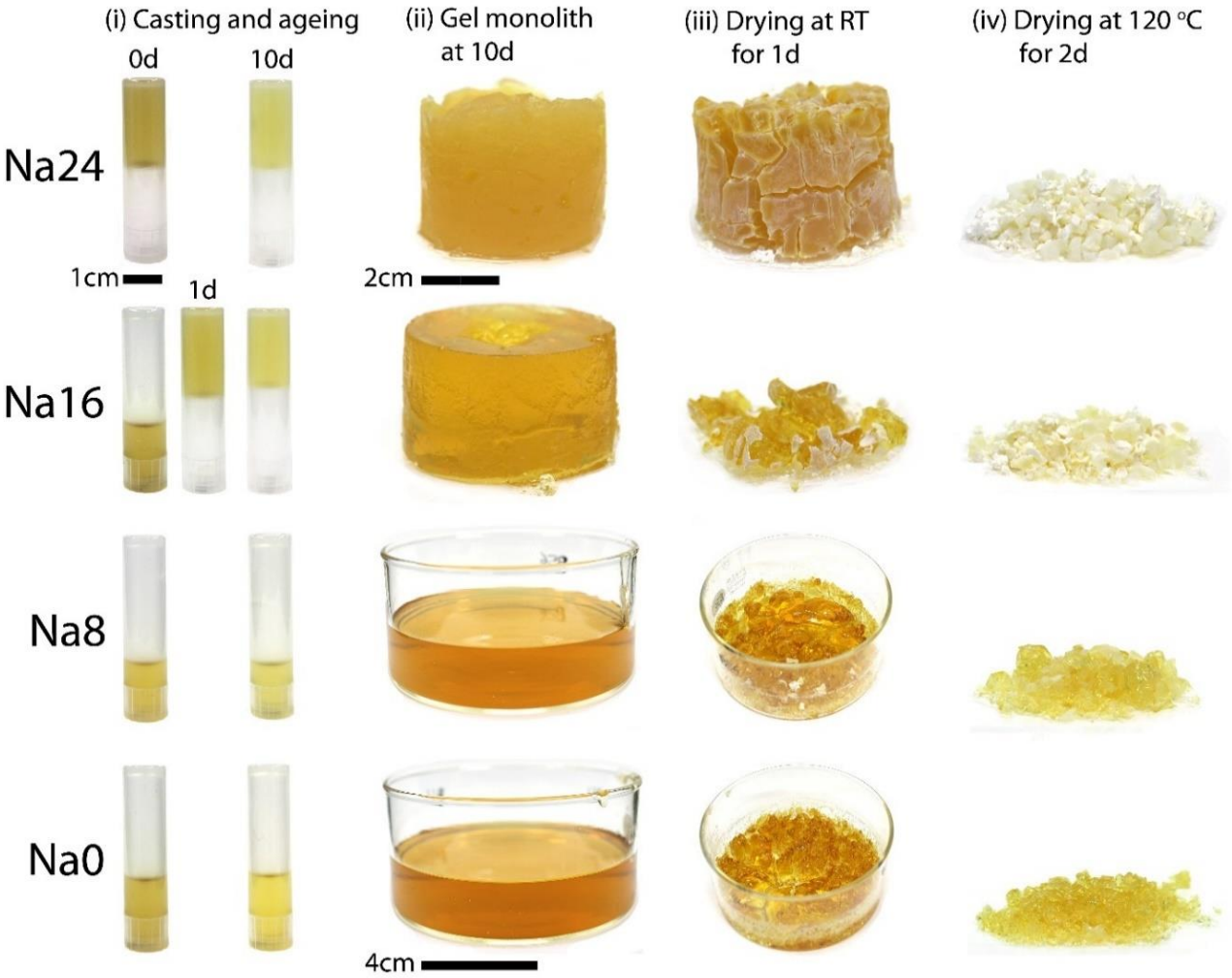

Figure 6.1 An overview of the effect of sodium content on the gelling of SGBGs. (i) casting and ageing, (ii) gel monoliths at day 10, (iii) drying at RT for 1 day, (iv) drying at 120 C for 2 days. Sodium influences the gelation behaviour of the glasses, possibly due to increasing pH.

interconnection. The gelling behavior of Na8 and Na0 was observed to be very similar to previously reported (Na24) compositions generated using trimethyl borate (TMB) and triethyl borate (TEB) as precursors [262]. The gelation process is also akin to the evaporation-induced self-assembly (EISA) used in the creation of mesoporous glasses [263], that is, the excess organic material is evaporated from the surface, resulting in the final material form. However, the method in this study does not result in a well-organized final structure due to the lack of structural directing agents during processing which is common using EISA. It is also interesting to note that the Na0 SGBG is very similar to one of the first, and now most commonly reported, silicate sol-gel composition "58S" (60)SiO_2-(36)CaO-(4)P_2O_5 (mol%) [15, 264].

SGBG textural properties

A summary of the glass textural properties is given in Table 6.2. All the particles were ground to similar median particle size (D_{50}) to directly compare their textural properties. Specific surface area values increased with decreasing sodium content, and was in contrast to the pore width values, which decreased with decreasing sodium content. In silicate-based systems, sodium is added as a network modifier that disrupts the glass structure, thus creating non-bridging oxygens (nbOs). In melt-quench derived glass systems, sodium improves the handling of the glasses by lowering the processing temperatures and, once incorporated into the glass structure, lowers the chemical durability increasing the dissolution [82]. The observed increased surface area can be attributed to a more connected glass

Table 6.2 Glass particle textural properties: Average Median (D_{50}) and Mean (D_{AVG}) Diameter, Specific Surface Area (SSA), Average Pore Width and Average Pore Volume

ID	Particle Size (µm)		SSA (m^2/g)	Pore Width (nm)	Pore Volume (cm^3/g)
	D_{AVG}	D_{50}			
Na24	44.88	39.23	37.26	32.62	0.44
Na16	36.99	29.91	71.24	27.35	0.57
Na8	30.53	29.25	138.95	18.3	0.99
Na0	42.85	43.94	159.18	10.74	0.64

network, as previously observed in other sol-gel systems [15]. Furthermore, the decreasing pore size might also be attributed to this effect as increasing nbOs would essentially create a larger glass network. The pore volume of each glass remained high, but did not follow a trend with composition.

Structural Analysis of as-calcined SGBGs

SGBG bonding regions were examined using ATR-FTIR spectroscopy (Figure 6.2 a). There are three main regions associated with borate-based glasses: the B–O stretching of the BO_4 units (850 – 1200 cm^{-1}), the B–O stretching of the BO_3 units (1200 – 1500 cm^{-1}), and the B–O–B bending of the BO_3 units indicated by the band at ~720 cm^{-1} [218-220]. B–O stretching of boroxol rings are characteristic of the shoulder peak at ~870 cm^{-1} and the B–O linkages of BO_4 are indicated by the broad band between ~942 and ~1000 cm^{-1} [165, 221-223]. SGBGs with decreasing sodium content demonstrated broader, smoother spectra peaks. XRD diffractograms (Figure 6.2 b) showed that all glasses remained amorphous, as indicated by the two broad humps after calcination at 400 °C.

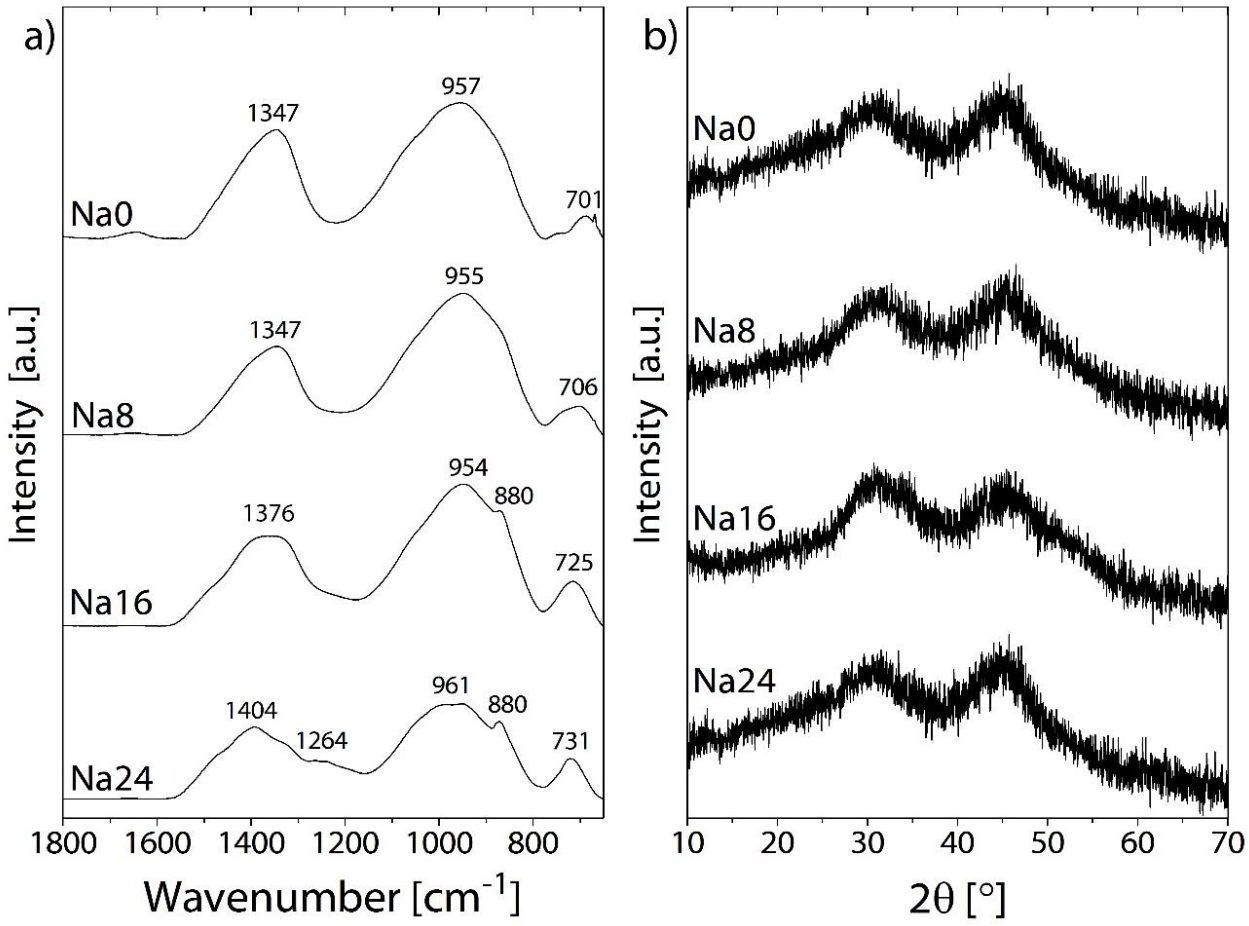

Figure 6.2 Characterisation of the calcined SGBGs (a) ATR-FTIR spectra and (b) XRD diffractograms of the glass particles produced as a function of sodium content.

Assessment of SGBG reactivity through aqueous interactions

As an indicator of their reactivity, DVS was used to investigate SGBG aqueous interactions by gravimetrically measuring their sorption and desorption of water vapour at direct exposure to 90% (RH) relative humidity. DVS has previously been used to examine the reactivity of bioactive glasses [265, 266]. All glasses demonstrated a rapid increase in mass within the first hour (Figure 6.3). The rate and extent of mass change after 6 h was highly dependent on composition, which decreased with a decrease in glass sodium content. Lowering the RH to 0% resulted in a rapid decrease in mass with the higher Na containing glasses demonstrating a greater extent of mass loss. However, the overall final mass change increased with an increase in glass sodium content.

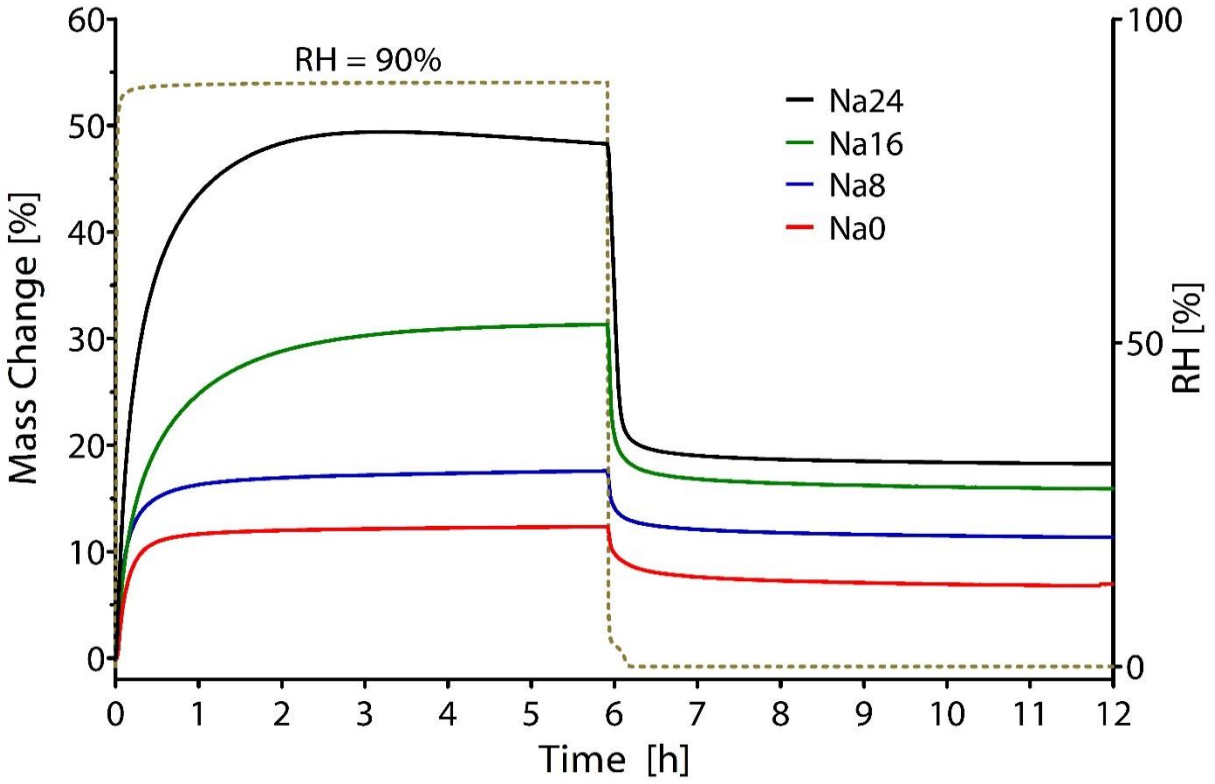

Figure 6.3 Reactivity through vapor adsorption using DVS. The direct exposure to 90% RH showed rapid increase in mass change which increased with sodium content.

Given that the mass change was independent of the SSA values (for example, Na0 particles of 159.2 m^2/g had a final mass change of ~9% compared to that of Na24 which was 37.3 m^2/g and resulted in a mass change of ~17%), this data confirmed that the atomic and molecular structures have dominant roles on the chemical durability of multicomponent glasses [82, 229], as also previously reported with SGBGs where the highest SSA glasses were the least reactive according to DVS [249]. The increased reactivity of SGBGs with higher sodium content can be attributed to a greater presence of nbOs in the glass structure, which reduce its network connectivity, making the glass more susceptible to chemical attack [267]. Interestingly, a similar DVS protocol on a previously created melt-quench derived Na24 glass equivalent resulted in an ~11% mass increase at 6 h [249], which is in a very similar range to the final mass change of ~12% observed for Na0 in this study. However, the SSA for the melt-quench derived glass was 0.2 ± 0.02 m^2/g while that of Na0 is 159 m^2/g. This further demonstrates the importance of composition on the reactivity of multi-component glasses.

SGBG bioactivity and ion release in SBF

The ability for SGBGs to form HCA was examined up to day 7 in SBF. After 0.5h, ATR-FTIR spectra of Na24, indicated the formation of a phosphate peak, as shown by the strong band at ~1020 cm^{-1} along with shoulders at ~961 and 1062 cm^{-1}, which are characteristic of the bending modes ν1 and ν3 of PO_4^{3-} [252], respectively (Figure 6.4). The formation of similar peaks also initiated in the case of the other SGBG formulations but at a slower rate in particular with lower sodium containing glasses, as observed by more gradual peak formation. Carbonate peaks at ~1470 and ~1421 cm^{-1}, which represent the stretching modes ν1 and ν3 of CO_3^{2-} were as well as a sharp peak at around 870 cm^{-1} that indicates the bending mode ν2 of CO_3^{2-} [231, 232] also formed. This band is thought to be a combination of the B-O stretching of boroxol rings found in the calcined glasses (Figure 6.2) as well as the bending mode ν2 of CO_3^{2-}. The ν2 bending mode of water can also be seen by the broad band at ~1640 cm^{-1} [233, 234]. At longer immersion times in SBF, more defined peaks were observed, suggesting the formation of carbonated apatite.

This SGBG-HCA conversion was confirmed by XRD diffractograms where hydroxyapatite-characteristic peaks at ~25 and ~32° 2θ ("•", JCPDS 9-0432), which were observed at the 2 h time point in SBF in all glasses (Figure 6.5). It has previously been reported that the broad apatite peaks, which become sharper with longer times in SBF, suggest nanometer-sized or partially crystallized HCA [17]. This rapid HCA formation is similar to previously studied SGBG formulations [249, 262], and demonstrates that, while sodium inclusion impacts the reactivity, the bioactivity is not largely affected by its presence in these glass systems. However, it should be noted that while the sodium content is

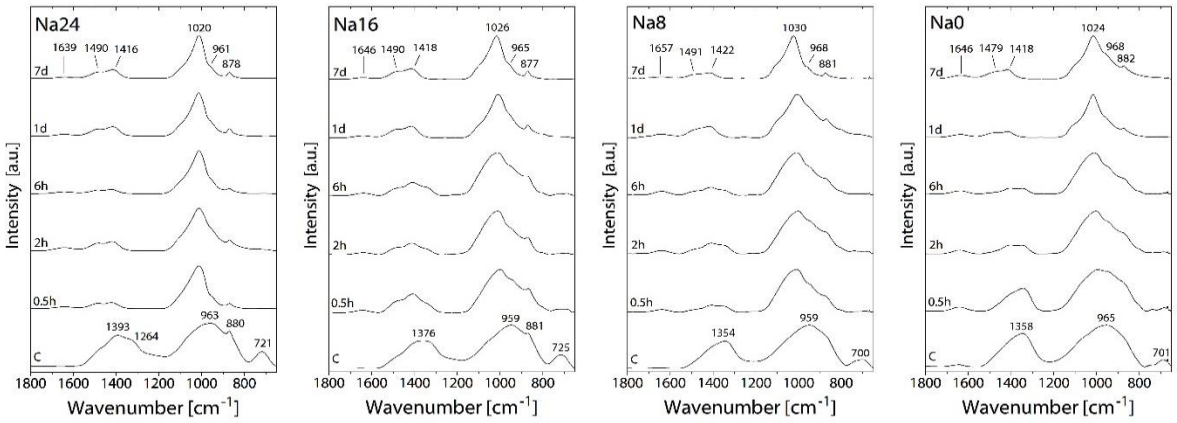

Figure 6.4 ATR-FTIR spectra as a function of immersion time in SBF. Characteristic apatite-like peaks began to form after 30 min in SBF for higher sodium containing glasses. Peak formation was less defined in lower sodium containing glasses.

decreasing, calcium and phosphate are increasing, both of which are known to be important in bioactivity [82]. These results are in contrast with those indicated by ATR-FTIR as strong phosphate peaks were not observed until after day 1. However, there is a noticeable shift in from the calcined glass pattern at early time points.

In order to provide greater insight into the effect of sodium content on SGBG bioactivity, the release of boron, calcium, sodium, and phosphorous ions in SBF were measured through ICP-OES [120]. Figure 6.6 shows the release profiles up to day 7, along with the neat SBF concentrations of calcium and phosphorous. All glasses released the majority of boron ions by 0.5 h and according to the total borate content in the glass as indicated by the relatively constant values at longer times. Similar to previously reported SGBGs, the there was a decreasing trend in calcium release after 0.5 h for each composition [249, 262], which indicates re-precipitation on the glass surface as confirmed by the HCA peaks in XRD diffractograms. A more rapid decreasing trend was observed for phosphorous between 2 h and 1d, which is thought to be an indicator for HCA formation [120]. Sodium release rates, on the other hand were difficult to measure as the amount of sodium in SBF is very high (142 mM) [117]. Nonetheless, the slightly increasing release rates corresponded well with composition in that higher sodium containing glasses released a larger amount of Na ions in solution. Previous dissolution studies with a Na24 equivalent in water showed that sodium release was fairly static from 6h – 168h (~ 225 ppm) [249]. Future studies in water may provide better understanding of sodium release rates in these glasses along with examination at earlier time points than 0.5 h.

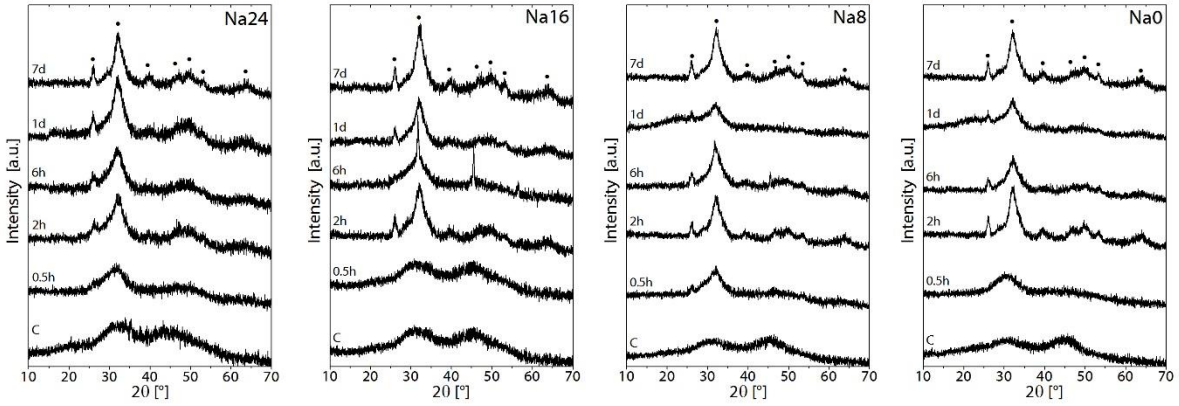

Figure 6.5 XRD diffractograms as a function of immersion time in SBF. All SGBG compositions rapidly converted to HCA ("•", JCPDS 9-0432).

Overall the ion release data supports the previously proposed dissolution-precipitation reactions that describe the "volume reduction" model (section 2.3.3.2) for borate glasses in that, HCA is formed on the glass surface and continues reacting towards the center until only HCA remains [17, 219]. This is in contrast to silicate-based glasses where a gel-like surface layer is formed on which the HCA is deposited [10]. The volume reduction model is supported by the fact that boron release rate and HCA formation is rapid, according to XRD (Figure 6.5). However, since the amount of borate increases with decreasing sodium content, further investigations with fixed borate content, are needed to observe the direct role of sodium in SGBGs.

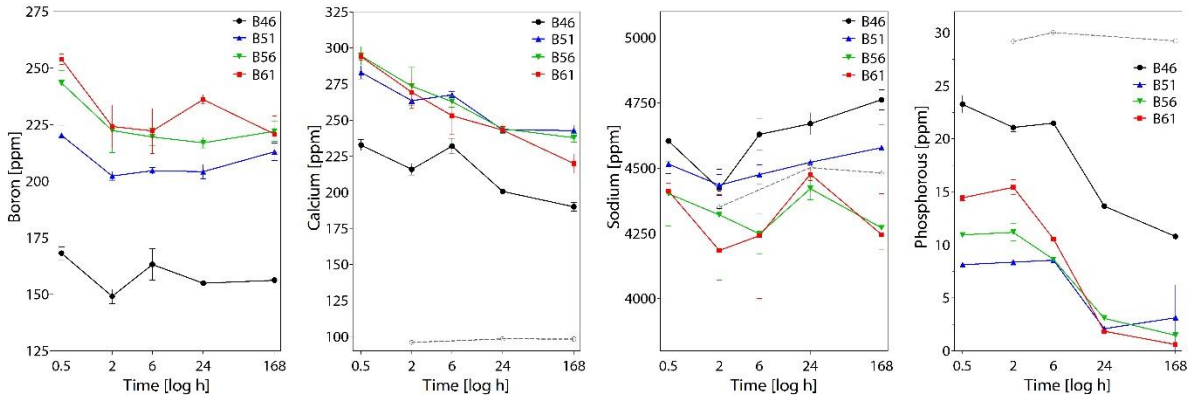

Figure 6.6 Release of boron, calcium, sodium, and phosphorus in SBF as measured through ICP-OES. Rapid ion release was observed with boron depending on composition and the decreasing release trend of calcium and phosphorous suggested their re-precipitation on the glass surface.

6.4 Conclusions

A new range of sol-gel derived bioactive borate glasses with decreasing amounts of sodium have been created. Lower amounts of sodium limit gel formation but increase the specific surface area values of the calcined glasses. Furthermore, in this study, sodium did not induce crystallization as is commonly observed in other sol-gel systems. Reactivity of the glasses was highly influenced by sodium content but there was no correlation with bioactivity as all glasses demonstrated rapid HCA conversion within 2 h according to XRD. The study represents a step towards more simple, three component SGBG for biomedical applications.

Acknowledgements

This study was supported by Canada NSERC, Québec MEIE, CFI and McGill University Faculty of Engineering Hatch Faculty Fellowship for S.N.N. W.C.L. is also supported by the McGill Engineering Doctoral Award, FQRNT.

7 Acellular Bioactivity of Sol-Gel Derived Borate Glass-Polycaprolactone Electrospun Scaffolds

The previous three chapters have demonstrated that a wide range of SGBGs can rapidly convert to bone-like HCA, *in vitro*. Therefore, their combination in a polymer may enhance the bioactivity of a composite system. Composite biomaterials offer synergistic advantages as the phases can work together to mimic more complex tissue targeted for repair. Chapter 7 focuses on a novel composite system of SGBG particle incorporated into electrospun polycaprolactone (PCL) fibers. PCL does not demonstrate bioactivity by itself, however, with up to only 5 wt.% addition of SGBG particles, the composite scaffolds converted to HCA within three days. The improved handling and increased bioactivity of these scaffolds might provide alternative options for tissue repair. This work was published in the Special Larry Hench memorial issue of the peer-reviewed journal, *Biomedical Glasses* and is reproduced below.

Acellular Bioactivity of Sol-Gel Derived Borate Glass-Polycaprolactone Electrospun Scaffolds

William C. Lepry[1], Sophia Smith[1], Liliana Liverani[2], Aldo R. Boccaccini[2], and Showan N. Nazhat[1]*

[1]Department of Mining and Materials Engineering, McGill University, Montreal, QC, Canada

[2]Institute of Biomaterials, Department of Materials Science and Engineering, University of Erlangen-Nuremberg, Erlangen, Germany

*corresponding author showan.nazhat@mcgill.ca

Abstract

Recently, sol-gel derived borate glasses (BGs) have shown unprecedented conversion rates to bone-like mineral (hydroxycarbonated apatite). In an effort to explore their potential applications in bone tissue engineering, this study reports on the fabrication and characterization of BG particle incorporated electrospun ε-polycaprolactone (PCL) fibrous composites. The electrospinning technique successfully incorporated PCL fibers with BG particles at 2.5 and 5 w/v%, with the higher BG loading creating a three-dimensional cotton-wool like morphology. Dynamic vapor sorption showed greater extents of mass change with BG content attributable to water sorption, and indicating greater reactivity in the composite systems. *In vitro* bioactivity was investigated in simulated body fluid for up to 7 days. Scanning electron microscopy, Fourier-transform infrared spectroscopy and x-ray diffraction indicated apatite formation in the 5 w/v% incorporated composite scaffold, which initiated as early as day 3. In summary, sol-gel derived BGs incorporated-fibrous electrospun PCL composites indicate rapid reactivity and bioactivity with potential applications in mineralized tissue engineering.

7.1 Introduction

Current procedures in the repair and augmentation of damaged or diseased bone rely mostly on using either autografts, where bone is sourced from another site of the patient, or allografts where it is sourced from another patient [268]. However, these have drawbacks in terms of limited supply, donor site morbidity, and the risk of infection [3], which have led to the field of tissue engineering as a viable alternative method to traditional bone repair techniques. Therefore, there is an ever-increasing demand for new bioactive and biodegradable three-dimensional (3D) scaffold compositions that mimic the native collagenous, fibrous-based bone extracellular matrix (ECM) [269].

Electrospinning (ES) is a common technique in scaffold fabrication attributable to its simplicity and reliable creation of long, continuous fibers [270]. ES involves the application of high voltage differences between a polymeric liquid and a collecting target in order to produce structures of different morphologies. ES has been widely used for tissue engineering due to the ability to attain diameters of fibers similar to that in the ECM [271]. In particular, it has been used with FDA approved biodegradable polyesters based on polycaprolactone (PCL) and polylactides (PLAs), amongst others [272]. However, while these polymers are biodegradable, they are hydrophobic in nature and, more importantly, in the context of bone tissue engineering, are not bioactive.

Indeed, bioactivity is recognized as a critical requirement for bone tissue engineering since bioactive materials (e.g. bio-ceramics and -glasses) have the ability to form hydroxycarbonated apatite (HCA), the mineral component of bone, in physiological fluids [12, 241]. Therefore, a composite of long continuous fibers incorporated with bioactive particles may prove to be a successful scaffold for bone tissue engineering; allowing for custom bone grafting and easier handling in a clinical setting. Surprisingly though, there has been very little studies on the effect inorganic particle additions to polyester fibers produced through ES. Hydroxyapatite [273], Mg,CO_3-doped HA particles [274], and $CaCO_3$ nanoparticles [275] have previously shown to improve the bioactive response of electrospun PCL fibers. Bioactive glass particles, (70)SiO_2-(25)CaO-(5)P_2O_5 (mol.%) have also been added to PLA fibers, which allowed for a calcium phosphate layer to form on the surface [276]. Using the sol-gel process, hybridised polymer-glass fibers have been generated using polyvinylbutyral [277] and PCL [278].

In addition to bioactive silicate-based glasses, recently there has been much interest in borate-based glasses (BGs) attributable to their lower chemical durability and more rapid HCA conversion rates [17]. Numerous studies have also shown that these glasses are able to re-grow bone with no

toxicity, *in vivo* [141, 198, 199]. Furthermore, while almost all bioactive glasses are produced by the melt-quench technique, the sol-gel process, a liquid based synthesis approach that typically uses metal alkoxide precursors, can offer many advantages for biomedical applications [82, 207]. In particular, higher surface areas and porosities, which have been shown to allow for rapid ion release and degradation thus increasing HCA formation rates [15, 82, 173]. Similar to melt-quench glasses, almost all of the research performed on bioactive sol-gel glasses has been silicate-based [20]. However, the processing of highly bioactive sol-gel derived BGs based on the four component system, B_2O_3-CaO-P_2O_5-Na_2O, with borate content ranging from 36 to 61 mol.% have recently demonstrated remarkable HCA conversion rates in as little as 30 minutes in simulated body fluid (SBF) [249]. The sol-gel processing of BGs combine their lower chemical durability with increased surface area and porosity resulting in rapid calcium and phosphate ion release and thus conversion to HCA.

Melt-quench bioactive BGs have been well represented in composite system. For example, BG incorporated chitosan composites have been created as an antibiotic delivery in the treatment of chronic osteomyelitis [279]. They have also been used as fillers in methacrylate-based composites [280]. However, bioactive BGs and in particular when processed through sol-gel technique have not been used as fillers in electrospun composite scaffolds. Herein, sol-gel derived BG incorporated electrospun PCL fibers were fabricated for potential applications in bone tissue engineering, and their reactivity and acellular bioactivity were investigated *in vitro*.

7.2 Methods

Sol-Gel borate glass production

Sol-gel-derived BG of the formulation $(46.1)B_2O_3-(26.9)CaO-(24.4)Na_2O-(2.6)P_2O_5$ (mol.%) was fabricated as previously reported [249]. Briefly, using a nitrogen filled glove box, boric acid (≥99.5% Sigma Aldrich) and anhydrous ethanol were mixed in a covered Teflon beaker and magnetically stirred at 40 ± 3°C until the solution became clear. This was followed by the addition of triethyl phosphate (>99.8%, Fisher Scientific), calcium methoxyethoxide (20% in methoxyethanol, Gelest, USA), and sodium methoxide (25 wt.% in methanol, Fisher Scientific) at 30 min intervals. The solution was then allowed to mix for another 30 min or until the viscosity became too high for further mixing. The resulting sol was then cast into polypropylene vials and sealed to undergo ageing for 10 days at 37 °C. The gels were then removed, placed in crystallization dishes, and dried in air at room temperature for one day followed by drying at 120 °C for a further two days. Calcination of the dried gels was carried out at 400 °C using a 3 °C/min ramp rate and a 2 h dwell time. Post calcination, the

glasses were pulverized using a planetary ball mill and sieved to < 25 μm. The median (D_{50}) and average diameter (D_{avg}) of the sieved glass particles were determined using a Horiba LA-920 (ATS Scientific Inc., Canada).

Electrospinning of PCL-BG composites

PCL (Number average molar mass of 80,000, Sigma Aldrich) was added to glacial acetic acid (Sigma Aldrich) at 20 w/v% and mixed overnight until the solution became clear. The solution was then ultrasonicated for 1 h to ensure homogeneity [281]. In another approach, the surfactant F127 1 w/v% (Sigma Aldrich), was added during sonication. For composite scaffold fabrication, along with 1 w/v% surfactant addition, BG particles were incorporated at either 2.5 or 5 w/v% (wt.%) relative to PCL solution. These mixtures underwent manual mixing for 1 min followed by sonication for a further 3 min to ensure homogeneity. The solutions was then loaded into a 3 mL syringe and placed in a commercial ES apparatus (Starter Kit 40KVWeb, Linari Engineering srl, GR), using 15 kV, 15 cm working distance, 21G needle (OD, 0.8 mm), and a flow rate of 0.4 mL/h collected on a flat grounded collector. Table I provides a summary of the compositions investigated and their codes.

Dynamic Vapor Sorption

The aqueous interactions of the electrospun scaffolds were investigated through dynamic vapor sorption (DVS) using a DVS Intrinsic (Surface Measurement Systems Ltd., U.K.), which measures mass changes (±0.1 μg) under controlled relative humidity (RH) and temperature. Approximately 20 mg of scaffold sections were placed in an aluminum pan and inserted into a chamber at 37 ± 0.05 °C. The scaffolds were then directly exposed to 90% relative humidity for 6 h and then to 0% RH for a further 6 h.

Bioactivity

The *in vitro* mineralization of the electrospun scaffolds were examined using Kokubo's SBF [117]. Scaffolds were added to SBF (pH 7.4) at a 0.25 mg/mL ratio and stored at 37 ± 1 °C. The SBF solution was replaced every third day. Mineralization was examined at days 1, 3, and 7 where the scaffolds were gently rinsed with deionized water then dried.

Scanning Electron Microscopy

Scanning electron microscopy (SEM) of the calcined BG particles and fibrous scaffolds before and after immersion in SBF was performed with an Inspect F50 Field Emission Scanning Electron Microscope (FEI Corporation, USA) using an accelerating voltage of 2kV. Samples were sputter coated with Pt prior to analysis. Measurement of fiber diameters was completed with ImageJ v.1.49 (NIH, USA) software (n = 200).

Attenuated total reflectance-Fourier transform infrared spectroscopy

Attenuated total reflectance-Fourier transform infrared (ATR-FTIR) spectroscopy was performed on the calcined BG particles and fibrous scaffolds before and after immersion in SBF. ATR-FTIR was carried out using a Spectrum 400 (Perkin-Elmer, USA) between wavenumbers 4000 and 650 cm^{-1} with a resolution of 4 cm^{-1} and 64 scans per sample. Spectra were baseline corrected and normalized to the total area surface area under absorption bands using Spectrum software (Perkin-Elmer, USA).

X-ray diffraction

X-ray diffraction (XRD) analysis was performed on performed on the calcined BG particles and fibrous scaffolds before and after immersion in SBF. XRD were analyzed using a Bruker D8 Discover X-ray diffractometer (Bruker AXSS Inc., USA) equipped with a CuKα (λ = 0.15406 nm) target set to 40 mV and 40 mA. Three frames of 25° were collected from 10 – 70 2 theta (°) using an area detector the merged. Phase identification was carried out using X'Pert Highscore Plus (PANalytical, Netherlands).

7.3 Results

Characterization of the BG and as-made electrospun PCL-BG scaffolds

The calcined BG particles were characterized in terms of particle size, morphology, and structure through ATR-FTIR and XRD (Figure 7.1). A histogram showing the particle size distribution of the calcined BG is shown in Figure 1a. The median particle size (D_{50}) of the as prepared powders was 10.64 μm with an average particle diameter of 11.59 ± 6.74 μm. SEM micrographs (Figure 7.1) showed the resultant nanotextured surface of the glass from the sol-gel process. ATR-FITR spectrum of BG particles (Figure 1c), indicated three regions at 850 – 1200 cm^{-1} (B–O stretching of BO_4 units), 1200 – 1500 cm^{-1} (B–O stretching of BO_3 units), and a band at ~720 cm^{-1}, attributable to the B–O–B bending of BO_3 units (Figure 7.1) [218-220]. The broad band around 1000 cm^{-1}, is attributed to the B–O linkages of BO_4 [165, 221-223] and the defined shoulder peak at ~870 cm^{-1}, is

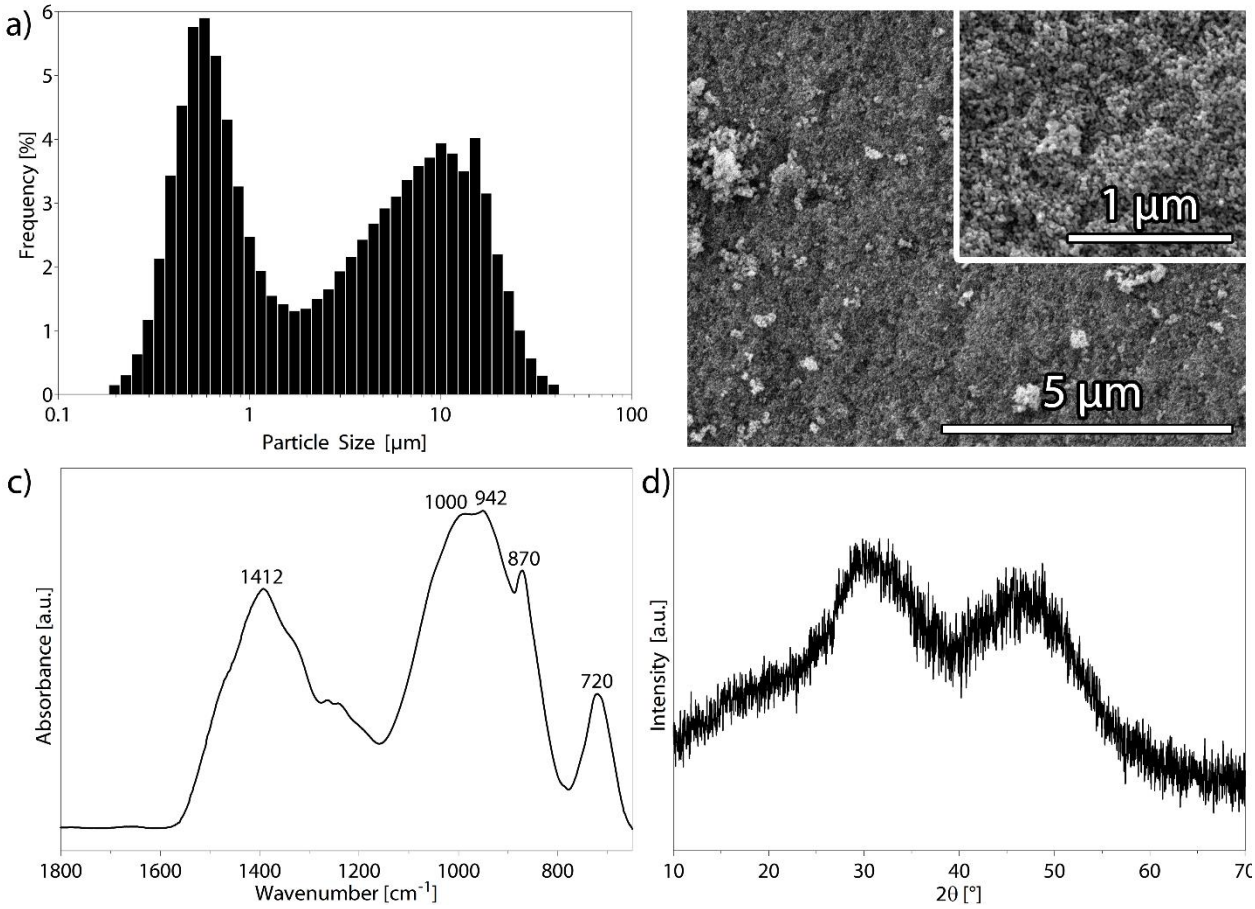

Figure 7.1 Characterization of BG particles. (a) Particle size distribution of the calcined BG particles. (b) Nanotextured morphology of the glass surface via SEM. (c) ATR-FTIR spectra showing the bonding moments for the BG particles and (d) XRD diffractograms displaying the typical amorphous humps.

characteristic of the B–O stretching of boroxol rings. XRD (Figure 7.1) confirmed the amorphous nature of the glass as observed by the two broad humps typical of this material [249].

SEM micrographs of as-made PCL and PCL-BG scaffolds confirmed the typical continuous fibrous structure achieved through the ES technique (Figure 7.2). Insets for PCL-2.5BG and PCL-5BG show that the BG particles were successfully incorporated within the PCL fibers. According to fiber diameter measurements (Figure 7.2 and summarized in Table 7.1) the addition of surfactant (PCL-S) resulted in a smaller, more uniform distribution of fibers compared to neat PCL. Furthermore, the addition of BG (PCL-2.5BG) generated a broader range of fiber size. This increase

in fiber diameter was significant ($p < 0.05$) in the case of PCL-5BG. The resultant cotton-wool like nature of the PCL-5BG and the potential handling ability can be seen in Figure 7.2.

Table 7.1 Scaffold compositions and their average fibre diameters as measured from SEM micrographs (n = 200).

ID	Surfactant (w/v%)	BG (w/v%)	Avg. Fibre Diameter (μm)
PCL	0	0	1.2 ± 0.5
PCL-S	1	0	0.8 ± 0.3
PCL-2.5BG	1	2.5	1.0 ± 0.7
PCL-5BG	1	5	3.5 ± 1.8

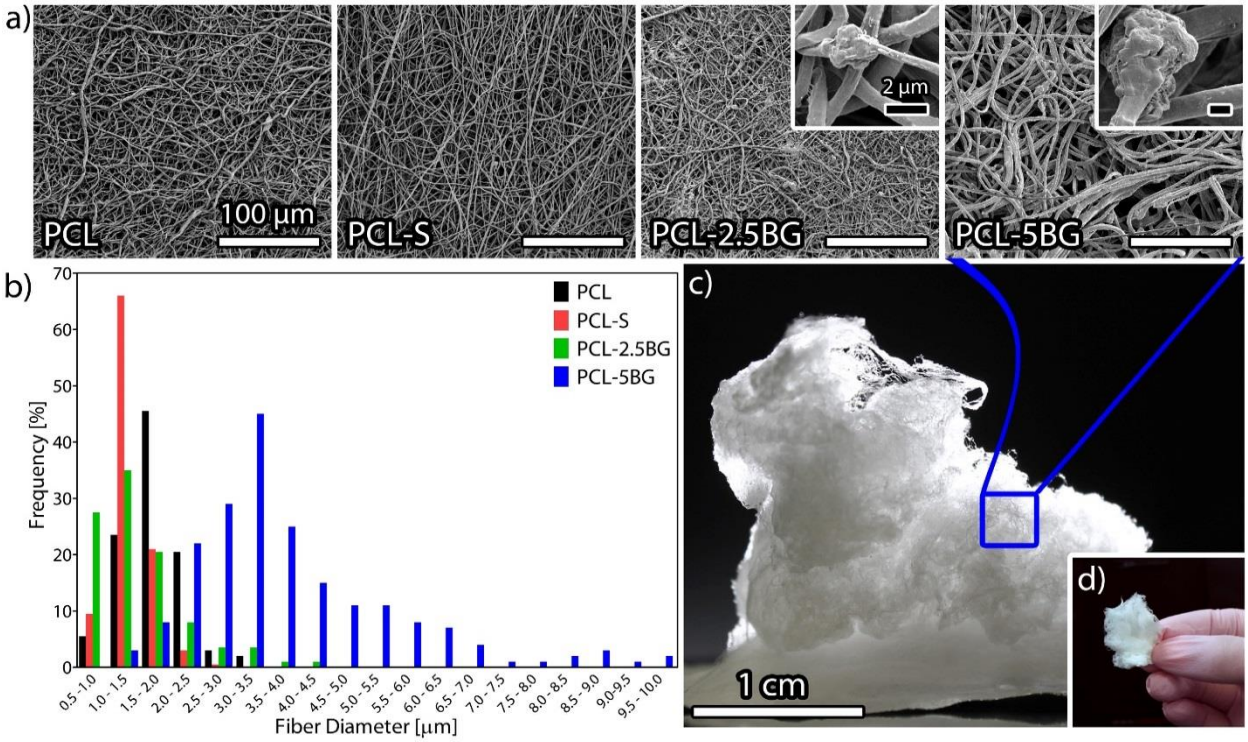

Figure 7.2 Morphology of as-made PCL and PCL-BG scaffolds. (a) SEM micrographs showing the fibrous morphologies and BG incorporation in composite scaffolds (inset scale bars = 2 μm). (b) Range of fibre diameters for the various scaffolds, indicating wider distribution of diameters with BG incorporation. (c) A macro view of PCL-5BG showing the cotton-wool like nature and (d) ease of handling of the scaffold.

The structural and chemical properties of the electrospun PCL and PCL-BG composite scaffolds were characterized through ATR-FTIR and XRD analyses. ATR-FTIR spectra of PCL and

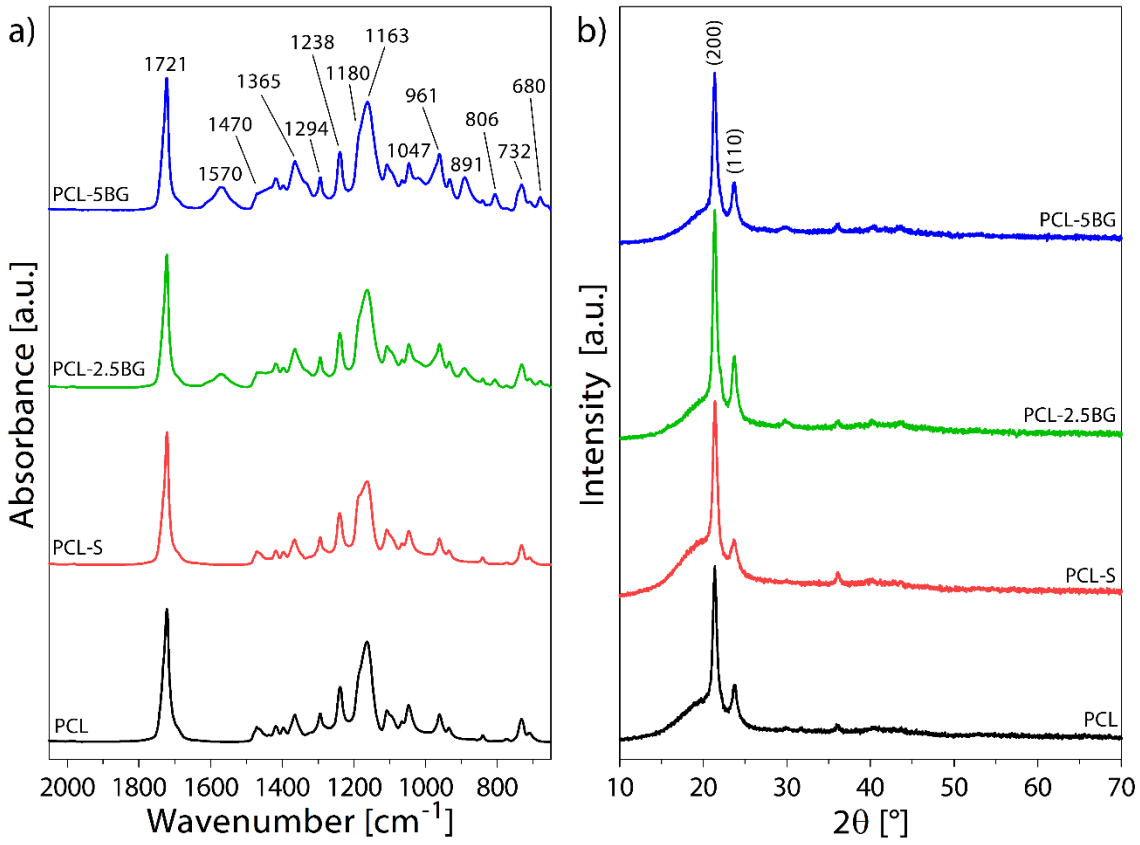

Figure 7.3 Structural analyses of as-made PCL and PCL-BG scaffolds. (a) ATR-FTIR spectra showing representative bonding moments of the electrospun PCL and PCL-BG scaffolds. (b) XRD diffractograms showing typical semi-crystalline peaks associated with PCL.

PCL-S showed common bands associated with the crystalline (1294 cm^{-1}) and amorphous (1163 cm^{-1}) phases [282]. Furthermore, the band at 1721 cm^{-1} [282] can be attributed to the stretching of υ_s(C=O) while the bands at 1238 and 1180 cm^{-1} represent the asymmetrical stretching of υ_{as}(C–O–C) and symmetric stretching of υ_s(C–O–C) respectively [283]. Peaks at 1047 cm^{-1} and 1470 cm^{-1} are associated with C–O stretching [284] and C–H bending [278], respectively. The incorporation of BG in PCL, resulted in new bands at 1570, 891, 806, and 680 cm^{-1}. Furthermore, the C–H bending at 1470 cm^{-1} begins to fade to form a shoulder region with increasing glass addition. In addition, the two defined diffraction peaks related to the (110) and (200) lattice planes at 21.5 and 23.6° 2-theta respectively, indicated the typical semi-crystalline morphology of PCL [285]. Compared to the amorphous BG (Figure 7.1), the PCL semicrystalline peaks dominate the XRD diffractograms of the composites.

Scaffold reactivity through vapor sorption

The aqueous interactions of the scaffolds, as an indicator of their reactivity and potential degradation, were investigated using DVS (Figure 7.4). Under direct exposure to 90% RH, BG incorporated PCL scaffolds demonstrated a rapid increase in mass within the first hour. This was followed by a plateauing region, ultimately leading to an equilibrium mass gain of ~24.8 and ~38.9% for PCL-2.5BG and PCL-5BG, respectively after 6h. Both of these values were below that observed for neat BG particles (~48.3%) and substantially greater that those observed for PCL (~1.2%) and PCL-S (~2.2%).

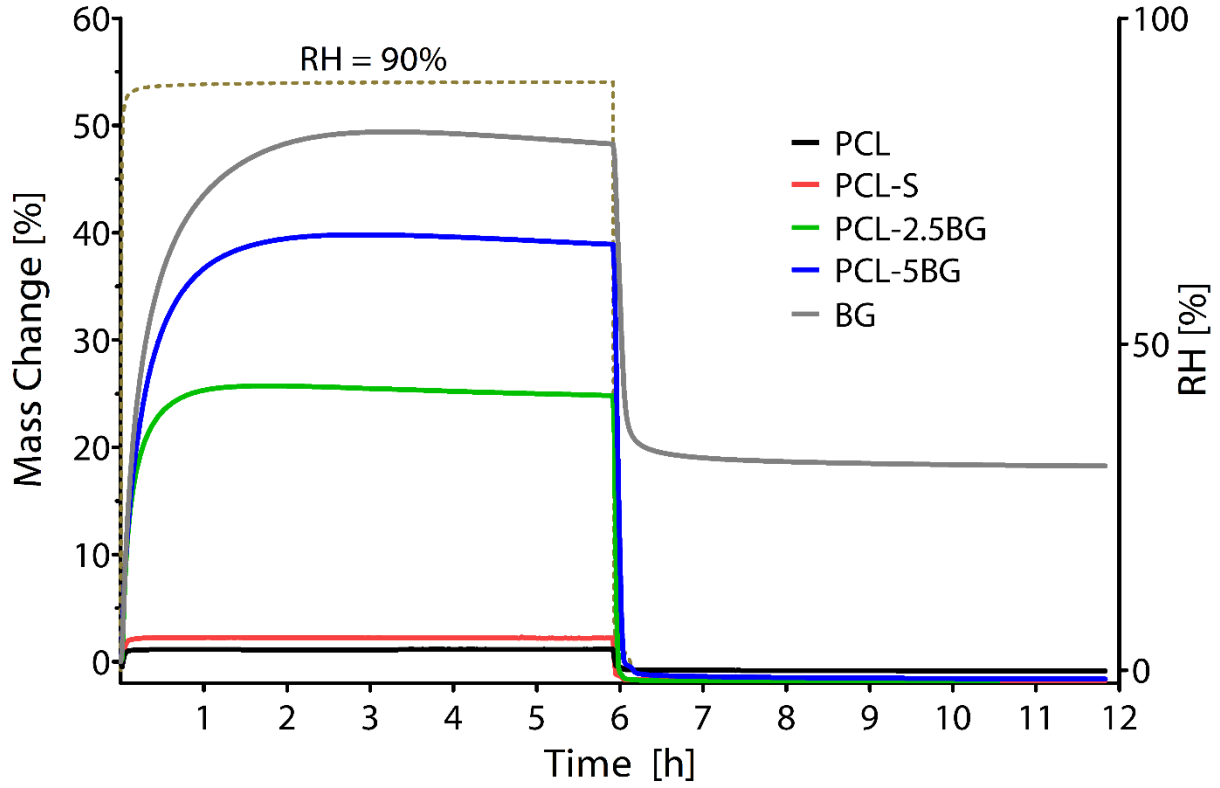

Figure 7.4 Reactivity of PCL and PCL-BG scaffolds through vapour sorption. The direct exposure to 90% RH, resulted in a rapid increase in mass of BG and BG incorporated PCL scaffolds. At 6 hours, the equilibrium increase in mass increased with BG content in composite scaffolds. The return to near 0% mass change after 12 hours for the PCL samples demonstrated their hydrophobic nature.

Scaffold bioactivity in SBF

The bioactivity of the PCL and PCL-BG scaffolds were investigated in SBF for up to 7 days. SEM micrographs of the PCL-5BG scaffolds indicated the progressive deposition of flower-like crystals as a function of time in SBF, which was prominent by day 7 (Figure 7.5). The surface at PCL-2.5BG showed a fairly similar formation, though to a much lesser extent. As immersion time increased

the fibrous scaffolds began to undergo surface transformation as observed by the roughening of PCL and PCL-S at day 7.

ATR-FTIR spectra of the PCL-5BG scaffolds as a function of time in SBF indicated the progressive increase in the intensity of the peak around 1020 cm^{-1}, which is attributed to PO_4^{3-} [252] and indicating apatite formation (Figure 7.6). In contrast, the spectra for the PCL, PCL-S, and PCL-2.5BG remained largely unchanged as a function of time in SBF. XRD diffractograms of the scaffolds at day 7 in SBF confirmed apatite formation in PCL-5BG (Figure 7.7). The presence of the peak at ~32° 2-theta, which is the main peak associated with hydroxyapatite, along with the development of other peaks, also related to hydroxyapatite ("•", JCPDS 9-0432) confirmed apatite formation.

7.4 Discussion

Electrospinning, a relative simple technique that generates fibrous scaffolds from polymer solutions, has been widely investigated for PCL, as well as other polyesters and their blends [271, 281, 284, 286]. However, compared to glacial acetic acid, other solvents, such as chloroform [271, 287], acetone [286], methylene chloride [288], and hexafluropropanol [289], amongst other combinations

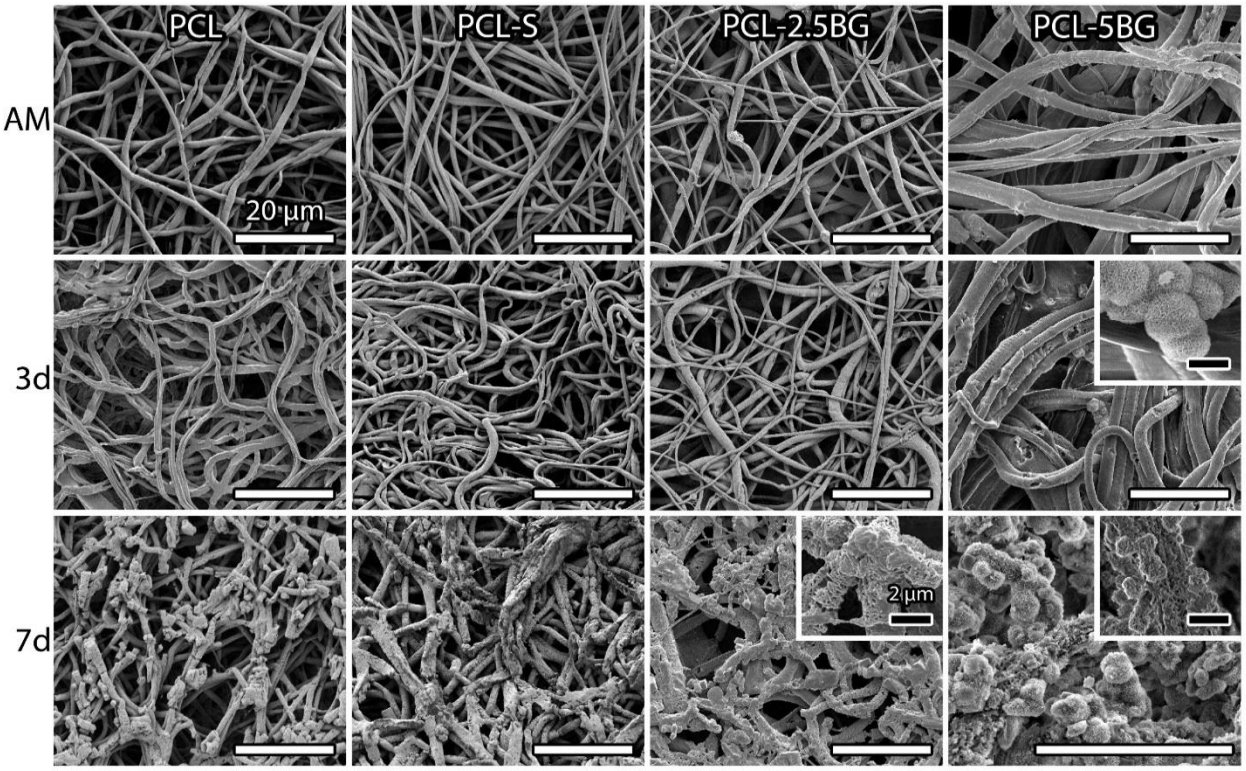

Figure 7.5 SEM micrographs of PCL and PCL-BG scaffolds as a function of immersion time in SBF. For PCL-5BG composite scaffolds, apatite-like crystals were visible at day 3 and rapidly increased by day 7. Surface changes were visible in the non-doped PCL samples at day 7.

[290, 291], have been more commonly used to dissolve PCL for electrospinning. Nevertheless, interest in the use of less toxic or potentially harmful solvents in ES arose with the introduction of the "Green Electrospinning" concept [292]. In particular, PCL electrospun fibers have also been generated by using less or non-toxic solvents (benign solvents), offering potential environmental and biomedical applications advantages [293, 294]. The suitability of this system has already been tested in the fabrication of neat PCL electrospun fibers [281] and blends of PCL/gelatine electrospun fibers [295]. Furthermore, PCL dissolved in glacial [293] and 90% acetic acid [290] and with the fiber size range is similar to reported values [293]. Previous research has shown that adding pyridine to acetic acid helped reduce the overall size of PCL fibers and generated predictable the fiber distributions [296] which may be a future approach to control fiber size. A previous study has also shown that using acetic acid, acetone, or a combination of both did not affect the chemical structure of ES-PCL, and indicated that the solvent was removed by evaporation during processing [297]. Solvent removal can also be performed by freeze drying and rotary evaporation, though this would likely initiate the conversion process of the BG particles.

The wider range of fiber distribution with increasing BG content might also be related to the electrical conductivity [298] or viscosity [295] of the solution. In ES, as the electric potential intensifies the polymer solution at the needle tip elongates to form a conical shape called the Taylor cone [299, 300]. With further electric potential increase, it reaches a threshold value causing the formation of a polymer jet as the surface tension is overcome by the repulsive electrostatic force. The polymer jet is then ejected from the Taylor cone towards the metal collector and collected after thinning due to solvent evaporation and bending instabilities that are electrically driven [301]. Therefore, a polymer solution with higher electrical conductivity exerts greater tensile force, which can increase the stretching and splitting of the jet, creating a broader distribution and overall smaller fibers. However, it is also possible that if the solution flow is not high enough, a thicker fiber diameter will form since a greater tensile force is exerted. Since the ES parameters were consistent across all materials, in order to compare the fabricated electrospun scaffolds, it is conceivable that the increase in BG loading also increased the viscosity which might have required a greater ejection rate in order to produce thinner fibers. In this study, it was found that the incorporation of BG at greater than 5w/v% (e.g. 7.5 and 10 w/v%) prevented the generation of fibrous matrices. Previously, it has been shown that the addition of up to 5 w/v% multi-walled carbon nanotubes increased both the diameter and distribution of the electrospun PCL fibers [298].

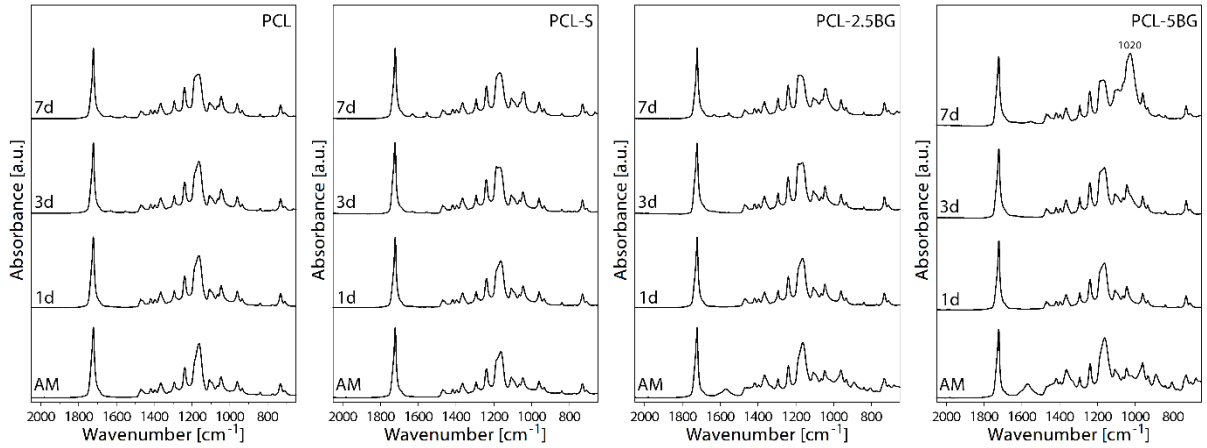

Figure 7.6 ATR-FTIR spectra of PCL and PCL-BG scaffolds as a function of immersion time in SBF. The presence of the peak at 1020 cm-1 in BG incorporated PCL scaffolds at day 7 suggested apatite peak formation.

An alternative approach to generate bioactive fibers involves the direct electrospinning from a sol, or sol-gel hybrid, which can be advantageous since it does not require a separate glass particle addition to the polymer and the resultant glass or glass-hybrid fibers are typically more uniform and homogenously distributed due to the nanoscale nature of the sol [82]. Nevertheless, the cotton-wool like appearance in this study, is reminiscent of previous work on glass fibers made by ES, directly from a sol with no polymer addition [302]. It was reported that the Ca^{2+} ions from the sol can act as charge carriers, which has previously been shown to increase the charge density on the surface of the jet [303], leading to greater branching from the primary jet. However, in this scenario, it leads to the splitting of several jets, known as "splaying" which has been previously described [270], and can result in a "bush-like" appearance. PCL and PCL-S did not show any signs of this build up making it likely that BG played a primary role in creating the 3D fiber morphology. PCL-2.5BG began to form fibrous mats that were not entirely flat but not nearly to the extent of the 3D morphologies generated with PCL-5BG. Since these glasses have previously demonstrated rapid dissolution rates [249], it is possible that during their mixing with the PCL solution, released Ca^{2+} and BO_3^{3-} ions that may have acted as charge carriers, increasing the electrical conductivity, and thus causing the cotton-wool like appearance. This 3D morphology may be desirable for many tissue engineering applications since it can be packed into various defects [302]. Moreover, it has been recently reported that fibrous, "cotton candy-like" BGs have been successfully used for wound healing applications [205, 244, 304].DVS has been used to predict the reactivity and potential solubility of bioactive glasses [249, 265, 266] and polymer coatings [305]. In the case of glass systems, it has been found that the extent of mass change is dependent primarily on the composition, followed by textural properties [249]. Here, since the

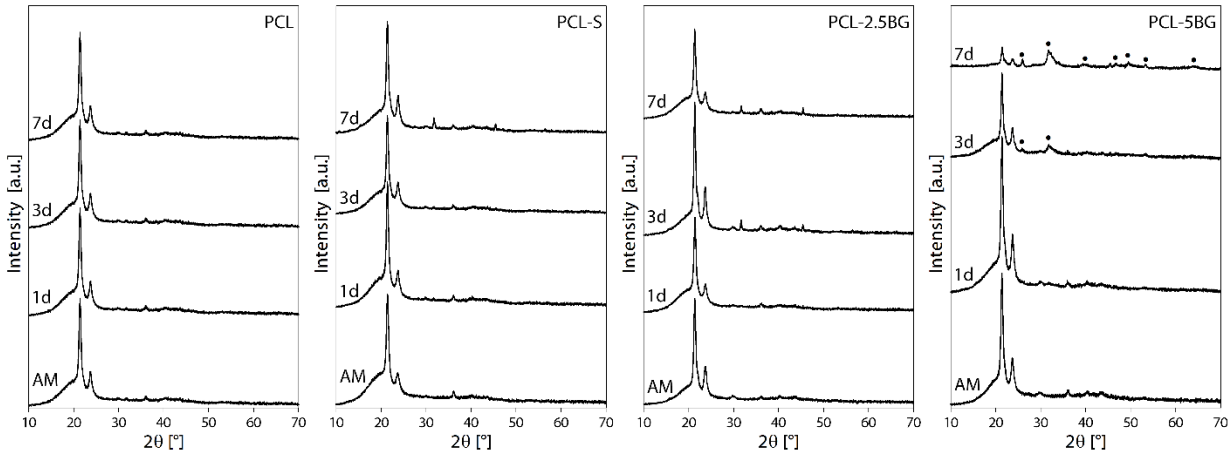

Figure 7.7 XRD diffractograms of PCL and PCL-BG scaffolds as a function of immersion time in SBF. Apatite conversion ("•", JCPDS 9-0432), which was initiated at day 3 for the BG incorporated PCL scaffolds were more defined by day 7 in SBF.

incorporated glass composition was the same in both BG incorporated scaffolds, the volume fraction of BG influenced the final mass change, increasing with BG content. The terminal –OH groups, that result on the surface of the BG from the sol-gel process [82], are thought to make the composites be more prone to aqueous interactions. Furthermore, the <2% mass change with the PCL and PCL-S samples have previously been observed with water sorption studies [306] and were expected due to the hydrophobic nature of the material. Therefore, it can be concluded that the mass change observed in the composites, was a direct result of the BG additions. This hydrophobicity of PCL was also demonstrated by the final mass change after 12 hours which was approximately 0% for all materials except for the BG particles, which has the ability to undergo permanent mass change [249].

Only PCL-5BG indicated apatite conversion as observed through SEM, ATR-FTIR and XRD analyses. SEM micrographs indicated significant apatite formation as well as fiber degradation. PCL surface degradation has been previously shown at day 7 in SBF by Joshi et al. [307]. Apatite formation was also supported by ATR-FTIR spectroscopy, in particular by the slight broadening of the peak around 1020 cm^{-1} in PCL-5BG at day 3, which was more pronounced by day 7, surpassing the intensity of the characteristic PCL υ_s(C=O) peak at 1721 cm^{-1}. This apatite conversion time scale was confirmed by XRD through the peak ~32° 2 theta apparent in PCL-5BG scaffolds, where at day 7 showed significant retardation of the inherent semi-crystalline peaks of PCL, as previously reported through the addition of other dopants to PCL or by changing the PCL fabrication process [298]. It also indicated the prominence of apatite presence at this time point, which can be confirmed by the additional peaks ("•", JCPDS 9-0432). Despite the higher DVS reactivity of the PCL-2.5BG scaffold compared to PCL and PCL-S, there was no indication of mineralization. While the surface

transformation of PCL-2.5BG appears to be similar to that of PCL-5BG, it cannot be concluded that HCA conversion has occurred based on the ATR-FTIR and XRD data. This suggests that the minimum particle loading needed for HCA conversion is above 2.5 w/v %. However, it is anticipated that this may be achieved by varying the sol-gel and electrospinning processing parameters.

In summary, electrospun PCL scaffolds incorporated with sol-gel derived bioactive BG particles were successfully fabricated. Despite their larger fiber diameters, PCL-5BG scaffolds demonstrated high reactivity according to DVS and significant conversion to apatite by day 7 in SBF according to SEM, ATR-FTIR, and XRD analyses. The cotton-wool like morphology produced with higher BG content is thought to be due to the increased electric conductivity of the solution due to dissolution of the glass during mixing and can potentially improve handling in the clinic to fill unique bone defect sites. Concluding, this a primary example of using sol-gel derived borate glasses to improve the reactivity and bioactivity of a biodegradable polymer can potentially be useful in mineralized tissue engineering applications. Further studies will focus on investigating cellular responses to these promising bioactive scaffolds.

Acknowledgements

This study was supported by Canada NSERC, CFI and McGill University Faculty of Engineering Hatch Faculty Fellowship for S.N.N. W.C.L. was also supported by the McGill Engineering Doctoral Award and Fonds de recherche du Québec (FQRNT) – Bourses de doctorat en recherché. L.L. acknowledges funding from the European Union's Horizon 2020 research and innovation programme under the Marie Skłodowska-Curie grant agreement No 657264. The authors would also like to thank Dr. Stefan Romeis for assistance with particle grinding, Prof. Kristian Waters for use of DVS, and Prof. Nate Quitoriano for use of the glovebox. This project was part of a German Academic Exchange Service (DAAD) short-term research grant received by W.C.L.

8 General Discussion

Due to the ever-ageing population, there is great demand for synthetic bone replacement materials. While many different types of materials excel at certain elements of bone repair, bioactive glasses have emerged as a leader in the field due to their ability to convert to HCA, which allows them to physically and chemically bond to native bone tissue [82]. The most successful and well-studied bioactive glass, was actually the first one to be invented in 1969 by Dr. Larry Hench [12] and since then, many different chemistries and processing methods of bioactive glasses have been investigated. Yet, despite great advancements in this field, bioactive sol-gel-derived borate glasses have not been studied investigated for mineralized tissue repair until now. This thesis investigated the sol-gel processing of bioactive four-component SGBGs. An overview of the glass compositions and selected properties are provided in Table 8.1.

Table 8.1 Summary of all glass compositions and selected properties

	ID[†]	mol %				N_C	D_{50} (μm)	SSA (m^2/g)	Pore Volume (cm^3/g)	HCA formation SBF (h)	
		B_2O_3	CaO	Na_2O	P_2O_5					ATR-FTIR	XRD
Chapter 4	B36	36.2	31.9	28.9	3.0	1.15	34.7	55 ± 8	0.4 ± 0.1	6	6
	B41	41.1	29.4	26.6	2.8	1.68	34.6	72 ± 8	0.7 ± 0.1	6	6
	B46	46.1	26.9	24.4	2.6	2.11	43.8	94 ± 8	0.7 ± 0.1	0.5	3
	B51	51.1	24.4	22.1	2.4	2.46	33.7	114 ± 15	0.9 ± 0.2	6	6
	B56	56.1	21.9	19.8	2.2	2.75	38.8	121 ± 13	1.0 ± 0.1	6	6
	B61	61.3	19.3	17.5	1.9	2.99	47.1	138 ± 12	1.2 ± 0.1	6	6
	45B5*	46.1	26.9	24.4	2.6	2.11	44.1	0.24 ± 0.02	0.0009	72	72
Chapter 5	AM	46.1	26.9	24.4	2.6	2.11	45.4	91± 6	0.6 ± 0.2	-	-
	TMB					2.11	49.1	75 ± 4	0.3 ± 0.02	0.5	6
	TEB					2.11	40.7	81 ± 2	0.4 ± 0.03	0.5	0.5
	0d					2.11	36.8	131 ± 7	0.8 ± 0.1	0.5	0.5
	30d					2.11	35.1	97 ± 1	0.7 ± 0.1	0.5	2
	RT					2.11	30.5	103 ± 2	0.7 ± 0.03	-	-
	65C					2.11	30.3	119 ± 6	0.8 ± 0.1	-	-
	1C/min					2.11	28.5	89 ± 3	0.8 ± 0.1	0.5	2
	10C/min					2.11	26.7	104 ± 20	0.8 ± 0.1	0.5	2
	BA 300					2.11	28.5	106 ± 1	0.8 ± 0.1	0.5	2
	BA 400					2.11	25.1	95 ± 3	0.7 ± 0.1	0.5	2
	BA 500[‡]					2.11	38.5	15 ± 1	0.2 ± 0.04	0.5	24
Chapter 6	Na24	46.1	26.9	24.4	2.6	2.11	39.2	37	0.4	0.5	2
	Na16	51.1	29.8	16.3	2.9	2.53	29.9	71	0.6	0.5	2
	Na8	56.0	32.7	8.1	3.2	2.88	29.3	139	1.0	0.5	2
	Na0	61.0	35.6	-	3.4	3.17	43.9	159	0.6	2	2

[†] Full compositional details given in Chapters 4, 5, and 6

* Melt-derived composition

[‡] BA 500 is a glass ceramic

8.1 SGBG composition and structure

To date, many of the melt-quench derived bioactive borate glass compositions have been based on the full substitution of silicate with borate in bioactive silicate-based glasses, *e.g.,* the creation of 45B5 (46.1)B_2O_3-(26.9)CaO-(24.4)Na_2O-(2.6)P_2O_5 (mol%) [17, 308] to mimic 45S5. This approach was also used as a starting point, where in Chapter 4, a series of six SGBG compositions (36 – 61 mol% B_2O_3) were fabricated based on a borate substituted 45S5 bioactive glass composition. Despite some phase separation during processing (Figure S4.11) with the lower borate containing glass (B36), all six SGBG compositions generated amorphous structures post calcination at 400 °C and demonstrated rapid conversion to HCA in SBF according to ATR-FITR, XRD, and also supported by SEM analysis. Although only B46 and 45B5 were tested at time points below 6h (Figure 4.9), it can be assumed that the conversion of the other glass compositions (*e.g.,* B36, B41, B51, B56, and B61) would be equally rapid based work presented in Chapters 5 and 6.

The bioactivity was predicted using the network connectivity (N_C) model [129] as discussed in section 2.3.3. While this model has served as a good indicator for predicting the bioactivity of multi-component glasses, there are some limitations based on the following assumptions [82, 129]:

1) The glass is homogeneous
2) Once a bO bond is broken, it disappears, and is replaced with an nbO
3) Subjective selection of glass network formers and modifiers
4) Network former is four-coordinated
5) Resultant high surface area and excess –OH groups from sol-gel processing are not considered

The first assumption implies that there exists a uniform distribution of ions within the glass (*e.g.,* homogeneity). Although the glasses were fully amorphous (except for B36) after calcination, which suggests homogeneity, it has also been shown that phase-separated amorphous glasses may be generated through both melt-quench [309] and sol-gel derived systems [310]. Considering the possibility of the existence of phase separation in SGBGs, there may be new insights on the structure and dissolution properties, where the various phases will have different dissolution or conversion rates, which in turn control the overall HCA conversion rates. Second, the model assumes that once a nbO is formed from breaking a bO, that the initial bond disappears. However, in practice this depends on the size and charge of the replacing ion, which can affect the properties of the glass network [129]. The equation leaves it to the user to determine whether ions are network formers or

modifiers. For example, many bioactive glasses have substituted MgO for CaO to create more dense glass networks and typically lowering degradation rates [311]. However, Watts et al. showed that in their glass composition, magnesium can enter the network as either a network former (MgO_4) and/or modifier (Mg^{2+}) when it replaces calcium [312]. Since the same four elements were used for each composition in Chapter 4, and phosphate is assumed not to be part of the glass network, this drawback was not considered. Another key assumption in this model is that the network former is four-coordinated, which is not always the case with borate systems as discussed in section 2.3.2. This would in turn affect the 2 to 2.6 range for N_C that is thought to be bioactive. Perhaps the most overarching assumption of this model is that it equates bioactivity with glass dissolution. For instance, Brauer and Hill described a scenario where substituting two Na^+ ions for one Ca^{2+} ion would likely increase the dissolution, and thus the predicted bioactivity [129]. However, since Na^+ does not directly contribute to apatite formation, this would not hold true in practice [129]. In Chapter 6, reduced sodium content led to slower phosphate peak formation according to ATR-FTIR, but equally rapid HCA formation according to XRD. Interestingly, since borate glasses follow a "volume-reduction" model based on dissolution and direct HCA precipitation [17, 18], the N_C model might be more effective for borate systems once and new calculation model is formulated based on the previously mentioned limitations.

In predicting N_C in Chapter 4, it was also assumed that the boron was four-coordinated, as based on NMR analysis. Thus, the resultant 2.12 N_C value was in a similar range to that of the original Bioglass® composition [82]. Yet, as discussed in section 4.3, a more advanced NMR magnet is needed in order to better decipher the exact amounts of three and four-coordinated boron ions in the glass structure. Additionally, more advanced NMR techniques are necessary to determine whether phosphates enter the borate glass network. Although this is not the case in the Bioglass® network [313], B–O–P bonds are known to exist in borate glasses [240]. These findings would influence the N_C calculation and possibly give better insight into the structure of SGBGs. Perhaps, the number "4" in eqn (1) would be changed to 3 or 3.5 to represent a combination of both three- and four-coordinated borate units in the glass structure. Similarly, Chapter 6 discusses the effect of sodium on SGBG network, where a reduction in sodium content increased N_C (Table 8.1) since a greater portion of network former is present.

The N_C calculation also does not factor in the high surface area and porosity values of glasses generated through the sol-gel process [82]. Thus, the sol-gel process leads to artificially lower N_C values since the H^+ can disrupt the glass network by acting as a modifier [170]. It has also been previously demonstrated in silicate sol-gel systems that, even after thermal treatment, OH^- groups

remain present which further increase dissolution rates [170]. Both of these factors are also not considered in the N_C calculations. These resultant processing properties allow sol-gel glasses to be bioactive [15] beyond the limit of 2 to 2.6 N_C values [128]. Yet, similar to melt-quench derived glasses, it has been shown that in silicate sol-gel systems, the phosphate is also present as an orthophosphate [314] however this might also depend on the amount of phosphate in the glass composition. For these reasons, the N_C model may not be ideal for non-silicate and sol-gel derived systems, and thus a new model that factors in the aforementioned limitations would provide new way to predict bioactivity. Furthermore, chemical analysis of these glasses to determine the actual composition would provide more accurate N_C calculation models.

The above limitations have led to a recent drive to model bioactive glasses through advanced molecular dynamic simulations [267, 315-317]. Since the molecular structure is the most important factor in determining glass dissolution and bioactivity [82, 229], understanding how the structural elements are connected can provide better insight into optimizing the glass composition compared to being based on previously made glasses. By modeling a series of four-component melt-quench derived glasses containing SiO_2-CaO-Na_2O-P_2O_5, Mathew et al. defined three key parameters for optimal bioactivity; the silicate N_C, the phosphate content (orthophosphate), and the molar ratio of Na to Ca [315]. These models become more complex in the case of sol-gel glasses due to the amount of water in the system. Nonetheless, simulations to model the influence of water on the dissolution and reactivity of these glasses have been investigated [318-320]. Simple models in a $(CaO)_x(SiO_2)1\text{-}_x(H_2O)_y$ system suggest that calcium distribution is more homogeneous with increasing OH^- content [321]. These models might prove useful for sol-gel compositions as the processing parameters can be easily varied and to overcome some inhomogeneity as was seen with B36 in Chapter 4. These simulations have increased the understanding of how compositions affect structure and dissolution behavior, and have also been applied for phosphate glass systems [322, 323]. However, although borate mixed alkali systems have been modeled [324], bioactive borate glasses compositions have not. Indeed, although the modeling of borate-based glasses may be more challenging than for silicate-based glasses since the boron ion can take many different forms, understanding when these superstructures form may help in designing borate glasses for different tissue engineering applications.

Chapter 5 focused mainly on the effect of processing parameters on SGBG structure and properties, with some of the compositions resulting in their partial crystallization when calcined at higher temperatures, thus forming glass-ceramics (Figure 5.3). Although the induction of crystallization is known to reduce the bioactivity of amorphous glasses [82], the ability to design glass-

ceramics with potentially increased mechanical properties may prove to be beneficial. In fact new glass-ceramic system, Biosilicate® [325], is being designed due to easier processing characteristics. In addition, although several 45S5 bioactive glass systems have been created through the sol-gel route [179, 181, 251, 258, 259], only a few remain amorphous after calcination [180, 261]. While this may be due to the effect of precursors, such as the use of nitrates, it mainly depends on the final calcination temperature. Thus, calcining below T_g results in amorphous forms, but depending on the precursor materials (*e.g.,* nitrates), the lower temperature may not be high enough to properly eliminate nitrates or organics, and thus some will remain in the glass which might inhibit bioactivity. In this study, nitrates were not used during the processing of SGBGs, and thus a lower calcination temperature was obtainable. Calcination at higher temperatures, *i.e.,* above T_g resulted in the partial crystallization of the glasses into various Na-Ca-B phases (Figure 4.2 and Figure 5.2). Further investigations of these created phases and their bioactivity have yet to be examined, which may provide greater insight on the semi-crystalline glass conversion to HCA.

8.2 SGBG sol-gel processing parameters

Compared to melt-derived equivalents, SGBGs have not been extensively studied. This may be due to their unique chemistry where the boron ion can achieve three- or four-fold coordination along with forming numerous boron ion species (section 2.3.2). In fact, many of the original SGBGs have been based on two- or three-component systems made using very similar precursors or processing conditions [158, 160, 162, 163, 210]. This dissertation, and in particular Chapter 5, demonstrated numerous different methods of producing SGBGs and their effects on the final structural, textural, and bioactive properties. Despite the variations in the processing parameters, all the resultant glasses demonstrated very similar overall bioactivity, with calcination temperature being the most influential factor. However, this calcination step is subjective, and there is no "standard temperature" in sol-gel processing, though it is the norm to use a temperature close to that of T_g. Therefore, a more interesting comparison would be between BA 400, TMB, and TEB since the generated glass is of the same composition is, but is fabricated using different borate precursors.

Work published by Brinker and Scherer provided a robust overview of the chemistry of sol-gel borates [21]. A possible mechanism of hydration and condensation, under neutral conditions, is given in Figure 2.13. Similar to what Brinker and Scherer proposed, the basis of this work started with boric acid which is mixed with an ethanol group, producing a $B(OR)_3$ group and water. It was postulated that instead of explicitly adding water, as in other sol-gel processing approaches, this initial

step produced enough excess water to hydrolyze the other components in the system. Therefore, the resultant $B(OR)_3$ starting group was likely TEB ($BO_3C_6H_{15}$), when boric acid and ethanol were mixed. However, in the case of the latter two methods of using either TMB or TEB, no water (or alcohol) was explicitly added to hydrolyze this system, since it has been shown that additional water rapidly causes precipitation of $B(OH)_3$ in both these precursor materials [326], which may have resulted in the lack of gel formation (Figure 5.1 and Figure 6.1). Nevertheless, upon evaporation a clear, gel-like layer did form which was similar to that reported on evaporation-induced self-assembly of mesoporous glasses [263]. This lack of gel formation (*i.e.,* 3D character) might be the cause in the slight decrease in the calcined glass textural properties when compared to those produced using boric acid as the precursor material (Table 5.2). Therefore, more possibilities regarding hydrolysis and condensation reactions, using different precursors and processing parameters, need to be examined using less complex, two or three-component system will allow for better deciphering of pH effects due to the reduced influence of precursor materials.

The other precursors in the four-component compositions included calcium (calcium methoxyethoxide 20% in methoxyethanol), which has been shown to be superior compared to calcium nitrate, since the former can enter the network during processing while the latter will only enter the glass network after heating [327]. The phosphate source was TEP, which is the most commonly used precursor for sol-gel bioactive glasses although not always used when phosphate is the main component in the sol-gel process [188, 189]. Sodium methoxide 25 wt.% in methanol was used as the sodium source and although the addition of sodium is not common the sol-gel process, it has been previously investigated to improve the glass mechanical strength and has also recently been added to create sol-gel derived Bioglass® equivalents as discussed in Chapter 6. For SGBGs, upon the final addition of sodium, the pH of the sol greatly increases, and gelation often occurs within a few minutes due to an inherently high pH. Further studies are required to explore the order of precursor addition, which may affect the hydrolysis and condensation reactions, thus impacting gel formation and possibly the generated glass structural and textural properties.

8.3 SGBG textural properties

This study has, for the first time, demonstrated that the specific surface area and porosity of an SGBG composition (B46) is two orders of magnitude higher than its melt-derived equivalent. It is well known that the sol-gel process increases these properties [82, 173] and that the surface of the material has a significant effect on its bioactivity [328], which has been shown using pure SiO_2 sol-

gels, where larger pore size and pore volume decreases the induction time of HCA formation, *in vivo* [329]. This was also supported by other *in vivo* studies where two implants of sol-gel-derived glasses of $(96)SiO_2$-$(4)B_2O_3$ (wt.%) with SSA > 200 m^2/g were found to bond to bone using the tibial pushout method in rats [330]. While it was observed that compositions with higher content of network formers had higher surface areas, the morphological surface differences between amorphous SGBGs were not directly compared in this study. However, differences were observed with the melt-quench derived glass (45B5) and the semi-crystalline BA500, which were smoother and less coarse, when compared to the amorphous SGBGs. Nevertheless, comparing and quantifying the amorphous SGBG surface morphologies may provide better insight into the ability to tailor their properties by altering the sol-gel processing parameters. Chapter 6 further demonstrates the influence of sodium content on the glass textural properties. As the sodium was decreased, SSA increased (Table 8.1). It is thought that this is due to less nbOs forming with a decrease in sodium content, which in term, increases the network connectivity, and thus surface area. Therefore, the addition of sodium might depend on the targeted final applications of the glasses.

8.4 SGBG Reactivity, dissolution, and HCA formation

Reactivity of the SGBGs was examined by investigating their interactions with water vapor, which has been shown to predict the dissolution behavior of bioactive and soluble glasses [265, 266]. It was found that the composition is the key determining factor in final mass change due to vapor sorption. This supports the previous notion that composition is the key determining factor in determining the dissolution of multicomponent glasses [82, 229]. In particular, and in addition to sodium influencing thermal and textural properties, it can also be inferred that sodium plays a key role in determining reactivity of a glass. Recently, modeling techniques have given new insights on the surfaces of silicate glass [267], where along with nbOs, it was shown that there is also an excess of sodium at the surface [320]. This more hydrophilic sodium surface interacts with vapor, which then allows the water molecules to penetrate into the glass network to initiate dissolution. By using DVS in this thesis, this was observed experimentally as the SGBG compositions with higher sodium content led to greater extent of final mass change (Figure 4.4 and Figure 6.3). Modeling studies, using borate glasses to determine if excess sodium exists on the surface, would also provide greater insight into the differences in reactivity as a function of composition. The effect of textural properties on reactivity was also analyzed by directly comparing the B46 SGBG with its melt-quench (45B5) derived equivalent. While 45B5 was also of high sodium content (24.4 mol%), the more dense structure

generated by its melt-derived processing, did not allow for as easy water penetration and interaction with sodium to initiate dissolution.

As previously reported for melt-quench derived 45S5 glass particles [265], a decrease in B46 particle size led to greater extent of aqueous interactions (Figure 8.1). Interestingly, above 75 μm, the effect of particle size was found to be negligible as all SGBGs experienced a similar, final mass change. This may represent the limit where glass structural properties override the textural properties but also brings into question the surface chemistry and potential dissolution kinetics of the glasses with higher particle size fractions. This finding also needs to be confirmed by using the alternative, step-wise DVS method previously used (Figure 4.4). The effect of both SGBG composition and texture could be observed when incorporated into electrospun PCL-matrix composite scaffolds. Increasing amounts of SGBG addition increased the final mass change, suggesting that only small additions (5 wt.%) of SGBGs are required to enhance the reactivity rate of scaffolds.

Bioactive borate glass buffer in solution as they dissolve in a pH range of 8 – 10 [16, 18, 331]. At physiological pH (7.4 ± 0.2), $B(OH)_3$ is the stable species in solution. However as the pH increases (*i.e.,* due to glass dissolution) greater amounts of $B(OH)_4^-$ form [332] according to equation 6:

$$B(OH)_3 + OH^- <> B(OH)_4^- \text{ (pKa = 9.24)} \quad (6)$$

Borate glass bulk dissolution has been previously studied by using lithium chloroborate glasses [333] where it was reported that the glass dissolution in water is controlled by a reaction controlled mechanism. Furthermore, unlike in silicate glasses, the inability of borate glasses to form a surface gel-like layer during dissolution, is likely to increase the importance of the pH environment during dissolution since the ions are directly released and HCA is deposited on the glass surface itself [333]. It has been shown that the pH of a solution determines the relative amounts of polyborate species in solution [334]. For bioactive borate glasses, a simple conversion mechanism (*i.e.,* dissolution without formation of a gel-like layer) was discussed in section 2.3.3.2.

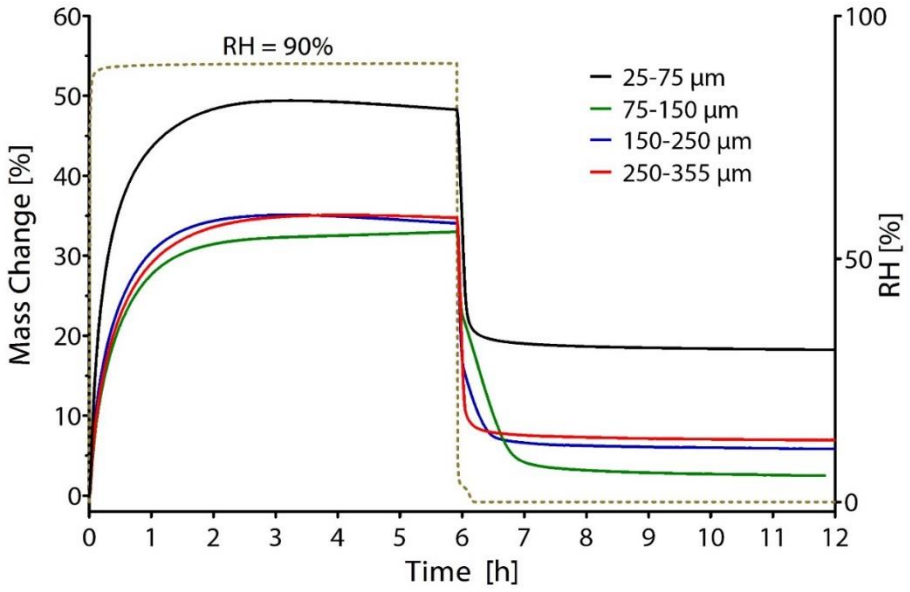

Figure 8.1 Aqueous interactions of a borate substituted Bioglass in 4 different size fractions. Above 75 µm, there seems to be no effect on the mass change.

In this dissertation, the SGBG ionic release in both water (Chapter 4) and SBF (Chapter 5 and 6) were measured through ICP-OES. Comparing the same composition in each dissolution environment (Figure 4.5 and Figure 5.5) demonstrated a similar trend: after an initial release of all ions, boron concentration in solution remained stable, whereas that of calcium showed a slight decreasing trend over time in solution. This decreasing trend was even more prominent in the case of phosphorous concentration at around 6h, indicating HCA formation. The rapid HCA formation after submersion in SBF, supports this dissolution model, however, shorter ICP time points (*i.e.,* < 30 min.) are required to examine the initiation of dissolution and better understand the mechanisms of HCA conversion for SGBGs. To this end, a single, sol-gel-derived borate substituted Bioglass® composition was submerged in four different environments Table 8.2.

Table 8.2 Ionic Concentrations of Various Dissolution Media

Media ID	pH	Na^+	K^+	Mg^{2+}	Ca^{2+}	Cl^-	HCO_3^-	HPO_4^{2-}	SO_4^{-2}
SBF	7.4	142.0	5.0	1.5	2.5	147.8	4.2	1.0	0.5
PBS	7	57.1	2.0	0.0	0.0	84.4	0.0	8.0	0
DMEM	7.4	155.3	5.3	0.8	1.8	119.3	0	0.9	0.8
DIW	~5.5	0	0	0	0	0	0	0	0

*DMEM also contains amino acids, vitamins, glucose, sodium pyruvate, and phenol red

Although, the effect of dissolution media was also examined in Chapter 4 where a K_2HPO_4 solution was compared (Figure S4.16), this resulted in artificially rapid HCA conversion rates due to the non-physiological pH and the excess of phosphorous in the solution which makes the calcium in the glass the limiting rate factor. Studies on silicate 13-93 glass in SBF and DMEM have shown that the ionic release of silicon and potassium is very similar however, HA formation was detected on the glass surface at week 2 in SBF and week 4 in DMEM, although by 2 weeks the DMEM formed HA obtained better crystallinity [335]. The XRD results of the four tested components can been seen in Figure 8.2. Interestingly, at day 7 B46 in PBS and SBF form HCA while glasses submerged in DIW and DMEM formed calcite (the first formation of these peaks was observed at 2h – data not shown). This is surprising as DMEM and SBF have very similar ionic concentrations with major difference being the HCO_3^- content (Table 8.2). Also interesting is that in DIW, B46 converts to HCA which suggests rapid dissolution and re-precipitation at a near ideal Ca/P ratio. To the best of our knowledge, the XRD patterns of 45S5 after immersion in water have not been recorded. However, when exposed to water vapour through DVS, the various $CaSiO_4$, NaP, CaP, $Ca_{10}Na(PO_4)_7$, and

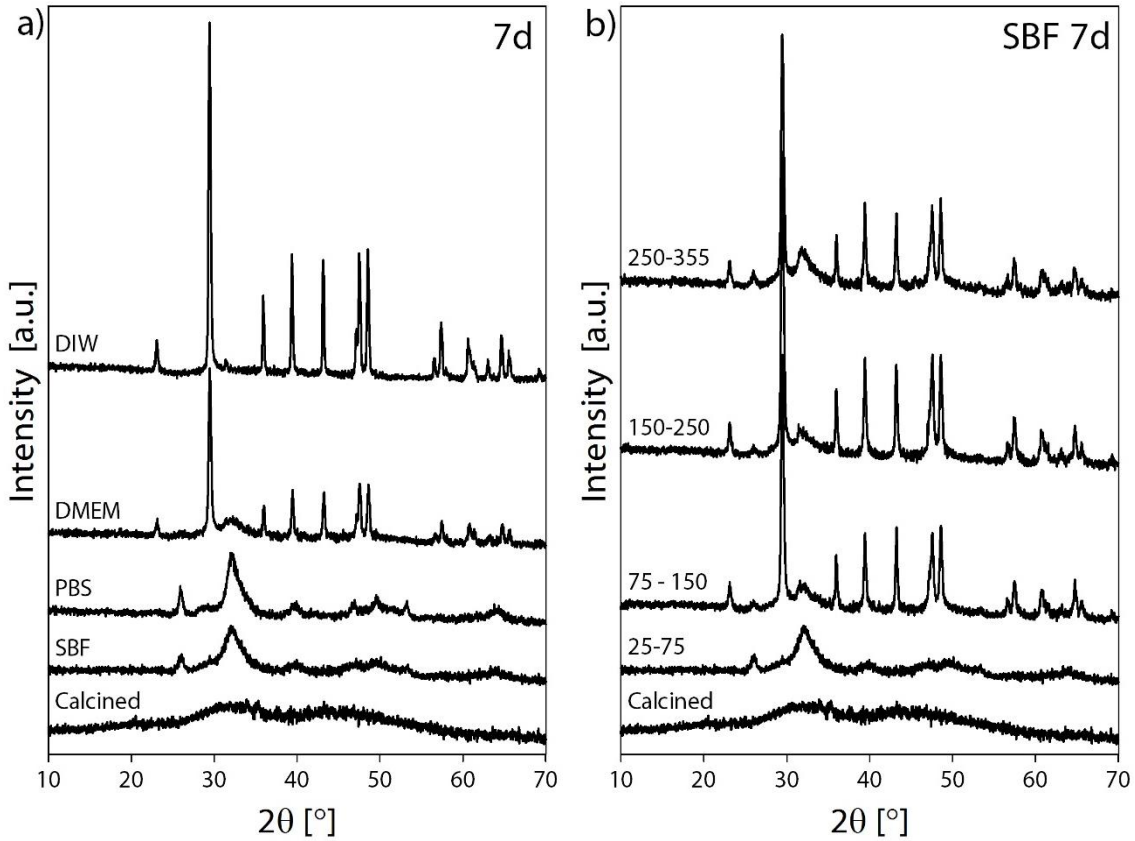

Figure 8.2 XRD diffractograms of (a) B46 submerged in 4 different types of media after 7d and (b) four different particle size fractions of B46 in SBF for 7d. Calcite formation is observed by the sharp peaks.

$NaCaPO_4$ phases formed, which were dependent on particle size suggesting surface area and particle size plays a role in conversion kinetics [265]. In another study, four different particle size fractions of B46 were submersed in SBF for 7 days (Figure 8.2). Interestingly, above 75 μm size fractions, the glasses converted to calcite as opposed to HCA with the 25 – 75 μm size fraction. This further brings into question the effect of bulk surface area as well as the dissolution and conversion mechanisms of SGBGs. It can be speculated that the lower surface area favors calcium release and re deposition, as seen with ion release overtime. However, further studies are needed to pin point the surface changes at shorter time points.

9 Conclusions and Future Perspectives

9.1 Conclusions

The following conclusions can be derived from this dissertation:

- A wide compositional range of bioactive sol-gel derived borate glasses can be processed for potential applications in mineralized tissue repair. Four-component glasses based on a borate substituted Bioglass® 45S5 formulation [$(46.1)B_2O_3-(26.9)CaO-(24.4)Na_2O-(2.6)P_2O_5$; mol%] ranging from 36 – 61 mol% B_2O_3 were fabricated using a unique sol-gel processing technique. Increasing the borate content increases the T_g, specific surface area, and porosity. Compared to the melt-quench-derived equivalent, the SSA and porosity of SGBGs were approximately 400 and 800 times greater, respectively. This is in direct correlation to lowered amounts of network modifiers which disrupt the glass network creating nbOs. These glasses demonstrated rapid HCA conversion in SBF according to XRD (3h), ATR-FITR (30 min), and SEM (6h). This can be attributed to the lower chemical durability of the borate glass system combined with the increased specific surface area and porosity which allows for faster dissolution and rapid ion release rates. Bioactivity of these glasses was relatively unaffected by composition.
- SGBGs can be fabricated through various precursor and processing conditions. Overall, regardless of the processing route, the glasses demonstrated similar structural and textural properties. Calcination temperature was found to have the most effect where higher temperatures generated partially crystalline glass with an order of magnitude lower specific surface area and slower conversion rates to HCA.
- According to the aqueous interactions of the SGBGs as measured through DVS, reactivity was found to be approximately four-fold greater than the melt-quench derived equivalent glass. Furthermore, total mass gain was inversely related to the amount of borate network former demonstrating the effect of network modifiers, especially sodium, on reactivity.

- Sodium is not a necessary component to fabricate bioactive SGBGs. Sodium free SGBGs demonstrated higher SSA and porosity and maintain the rapid HCA conversion rates per XRD and ATR-FTIR.
- SGBG particles can increase the bioactivity of non-bioactive systems. The addition of 5 wt.% SGBG to electrospun PCL scaffolds, generated bioactive fibrous composites as characterized through HCA formation by day 3 in SBF.

9.2 Future Perspectives

The high bioactivity of SGBGs has demonstrated great potential in mineralized tissue repair. The research reported in this dissertation are anticipated to lay the ground work for all future bioactive investigations of SGBGs aiming to examine composition, sol-gel processing, ion release, and composite or hybrid scaffold formation. Nonetheless, due to the limitations of this research many different areas can be expanded upon for future work.

While the structure of SGBGs was examined using various techniques, more advanced NMR studies are needed to decode the amounts of three- and four-coordinated borate species and how these are influenced by network modifiers such as sodium. As structure is the determining factor for chemical durability of multi-component glasses [82, 229], this data will be essential in creating new compositions for targeted tissue engineering applications. New computer modeling [229, 317] of bioactive borate glass systems will also be helpful in determining the structure of these glasses along with the more complex structural units inherent to borate systems and their effect on the bioactive properties. From this information, modified network connectivity models can be created to better predict the bioactivity of the borate glass network.

The sol-gel process contains many variables which have been thoroughly examined using silicate based glass systems [336]. However, these have not been systematically examined in borate systems. Chapter 5 examined many of these parameters, and while the final results demonstrated similar overall glass structural and textural characteristics, additional work is needed to examine some fundamental chemistry questions such as the effects of pH, alcohol, and water, which will also serve to expand the work of Brinker and Scherer [21] and others [157, 158, 160, 162]. While it has been suggested that a certain amount of four-coordinated borate units is needed for gel formation, this has not been specifically examined in this work. Understanding the effect of precursor materials will provide new insights to borate gel formation. After the gel has formed, the drying rate of the gels is another key parameter that can be further examined in these systems. Step by step, or gradual drying

of gels has been previously examined in other sol-gel systems [337]. This might help achieve monolithic forms which can be used for a variety of applications beyond the medical focus. Additionally, there are numerous other precursor materials that might influence these aforementioned properties. Further examinations on different SGBG chemistries are also needed to investigate the dissolution effects on SGBG compositions and how these correlate with bioactivity. These parameters will also greatly influence the textural properties which also play an important role in reactivity and bioactivity properties.

Perhaps the key remaining studies are those using cells *in vitro* along with *in vivo* animal models. While borate glasses can be toxic in static cell cultures conditions [196], the toxicity can be reduced by providing a dynamic environment [132] and they have been successfully studied using multiple cell lines [135, 136, 338]. The importance of the dynamic environment is seen by the numerous *in vivo* with animal bone [339, 340] and skin models [205, 341] and even in human trials [244, 342]. Thus, to truly evaluate the potential of SGBGs in repairing tissues, these studies will be crucial.

10 References

[1] Cauley JA. Public Health Impact of Osteoporosis. The Journals of Gerontology Series A: Biological Sciences and Medical Sciences. 2013;68:1243-51.
[2] Dawson JI, Kanczler J, Aarvold A, Smith J, Oreffo ROC. 5.22 - Tissue Engineering: Bone. In: Editor-in-Chief: Murray M-Y, editor. Comprehensive Biotechnology (Second Edition). Burlington: Academic Press; 2011. p. 275-90.
[3] Laurencin C, Khan Y, El-Amin SF. Bone graft substitutes. Expert Review of Medical Devices. 2006;3:49-57.
[4] Van Heest A, Swiontkowski M. Bone-graft substitutes. The Lancet. 1999;353:S28-S9.
[5] Silber JS, Anderson DG, Daffner SD, Brislin BT, Leland JM, Hilibrand AS, et al. Donor site morbidity after anterior iliac crest bone harvest for single-level anterior cervical discectomy and fusion. Spine. 2003;28:134-9.
[6] Finkemeier CG. Bone-Grafting and Bone-Graft Substitutes. The Journal of Bone & Joint Surgery. 2002;84:454-64.
[7] Greenwald MA, Kuehnert MJ, Fishman JA. Infectious Disease Transmission during Organ and Tissue Transplantation. Emerging Infectious Diseases. 2012;18:e1-e.
[8] Boyce T, Edwards J, Scarborough N. Allograft bone: the influence of processing on safety and performance. Orthopedic Clinics of North America. 1999;30:571-81.
[9] Wilson J, Nolletti D. Bonding of soft tissues to Bioglass®. Handbook of bioactive ceramics. 1990;1:283-302.
[10] Hench LL. Bioceramics: from concept to clinic. J Am Ceram Soc. 1991;74:1487-510.
[11] Hench LL, Paschall HA. Direct chemical bond of bioactive glass-ceramic materials to bone and muscle. J Biomed Mater Res. 1973;7:25-42.
[12] Hench LL. The story of Bioglass®. J Mater Sci: Mater Med. 2006;17:967-78.
[13] Hench LL, Splinter RJ, Allen W, Greenlee T. Bonding mechanisms at the interface of ceramic prosthetic materials. Journal of Biomedical Materials Research. 1971;5:117-41.
[14] Rahaman MN, Day DE, Bal BS, Fu Q, Jung SB, Bonewald LF, et al. Bioactive glass in tissue engineering. Acta biomaterialia. 2011;7:2355-73.
[15] Li R, Clark A, Hench L. An investigation of bioactive glass powders by sol-gel processing. J Appl Biomater. 1991;2:231-9.
[16] Fu Q, Rahaman MN, Fu H, Liu X. Silicate, borosilicate, and borate bioactive glass scaffolds with controllable degradation rate for bone tissue engineering applications. I. Preparation and in vitro degradation. J Biomed Mater Res, Part A. 2010;95:164-71.
[17] Huang W, Day DE, Kittiratanapiboon K, Rahaman MN. Kinetics and mechanisms of the conversion of silicate (45S5), borate, and borosilicate glasses to hydroxyapatite in dilute phosphate solutions. J Mater Sci: Mater Med. 2006;17:583-96.
[18] Huang W, Rahaman MN, Day DE, Li Y. Mechanisms for converting bioactive silicate, borate, and borosilicate glasses to hydroxyapatite in dilute phosphate solutions. Phys Chem Glasses. 2006;47:1.
[19] Day D, White J, Brown R, McMenamin K. Transformation of borate glasses into biologically useful materials. Glass Technol: Eur J Glass Sci Technol, Part A. 2003;44:75-81.
[20] Arcos D, Vallet-Regí M. Sol–gel silica-based biomaterials and bone tissue regeneration. Acta Biomater. 2010;6:2874-88.

[21] Brinker CJ, Scherer GW. Sol-gel science: the physics and chemistry of sol-gel processing: Academic press; 1990.
[22] Mitton D, Roux C, Laugier P. Bone overview. Bone Quantitative Ultrasound. 2011:1-28.
[23] Clarke B. Normal bone anatomy and physiology. Clinical journal of the American Society of Nephrology. 2008;3:S131-S9.
[24] Doblaré M, Garcıa J, Gómez M. Modelling bone tissue fracture and healing: a review. Engineering Fracture Mechanics. 2004;71:1809-40.
[25] Rodan GA. Introduction to bone biology. Bone. 1992;13, Supplement 1:S3-S6.
[26] Nalla RK, Kruzic JJ, Kinney JH, Balooch M, Ager Iii JW, Ritchie RO. Role of microstructure in the aging-related deterioration of the toughness of human cortical bone. Mater Sci Eng, C. 2006;26:1251-60.
[27] Burr D. Targeted and nontargeted remodeling. Bone. 2002;30:2-4.
[28] Eastell R, Mosekilde L, Hodgson SF, Riggs BL. Proportion of human vertebral body bone that is cancellous. Journal of Bone and Mineral Research. 2009;5:1237-41.
[29] Eriksen EF, Axelrod DW, Melsen F. Bone histomorphometry: Raven Press New York; 1994.
[30] Guise TA, Mundy GR. Cancer and bone. Endocrine Reviews. 1998;19:18-54.
[31] Rho J-Y, Kuhn-Spearing L, Zioupos P. Mechanical properties and the hierarchical structure of bone. Medical Engineering & Physics. 1998;20:92-102.
[32] Weiner S, Wagner HD. The material bone: structure-mechanical function relations. Annual Review of Materials Science. 1998;28:271-98.
[33] Posner AS. Crystal chemistry of bone mineral. Physiological reviews. 1969;49:760-92.
[34] Hench LL. New Materials and Technologies for Healthcare: World Scientific; 2011.
[35] Jones J, Clare A. Bio-Glasses: An Introduction: John Wiley & Sons; 2012.
[36] Young M. Bone matrix proteins: their function, regulation, and relationship to osteoporosis. Osteoporos Int. 2003;14:35-42.
[37] Robey PG, Boskey AL, Asbmr. Chapter 6. The Composition of Bone. Primer on the Metabolic Bone Diseases and Disorders of Mineral Metabolism: John Wiley & Sons, Inc.; 2009. p. 32-8.
[38] Bilezikian JP, Raisz LG, Martin TJ. Principles of bone biology, two-volume set: Academic Press; 2008.
[39] Hollinger JO, Srinivasan A, Alvarez P, Hsu E, McBride S, Eppell S, et al. 5.522 - Bone Tissue Engineering: Growth Factors and Cytokines. In: Editor-in-Chief: Paul D, editor. Comprehensive Biomaterials. Oxford: Elsevier; 2011. p. 281-301.
[40] Datta B. Textbook of Pathology. Jaypee Brothers Medical; 2008.
[41] Christodoulou C, Cooper C. What is osteoporosis? Postgraduate medical journal. 2003;79:133-8.
[42] Harvey N, Dennison E, Cooper C. Osteoporosis: impact on health and economics. Nature Reviews Rheumatology. 2010;6:99-105.
[43] Consensus development conference: diagnosis, prophylaxis and treatment of osteoporosis. The American Journal of Medicine. 1993;94:646-50.
[44] Ilich JZ, Kerstetter JE. Nutrition in bone health revisited: a story beyond calcium. Journal of the American College of Nutrition. 2000;19:715-37.
[45] Lakhkar NJ, Lee I-H, Kim H-W, Salih V, Wall IB, Knowles JC. Bone formation controlled by biologically relevant inorganic ions: Role and controlled delivery from phosphate-based glasses. Advanced Drug Delivery Reviews. 2012.
[46] Hynes RO. The extracellular matrix: not just pretty fibrils. Science. 2009;326:1216-9.
[47] Bilezikian JP. Management of Acute Hypercalcemia. New England Journal of Medicine. 1992;326:1196-203.
[48] Heaney RP, Gallagher J, Johnston C, Neer R, Parfitt A, Whedon G. Calcium nutrition and bone health in the elderly. The American journal of clinical nutrition. 1982;36:986-1013.

[49] Ilich JZ, Brownbill R, Tamborini L. Bone and nutrition in elderly women: protein, energy, and calcium as main determinants of bone mineral density. European journal of clinical nutrition. 2003;57:554-65.
[50] Bonjour JP. Calcium and phosphate: a duet of ions playing for bone health. Journal of the American College of Nutrition. 2011;30:438S-48S.
[51] Chan GM. Dietary calcium and bone mineral status of children and adolescents. Archives of Pediatrics & Adolescent Medicine. 1991;145:631.
[52] Johnston Jr CC, Miller JZ, Slemenda CW, Reister TK, Hui S, Christian JC, et al. Calcium supplementation and increases in bone mineral density in children. New England journal of medicine. 1992;327:82-7.
[53] Hoac B, Kiffer-Moreira T, Millán JL, McKee MD. Polyphosphates inhibit extracellular matrix mineralization in MC3T3-E1 osteoblast cultures. Bone. 2013;53:478-86.
[54] Foster BL, Tompkins KA, Rutherford RB, Zhang H, Chu EY, Fong H, et al. Phosphate: Known and potential roles during development and regeneration of teeth and supporting structures. Birth Defects Research Part C: Embryo Today: Reviews. 2008;84:281-314.
[55] Takeda E, Yamamoto H, Nashiki K, Sato T, Arai H, Taketani Y. Inorganic phosphate homeostasis and the role of dietary phosphorus. Journal of cellular and molecular medicine. 2004;8:191-200.
[56] Tenenbaum H. Role of organic phosphate in mineralization of bone in vitro. Journal of Dental Research. 1981;60:1586-9.
[57] Beck GR. Inorganic phosphate as a signaling molecule in osteoblast differentiation. Journal of cellular biochemistry. 2003;90:234-43.
[58] Beck GR, Zerler B, Moran E. Phosphate is a specific signal for induction of osteopontin gene expression. Proceedings of the National Academy of Sciences. 2000;97:8352-7.
[59] Carlisle EM. Silicon: a requirement in bone formation independent of vitamin D1. Calcif Tissue Int. 1981;33:27-34.
[60] Jugdaohsingh R. Silicon and bone health. The journal of nutrition, health & aging. 2007;11:99.
[61] Sripanyakorn S, Jugdaohsingh R, Thompson RP, Powell JJ. Dietary silicon and bone health. Nutrition Bulletin. 2005;30:222-30.
[62] Landis W, Lee D, Brenna J, Chandra S, Morrison G. Detection and localization of silicon and associated elements in vertebrate bone tissue by imaging ion microscopy. Calcif Tissue Int. 1986;38:52-9.
[63] Schwarz K, Milne DB. Growth-promoting effects of silicon in rats. 1972.
[64] Carlisle EM. Silicon: an essential element for the chick. Science. 1972;178:619-21.
[65] Keeting PE, Oursler MJ, Wiegand KE, Bonde SK, Spelsberg TC, Riggs BL. Zeolite a increases proliferation, differentiation, and transforming growth factor β production in normal adult human osteoblast-like cells in vitro. Journal of Bone and Mineral Research. 1992;7:1281-9.
[66] Botelho CM, Brooks RA, Best SM, Lopes MA, Santos JD, Rushton N, et al. Human osteoblast response to silicon-substituted hydroxyapatite. J Biomed Mater Res, Part A. 2006;79A:723-30.
[67] Xynos ID, Edgar AJ, Buttery LD, Hench LL, Polak JM. Ionic products of bioactive glass dissolution increase proliferation of human osteoblasts and induce insulin-like growth factor II mRNA expression and protein synthesis. Biochemical and biophysical research communications. 2000;276:461-5.
[68] Boonrungsiman S, Fearn S, Gentleman E, Spillane L, Carzaniga R, McComb DW, et al. Correlative spectroscopy of silicates in mineralised nodules formed from osteoblasts. Nanoscale. 2013;5:7544-51.
[69] Nieves J. Skeletal effects of nutrients and nutraceuticals, beyond calcium and vitamin D. Osteoporos Int. 2013;24:771-86.

[70] Nielsen FH. The justification for providing dietary guidance for the nutritional intake of boron. Biological trace element research. 1998;66:319-30.
[71] Nielsen FH. Is boron nutritionally relevant? Nutrition reviews. 2008;66:183-91.
[72] Nielsen FH, Hunt CD, Mullen LM, Hunt J. Effect of dietary boron on mineral, estrogen, and testosterone metabolism in postmenopausal women. The FASEB journal. 1987;1:394-7.
[73] Hunt CD, Herbel JL, Nielsen FH. Metabolic responses of postmenopausal women to supplemental dietary boron and aluminum during usual and low magnesium intake: boron, calcium, and magnesium absorption and retention and blood mineral concentrations. The American journal of clinical nutrition. 1997;65:803-13.
[74] Meacham SL, Taper LJ, Volpe SL. Effect of boron supplementation on blood and urinary calcium, magnesium, and phosphorus, and urinary boron in athletic and sedentary women. The American journal of clinical nutrition. 1995;61:341-5.
[75] Kerstetter JE, Allen LH. Dietary protein increases urinary calcium. Journal of Nutrition. 1990;120:134-6.
[76] Hakki SS, Dundar N, Kayis SA, Hakki EE, Hamurcu M, Kerimoglu U, et al. Boron enhances strength and alters mineral composition of bone in rabbits fed a high energy diet. Journal of Trace Elements in Medicine and Biology. 2013;27:148-53.
[77] Armstrong TA, Spears JW, Crenshaw TD, Nielsen FH. Boron supplementation of a semipurified diet for weanling pigs improves feed efficiency and bone strength characteristics and alters plasma lipid metabolites. The Journal of nutrition. 2000;130:2575-81.
[78] Nielsen FH, Stoecker BJ. Boron and fish oil have different beneficial effects on strength and trabecular microarchitecture of bone. Journal of Trace Elements in Medicine and Biology. 2009;23:195-203.
[79] Ratner BD, Hoffman AS, Schoen FJ, Lemons JE. Biomaterials science: an introduction to materials in medicine: Academic press; 2004.
[80] Hench L. Biomaterials. Science. 1980;208:826-31.
[81] Hench LL, Polak JM. Third-generation biomedical materials. Science. 2002;295:1014-7.
[82] Jones JR. Review of bioactive glass–from Hench to hybrids. Acta Biomater. 2012.
[83] Hutmacher DW. Scaffold design and fabrication technologies for engineering tissues—state of the art and future perspectives. J Biomater Sci, Polym Ed. 2001;12:107-24.
[84] Karageorgiou V, Kaplan D. Porosity of 3D biomaterial scaffolds and osteogenesis. Biomaterials. 2005;26:5474-91.
[85] Jones JR. New trends in bioactive scaffolds: The importance of nanostructure. J Eur Ceram Soc. 2009;29:1275-81.
[86] Okii N, Nishimura S, Kurisu K, Takeshima Y, Uozumi T. In Vivo Histological Changes Occurring in Hydroxyapatite Cranial Reconstruction
—Case Report&mdash. Neurologia medico-chirurgica. 2001;41:100-4.
[87] Loh QL, Choong C. Three-Dimensional Scaffolds for Tissue Engineering Applications: Role of Porosity and Pore Size. Tissue Engineering Part B, Reviews. 2013;19:485-502.
[88] Hench LL. Sol-gel materials for bioceramic applications. Curr Opin Solid State Mater Sci. 1997;2:604-10.
[89] Vallet-Regí M, Ruiz-Hernández E. Bioceramics: From Bone Regeneration to Cancer Nanomedicine. Adv Mater. 2011;23:5177-218.
[90] Sabir MI, Xu X, Li L. A review on biodegradable polymeric materials for bone tissue engineering applications. J Mater Sci. 2009;44:5713-24.
[91] Liu X, Ma PX. Polymeric Scaffolds for Bone Tissue Engineering. Ann Biomed Eng. 2004;32:477-86.

[92] Rahaman MN, Day DE, Sonny Bal B, Fu Q, Jung SB, Bonewald LF, et al. Bioactive glass in tissue engineering. Acta Biomater. 2011;7:2355-73.
[93] Marelli B, Ghezzi CE, Mohn D, Stark WJ, Barralet JE, Boccaccini AR, et al. Accelerated mineralization of dense collagen-nano bioactive glass hybrid gels increases scaffold stiffness and regulates osteoblastic function. Biomaterials. 2011;32:8915-26.
[94] Pham QP, Sharma U, Mikos AG. Electrospinning of polymeric nanofibers for tissue engineering applications: a review. Tissue engineering. 2006;12:1197-211.
[95] Prabhakaran MP, Venugopal J, Ramakrishna S. Electrospun nanostructured scaffolds for bone tissue engineering. Acta Biomater. 2009;5:2884-93.
[96] Khajavi R, Abbasipour M, Bahador A. Electrospun biodegradable nanofibers scaffolds for bone tissue engineering. J Appl Polym Sci. 2016;133:n/a-n/a.
[97] Di Martino A, Liverani L, Rainer A, Salvatore G, Trombetta M, Denaro V. Electrospun scaffolds for bone tissue engineering. Musculoskeletal surgery. 2011;95:69-80.
[98] Earl J, Leary R, Muller K, Langford R, Greenspan D. Physical and chemical characterization of dentin surface following treatment with NovaMin technology. The Journal of clinical dentistry. 2011;22:62.
[99] Shelby JE. Introduction to Glass Science and Technology: Royal Society of Chemistry; 2005.
[100] Zachariasen WH. The atomic arrangement in glass. J Am Chem Soc. 1932;54:3841-51.
[101] Fagerlund S, Hupa L. Chapter 1 Melt-derived Bioactive Silicate Glasses. Bioactive Glasses: Fundamentals, Technology and Applications: The Royal Society of Chemistry; 2017. p. 1-26.
[102] Uhlmann DR. A kinetic treatment of glass formation. J Non-Cryst Solids. 1972;7:337-48.
[103] Hopper RW, Scherer G, Uhlmann DR. Crystallization statistics, thermal history and glass formation. J Non-Cryst Solids. 1974;15:45-62.
[104] Brauer DS, Moncke D. Chapter 3 Introduction to the Structure of Silicate, Phosphate and Borate Glasses. Bioactive Glasses: Fundamentals, Technology and Applications: The Royal Society of Chemistry; 2017. p. 61-88.
[105] National Institute of Industrial R. The complete book on glass and ceramics technology. New Delhi: Asian Pacific Business Press; 2006.
[106] Brow RK. Review: the structure of simple phosphate glasses. J Non-Cryst Solids. 2000;263:1-28.
[107] Kirkpatrick RJ, Brow RK. Nuclear magnetic resonance investigation of the structures of phosphate and phosphate-containing glasses: a review. Solid state nuclear magnetic resonance. 1995;5:9-21.
[108] Brow RK, Alam TM, Tallant DR, Kirkpatrick RJ. Spectroscopic studies on the structures of phosphate sealing glasses. MRS Bulletin. 1998;23:63-7.
[109] Peng Y, Day D. High thermal expansion phosphate glasses. II. Glass technology. 1991;32:200-5.
[110] Neel EAA, Pickup DM, Valappil SP, Newport RJ, Knowles JC. Bioactive functional materials: a perspective on phosphate-based glasses. J Mater Chem. 2008;19:690-701.
[111] Krogh-Moe J. The structure of vitreous and liquid boron oxide. J Non-Cryst Solids. 1969;1:269-84.
[112] Goubeau J, Keller H. RAMAN-Spektren und Struktur von Boroxol-Verbindungen. Zeitschrift für anorganische und allgemeine Chemie. 1953;272:303-12.
[113] Wright AC. Borate structures: crystalline and vitreous. Physics and Chemistry of Glasses-European Journal of Glass Science and Technology Part B. 2010;51:1-39.
[114] Wright AC. My Borate Life: An Enigmatic Journey. Int J Appl Glass Sci. 2015;6:45-63.
[115] Warren BE. SUMMARY OF WORK ON ATOMIC ARRANGEMENT IN GLASS*. Journal of the American Ceramic Society. 1941;24:256-61.

[116] Yiannopoulos YD, Chryssikos GD, Kamitsos EI. Structure and properties of alkaline earth borate glasses. Phys Chem Glasses. 2001;42:164-72.
[117] Kokubo T, Takadama H. How useful is SBF in predicting in vivo bone bioactivity? Biomaterials. 2006;27:2907-15.
[118] Kokubo T, Kushitani H, Sakka S, Kitsugi T, Yamamuro T. Solutions able to reproduce in vivo surface-structure changes in bioactive glass-ceramic A-W3. J Biomed Mater Res. 1990;24:721-34.
[119] Bohner M, Lemaitre J. Can bioactivity be tested in vitro with SBF solution? Biomaterials. 2009;30:2175-9.
[120] Maçon ALB, Kim TB, Valliant EM, Goetschius K, Brow RK, Day DE, et al. A unified in vitro evaluation for apatite-forming ability of bioactive glasses and their variants. J Mater Sci: Mater Med. 2015;26:1-10.
[121] Miguez-Pacheco V, Hench LL, Boccaccini AR. Bioactive glasses beyond bone and teeth: Emerging applications in contact with soft tissues. Acta Biomater. 2015;13:1-15.
[122] Hench LL. Bioceramics. J Am Ceram Soc. 1998;81:1705-28.
[123] Habraken W, Habibovic P, Epple M, Bohner M. Calcium phosphates in biomedical applications: materials for the future? Materials Today. 2016;19:69-87.
[124] Li P, Yang Q, Zhang F, Kokubo T. The effect of residual glassy phase in a bioactive glass-ceramic on the formation of its surface apatite layerin vitro. J Mater Sci: Mater Med. 1992;3:452-6.
[125] Peitl Filho O, Latorre GP, Hench L. Effect of crystallization on apatite-layer formation of bioactive glass 45%. J Biomed Mater Res. 1996;30:509-14.
[126] Gross UM, Strunz V. The anchoring of glass ceramics of different solubility in the femur of the rat. J Biomed Mater Res, Part A. 1980;14:607-18.
[127] Hill R. An alternative view of the degradation of bioglass. Journal of Materials Science Letters. 1996;15:1122-5.
[128] Edén M. The split network analysis for exploring composition–structure correlations in multi-component glasses: I. Rationalizing bioactivity-composition trends of bioglasses. J Non-Cryst Solids. 2011;357:1595-602.
[129] Hill RG, Brauer DS. Predicting the bioactivity of glasses using the network connectivity or split network models. J Non-Cryst Solids. 2011;357:3884-7.
[130] Li A, Wang D, Xiang J, Newport RJ, Reinholdt M, Mutin PH, et al. Insights into new calcium phosphosilicate xerogels using an advanced characterization methodology. J Non-Cryst Solids. 2011;357:3548-55.
[131] Yao A, Wang D, Huang W, Fu Q, Rahaman MN, Day DE. In Vitro Bioactive Characteristics of Borate-Based Glasses with Controllable Degradation Behavior. J Am Ceram Soc. 2006;90:303-6.
[132] Brown RF, Rahaman MN, Dwilewicz AB, Huang W, Day DE, Li Y, et al. Effect of borate glass composition on its conversion to hydroxyapatite and on the proliferation of MC3T3-E1 cells. J Biomed Mater Res, Part A. 2008;88:392-400.
[133] Day DE, White J, Brown RF, McMenamin K. Transformation of borate glasses into biologically useful materials. Glass Technol: Eur J Glass Sci Technol, Part A. 2003;44:75-81.
[134] Ning J, Yao A, Wang D, Huang W, Fu H, Liu X, et al. Synthesis and in vitro bioactivity of a borate-based bioglass. Mater Lett. 2007;61:5223-6.
[135] Fu H, Fu Q, Zhou N, Huang W, Rahaman MN, Wang D, et al. In vitro evaluation of borate-based bioactive glass scaffolds prepared by a polymer foam replication method. Mater Sci Eng, C. 2009;29:2275-81.
[136] Marion NW, Liang W, Liang W, Reilly GC, Day DE, Rahaman MN, et al. Borate glass supports the in vitro osteogenic differentiation of human mesenchymal stem cells. Mechanics of Advanced Materials and Structures. 2005;12:239-46.

[137] Liang W, Rahaman MN, Day DE, Marion NW, Riley GC, Mao JJ. Bioactive borate glass scaffold for bone tissue engineering. J Non-Cryst Solids. 2008;354:1690-6.
[138] Han X, Day DE. Reaction of sodium calcium borate glasses to form hydroxyapatite. J Mater Sci: Mater Med. 2007;18:1837-47.
[139] Pan H, Zhao X, Zhang X, Zhang K, Li L, Li Z, et al. Strontium borate glass: potential biomaterial for bone regeneration. Journal of The Royal Society Interface. 2010;7:1025-31.
[140] Yao A, Ai F, Liu X, Wang D, Huang W, Xu W. Preparation of hollow hydroxyapatite microspheres by the conversion of borate glass at near room temperature. Materials Research Bulletin. 2010;45:25-8.
[141] Bi L, Rahaman MN, Day DE, Brown Z, Samujh C, Liu X, et al. Effect of bioactive borate glass microstructure on bone regeneration, angiogenesis, and hydroxyapatite conversion in a rat calvarial defect model. Acta Biomater. 2013;9:8015-26.
[142] Bi L, Zobell B, Liu X, Rahaman MN, Bonewald LF. Healing of critical-size segmental defects in rat femora using strong porous bioactive glass scaffolds. Mater Sci Eng, C. 2014;42:816-24.
[143] Wray P. 'Cotton candy'that heals? American Ceramic Society Bulletin. 2011;90.
[144] http://etissuesolutions.com. 2017.
[145] Castricum HL, Sah A, Mittelmeijer-Hazeleger MC, Huiskes C, Johan E. Microporous structure and enhanced hydrophobicity in methylated SiO 2 for molecular separation. J Mater Chem. 2007;17:1509-17.
[146] Ebelmen M. Chimie sur une production artificielle de silice diaphane. Comptes-rendus de l'Académie des Sciences. 1845;21:502-5.
[147] Patrick WA. Silica gel and process of making same. Google Patents; 1919.
[148] Geffcken W, Berger E. Verfahren zur anderung des reflexionsvermogens optischer glaser. Deutsches Reichspatent, assigned to Jenaer Glaswerk Schott & Gen, Jena. 1939;736:411.
[149] Schroeder H. Oxide layers deposited from organic solutions. Physics of thin films. 1969;5:87-141.
[150] Yoldas BE. Alumina gels that form porous transparent Al 2 O 3. J Mater Sci. 1975;10:1856-60.
[151] Yamane M, Aso S, Sakaino T. Preparation of a gel from metal alkoxide and its properties as a precursor of oxide glass. J Mater Sci. 1978;13:865-70.
[152] Hench LL, West JK. The sol-gel process. Chem Rev. 1990;90:33-72.
[153] Boccaccini AR, Erol M, Stark WJ, Mohn D, Hong Z, Mano JF. Polymer/bioactive glass nanocomposites for biomedical applications: A review. Composites Science and Technology. 2010;70:1764-76.
[154] Livage J. Basic principles of sol-gel chemistry. Sol-Gel Technologies for Glass Producers and Users: Springer; 2004. p. 3-14.
[155] Scherer GW. Characterization of aerogels. Advances in Colloid and Interface Science. 1998;76–77:321-39.
[156] Yin W, Rubenstein DA. Biomedical Applications of Aerogels. Aerogels Handbook: Springer; 2011. p. 683-94.
[157] Brinker C, Ward K, Keefer K, Holupka E, Bray P, Pearson R. Synthesis and Structure of Borate Based Aerogels. Aerogels: Springer; 1986. p. 57-67.
[158] Tohge N, Mackenzie J. Preparation of 20Na2O·80B2O3 glasses by sol-gel method. J Non-Cryst Solids. 1984;68:411-8.
[159] Tohge N, Mackenzie J. Preparation of 20Na< sub> 2</sub> O· 80B< sub> 2</sub> O< sub> 3</sub> glasses by sol-gel method. J Non-Cryst Solids. 1984;68:411-8.
[160] Weinberg MC, Neilson GF, Smith GL, Dunn B, Moore G, Mackenzie J. The preparation and characterization of a lithium borate glass prepared by the gel technique. J Mater Sci. 1985;20:1501-8.

[161] Lu C, Dimov S, Lipson R. Enhanced Nonlinear Thin Films of β-Barium Borate by Sol− Gel Synthesis. Chem Mater. 2008;20:5296-300.
[162] Irwin A, Holmgren J, Zerda T, Jonas J. Spectroscopic investigations of borosiloxane bond formation in the sol-gel process. J Non-Cryst Solids. 1987;89:191-205.
[163] Ota R, Asagi N, Fukunaga J, Yoshida N, Fujii T. Variation of the gel region with heat-treatment in the B2O3-Na2O-TiO2 system compared with the melt-quenched glass region. J Mater Sci. 1990;25:4259-65.
[164] Bengisu M, Yilmaz E, Farzad H, Reis ST. Borate, lithium borate, and borophosphate powders by sol–gel precipitation. J Sol-Gel Sci Technol. 2008;45:237-43.
[165] Carta D, Qiu D, Guerry P, Ahmed I, Abou Neel EA, Knowles JC, et al. The effect of composition on the structure of sodium borophosphate glasses. J Non-Cryst Solids. 2008;354:3671-7.
[166] Carta D, Knowles JC, Guerry P, Smith ME, Newport RJ. Sol–gel synthesis and structural characterisation of P2O5–B2O3–Na2O glasses for biomedical applications. J Mater Chem. 2009;19:150-8.
[167] De La Rocha C, Conley DJ. Glass Houses and Nanotechnology. Silica Stories. Cham: Springer International Publishing; 2017. p. 69-93.
[168] Kurkjian CR, Prindle WR. Perspectives on the history of glass composition. J Am Ceram Soc. 1998;81:795-813.
[169] Stuart BW, Gimeno-Fabra M, Segal J, Ahmed I, Grant DM. Mechanical, structural and dissolution properties of heat treated thin-film phosphate based glasses. Applied Surface Science. 2017;416:605-17.
[170] Lin S, Ionescu C, Pike KJ, Smith ME, Jones JR. Nanostructure evolution and calcium distribution in sol–gel derived bioactive glass. J Mater Chem. 2009;19:1276-82.
[171] Pereira M, Clark A, Hench L. Calcium phosphate formation on sol-gel-derived bioactive glasses in vitro. J Biomed Mater Res. 1994;28:693-8.
[172] Sepulveda P, Jones JR, Hench LL. Bioactive sol-gel foams for tissue repair. J Biomed Mater Res. 2002;59:340-8.
[173] Sepulveda P, Jones JR, Hench LL. Characterization of melt-derived 45S5 and sol-gel–derived 58S bioactive glasses. J Biomed Mater Res. 2001;58:734-40.
[174] Christodoulou I, Buttery LD, Saravanapavan P, Tai G, Hench LL, Polak JM. Dose-and time-dependent effect of bioactive gel-glass ionic-dissolution products on human fetal osteoblast-specific gene expression. J Biomed Mater Res, Part B. 2005;74:529-37.
[175] Zhang J, Wang M, Cha JM, Mantalaris A. The incorporation of 70s bioactive glass to the osteogenic differentiation of murine embryonic stem cells in 3D bioreactors. J Tissue Eng Regener Med. 2009;3:63-71.
[176] Radev L, Hristova K, Jordanov V, Fernandes M, Salvado I. In vitro bioactivity of 70 wt.% SiO2—30 wt.% CaO sol-gel glass, doped with 1, 3 and 5 wt.% NbF5. Open Chemistry. 2012;10:137-45.
[177] Lin S, Ionescu C, Valliant EM, Hanna JV, Smith ME, Jones JR. Tailoring the nanoporosity of sol-gel derived bioactive glass using trimethylethoxysilane. J Mater Chem. 2010;20:1489-96.
[178] Lin S, Van den Bergh W, Baker S, Jones JR. Protein interactions with nanoporous sol–gel derived bioactive glasses. Acta Biomater. 2011;7:3606-15.
[179] Pirayesh H, Nychka JA. Sol–Gel Synthesis of Bioactive Glass-Ceramic 45S5 and its in vitro Dissolution and Mineralization Behavior. J Am Ceram Soc. 2013;96:1643-50.

[180] Cacciotti I, Lombardi M, Bianco A, Ravaglioli A, Montanaro L. Sol–gel derived 45S5 bioglass: synthesis, microstructural evolution and thermal behaviour. J Mater Sci: Mater Med. 2012;23:1849-66.
[181] Faure J, Drevet R, Lemelle A, Jaber NB, Tara A, El Btaouri H, et al. A new sol–gel synthesis of 45S5 bioactive glass using an organic acid as catalyst. Mater Sci Eng, C. 2015;47:407-12.
[182] Rezabeigi E, Wood-Adams PM, Drew RA. Synthesis of 45S5 Bioglass® via a straightforward organic, nitrate-free sol–gel process. Mater Sci Eng, C. 2014;40:248-52.
[183] Jones JR, Ehrenfried LM, Hench LL. Optimising bioactive glass scaffolds for bone tissue engineering. Biomaterials. 2006;27:964-73.
[184] Jia W, Lau GY, Huang W, Zhang C, Tomsia AP, Fu Q. Bioactive glass for large bone repair. Adv Healthcare Mater. 2015;4:2842-8.
[185] Ciceo RL, Trandafir D-L, Radu T, Ponta O, Simon V. Synthesis, characterisation and in vitro evaluation of sol–gel derived SiO2–P2O5–CaO–B2O3 bioactive system. Ceram Int. 2014;40:9517-24.
[186] Seyedmomeni SS, Naeimi M, Raz M, Mohandesi JA, Moztarzadeh F, Baghbani F, et al. Synthesis, Characterization and Biological Evaluation of a New Sol-Gel Derived B and Zn-Containing Bioactive Glass: In Vitro Study. Silicon. 2016:1-7.
[187] Döhler F, Mandlule A, van Wüllen L, Friedrich M, Brauer DS. 31 P NMR characterisation of phosphate fragments during dissolution of calcium sodium phosphate glasses. J Mater Chem B. 2015;3:1125-34.
[188] Carta D, Pickup DM, Knowles JC, Smith ME, Newport RJ. Sol-gel synthesis of the P2O5-CaO-Na2O-SiO2 system as a novel bioresorbable glass. J Mater Chem. 2005;15:2134-40.
[189] Pickup DM, Guerry P, Moss RM, Knowles JC, Smith ME, Newport RJ. New sol–gel synthesis of a (CaO) 0.3 (Na 2 O) 0.2 (P 2 O 5) 0.5 bioresorbable glass and its structural characterisation. J Mater Chem. 2007;17:4777-84.
[190] Pickup DM, Newport RJ, Knowles JC. Sol–Gel Phosphate-based Glass for Drug Delivery Applications. J Biomater Appl. 2012;26:613-22.
[191] Pickup DM, Valappil SP, Moss RM, Twyman HL, Guerry P, Smith ME, et al. Preparation, structural characterisation and antibacterial properties of Ga-doped sol-gel phosphate-based glass. J Mater Sci. 2009;44:1858-67.
[192] Rust KR, Singleton GT, Wilson J, Antonelli PJ. Bioglass middle ear prosthesis: long-term results. Otology & Neurotology. 1996;17:371-4.
[193] Liu X, Rahaman MN, Day DE. In Vitro Degradation and Conversion of Melt-Derived Microfibrous Borate (13-93B3) Bioactive Glass Doped with Metal Ions. J Am Ceram Soc. 2014;97:3501-9.
[194] Stähli C, James-Bhasin M, Nazhat SN. Three-dimensional endothelial cell morphogenesis under controlled ion release from copper-doped phosphate glass. Journal of Controlled Release. 2015;200:222-32.
[195] Abdelghany A, ElBatal H, EzzElDin F. Bone bonding ability behavior of some ternary borate glasses by immersion in sodium phosphate solution. Ceram Int. 2012;38:1105-13.
[196] Modglin VC, Brown RF, Jung SB, Day DE. Cytotoxicity assessment of modified bioactive glasses with MLO-A5 osteogenic cells in vitro. J Mater Sci: Mater Med. 2013;24:1191-9.
[197] Wei X, Xi T, Zheng Y, Zhang C, Huang W. In Vitro Comparative Effect of Three Novel Borate Bioglasses on the Behaviors of Osteoblastic MC3T3-E1 Cells. Journal of Materials Science & Technology. 2014;30:979-83.

[198] Wang H, Zhao S, Zhou J, Shen Y, Huang W, Zhang C, et al. Evaluation of borate bioactive glass scaffolds as a controlled delivery system for copper ions in stimulating osteogenesis and angiogenesis in bone healing. J Mater Chem B. 2014;2:8547-57.
[199] Deliormanlı AM, Liu X, Rahaman MN. Evaluation of borate bioactive glass scaffolds with different pore sizes in a rat subcutaneous implantation model. J Biomater Appl. 2014;28:643-53.
[200] Zhang X, Jia W, Gu Y, Xiao W, Liu X, Wang D, et al. Teicoplanin-loaded borate bioactive glass implants for treating chronic bone infection in a rabbit tibia osteomyelitis model. Biomaterials. 2010;31:5865-74.
[201] Xie Z, Cui X, Zhao C, Huang W, Wang J, Zhang C. Gentamicin-Loaded Borate Bioactive Glass Eradicates Osteomyelitis Due to Escherichia coli in a Rabbit Model. Antimicrob Agents Chemother. 2013;57:3293-8.
[202] Ding H, Zhao C-J, Cui X, Gu Y-F, Jia W-T, Rahaman MN, et al. A Novel Injectable Borate Bioactive Glass Cement as an Antibiotic Delivery Vehicle for Treating Osteomyelitis. Plos One. 2014;9:e85472.
[203] Lin Y, Brown RF, Jung SB, Day DE. Angiogenic effects of borate glass microfibers in a rodent model. Journal of Biomedical Materials Research Part A. 2014:n/a-n/a.
[204] Liu X, Rahaman MN, Day DE. Conversion of melt-derived microfibrous borate (13-93B3) and silicate (45S5) bioactive glass in a simulated body fluid. Journal of Materials Science: Materials in Medicine. 2013;24:583-95.
[205] Zhao S, Li L, Wang H, Zhang Y, Cheng X, Zhou N, et al. Wound dressings composed of copper-doped borate bioactive glass microfibers stimulate angiogenesis and heal full-thickness skin defects in a rodent model. Biomaterials. 2015;53:379-91.
[206] Marquardt LM, Day D, Sakiyama-Elbert SE, Harkins AB. Effects of borate-based bioactive glass on neuron viability and neurite extension. Journal of Biomedical Materials Research Part A. 2013:n/a-n/a.
[207] Lei B, Chen X, Wang Y, Zhao N, Du C, Fang L. Surface nanoscale patterning of bioactive glass to support cellular growth and differentiation. J Biomed Mater Res, Part A. 2010;94:1091-9.
[208] Shelby JE. Thermal Expansion of Alkali Borate Glasses. Journal of the American Ceramic Society. 1983;66:225-7.
[209] Kamitsos E. Modifying role of alkali-metal cations in borate glass networks. The Journal of Physical Chemistry. 1989;93:1604-11.
[210] Krüner G, Frischat G. Some properties of n-containing lithium borate glasses prepared by different sol-gel methods. J Non-Cryst Solids. 1990;121:167-70.
[211] Yogo T, Kikuta K, Niwa K, Ichida M, Nakamura A, Hirano S-i. Sol-gel processing of β-BaB2O4 thin films through metal organics. 1994. p. 484-92.
[212] Li HC, Wang DG, Hu JH, Chen CZ. Effect of the partial substitution of K2O, MgO, B2O3 for CaO on crystallization, structure and properties of Na2O–CaO–SiO2–P2O5 system glass-ceramics. Mater Lett. 2013;106:373-6.
[213] Qiu D, Martin RA, Knowles JC, Smith ME, Newport RJ. A comparative study of the structure of sodium borophosphates made by sol–gel and melt-quench methods. Journal of Non-Crystalline Solids. 2010;356:490-4.
[214] Bengisu M, Yilmaz E, Farzad H, Reis S. Borate, lithium borate, and borophosphate powders by sol–gel precipitation. Journal of Sol-Gel Science and Technology. 2008;45:237-43.
[215] Brunauer S, Emmett PH, Teller E. Adsorption of gases in multimolecular layers. J Am Chem Soc. 1938;60:309-19.
[216] Joyner LG, Barrett EP, Skold R. The Determination of Pore Volume and Area Distributions in Porous Substances. II. Comparison between Nitrogen Isotherm and Mercury Porosimeter Methods. J Am Chem Soc. 1951;73:3155-8.

[217] Whittemore Jr O, Sipe J. Pore growth during the initial stages of sintering ceramics. Powder Technology. 1974;9:159-64.
[218] Kamitsos E, Karakassides M, Chryssikos GD. A vibrational study of lithium borate glasses with high Li2O content. Phys Chem Glasses. 1987;28:203-9.
[219] Deliormanlı AM. In vitro assessment of degradation and bioactivity of robocast bioactive glass scaffolds in simulated body fluid. Ceram Int. 2012;38:6435-44.
[220] Kamitsos E, Karakassides M, Chryssikos GD. Vibrational spectra of magnesium-sodium-borate glasses. 2. Raman and mid-infrared investigation of the network structure. J Phys Chem. 1987;91:1073-9.
[221] Gautam C, Yadav AK, Singh AK. A Review on Infrared Spectroscopy of Borate Glasses with Effects of Different Additives. ISRN Ceram. 2012;2012.
[222] Agathopoulos S, Tulyaganov D, Ventura J, Kannan S, Karakassides M, Ferreira J. Formation of hydroxyapatite onto glasses of the CaO-MgO-SiO2 system with B2O3, Na2O, CaF2 and P2O5 additives. Biomaterials. 2006;27:1832-40.
[223] Balachandera L, Ramadevudub G, Shareefuddina M, Sayannac R, Venudharc Y. IR analysis of borate glasses containing three alkali oxides. ScienceAsia. 2013;39:278-83.
[224] Repkova M, Nemec P, Frumar M. Structure and thermal properties of Ge-In-S chalcogenide glasses. J Optoelectronics Adv Mater. 2006;8:1796-800.
[225] Ersundu A, Çelikbilek M, Solak N, Aydin S. Glass formation area and characterization studies in the CdO–WO 3–TeO 2 ternary system. Journal of the European Ceramic Society. 2011;31:2775-81.
[226] Liang W, Rüssel C, Day DE, Völksch G. Bioactive comparison of a borate, phosphate and silicate glass. Journal of materials research. 2006;21:125-31.
[227] Stähli C, Shah Mohammadi M, Waters KE, Nazhat SN. Characterization of aqueous interactions of copper-doped phosphate-based glasses by vapour sorption. Acta biomaterialia. 2014.
[228] Naseri S, Lepry WC, Li W, Waters KE, Boccaccini AR, Nazhat SN. 45S5 bioactive glass reactivity by dynamic vapour sorption. Journal of Non-Crystalline Solids. 2015.
[229] Tilocca A. Structural models of bioactive glasses from molecular dynamics simulations. Proc R Soc A. 2009;465:1003-27.
[230] Rey C, Shimizu M, Collins B, Glimcher MJ. Resolution-enhanced fourier transform infrared spectroscopy study of the environment of phosphate ion in the early deposits of a solid phase of calcium phosphate in bone and enamel and their evolution with age: 2. Investigations in thev 3 PO4 domain. Calcified Tissue International. 1991;49:383-8.
[231] Chickerur N, Tung M, Brown W. A mechanism for incorporation of carbonate into apatite. Calcif Tissue Int. 1980;32:55-62.
[232] Nelson D, Featherstone J. Preparation, analysis, and characterization of carbonated apatites. Calcif Tissue Int. 1981;34:S69-81.
[233] LeGeros RZ. The unit-cell dimensions of human enamel apatite: effect of chloride incorporation. Arch Oral Biol. 1975;20:63-71.
[234] Fowler B, Moreno E, Brown W. Infra-red spectra of hydroxyapatite, octacalcium phosphate and pyrolysed octacalcium phosphate. Arch Oral Biol. 1966;11:477-92.
[235] Gu Y, Xiao W, Lu L, Huang W, Rahaman MN, Wang D. Kinetics and mechanisms of converting bioactive borate glasses to hydroxyapatite in aqueous phosphate solution. Journal of Materials Science. 2011;46:47-54.
[236] Peddi L, Brow RK, Brown RF. Bioactive borate glass coatings for titanium alloys. Journal of Materials Science: Materials in Medicine. 2008;19:3145-52.
[237] Ouis MA, Abdelghany AM, ElBatal HA. Corrosion mechanism and bioactivity of borate glasses analogue to Hench's bioglass. Processing and Application of Ceramics. 2012;6:141-9.

[238] Liu X, Xie Z, Zhang C, Pan H, Rahaman MN, Zhang X, et al. Bioactive borate glass scaffolds: in vitro and in vivo evaluation for use as a drug delivery system in the treatment of bone infection. J Mater Sci: Mater Med. 2010;21:575-82.
[239] Brinker CJ, Scherer GW. Sol-gel science1990.
[240] Sharmin N, Hasan MS, Parsons AJ, Furniss D, Scotchford CA, Ahmed I, et al. Effect of boron addition on the thermal, degradation, and cytocompatibility properties of phosphate-based glasses. BioMed research international. 2013;2013.
[241] Hench LL. Biomaterials: a forecast for the future. Biomaterials. 1998;19:1419-23.
[242] Jia W-T, Fu Q, Huang W-H, Zhang C-Q, Rahaman MN. Comparison of borate bioactive glass and calcium sulfate as implants for the local delivery of teicoplanin in the treatment of methicillin-resistant Staphylococcus aureus-induced osteomyelitis in a rabbit model. Antimicrob Agents Chemother. 2015;59:7571-80.
[243] Lin Y, Brown RF, Jung SB, Day DE. Angiogenic effects of borate glass microfibers in a rodent model. J Biomed Mater Res, Part A. 2014:4491-9.
[244] Wray P. 'Cotton candy'that heals? Am Ceram Soc Bull. 2011;90:25-9.
[245] Marquardt LM, Day D, Sakiyama-Elbert SE, Harkins AB. Effects of borate-based bioactive glass on neuron viability and neurite extension. J Biomed Mater Res, Part A. 2013:2767-75.
[246] Gupta B, Papke JB, Mohammadkhah A, Day DE, Harkins AB. Effects of Chemically Doped Bioactive Borate Glass on Neuron Regrowth and Regeneration. Ann Biomed Eng. 2016:1-10.
[247] Hoppe A, Güldal NS, Boccaccini AR. A review of the biological response to ionic dissolution products from bioactive glasses and glass-ceramics. Biomaterials. 2011;32:2757-74.
[248] Tohge N, Moore GS, Mackenzie JD. Structural developments during the gel to glass transition. J Non-Cryst Solids. 1984;63:95-103.
[249] Lepry WC, Nazhat SN. Highly Bioactive Sol-Gel-Derived Borate Glasses. Chem Mater. 2015;27:4821-31.
[250] Osaka A, Yuasa M, Miura Y, Takahashi K. Sodium borosilicate glasses prepared by the sol-gel process. J Non-Cryst Solids. 1988;100:409-12.
[251] Zheng K, Solodovnyk A, Li W, Goudouri OM, Stähli C, Nazhat SN, et al. Aging Time and Temperature Effects on the Structure and Bioactivity of Gel-Derived 45S5 Glass-Ceramics. J Am Ceram Soc. 2015;98:30-8.
[252] Rey C, Shimizu M, Collins B, Glimcher MJ. Resolution-enhanced fourier transform infrared spectroscopy study of the environment of phosphate ion in the early deposits of a solid phase of calcium phosphate in bone and enamel and their evolution with age: 2. Investigations in the nu3PO4 domain. Calcif Tissue Int. 1991;49:383-8.
[253] Xie K, Zhang L, Yang X, Wang X, Yang G, Zhang L, et al. Preparation and characterization of low temperature heat-treated 45S5 bioactive glass-ceramic analogues. Biomed Glasses. 2015;1:80-92.
[254] Thomas A, Bera J. Sol–gel synthesis and in vitro bioactivity of glass–ceramics in SiO2–CaO–Na2O–P2O5 system. J Sol-Gel Sci Technol. 2016;80:411-6.
[255] Chen Q-Z, Li Y, Jin L-Y, Quinn JM, Komesaroff PA. A new sol–gel process for producing Na 2 O-containing bioactive glass ceramics. Acta Biomater. 2010;6:4143-53.
[256] Holand W, Beall GH. Glass ceramic technology: John Wiley & Sons; 2012.
[257] Jones JR, Brauer DS, Hupa L, Greenspan DC. Bioglass and Bioactive Glasses and Their Impact on Healthcare. Int J Appl Glass Sci. 2016;7:423–34.
[258] Bahniuk MS, Pirayesh H, Singh HD, Nychka JA, Unsworth LD. Bioactive Glass 45S5 Powders: Effect of Synthesis Route and Resultant Surface Chemistry and Crystallinity on Protein Adsorption from Human Plasma. Biointerphases. 2012;7:1-15.

[259] Li HC, Wang DG, Hu JH, Chen CZ. Crystallization, mechanical properties and in vitro bioactivity of sol–gel derived Na2O–CaO–SiO2–P2O5 glass–ceramics by partial substitution of CaF2 for CaO. J Sol-Gel Sci Technol. 2013;67:56-65.
[260] Siqueira RL, Peitl O, Zanotto ED. Gel-derived SiO2–CaO–Na2O–P2O5 bioactive powders: Synthesis and in vitro bioactivity. Mater Sci Eng, C. 2011;31:983-91.
[261] Siqueira RL, Costa LC, Schiavon MA, de Castro DT, dos Reis AC, Peitl O, et al. Bioglass® and resulting crystalline materials synthesized via an acetic acid-assisted sol–gel route. J Sol-Gel Sci Technol. 2017:1-9.
[262] Lepry WC, Naseri S, Nazhat SN. Effect of processing parameters on textural and bioactive properties of sol–gel-derived borate glasses. J Mater Sci. 2017:1-13.
[263] Wu C, Chang J. Mesoporous bioactive glasses: structure characteristics, drug/growth factor delivery and bone regeneration application. Interface Focus. 2012;2:292.
[264] Ma J, Chen C, Wang D, Meng X, Shi J. Influence of the sintering temperature on the structural feature and bioactivity of sol–gel derived SiO 2–CaO–P 2 O 5 bioglass. Ceram Int. 2010;36:1911-6.
[265] Naseri S, Lepry WC, Li W, Waters KE, Boccaccini AR, Nazhat SN. 45S5 bioactive glass reactivity by dynamic vapour sorption. J Non-Cryst Solids. 2016;432, Part A:47-52.
[266] Stähli C, Shah Mohammadi M, Waters KE, Nazhat SN. Characterization of aqueous interactions of copper-doped phosphate-based glasses by vapour sorption. Acta Biomater. 2014;10:3317-26.
[267] Cormack AN. The Structure of Bioactive Glasses and Their Surfaces. Bio-Glasses: John Wiley & Sons, Ltd; 2012. p. 65-74.
[268] Giannoudis PV, Dinopoulos H, Tsiridis E. Bone substitutes: an update. Injury. 2005;36:S20-S7.
[269] Bose S, Roy M, Bandyopadhyay A. Recent advances in bone tissue engineering scaffolds. Trends Biotechnol. 2012;30:546-54.
[270] Darrell HR, Iksoo C. Nanometre diameter fibres of polymer, produced by electrospinning. Nanotechnology. 1996;7:216.
[271] Hsu C-M, Shivkumar S. Nano-sized beads and porous fiber constructs of poly (ε-caprolactone) produced by electrospinning. J Mater Sci. 2004;39:3003-13.
[272] Woodruff MA, Hutmacher DW. The return of a forgotten polymer—polycaprolactone in the 21st century. Prog Polym Sci. 2010;35:1217-56.
[273] Guarino V, Causa F, Netti PA, Ciapetti G, Pagani S, Martini D, et al. The role of hydroxyapatite as solid signal on performance of PCL porous scaffolds for bone tissue regeneration. J Biomed Mater Res, Part B. 2008;86:548-57.
[274] Guarino V, Scaglione S, Sandri M, Alvarez-Perez MA, Tampieri A, Quarto R, et al. MgCHA particles dispersion in porous PCL scaffolds: in vitro mineralization and in vivo bone formation. J Tissue Eng Regener Med. 2014;8:291-303.
[275] Fujihara K, Kotaki M, Ramakrishna S. Guided bone regeneration membrane made of polycaprolactone/calcium carbonate composite nano-fibers. Biomaterials. 2005;26:4139-47.
[276] Noh K-T, Lee H-Y, Shin U-S, Kim H-W. Composite nanofiber of bioactive glass nanofiller incorporated poly(lactic acid) for bone regeneration. Mater Lett. 2010;64:802-5.
[277] Kim HW, Kim HE, Knowles JC. Production and Potential of Bioactive Glass Nanofibers as a Next-Generation Biomaterial. Adv Funct Mater. 2006;16:1529-35.
[278] Allo BA, Rizkalla AS, Mequanint K. Synthesis and electrospinning of ε-polycaprolactone-bioactive glass hybrid biomaterials via a sol− gel process. Langmuir. 2010;26:18340-8.

[279] Jia W-T, Zhang X, Luo S-H, Liu X, Huang W-H, Rahaman MN, et al. Novel borate glass/chitosan composite as a delivery vehicle for teicoplanin in the treatment of chronic osteomyelitis. Acta Biomater. 2010;6:812-9.
[280] Lopes P, Ferreira BL, Gomes P, Correia R, Fernandes M, Fernandes M. Silicate and borate glasses as composite fillers: a bioactivity and biocompatibility study. J Mater Sci: Mater Med. 2011;22:1501-10.
[281] Liverani L, Boccaccini AR. Versatile Production of Poly (Epsilon-Caprolactone) Fibers by Electrospinning Using Benign Solvents. Nanomaterials. 2016;6:75.
[282] Coleman MM, Zarian J. Fourier-transform infrared studies of polymer blends. II. Poly(ϵ-caprolactone)–poly(vinyl chloride) system. J Polym Sci, Polym Phys Ed. 1979;17:837-50.
[283] Oliveira JE, Mattoso LH, Orts WJ, Medeiros ES. Structural and morphological characterization of micro and nanofibers produced by electrospinning and solution blow spinning: a comparative study. Adv Mater Sci Eng. 2013;2013.
[284] Edwards A, Jarvis D, Hopkins T, Pixley S, Bhattarai N. Poly (ε-caprolactone)/keratin-based composite nanofibers for biomedical applications. J Biomed Mater Res, Part B. 2015;103:21-30.
[285] Lee K, Kim H, Khil M, Ra Y, Lee D. Characterization of nano-structured poly (ε-caprolactone) nonwoven mats via electrospinning. Polymer. 2003;44:1287-94.
[286] Bosworth LA, Downes S. Acetone, a sustainable solvent for electrospinning poly (ε-caprolactone) fibres: effect of varying parameters and solution concentrations on fibre diameter. J Polym Environ. 2012;20:879-86.
[287] Yoshimoto H, Shin YM, Terai H, Vacanti JP. A biodegradable nanofiber scaffold by electrospinning and its potential for bone tissue engineering. Biomaterials. 2003;24:2077-82.
[288] Soliman S, Sant S, Nichol JW, Khabiry M, Traversa E, Khademhosseini A. Controlling the porosity of fibrous scaffolds by modulating the fiber diameter and packing density. J Biomed Mater Res, Part A. 2011;96:566-74.
[289] Lee SJ, Oh SH, Liu J, Soker S, Atala A, Yoo JJ. The use of thermal treatments to enhance the mechanical properties of electrospun poly(ε-caprolactone) scaffolds. Biomaterials. 2008;29:1422-30.
[290] Kanani AG, Bahrami SH. Effect of changing solvents on poly (ε-caprolactone) nanofibrous webs morphology. J Nanomater. 2011;2011:31.
[291] Khil MS, Bhattarai SR, Kim HY, Kim SZ, Lee KH. Novel fabricated matrix via electrospinning for tissue engineering. J Biomed Mater Res, Part B. 2005;72:117-24.
[292] Agarwal S, Greiner A. On the way to clean and safe electrospinning—green electrospinning: emulsion and suspension electrospinning. Polym Adv Technol. 2011;22:372-8.
[293] Ferreira JL, Gomes S, Henriques C, Borges JP, Silva JC. Electrospinning polycaprolactone dissolved in glacial acetic acid: Fiber production, nonwoven characterization, and in vitro evaluation. J Appl Polym Sci. 2014;131.
[294] Van der Schueren L, De Schoenmaker B, Kalaoglu ÖI, De Clerck K. An alternative solvent system for the steady state electrospinning of polycaprolactone. Eur Polym J. 2011;47:1256-63.
[295] Gönen SÖ, Taygun ME, Küçükbayrak S. Fabrication of bioactive glass containing nanocomposite fiber mats for bone tissue engineering applications. Compos Struct. 2016;138:96-106.
[296] Moghe AK, Hufenus R, Hudson SM, Gupta BS. Effect of the addition of a fugitive salt on electrospinnability of poly(ε-caprolactone). Polymer. 2009;50:3311-8.
[297] Augustine R, Kalarikkal N, Thomas S. Clogging-Free Electrospinning of Polycaprolactone Using Acetic Acid/Acetone Mixture. Polym-Plast Technol Eng. 2016;55:518-29.
[298] Meng Z, Zheng W, Li L, Zheng Y. Fabrication and characterization of three-dimensional nanofiber membrance of PCL–MWCNTs by electrospinning. Mater Sci Eng, C. 2010;30:1014-21.

[299] Taylor G. Disintegration of water drops in an electric field. Proceedings of the Royal Society of London A: Mathematical, Physical and Engineering Sciences: The Royal Society; 1964. p. 383-97.
[300] Reneker DH, Chun I. Nanometre diameter fibres of polymer, produced by electrospinning. Nanotechnology. 1996;7:216.
[301] Jiang T, Carbone EJ, Lo KWH, Laurencin CT. Electrospinning of polymer nanofibers for tissue regeneration. Prog Polym Sci. 2015;46:1-24.
[302] Poologasundarampillai G, Wang D, Li S, Nakamura J, Bradley R, Lee P, et al. Cotton-wool-like bioactive glasses for bone regeneration. Acta Biomater. 2014;10:3733-46.
[303] Zong X, Kim K, Fang D, Ran S, Hsiao BS, Chu B. Structure and process relationship of electrospun bioabsorbable nanofiber membranes. Polymer. 2002;43:4403-12.
[304] Yang Q, Chen S, Shi H, Xiao H, Ma Y. In vitro study of improved wound-healing effect of bioactive borate-based glass nano-/micro-fibers. Mater Sci Eng, C. 2015;55:105-17.
[305] Bley O, Siepmann J, Bodmeier R. Characterization of moisture-protective polymer coatings using differential scanning calorimetry and dynamic vapor sorption. J Pharm Sci. 2009;98:651-64.
[306] Musto P, Galizia M, Scherillo G, Mensitieri G. Water Sorption Thermodynamics and Mass Transport in Poly (ϵ-Caprolactone): Interactional Issues Emerging from Vibrational Spectroscopy. Macromol Chem Phys. 2013;214:1921-30.
[307] Joshi MK, Tiwari AP, Pant HR, Shrestha BK, Kim HJ, Park CH, et al. In situ generation of cellulose nanocrystals in polycaprolactone nanofibers: Effects on crystallinity, mechanical strength, biocompatibility, and biomimetic mineralization. ACS Appl Mater Interfaces. 2015;7:19672-83.
[308] Gu Y, Huang W, Rahaman MN. In vivo evaluation of scaffolds with a grid-like microstructure composed of a mixture of silicate (13-93) and borate (13-93B3) bioactive glasses. Ceram Eng Sci Proc. 5 ed2014. p. 53-64.
[309] Vogel W. Phase separation in glass. J Non-Cryst Solids. 1977;25:170-214.
[310] Nakanishi K, Tanaka N. Sol–Gel with Phase Separation. Hierarchically Porous Materials Optimized for High-Performance Liquid Chromatography Separations. Accounts of Chemical Research. 2007;40:863-73.
[311] Diba M, Tapia F, Boccaccini AR, Strobel LA. Magnesium-containing bioactive glasses for biomedical applications. Int J Appl Glass Sci. 2012;3:221-53.
[312] Watts S, Hill R, O'Donnell M, Law R. Influence of magnesia on the structure and properties of bioactive glasses. J Non-Cryst Solids. 2010;356:517-24.
[313] O'Donnell MD, Watts SJ, Law RV, Hill RG. Effect of P2O5 content in two series of soda lime phosphosilicate glasses on structure and properties – Part I: NMR. J Non-Cryst Solids. 2008;354:3554-60.
[314] Jones J, Hench L. Effect of surfactant concentration and composition on the structure and properties of sol-gel-derived bioactive glass foam scaffolds for tissue engineering. J Mater Sci. 2003;38:3783-90.
[315] Mathew R, Stevensson B, Tilocca A, Edén M. Toward a rational design of bioactive glasses with optimal structural features: composition–structure correlations unveiled by solid-state NMR and MD simulations. The Journal of Physical Chemistry B. 2014;118:833-44.
[316] Tilocca A. Short-and medium-range structure of multicomponent bioactive glasses and melts: an assessment of the performances of shell-model and rigid-ion potentials. The Journal of chemical physics. 2008;129:08B614.
[317] Mathew R, Stevensson B, Tilocca A, Edén M. Toward a Rational Design of Bioactive Glasses with Optimal Structural Features: Composition–Structure Correlations Unveiled by Solid-State NMR and MD Simulations. The Journal of Physical Chemistry B. 2014;118:833-44.

[318] Zeitler TR, Cormack A. Interaction of water with bioactive glass surfaces. Journal of crystal growth. 2006;294:96-102.
[319] Tilocca A, Cormack AN. Exploring the surface of bioactive glasses: water adsorption and reactivity. The Journal of Physical Chemistry C. 2008;112:11936-45.
[320] Tilocca A, Cormack AN. Modeling the Water− Bioglass Interface by Ab Initio Molecular Dynamics Simulations. ACS Appl Mater Interfaces. 2009;1:1324-33.
[321] Mead R, Mountjoy G. Modeling the Local Atomic Structure of Bioactive Sol− Gel-Derived Calcium Silicates. Chem Mater. 2006;18:3956-64.
[322] Christie JK, Ainsworth RI, de Leeuw NH. Investigating structural features which control the dissolution of bioactive phosphate glasses: Beyond the network connectivity. J Non-Cryst Solids. 2016;432, Part A:31-4.
[323] Christie JK, Ainsworth RI, de Leeuw NH. Ab initio molecular dynamics simulations of structural changes associated with the incorporation of fluorine in bioactive phosphate glasses. Biomaterials. 2014;35:6164-71.
[324] Vegiri A, Varsamis C-P, Kamitsos E. Molecular dynamics investigation of mixed-alkali borate glasses: Short-range order structure and alkali-ion environments. Physical Review B. 2009;80:184202.
[325] Crovace MC, Souza MT, Chinaglia CR, Peitl O, Zanotto ED. Biosilicate®—A multipurpose, highly bioactive glass-ceramic. In vitro, in vivo and clinical trials. J Non-Cryst Solids. 2016;432:90-110.
[326] Docks EL. Boric Acid Esters. Kirk-Othmer Encyclopedia of Chemical Technology: John Wiley & Sons, Inc.; 2000.
[327] Yu B, Turdean-Ionescu CA, Martin RA, Newport RJ, Hanna JV, Smith ME, et al. Effect of Calcium Source on Structure and Properties of Sol–Gel Derived Bioactive Glasses. Langmuir. 2012;28:17465-76.
[328] Li N, Chen G, Liu J, Xia Y, Chen H, Tang H, et al. Effect of Surface Topography and Bioactive Properties on Early Adhesion and Growth Behavior of Mouse Preosteoblast MC3T3-E1 Cells. ACS Appl Mater Interfaces. 2014;6:17134-43.
[329] Pereira MM, Clark AE, Hench LL. Effect of Texture on the Rate of Hydroxyapatite Formation on Gel-Silica Surface. J Am Ceram Soc. 1995;78:2463-8.
[330] Hench LL, Walker MM. Bonding of bone to materials presenting a high specific area, porous, silica-rich surface. Google Patents; 1979.
[331] Li Y, Rahaman MN, Fu Q, Bal BS, Yao A, Day DE. Conversion of bioactive borosilicate glass to multilayered hydroxyapatite in dilute phosphate solution. J Am Ceram Soc. 2007;90:3804-10.
[332] Zhou Y, Fang C, Fang Y, Zhu F, Cao L. Polyborates in aqueous sodium borate solution at 298.15 K. Asian Journal of Chemistry. 2012;24:29.
[333] Velez M, Tuller HL, Uhlmann DR. Chemical durability of lithium borate glasses. J Non-Cryst Solids. 1982;49:351-62.
[334] Anderson J, Eyring E, Whittaker M. Temperature Jump Rate Studies of Polyborate Formation in Aqueous Boric Acid1. The Journal of Physical Chemistry. 1964;68:1128-32.
[335] Yifei G, Huang W, Rahaman MN. Effect of Immersion Medium on the Degradation and Conversion of Silicate (13-93) Bioactive Glass Scaffolds. Biomaterials Science: Processing, Properties, and Applications V: Ceramic Transactions, Volume 254. 2015:73-83.
[336] Kaur G, Pickrell G, Sriranganathan N, Kumar V, Homa D. Review and the state of the art: Sol–gel and melt quenched bioactive glasses for tissue engineering. J Biomed Mater Res, Part B. 2015.
[337] Zhong J, Greenspan DC. Processing and properties of sol–gel bioactive glasses. J Biomed Mater Res, Part A. 2000;53:694-701.

[338] Wei X, Xi T, Zheng Y, Zhang C, Huang W. In Vitro Comparative Effect of Three Novel Borate Bioglasses on the Behaviors of Osteoblastic MC3T3-E1 Cells. Journal of Materials Science & Technology. 2014;30:979-83.
[339] Gu Y, Huang W, Rahaman MN. In vivo evaluation of scaffolds with a grid-like microstructure composed of a mixture of silicate (13-93) and borate (13-93B3) bioactive glasses. Ceram Eng Sci Proc. 5 ed2014. p. 53-64.
[340] Bi L, Zobell B, Liu X, Rahaman MN, Bonewald LF. Healing of critical-size segmental defects in rat femora using strong porous bioactive glass scaffolds. Materials Science and Engineering C. 2014;42:816-24.
[341] Zhou J, Wang H, Zhao S, Zhou N, Li L, Huang W, et al. In vivo and in vitro studies of borate based glass micro-fibers for dermal repairing. Mater Sci Eng, C. 2016;60:437-45.
[342] Wray P. Wound healing: An update on Mo-Sci's novel borate glass fibers. Am Ceram Soc Bull. 2013;92:30-5.